SENSITIVITY AND ERROR ANALYSIS OF A DIFFERENTIAL RECTIFICATION METHOD FOR CCD FRAME CAMERAS AND PUSHBROOM SCANNERS

A THESIS SUBMITTED TO
THE GRADUATE SCHOOL OF NATURAL AND APPLIED SCIENCES
OF
MIDDLE EAST TECHNICAL UNIVERSITY

BY

ÖNDER HALİS BETTEMİR

IN PARTIAL FULFILLMENT OF THE REQUIREMENTS
FOR
THE DEGREE OF MASTER OF SCIENCE
IN
CIVIL ENGINEERING

SEPTEMBER 2006

Approval of the Graduate School of Natural and Applied Sciences

Prof. Dr. Canan Özgen
Director

I certify that this thesis satisfies all the requirements as a thesis for the degree of Master of Science.

Prof. Dr. Erdal Çokça
Head of Department

This is to certify that we have read this thesis and that in our opinion it is fully adequate, in scope and quality, as a thesis for the degree of Master of Science.

Assoc. Prof. Dr. Mahmut Onur Karslıoğlu
Supervisor

Examining Committee Members

Assist. Prof. Bahattin Coşkun	(METU,CE)	
Assoc. Prof. Mahmut O. Karslıoğlu	(METU,CE)	
Prof. Dr. Vedat Toprak	(METU, GEOE)	
Dr. Uğur Murat Leloğlu	(TÜBİTAK UZAY)	
Dr. Jurgen Friedrich	(Başkent Unv, CENG)	

I hereby declare that all information in this document has been obtained and presented in accordance with academic rules and ethical conduct. I also declare that, as required by these rules and conduct, I have fully cited and referenced all material and results that are not original to this work.

Name, Last name: Önder Halis BETTEMİR

Signature :

ABSTRACT

SENSITIVITY AND ERROR ANALYSIS OF A DIFFERENTIAL RECTIFICATION METHOD FOR CCD FRAME CAMERAS AND PUSHBROOM SCANNERS

Bettemir, Önder Halis

MSc., Department of Civil Engineering

Supervisor : Assoc. Prof. Mahmut Onur Karslıoğlu

September 2006, 252 pages

In this thesis, sensitivity and error analysis of a differential rectification method were performed by using digital images taken by a frame camera onboard BILSAT and pushbroom scanner on ASTER. Three methods were implemented for Sensitivity and Uncertainty analysis: Monte Carlo, covariance analysis and FAST (Fourier Amplitude Sensitivity Test).

A parameter estimation procedure was carried out on the basis of so called Mixed Model extended by some suitable additional regularization parameters to stabilize the solution for improper geometrical conditions of the imaging system.

The effectiveness and accuracy of the differential rectification method were compared with other rectification methods and the results were analyzed. Furthermore the differential method is adapted to the pushbroom scanners and software which provides rectified images from raw satellite images was developed.

Keywords: Orthoimages, rectification, sensitivity analysis, error analysis, Mixed Model (Gauss-Helmert model)

ÖZ

CCD VE PUSHBROOM KAMERALAR İÇİN GELİŞTİRİLMİŞ DİFERANSİYEL REKTİFİKASYON YÖNTEMİNİN DUYARLILIK VE HATA ANALİZİ

Bettemir, Önder Halis
Y. Lisans, İnşaat Mühendisliği Bölümü
Tez Yöneticisi : Doç. Dr. Mahmut Onur Karslıoğlu

Eylül 2006, 252 sayfa

Bu tezde BİLSAT üzerindeki Metrik kamera (frame camera) ve ASTER üzerindeki pushbroom tarayıcı ile çekilen görüntüler kullanılarak diferansiyel rektifikasyon yönteminin duyarlılık ve hata analizi yapıldı. Duyarlılık ve hata analizinde Diferansiyel Analiz, Monte Carlo Hassasiyet Analizi ve Fourier Genlik Duyarlılık Testi (FGDT) metodları kullanıldı.

Parametre kestirimi, Karışık Model (Gauss-Helmert) yöntemi ile görüntü alım geometrisinin bozukluğundan etkilenen çözümü stabilize etmek için uygun düzeltme yöntemleri kullanılarak yapıldı.

Algoritmanın verimliliği ve duyarlılığı diğer görüntü rektifikasyon methodları ile karşılaştırıldı ve sonuçları analiz edildi. Bununla beraber yeni geliştirilen rektifikasyon yöntemi *pushbroom* tarayıcılara uyarlandı ve uydu fotoğraflarının rektifikasyonunu yapan bir yazılım geliştirildi.

Anahtar Kelimeler: Sayısal Ortofoto, rektifikasyon (rödresman), duyarlılık analizi, hata analizi, Karışık Model (Gauss-Helmert modeli).

To My Parents,

ACKNOWLEDGMENTS

The author wishes to express his deepest gratitude to his supervisor Assoc. Prof. Mahmut Onur Karslıoğlu for his guidance, advice, criticism and insight throughout the research.

The author would also like to thank Dr. Jurgen Friedrich for his suggestions and comments.

Special thanks to Assist. Prof. Bahattin Coşkun, Dr. Uğur Murat Leloğlu and Prof. Dr. Vedat Toprak for their advices, comments and believing in my determination on the subject and their patience.

Thanks to Birol Güçlüer for supplying devices and technical support during the fieldworks.

Thanks to Ali Özdemir for his help in enhancing the images and printing out the thesis.

Finally endless thanks to my father Veli Bettemir and my mother Nazife Bettemir for their support and encouragements during the thesis study.

TABLE OF CONTENTS

LIST OF TABLES

TABLES

LIST OF FIGURES

FIGURES

CHAPTER 1

INTRODUCTION

In this thesis it is aimed to implement and derive the algorithm of the differential rectification method (DRM) developed for charge coupled device (CCD) cameras in detail, to adopt DRM to pushbroom scanners, to perform a sensitivity and uncertainty analysis of the DRM for both CCD and pushbroom scanner images, and to compare the accuracy of DRM with some of the existing rectification methods. For the implementation of the algorithm, images taken by BiLSAT and ASTER will be used as the data source in the study.

There are many rectification methods and each method has unique algorithms and as a result unique accuracy. However, in general the methods project the image coordinates to the earth surface considering the earth as a planar surface and then apply the necessary corrections for the curvature of the earth. A new differential method (DRM) was proposed for orthorectification [1] that projects the pixel coordinates directly on to the reference ellipsoid as an earth model, thus requiring no additional corrections.

1.1 Necessity of Rectification

There are several reasons that prevent an image to be used directly as image map. These are explained in the following subsections

1.1.1 Tilted Image

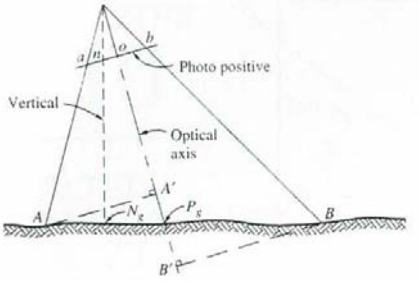

(a)

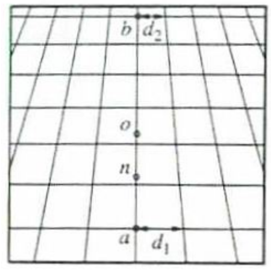

(b)

Figure 1.1 (a) Geometry of a tilted image (b) Appearances of grids in a tilted image [2].

Satellites can not always pass exactly over the ground object that is desired to be imaged because of the orbit characteristics of satellites. In order to image the intended ground object, imaging system of satellite is tilted from the nadir direction. Because of this, the ratio of the distance between the sensor and the ground surface, and the ratio of the distance between camera focus and the imaging sensor of all image points will not be the same (Figure 1.1a). The scale of the image is directly related with this ratio, different ratio results in scale variations in the image. In order to use the image as an image map, the scale variations due to tilt should be eliminated [2].

It is easily seen that the ratio of the lines Lb to bB and La to LA (Figure 1.1a) are not the same. Because of the tilt of the sensor ration of Lb to bB is smaller, resulting different scales in different portions of the image. Figure 1.1b shows the appearance of the same sized grids in a tilted image. The scale at the top of the image is considerably smaller than the bottom part which is a good representation of the tilt effect on scale.

1.1.2 Earth's Curvature

The surface of the earth is not a flat surface and especially satellite images cover a wide area and the curvature of the earth becomes an important factor that affects the ratio of the distance between the focus and sensor, sensor and the ground point (Figure 1.2). Although the image is not tilted, the ratio of Ad to dD is not the same with the ratio of Ac to cC because of the earth's curvature. In order to keep scale constant all over the image, the earth's curvature effect should be eliminated.

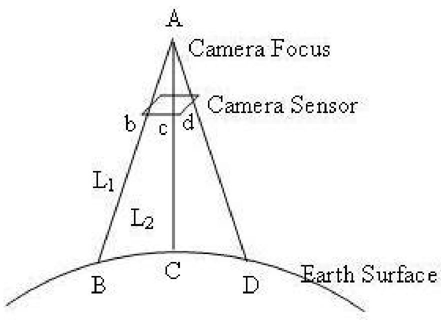

Figure 1.2 Earth curvature effect on the scale of the image

1.1.3 Relief Displacements

Relief displacement is the shift or displacement in the photographic position of an image caused by the relief, elevation with respect to a selected datum, of the object (Figure 1.3). Relief displacement is outward for points whose elevations are above datum and inwards for points whose elevations are below datum [2, p137].

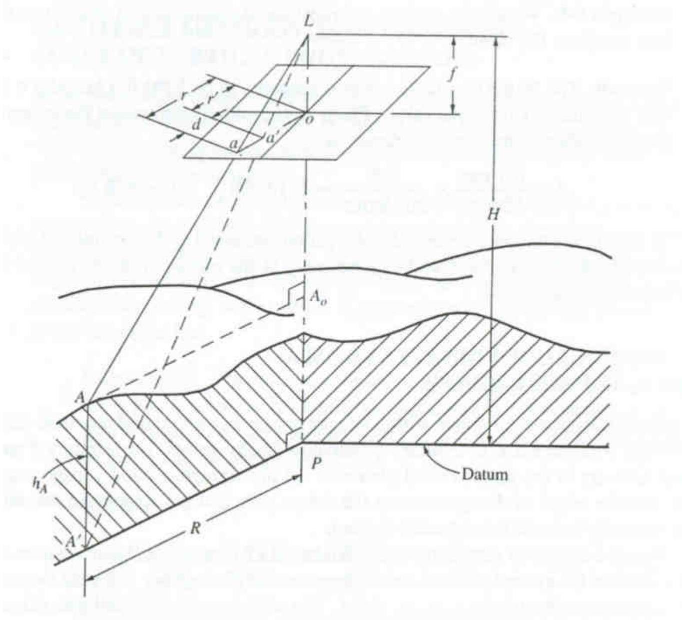

Figure 1.3 Effect of relief displacement, the exact location of the point A is further from the A' [2].

Relief displacements change the relative positions, in other words the relative distance between the objects in the image. For this reason the image cannot be used as a map unless the relief displacements are eliminated. The relief displacement effect increases if the ground point is further from the image center. Furthermore, the displacement direction is same with the direction to the image center.

1.1.4 Atmospheric Refraction

Propagation direction of light ray changes (Figure 1.4) when the density of the medium changes [2, p102]. It is known that density of the atmosphere decreases with increasing altitude. For this reason, light rays do not travel in straight lines through the atmosphere; they are bent according to the Snell's law. Since analytic photogrammetric equations are derived with the assumption of light rays travel in straight lines, corrections should be applied in order to eliminate the error caused by atmospheric refraction.

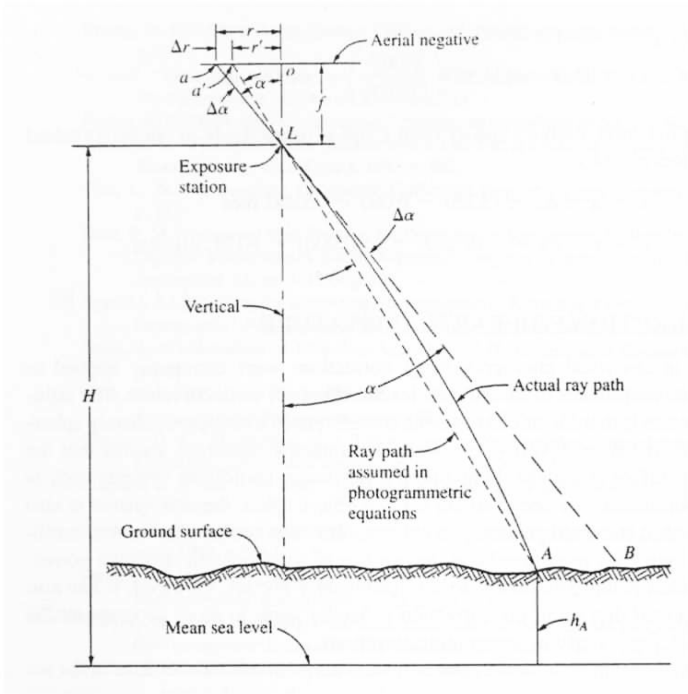

Figure 1.4 Refraction of light rays while propagating through atmosphere [2]

1.1.5 Lens Distortion

Characteristics of camera lens have an important effect on the image. Although they are produced very cautiously, some malfunctioning will be present in the device and the lens will distort the light rays according to the distance from the image center, causing the changes at the relative positions between the ground points. Lens distortion effect can be eliminated by mathematical corrections derived after the lens calibration [2, p.97].

1.2 Common Rectification Methods

In this subchapter some of the widespread rectification methods will be presented.

1.2.1 Helmert Transformation

In 2-D Helmert transformation, there are only four parameters for the scale, shift and rotation. Two axes are rotated by same amount so the rotation is orthogonal [3]. The formula of Helmert transformation (HT) can be given as;

$$\begin{aligned} x &= au + bv + c \\ y &= -bu + av + d \end{aligned} \tag{1.1}$$

In Equation 1.1 a and b are the rotation parameters, c and d are translation parameters, u and v are the image coordinates. Scale is the norm of a and b. In order to determine the parameters at least two GCPs should be collected. Since this is an orthogonal transformation, this method can not be used in the rectification of satellite images. HT can not eliminate effect of tilt and curvature of the earth successfully.

1.2.2 Affine Transformation

In affine transformation the raw satellite or airborne image is rectified by a transformation operation. The transformation parameters are computed after the optimization process of the residuals of the GCPs collected at the field. Rotation of the two axes is not the same. In Affine Transformation rotation is not orthogonal but parallel lines remains parallel after the rotation [3]. The mathematical formula of the transformation can be written as;

$$\begin{aligned} X &= au + bv + c \\ Y &= du + ev + f \end{aligned} \tag{1.2}$$

In Equation 1.2 a and b are the both rotation and scaling, c is the translation parameters of the x axis, similarly d and e are the rotation and scaling parameters and f is the translation parameter for the y axis. X and Y are the ground coordinates of the corresponding pixel with respect to a certain datum and finally u and v are image coordinates. Totally there are 6 parameters to be solved, so at least 3 GCPs are required in order to determine the transformation parameters.

1.2.3 Pseudo Affine Transformation

Pseudo Affine is an eight parameter transformation used for the rectification of satellite images. In order to solve eight parameters at least four GCPs are required. This method has three rotation parameters and one translation parameter for each axis [3]. The mathematical formula of the Pseudo Affine Transform is given as;

$$\begin{aligned} x &= a_1uv + a_2u + a_3v + a_4 \\ y &= a_5uv + a_6u + a_7v + a_8 \end{aligned} \tag{1.3}$$

Pseudo Affine Transformation is neither an orthogonal transformation nor parallel lines stay parallel. Because of a_1 and a_5 terms rotation and scaling will not be the same for every pixel in the raw image.

1.2.4 Projective Transformation

Projective transformation is an 8 parameter transformation generally used for the rectification of images shot by CCD array. 8 parameters are computed after the optimization process of the GCPs collected from the field [2, p548]. The transformation equations are derived from colinearity equations;

$$X = \frac{a_1 x + b_1 y + c_1}{a_3 x + b_3 y + 1}$$

$$Y = \frac{a_2 x + b_2 y + c_2}{a_3 x + b_3 y + 1} \tag{1.4}$$

In Equation 1.4 X and Y are the rectified coordinates expressed in terms of x and y, which are tilted photo coordinates. a_1, b_1, c_1, a_2, b_2, c_2, a_3 and b_3 are the transformation parameters to be solved. The method requires collection of at least four GCPs for the solution of parameters. Projective transformation is generally used for the rectification of airborne images.

1.2.5 Second Order Conformal Transform

As its name implies, this method rotates the image axes with same angle but the amount of rotation is not the same at every location of the image. In other words rotation amount may not be the same for different pixel locations but the both axis will be rotated by the same amount. There are four parameters for rotation of the two axes and one parameter for the translation of each axis. In order to determine all parameters, at least three GCPs are required [3]. The mathematical formula of the method can be written as;

$$\begin{aligned} x &= a_1 u + a_2 v + a_3\left(u^2 - v^2\right) + 2a_4 uv + a_5 \\ y &= -a_2 u + a_1 v + 2a_3 uv - a_4\left(u^2 - v^2\right) + a_6 \end{aligned} \tag{1.5}$$

When second order conformal transformation is applied, parallel lines may not remain parallel after the transformation.

1.2.6 Polynomial Transformation

For the rectification of satellite images, Polynomial Transformations are generally used. The order of polynomial can be taken as two or three. Higher order polynomials increase the parameter number considerably which results an increase in demand for GCPs. Furthermore higher order terms may be correlated with each other and cause rank deficiency in the coefficient matrix leading to inaccurate solution. The general formula for the polynomial transform can be written as;

$$x = \sum_i \sum_j a_{ij} u^{i-1} v^{j-1}$$
$$y = \sum_i \sum_j b_{ij} u^{i-1} v^{j-1} \tag{1.6}$$

In Equation 1.6 a and b are coefficients to be determined for rectification, u and v are raw image coordinates of the ground point and x and y are the assigned ground point for the corresponding image point [3].

1.2.7 Orthorectification

In orthorectification method, colinearity equations are applied in order to provide a relationship between image and ground points. Additionally, elevation information of the ground points are required for the elimination of relief displacements. For this reason, a Digital Elevation Model (DEM) is required in orthorectification process. Furthermore computational demand of this method is much higher than other rectification methods. On the other hand, if inner and outer orientation parameters of the camera are known accurately, the accuracy of the rectification will be better than the other methods. To improve the accuracy of these parameters parameter estimation procedure may be carried out within the rectification process. Besides, orthorectification provides the elevation information for each pixel of the rectified image.

Colinearity equations are usually written with an assumption of a flat earth surface in order to make equations easier to solve [4]. After the rectification process corrections are made for curvature of the earth (Figure 1.5). DRM directly rectifies the ground points on to reference ellipsoid as an earth model and avoids earth curvature corrections [1]. One of the tasks in this thesis is to compare the accuracy of DRM with present orthorectification methods for regions with different topographic characteristics.

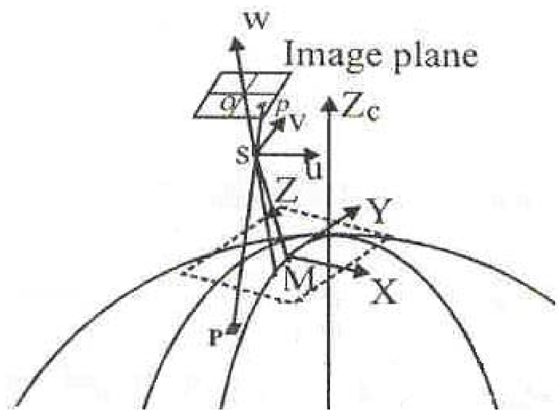

Figure 1.5 Classical orthorectification methods [4].

1.3 Related Works About Image Rectification

There are many techniques developed for the rectification of orthoimages. Most commonly used technique is affine and polynomial transformation methods. Another widespread technique is differential rectification. The literature related with the image rectification is presented briefly as below;

Besides “ill-conditioned” analytical relationships, an alternative approach was proposed by Okamato to the triangulation of satellite line scanner imagery [5]. In his approach an initial transformation of the original perspective line image into an affine projection which is then followed by a linear transformation from image to object space for stereo geometries is performed. The advantage of the method can be considered as avoiding very high correlations arising between the orientation parameters due to very narrow view angle of the imaging device.

Direct Linear Transformation (DLT) was suggested by El-Manadili and Novak for the geometric modeling of SPOT imagery [6]. DLT approach does not require parameters of the interior and ephemeris information. The solution is based only on ground control points. This is advantageous for processing of the new high resolution satellite images, especially if their sensor model and ephemeris information are not available. DLT is employed after correcting the image coordinates for systematic distortions caused by Earth rotation and cell size variations due to off-nadir viewing. Corrections for other systematic errors are considered through the adjustment.

The principle of orientation images was used by Kornus for the geometric inflight calibration of MOMS-2P imagery [7]. This method is based on extended collinear equations [8]. The exterior orientation parameters are determined in the so called orientation images. Between the orientation images, parameters of an arbitrary scan line are interpolated using Lagrange polynomials. For modeling of the interior orientation for each CCD array, five parameters are introduced. All unknown parameters are estimated in a bundle block adjustment using threefold stereo imagery. For the determination of the unknown parameters, a large number of tie points is required which are automatically measured.

An orbital parameter model was suggested by Gugan [9]. The collinear equations are expanded by two orbital parameters to model the satellite movement along the path and the earth’s rotation: the linear angular changes with time of the true anomaly and the right ascension of the ascending node. The attitude variations are modeled by drift rates. This model was successfully adopted by Valadan Zoej and Petrie and applied for SPOT level 1A and 1B, MOMS – 02 and IRS-1C imagery [10].

For the photogrammetric triangulation using MOMS-02, MOMS-02/D2 and MOMS-2P/PRIRODA imageries good results are obtained using the program SPOTCHECK+ [11-12]. This solution was successfully applied on various sensors eg. SPOT, Landsat, TM5 and JERS-1 [13]. The approach is based on a photogrammetric strict sensor model which needs only 10 ground control points. Furthermore, the sensor model can be easily extended to process images from other high resolution imaging systems as they become available.

Applicability and accuracy of the rectification methods were compared by Ok. A. Ö. in his MS thesis [14]. The study examines rectification models including affine transformation to rigorous analytical rectification.

DRM for monoscopic images taken by CCD frame cameras was proposed by Karslıoğlu and Friedrich [1]. The method directly assigns the geodetic coordinates of the images by avoiding earth curvature corrections. In this thesis, sensitivity and accuracy analysis of DRM will be performed for both CCD frame cameras and pushbroom scanners.

1.4 Sensitivity and Uncertainty Analysis

Sensitivity refers to the variation in output of a mathematical model with respect to changes in the values of the model's parameters. A sensitivity analysis attempts to provide a ranking to the assumptions of the model's parameters with respect to their contribution to model output variability or uncertainty [15]. The difficulty of a sensitivity analysis increases when the underlying model is nonlinear, non-monotonic or when the input parameters range over several orders of magnitude. In a broader sense, sensitivity can refer to how conclusions may change if models, data, or assessment assumptions are changed.

Uncertainty refers to lack of knowledge about specific factors, parameters, or models. Uncertainty includes parameter uncertainty, i.e. measurement errors, sampling errors, systematic errors, model uncertainty, i.e. uncertainty due to necessary simplification of real-world processes, misspecification of the model structure, model misuse, use of inappropriate surrogate variables, and scenario uncertainty, i.e. descriptive errors, aggregation errors, errors in professional judgment, and incomplete analysis [16].

Sensitivity analysis is conducted to determine which input parameters have significant effect on the outputs and which parameters contribute most to output variability, thus require more attention when performing uncertainty analysis. Sensitivity analyses are often referred to as local or global. Local analysis considers one parameter at a time and addresses sensitivity relative to the point estimates of parameters. Global analysis examines sensitivity with respect to the entire parameter distribution.

The main objective of uncertainty analysis is to assess the statistical properties of model outputs as a function of stochastic input parameters. Methods generally used for uncertainty analysis can be listed as First Order Analysis, Monte Carlo Simulation, Latin Hypercube Sampling, Response Surface Methodology, Fourier Amplitude Sensitivity Test and Point Estimate Method [17].

In literature there are many works on sensitivity and uncertainty. Some of them are listed below;

Rank transformed data had been used by Conover and Iman at covariance analysis which is a combination of regression, and analysis of variance [18]. Rank transformed data have properties of robustness and power in both regression, and analysis of variance. The authors examined a robust ANCOVA procedure based on replacing the data with their ranks and performed the parametric calculations with their ranks.

A Performance Assessment study was made by Helton aiming to find “What occurrences can take place?”, “How likely are these occurrences?”, “What are the consequences of individual occurrences?” and “How much confidence exists in the answers?” In his study the author divided the uncertainty in two components; stochastic (aleatory) uncertainty which arises because the system under study can potentially behave in many different ways, and subjective (epistemic) uncertainty, which arises from a lack of knowledge about quantities that are assumed to have fixed values within the computational implementation of the Performance Assessment [19].

A Monte Carlo method to study the effect of systematic and random errors on computer models mainly dealing with experimental data was presented by Vasques [20]. The uncertainty analysis approach presented in his work is based on the analysis of cumulative probability distributions of output variables of the models involved taking into account the effect of both random and systematic errors. The main objectives of his study were to detect the error source with stochastic dominance on the uncertainty propagation, and the combined effect on output variables of the models.

Uncertainty and sensitivity analysis results obtained with random and Latin Hypercube sampling were compared by Helton [21]. In order to assess the stability of the sensitivity analysis results caused by inadequate sample size, he used Kendall’s coefficient of concordance and the top down coefficient of concordance.

Some of the variance based methods used in sensitivity analysis to ascertain how much a model depends on each or some of its input parameters were reviewed by Chan, Saltelli and Tarantola [22]. In their analysis “Correlation ratios or Importance Measures”, “Sobol’ Indices” and FAST Indices” are used. At the end of their study they concluded that all the alternative global methods, variance-based or not, can offer, at best, a qualitative picture of the model sensitivity. The variance based methods such as correlation ratio or importance measures are model independent and can evaluate main effect contributions.

Methods for the sensitivity and uncertainty analysis of signalized intersections had been compared by Ji [17]. In his analysis he has used four sensitivity analysis methods; Partial Differential Analysis, Partial Correlation Coefficients, Standardized Regression Coefficients and Fourier Amplitude Sensitivity Test and four uncertainty analysis methods; First Order Analysis, Monte Carlo Simulation, FAST, and Point Estimate Method.

A new method of sensitivity analysis of model output based on Fourier Amplitude Sensitivity Test (FAST) had been proposed by Saltelli [23]. The method allows the computation of the total contribution of each parameter to the output's variance. The term "total contribution" means the parameters' main effects, as well as all the interaction terms involving that factor, are included. In his study Saltelli addresses the limitations of other sensitivity analysis methods and suggest that the total-effect indices are ideally suited to perform a global, quantitative, model-independent sensitivity analysis.

1.5 Prospects from This Thesis

In this thesis, it is aimed to find the accuracy and effectiveness of the DRM by comparing it with some of the other rectification methods. At the end of the study software which can generate orthoimages acquired by CCD frame cameras and Pushbroom scanners will be developed.

Additionally, three sensitivity analysis methods, Differential Sensitivity, Monte Carlo and Fourier Amplitude Sensitivity Test (FAST) will be applied to compute the uncertainty in the rectified coordinates and the sensitivity of the rectification parameters. These analyses will be performed by using both BilSAT and ASTER images and the computed sensitivity will be on the basis of both BilSAT and ASTER geometry.

The new method will be implemented for pushbroom scanners which have continuous attitude and position information. In case of missing information in terms of position or attitude, these will be predicted by interpolation.

During the research BilSAT and ASTER images and SRTM DEM will be used as data source and Matlab mathematical programming software will be used for programming of the algorithms.

In Chapter 2, reference and time systems used in rectification process are briefly introduced. Additionally, assumptions made in the definition of some of the reference frames are explained and illustrated.

In Chapter 3, region of analysis is described. Both BilSAT and ASTER images used in the analysis are presented. Additionally, Ground Control Points (GCP) distribution is defined and measurement method of ground coordinates and image coordinates are explained.

In Chapter 4, derivation of colinearity equations are described for both CCD cameras and pushbroom scanners. In this chapter; lens distortion, precession, nutation, polar motion, atmospheric refraction and relief displacement corrections are explained. Additionally, all transformation procedures in the rectification process explained in detail. In this chapter some modifications on DRM is illustrated also. Convergence of the iteration process is brushed up and the convergence of the method is accelerated.

In Chapter 5, parameter estimation procedure used in this thesis is introduced. The solution of the parameter estimation equations is not stable because of the weak camera geometry of the satellites and correlations between the parameters. This prevents obtaining an accurate solution for the parameters. For this reason, solution of the system is stabilized by applying regularization methods. Three regularization algorithms used for the stabilization of the solution are introduced in this chapter. Furthermore, improvement obtained in the accuracy of the solution by applying regularization methods is also tested.

In Chapter 6, the parameter estimation methods are implemented to improve the accuracy of the parameters. Additionally, performance of the regularization methods is compared in terms of accuracy and convergence. Furthermore, DRM for both CCD frame and pushbroom scanners are implemented by using improved parameters. For the CCD frame cameras some constraints are introduced to improve the result of the parameter estimation and an outlier test is performed to check the result of the parameter estimation and GCPs.

In Chapter 7 DRM is compared with some of the existing rectification methods. The comparison is performed in terms of accuracy, speed and complexity of the methods. Additionally, changes in the estimated parameters with respect to initial conditions are examined by adding blunders to the initial values of the parameters. At the end of the chapter the analysis results are commented.

In Chapter 8 sensitivity and uncertainty analysis is performed for the rectification methods of CCD frame camera and pushbroom scanners. First the sensitivity analysis methods used in the analysis are introduced then the methods are implemented for both CCD frame cameras and pushbroom scanners. The sensitivity and uncertainty results are also commented.

In Chapter 9 an overall discussion of the thesis study is made. Analysis results are commented briefly and some recommendations are suggested for future studies related with DRM and sensitivity and uncertainty analysis.

CHAPTER 2

REFERENCE AND TIME SYSTEMS USED IN RECTIFICATION PROCEDURE

In this chapter, reference and time systems used in the thesis will be briefly introduced. Assumptions in the definition of the reference systems are also clearly illustrated.

2.1 REFERENCE SYSTEMS USED IN RECTIFICATION PROCEDURE

In this section ten reference systems used in the rectification procedure are illustrated.

2.1.1 Image Coordinate System (S_{IM})

Image coordinate system is denoted by S_{IM}.

This coordinate system is used for positioning the pixels of the image. Since an image is 2 dimensional, image coordinate system is also 2 dimensional. The origin of this system is at the upper left corner of the image, x and y axis are orthogonal to each other. Direction of these axes are shown in Figure 2.1. Unit of image coordinate system is pixel; in other words the smallest picture element. S_{IM} is a Left Hand coordinate system.

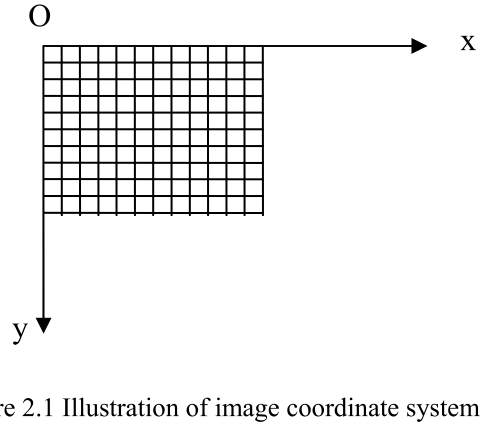

Figure 2.1 Illustration of image coordinate system

2.1.2 Photo Coordinate System (S_P)

Photo coordinate system is denoted by S_P.

Similar to S_{IM}, S_P is a 2D coordinate system. Origin of photo coordinate system is the principal point of the CCD frame. For the images scanned by pushbroom sensors x coordinate of the origin is the principal point of pushbroom scanner and y coordinate of origin is the half of the image height. Direction of x axis is same with S_{IM} but y axis is reversed (Figure 2.2). For this reason S_P is a Right Hand coordinate system. Unit of S_P is mm, therefore a scale factor c is required to perform the transformation from S_{IM} to S_P. Parameters required to transform S_{IM} to S_P are: principal coordinates (Δx, Δy), and size of the sensing element (c) of the sensor.

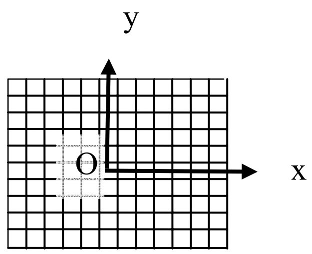

Figure 2.2 Illustration of photo coordinate system

2.1.3 Camera Coordinate System (S_C)

Camera coordinate system is denoted by S_C.

S_C is a 3D coordinate system that has the origin at satellite camera focus. In S_C direction of x and y axes are same with S_P. z axis's direction is defined to complete a 3D right hand reference system. Orientation of axis of S_C is shown in Figure 2.3. Similar to S_P unit of the S_C is mm. Transformation from S_P to S_C requires focal length, f, of the camera.

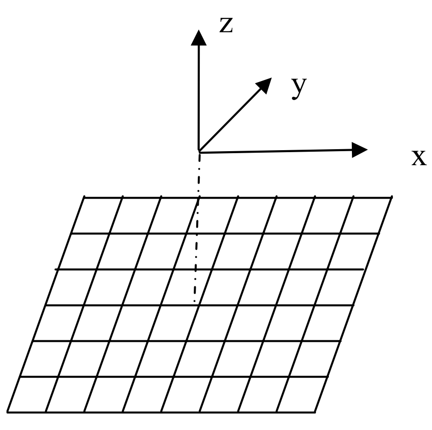

Figure 2.3 Illustration of camera coordinate system

2.1.4 Body Fixed Reference System (S_B)

Body fixed reference system denoted by S_B.

Origin of S_B is mass center of the satellite. Axis of body fixed reference system coincide with the principal axis of the inertia tensor of the satellite. If a satellite rotates around the earth as earth oriented, axis of S_B coincide almost with orbital coordinate system and the angles between the two corresponding coordinate axes are considered as the attitude angles of the satellite (Figure 2.4). Transformation from S_C to S_B is performed by a rotation of 180^o around the x axis and -90^o around z axis.

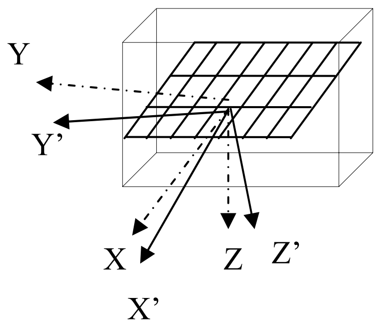

Figure 2.4 Orientation of body fixed reference system and orbital reference system

2.1.5 Orbital Reference System (S_O)

Orbital reference system is denoted by S_O.

S_O is a reference system with its origin defined at the satellite's center of mass. Z-axis is pointing in the same direction as the satellite's nadir direction, given in Earth Centered Inertial reference frame (Figure 2.5). Y-axis is defined in the opposite direction of the angular momentum vector of the satellite orbit. X-axis completes a 3D right hand reference system. In this sense if eccentricity of the orbit is too small, direction of the X-axis can be considered as the same direction with the velocity vector of the satellite. Transformation from S_B to S_O is performed by means of a rotation matrix constructed by the attitude angles of the satellite [24].

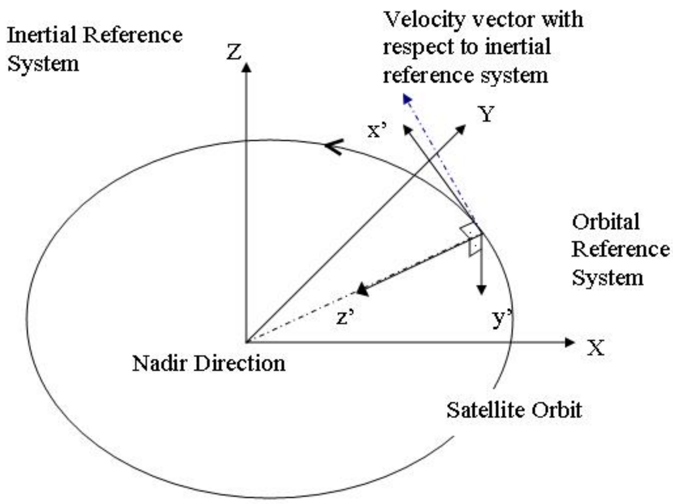

Figure 2.5 Orientation of orbital reference system with respect to inertial reference frame

2.1.6 Earth Fixed Reference Frame (S_E)

Earth centered earth fixed reference frame is denoted by S_E.

The origin of this reference system is the mass center of the earth. Orientation of this system changes with time and with respect to the solid earth's body as well as to the celestial reference system. Z-axis is directed towards a conventional mean terrestrial (north) pole (Figure 2.6). XZ plane is generated by the conventional mean meridian plane of Greenwich, which is spanned by the axis of rotation and the Greenwich zero meridian. Y axis is directed so as to obtain a right handed system [25, p 31].

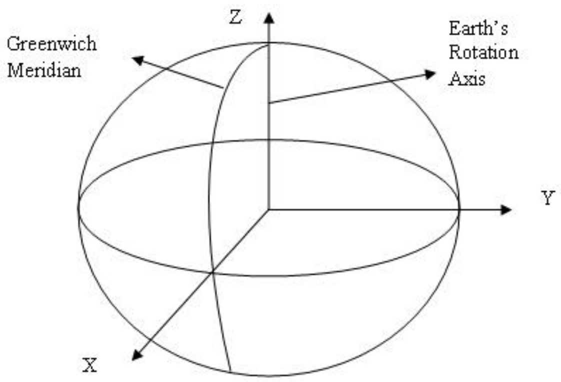

Figure 2.6 Illustration of earth centered earth fixed reference frame

2.1.7 Quasi Inertial Reference Frame (S_I)

Quasi-Inertial reference system is denoted by S_I.

Origin of the Quasi-inertial reference system is the mass center of the Earth. Rotation axis of the earth forms the Z axis, direction from mass center of the earth to the true vernal equinox defines the X axis and the Y axis completes a 3D right hand coordinate system (Figure 2.7). The unit of S_I is meters [25, p 25].

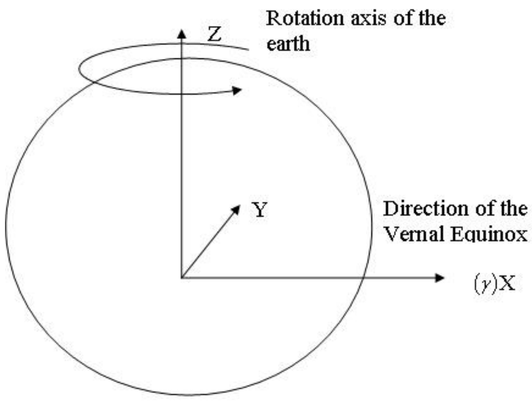

Figure 2.7 Illustration of the inertial reference frame

2.1.8 Geodetic Reference System (Global Ellipsoidal Reference System) (S_G)

Geodetic reference system is denoted by S_G.

In Figure 2.8 geocentric ellipsoidal coordinates are shown. WGS84 ellipsoid is used as a datum for the reference frame with coordinates expressed in geodetic latitude, longitude and height above the reference Earth ellipsoid. Geodetic latitude and longitude are defined as the angle between the ellipsoid normal and its projection onto the equator, and the angle between the local meridian and the Greenwich meridian respectively. The frame parameters are;

- Semimajor axis *a;* 6378137 meters
- Semiminor axis *b;* 6356752,314 meters
- Flattening *f* ; 1/298,257223560

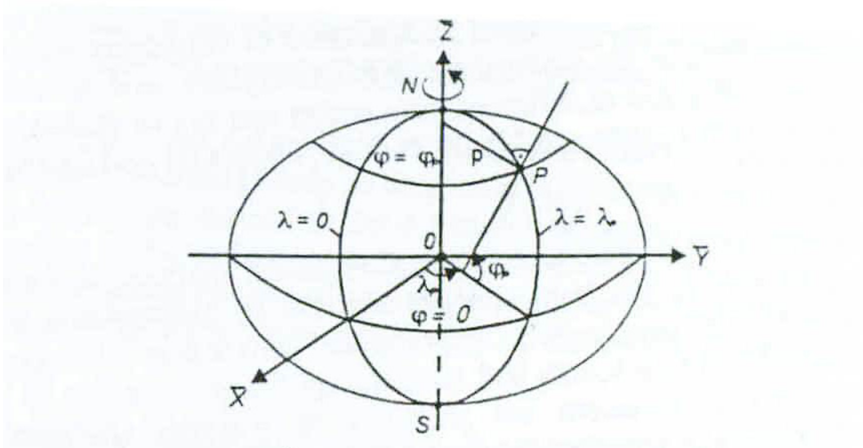

Figure 2.8 Illustration of geodetic coordinate system [25, p 93].

2.1.9 Local Ellipsoidal Reference Frame (S_L)

Local Ellipsoidal Coordinate system is denoted by S_L.

S_L is defined by the zenith, east and north directions. Zenith direction is the direction of the Ellipsoidal normal and defines the direction of the z axis, x axis directs through the North Pole and the y axis directs to the East which makes the coordinate system a Left Hand System (Figure 2.9). Origin of the S_L is taken as the observer's position [25, p 43].

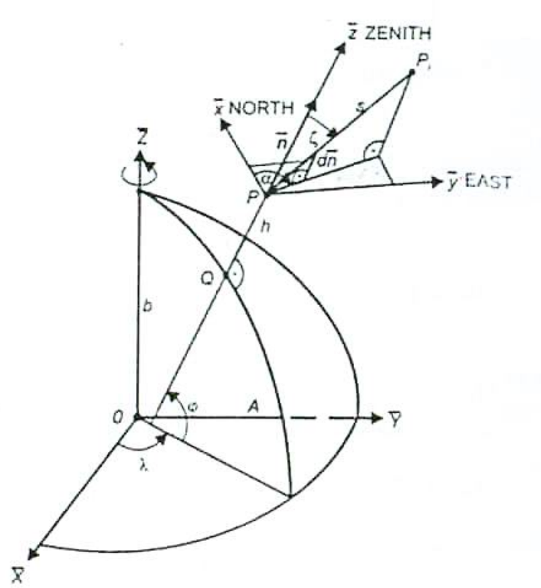

Figure 2.9 Illustration of local ellipsoidal reference frame [25, p 101]

2.1.10 Map Projection Coordinate Frame (S_M)

Map projection coordinate system is denoted by S_M.

Universal Transverse Mercator (UTM) map projection coordinate system is used in order to provide a mapping from latitude and longitude to a plane coordinate system which is an approximation to a Cartesian coordinate system for a portion of the Earth’s surface [2, p.571].

These reference and coordinate systems will be used in the orthorectification and error analysis of the new differential image rectification method.

2.2 TIME SYSTEMS USED IN RECTIFICATION PROCEDURE

2.2.1 UTC Time

Coordinated Universal Time (UTC) is a high-precision atomic time standard which approximately tracks Universal Time (UT). It is the basis for legal civil time all over the Earth: time zones around the world are expressed as positive and negative offsets from UTC. In this role it is also referred to as Zulu time (Z), or using the term "Greenwich Mean Time" (GMT).

As a time scale, UTC divides time up into days, and days into hours, minutes, and seconds. Days are conventionally identified using the Gregorian calendar, but Julian Day Numbers can also be used. Each day contains 24 hours and each hour contains 60 minutes, but the number of seconds in a minute is slightly variable.

Most UTC days contain exactly 86400 seconds, with exactly 60 seconds in each minute. Occasionally the last minute of a day has 59 or 61 seconds, or prior to 1972 other lengths. These irregular days have 86399 seconds, 86401 seconds, or some other number of seconds. The irregular day lengths mean that Julian Dates don't work properly with UTC. The intercalary seconds are known as "leap seconds" [26].

2.2.2 Universal Time

UT0 is Universal Time determined at an observatory by observing the diurnal motion of stars or extragalactic radio sources, and also from ranging observations of the Moon and artificial Earth satellites. It is uncorrected for the displacement of Earth's geographic pole from its rotational pole. This displacement, called polar motion, causes the geographic position of any place on Earth to vary by several meters, and different observatories will find a different value for UT0 at the same moment. It is thus not, strictly speaking, Universal [27].

UT1 is computed by correcting UT0 for the effect of polar motion on the longitude of the observing site. UT1 is the same everywhere on Earth, and defines the true rotation angle of the Earth with respect to a fixed frame of reference. Since the rotational speed of the earth is not uniform, UT1 has an uncertainty of plus or minus 3 milliseconds per day.

2.2.3 Unix Time

Unix time, or POSIX time, is a system for describing points in time. It is widely used not only on Unix-like operating systems but in many other computing systems, including the Java programming language. It is an encoding of UTC, and is sufficiently similar to a linear representation of the passage of time that it is frequently mistaken for one. The Unix epoch is the time 00:00:00 UTC on January 1, 1970 [28].

CHAPTER 3

STUDY AREA AND IMAGES

Error Analysis of the new orthorectification method is performed around Ankara region in Turkey. Bilsat and ASTER images are used in order to test the accuracy of the new method coverage of these images are shown by blue rectangle in Figure 3.1. Additionally sensitivity and uncertainty analysis are based on the geometry of Ankara images.

Figure 3.1 Snapshot of Ankara and Anatolia region.

In the Figure 3.1 Ankara and the neighboring cities are shown. In the error Analysis one BilSAT and one ASTER images are used each covering approximately 3600 km^2. The region is mountainous area having up to 2000 meter high top elevations. Elmadağ and Altındağ are the examples of the mountains near Ankara. Steep slopes exist in the region and elevation differences up to 1000 meters can be measured in close regions. However, the region has smooth surfaces near Gölbaşı and

Haymana Plato. This property of the study region will allow us to compare the accuracy of the method both for mountainous and flat areas.

3.1 CCD Frame Camera Image

Error analysis of the new orthorectification method for CCD arrays is performed with one BilSAT image. BilSAT is launched with a cooperation between TÜBİTAK-Bilten and Surrey Satellite Technology Limited (SSTL) of Surrey University, UK. It is a technology transfer project aimed at acquiring small satellite technologies. BilSAT has the properties represented in Table 3.1 [29].

Table 3.1 Technical properties of BilSAT

Weight:	129 kg
Orbit:	686 km, circular, sun synchronous
Attitude Control:	3-axis stabilized
Orbit alignment by propulsion engine	
Life time:	(5+10) year
Cameras:	Multispectral Camera Properties:
	Ground Sampling Distance : 27,6 m
	Radiometric ranges: (μm)
	Band 1: 0.45 - 0.52 (Blue)
	Band 2: 0.52 - 0.60 (Green)
	Band 3: 0.63 - 0.69 (Red)
	Band 4: 0.76 - 0.90 (Near Infrared)

In order to examine the rectification accuracy, Ground Control Points (GCP) are collected from several sites seen on the image. Measured and computed coordinates of GCPs are compared during the error analysis. During the selection of GCPs some important facts are considered such as;

- GCPs should easily be detectable both in the image and in the ground.
- GCPs should be stationary and permanent.
- GCP should be well distributed in the image and cover all image.
- GCP positions should not be collinear on the image.

Bilsat image taken on August 3rd 2005 is used in the analysis. 28 GCPs were collected and distribution of GCPs is shown in the Figure 3.2.

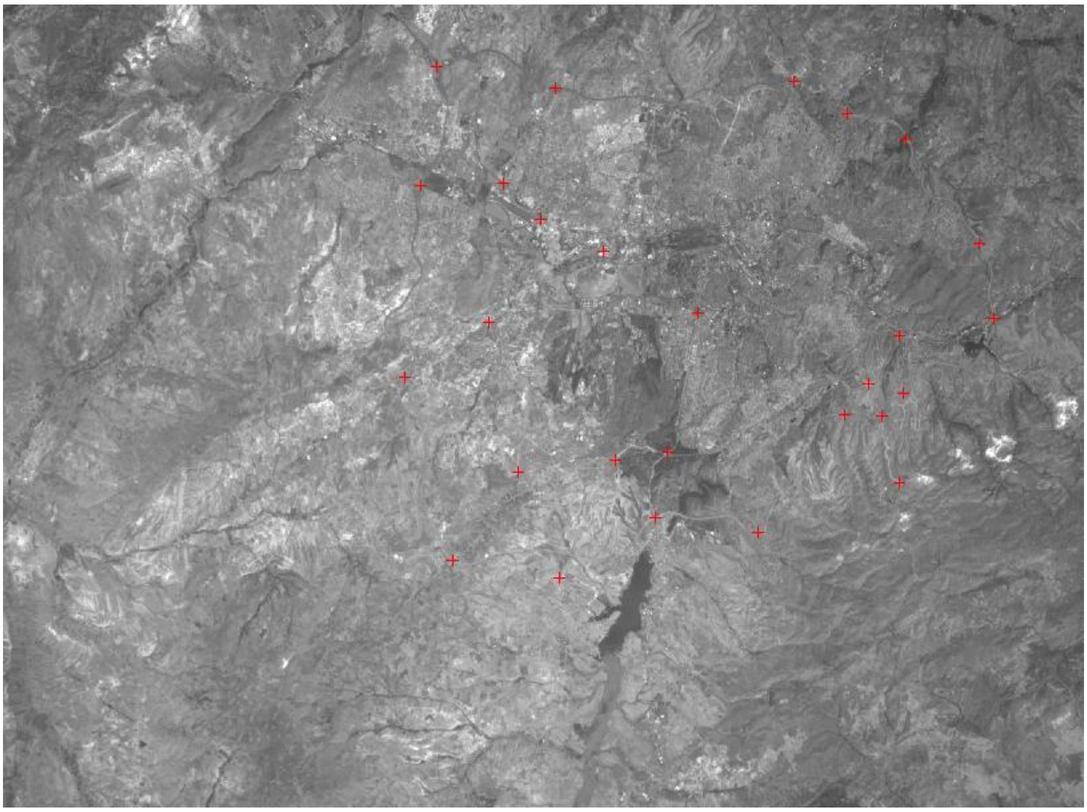

Figure 3.2 Distribution of GCPs for the image shot on August 3rd 2005.

Spatial resolution of BilSAT can be considered as low compared with new generation commercial remote sensing satellites. Most of the detectable objects in high resolution satellite images was undetectable in Bilsat images. For this reason collecting GCPs was relatively difficult. GCPs are collected mainly from highway bridges, road intersections and airports. Building corners, minor roads or monuments were impossible to detect from the image.

3.2 Pushbroom Scanner Image

An ASTER image is used for the sensitivity and uncertainty analysis and implementation of the new method adopted for pushbroom scanners. ASTER is a cooperative effort between NASA and Japan's Ministry of Economy Trade and Industry (METI), with the collaboration of scientific and industry organizations in both countries [30]. ASTER captures high spatial resolution data in 14 bands, from the visible to the thermal infrared wavelengths; and provides stereo viewing capability for digital elevation model creation. Technical properties of the Visible Near Infrared (VNIR) band of the ASTER is represented in Table 3.2 [30].

Table 3.2 Technical properties of VNIR band of ASTER

Characteristic	VNIR
Spectral Range	Band 1: 0.52 - 0.60 µm
	Nadir looking
	Band 2: 0.63 - 0.69 µm
	Nadir looking
	Band 3: 0.76 - 0.86 µm
	Nadir looking
	Band 3: 0.76 - 0.86 µm
	Backward looking
Ground Resolution	15 m
Swath Width (km)	60
Quantization (bits)	8

The image is acquired in August 27th 2002. ASTER has approximately 15 meter ground resolution in visible bands. In ASTER images; airports, highways and road intersections can easily be detected. If there is a sharp contrast, even the minor roads can also be detected (Figure 3.3).

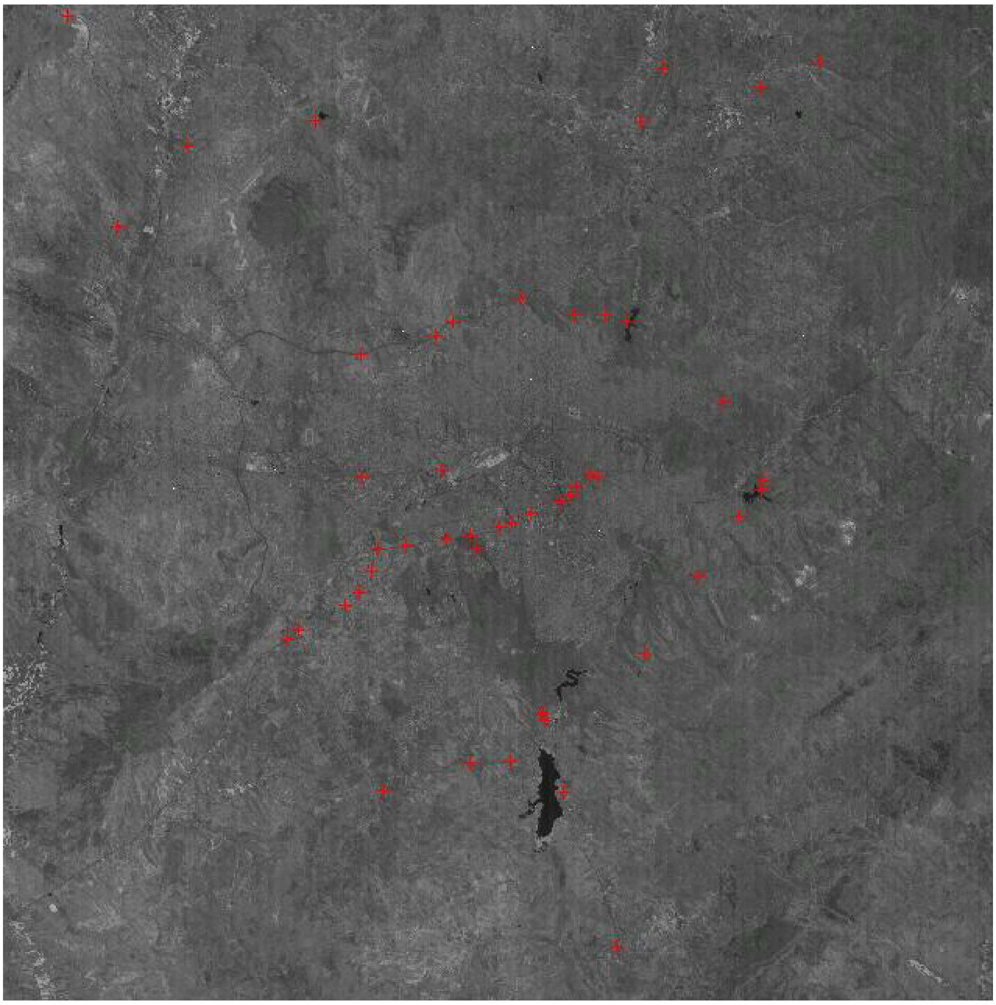

Figure 3.3 Distribution of GCPs of the image shot by ASTER

3.3 GCP Coordinate Measurements

Distribution of GCPs with their geodetic coordinates with respect to WGS 84 datum is shown in Figure 3.4. GCPs are collected by means of a hand held Magellan GPS receiver by absolute positioning. Accuracy of the GCP coordinates is expected to be within 15 meters. To check if there is a blunder in the measurements, the measured ground coordinates are compared by a topographic map and it is seen that there is not any considerable error. The snapshot is obtained from Trackmaker software.

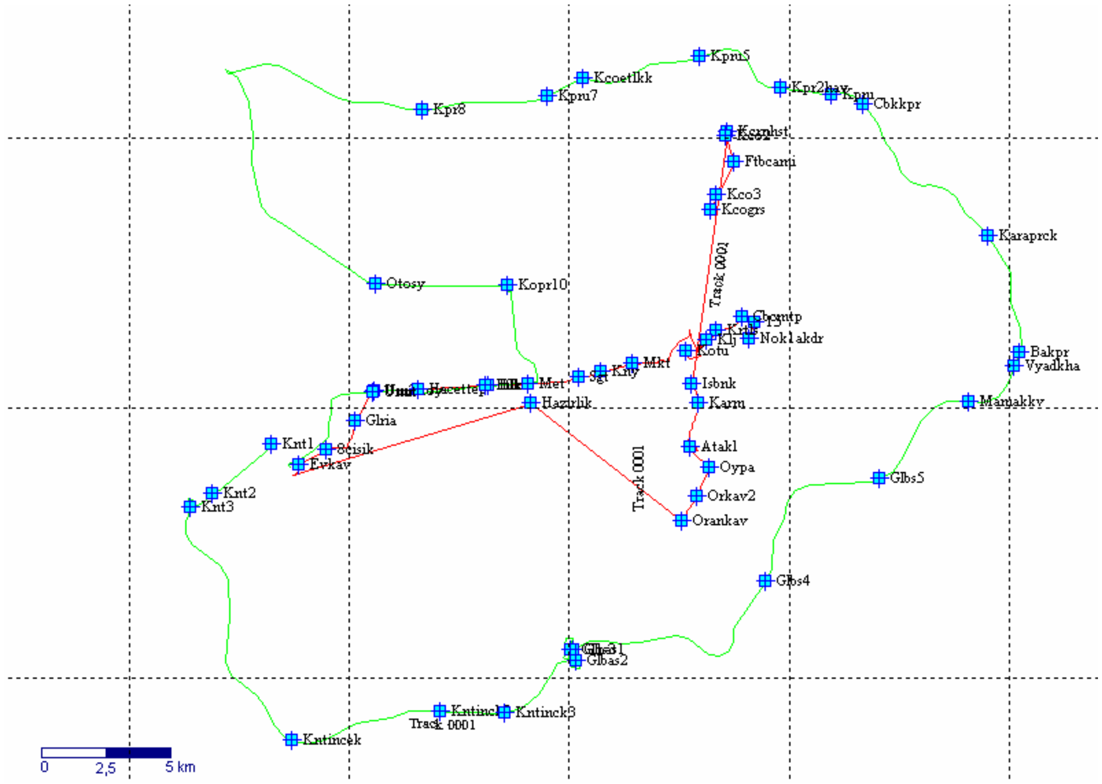

Figure 3.4 Distribution of ground control points shown on Trackmaker software

3.4 DEM Data

In this thesis for the elevation data SRTM DEM will be used. The data is produced by The Shuttle Radar Topography Mission (SRTM). The mission obtained elevation data on a near-global scale to generate the most complete high-resolution digital topographic database of Earth. SRTM consisted of a specially modified radar system that flew onboard the Space Shuttle Endeavour during an 11-day mission in February of 2000 [31].

SRTM DEM data has an accuracy of approximately 5 meters for the region of Ankara. Elevation accuracy of 5 meters is adequate for the orthorectification of BilSAT and ASTER images, since both satellites have coarse spatial resolution and the images are not oblique.

SRTM DEM stores elevation data in 3 arc second intervals. Each DEM file contains 1201x1201 elevation value thus covers a region of 1 degree of latitude and longitude.

CHAPTER 4

DRM ALGORITHM FOR CCD FRAME CAMERA AND PUSHBROOM SCANNERS

4.1 DRM Algorithm for CCD Frame Cameras

DRM is based on colinearity equations to provide a relationship between pixel positions and corresponding positions on ground. Colinearity is the condition which requires that all three points; the exposure station of photograph (focus), an object point, and its photo image lie on a straight line (Figure 4.1). The equations expressing this condition are called colinearity equations.

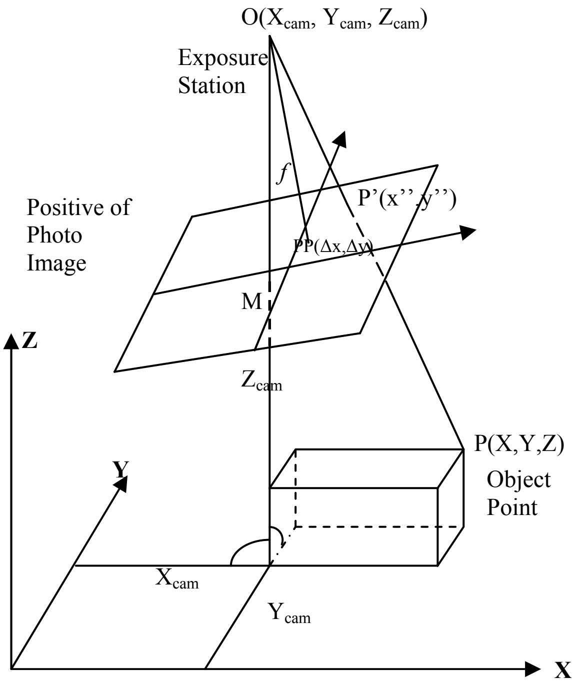

Figure 4.1 Illustration of Colinearity Conditions [31]

Abbreviations used in Figure 4.1 are explained as;

M is the photographic nadir point,

PP is the principal point,

P' is the image position of the object point P and x", y" are the image coordinates of point P.

Colinearity equations are written with respect to interior and exterior camera parameters Interior orientation parameters of the camera can be listed as;

- f focal length (mm)
- Δx, Δy principal point coordinates (mm)
- k_1, k_2 radial lens distortion (1/mm^2 and 1/mm^4 respectively)
- p_1, p_2 asymmetric radial lens distortion (1/mm)

Exterior orientation parameters of the camera can be listed as;

- X_{cam}, Y_{cam}, Z_{cam} Object coordinates of camera position with respect to a given datum (meter)
- ω, φ, κ Attitude angles of the S_O with respect to S_B

4.1.1 Transformation from S_{IM} to S_P

Implementation of the DRM for CCD frame cameras consists of 6 stages and the data required for each step are shown in Figure 4.2, where the transformation steps and required parameters and data are explained. To begin the rectification procedure pixel coordinates are obtained from image in S_{IM}.

The first step of the algorithm consists of transformation of image coordinates from S_{IM} to S_C. Image coordinates are converted to S_P by using Equation 4.1. In this transformation, origin of coordinate system is translated from left corner to the middle of the CCD array not only by moving half of the size of the CCD array but also by applying the correction of the misalignment of the principal point to the CCD center by an amount of Δx and Δy. Furthermore, direction of y axis is reversed and coordinate system is shifted from Left Hand system to Right Hand system. Additionally, unit of this coordinate system is converted from pixel to mm by using parameter 'c' the size of the sensing element in CCD array. Transformation from S_{IM} to S_P can be formulated as in Equation 4.1.

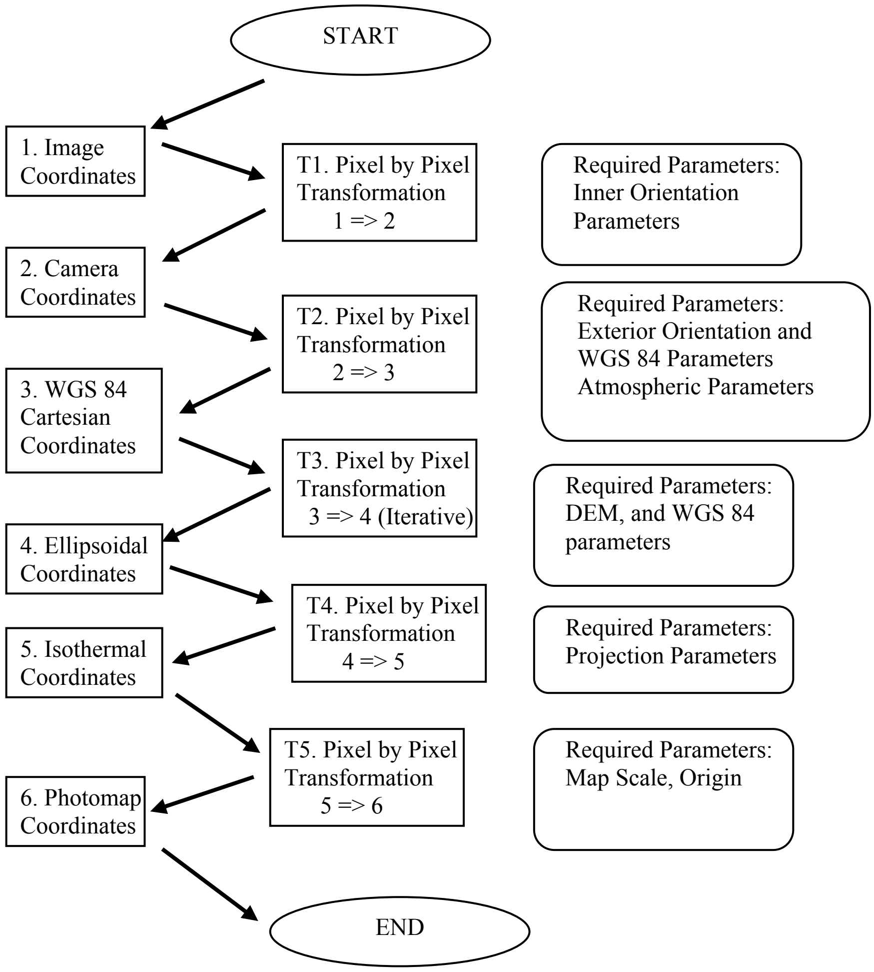

Figure 4.2 Illustration of the algorithm of DRM

$$x' = \left(x'' - \frac{width}{2} \right) * c - \Delta x \qquad (4.1)$$

$$y' = \left(-y'' + \frac{heigth}{2} \right) * c - \Delta y$$

where;

x'' and y'' are the cartesian coordinates of the image point in pixel read from the digital image (pixel)

width and *height* are the image width and image height (pixel)

Δx, Δy are the x and y coordinates of the principal point (mm)

c is the image scale (mm/pixel).

x' and y' are the position in S_C (mm)

The transformed pixel coordinates from S_{IM} to S_P are not the ideal pixel positions. There are small displacements in their ideal positions because of the distorting effect of the camera lens. These displacements can be corrected by using mathematical models.

4.1.2 Lens Distortion Corrections

Lens distortions are corrected by a polynomial model. The radial distortion value is the radial displacement from the ideal location to the actual image of the collimator cross, with positive values indicating outward displacements. Radial and asymmetric lens distortions are corrected by the following formulae [33];

$$x = x' * (1 - k_1 * r^2 - k \ \ * r^4 - 2 * p_1 * x' - 2 * p_2 * y' - \frac{p_1 * r^2}{x'}) \tag{4.2}$$

$$y = y' * (1 - k_1 * r^2 - k_2 * r^4 - 2 * p_2 * y - 2 * p_1 * x' - \frac{p_2 * r^2}{y'})$$

$$z = -f$$

$$r = \sqrt{x'^2 + y'^2} \tag{4.3}$$

where;

r is the distance of the corresponding pixel from the principal point on the CCD array (mm)

x' is the x coordinate of the image point in S_P

y' is the y coordinate of the image point in S_P

x, y and z values are the for lens distortion free image coordinates in S_C

k_1 and k_2 are radial lens distortion parameters

p_1 and p_2 are decentering lens distortion parameters

f is the focal length of the camera

4.1.3 Transformation from S_P to S_C

By using focal length of the camera and pixel positions in S_P, transformation to S_C can be performed. The origin of coordinate system is moved from principal point to focus, for this reason all image points' z coordinates are $-f$ (Equation 4.3).

Direction vector of each pixel with respect to the camera coordinate system is calculated by using the formula,

$$\overset{C}{D} = [x, y, z]' / \sqrt{x^2 + y^2 + z^2} \tag{4.4}$$

where;

x and y are the corrected pixel coordinates in S_P and z is the negative value of focal length

$\overset{C}{D}$ is the direction vector with respect to S_C

4.1.4 Computation of Intersection Point

Applying Equation 4.4 completes the first step of the rectification algorithm. Second step of the algorithm involves the computation of cartesian coordinates of intersection point with the direction vector computed in step 1 with the WGS84 ellipsoid. To compute the cartesian coordinates of the intersection point, first the direction vector with respect to S_C should be transformed to S_E and the intersection equation involving the direction vector in S_E and camera position should be generated. Whole transformation sequence can be illustrated as;

$$S_C \to S_E = S_C \to S_B \to S_O \to S_I \to S_E$$

4.1.4.1 Transformation from S_C to S_B

To transform from S_C to S_B 180^o rotation respect to X axis and - 90^o rotation with respect to Z axis is required. The orientations of two coordinate systems are shown in Figure 4.3a and 4.3b.

$$\overset{B}{D} = \boldsymbol{R_3}\left(-90^o\right)\boldsymbol{R_1}\left(180^o\right)\overset{C}{D} \tag{4.5}$$

where;

$\overset{B}{D}$ is the direction vector of the corresponding image point with respect to S_B

$$R_1\left(180^o\right) = \begin{bmatrix} 1 & 0 & 0 \\ 0 & -1 & 0 \\ 0 & 0 & -1 \end{bmatrix}$$

$$R_3\left(-90^o\right) = \begin{bmatrix} 0 & -1 & 0 \\ 1 & 0 & 0 \\ 0 & 0 & 1 \end{bmatrix}$$

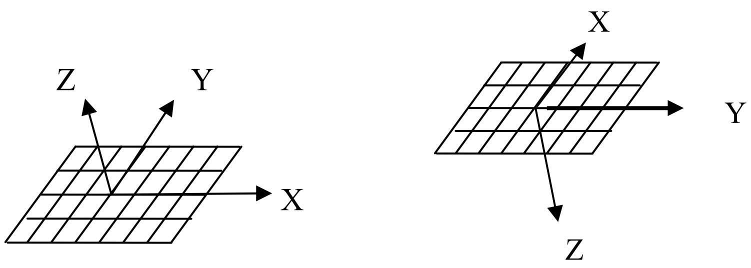

(a) (b)

Figure 4.3 (a) Orientation of S_C (b) Orientation of S_B

4.1.4.2 Transformation from S_B to S_O

After performing the transformation from S_C to S_B the next transformation is from S_B to S_O. To perform this transformation, attitude of the satellite is required.

Attitude angles (Roll, Pitch and Yaw (ω, φ, κ)) between S_B and S_O are obtained from telemetry file. By $\mathbf{R}_{213}(-\omega, -\varphi, -\kappa)$ rotation matrix constructed with minus signs of the attitude angles the direction vector will be transformed from S_C to S_O. Transformation from S_C to S_O can be shown as;

$$S_O = R_{213}(-\omega, -\phi, -\kappa)S_B \tag{4.6}$$

$$\overset{O}{D} = \begin{bmatrix} \cos\kappa\cos\phi - \sin\kappa\sin\omega\sin\phi & -\sin\kappa\cos\omega & \cos\kappa\sin\phi + \sin\kappa\sin\omega\cos\phi \\ \sin\kappa\cos\phi + \cos\kappa\sin\omega\sin\phi & \cos\kappa\cos\omega & \sin\kappa\sin\phi - \cos\kappa\sin\omega\cos\phi \\ -\cos\omega\sin\phi & \sin\omega & \cos\omega\cos\phi \end{bmatrix} \overset{B}{D} \tag{4.7}$$

where; $\overset{O}{D}$ is the direction vector of the corresponding image pixel with respect to S_O

In this section transformation equations are explained if the attitude between S_B and S_O is given in rotation angles. However, the transformation parameter can be obtained in terms of quaternion. In this case the transformation from S_B to S_O will be as fallowing;

Quaternions are given as;

$$q = [q_1 \quad q_2 \quad q_3 \quad q_4]' \tag{4.8}$$

Rotation matrix in Equation 4.6 required for the transformation can be written in terms of quaternions as;

$$C = \begin{bmatrix} q_1^2 - q_2^2 - q_3^2 + q_4^2 & 2(q_1 q_2 + q_3 q_4) & 2(q_1 q_3 - q_2 q_4) \\ 2(q_1 q_2 - q_3 q_4) & -q_1^2 + q_2^2 - q_3^2 + q_4^2 & 2(q_2 q_3 + q_1 q_4) \\ 2(q_1 q_3 + q_2 q_4) & 2(q_2 q_3 - q_1 q_4) & -q_1^2 - q_2^2 + q_3^2 + q_4^2 \end{bmatrix} \tag{4.9}$$

The rotation matrix defined in Equation 4.9 can be used for the transformation from S_B to S_O. However, if Euler angles are required for comparison by the fallowing procedure Euler angles can be computed. By equating two matrix represented in Equations 4.7 and 4.9, the attitude angles can be computed by the following equations;

The quaternions can be expressed in terms of Euler angles by the following equations[24];

$$q_1 = \cos\left(\frac{\kappa}{2}\right)\cos\left(\frac{\phi}{2}\right)\sin\left(\frac{\omega}{2}\right) - \sin\left(\frac{\kappa}{2}\right)\sin\left(\frac{\phi}{2}\right)\cos\left(\frac{\omega}{2}\right)$$

$$q_2 = \cos\left(\frac{\kappa}{2}\right)\sin\left(\frac{\phi}{2}\right)\cos\left(\frac{\omega}{2}\right) + \sin\left(\frac{\kappa}{2}\right)\cos\left(\frac{\phi}{2}\right)\sin\left(\frac{\omega}{2}\right)$$

$$q_3 = \sin\left(\frac{\kappa}{2}\right)\cos\left(\frac{\phi}{2}\right)\cos\left(\frac{\omega}{2}\right) - \cos\left(\frac{\kappa}{2}\right)\sin\left(\frac{\phi}{2}\right)\sin\left(\frac{\omega}{2}\right)$$

$$q_4 = \cos\left(\frac{\kappa}{2}\right)\cos\left(\frac{\phi}{2}\right)\cos\left(\frac{\omega}{2}\right) + \sin\left(\frac{\kappa}{2}\right)\sin\left(\frac{\phi}{2}\right)\sin\left(\frac{\omega}{2}\right) \tag{4.10}$$

$$\tan(\kappa) = \frac{2(q_1 q_2 + q_3 q_4)}{q_1^2 - q_2^2 - q_3^2 + q_4^2} \tag{4.11}$$

$$\sin(\phi) = -2(q_1 q_3 - q_2 q_4) \tag{4.12}$$

$$\tan(\omega) = \frac{2(q_1 q_4 + q_2 q_3)}{-q_1^2 - q_2^2 + q_3^2 + q_4^2} \tag{4.13}$$

The obtained Euler angles are the same with the rotation angles defined in Equation 4.6. For this reason, the rotation angles computed by the Equations 4.11 to 4.13 can be substituted into the matrix defined in Equation 4.7 and the two attitude angle set can also be compared.

4.1.4.3 Transformation from S_O to S_E

To proceed to the next step, direction vector should be transformed from S_O to S_E, rotation matrix of this transformation is calculated by using the definition of S_O.

The orbital reference frame is defined by the position and velocity of the satellite measured in the quasi-inertial frame. However, position and velocity are obtained in S_E. When performing the transformation from S_O to S_E, position and velocity should be transformed from S_E to S_I. Then the rotation matrix from S_O to S_I can be computed. After transforming the direction vector with respect to

S_I, it can be transformed with respect to S_E. By using position and velocity vectors in S_I direction cosines are computed which rotates S_O to S_I (Figure 4.4). Transformation from S_I to S_E is performed by applying precession, nutation and polar motion corrections and GAST rotation.

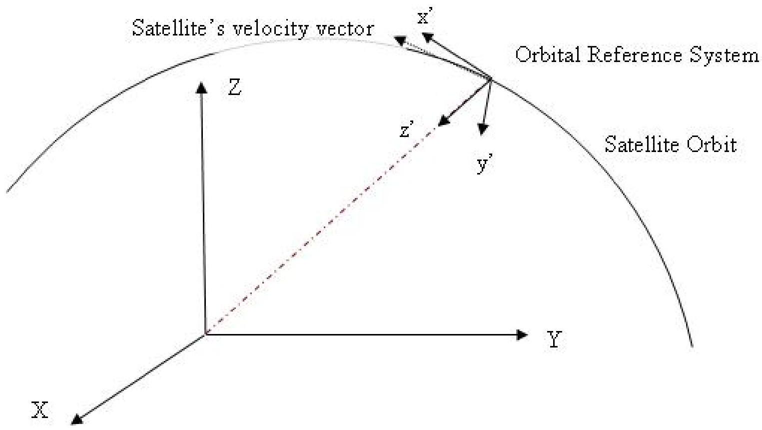

Figure 4.4 Orientation of S_O with respect to S_I

Velocity of satellite is computed from two successive position measurement of satellite by the GPS receiver installed on the satellite. GPS receiver gives geodetic coordinates of the satellite with respect to WGS84 reference ellipsoid. For a small time interval, the angular velocity of the satellite and change in altitude can be assumed to be constant. Hence velocity of the satellite can be computed without a considerable error. To derive the rate of change of cartesian coordinates with respect to time, rate of change of geodetic coordinates with respect to time and rate of change of cartesian coordinates with respect to geodetic coordinates are used by applying chain rule for three orthogonal axes. The whole equation is shown below.

$$
\begin{aligned}
v_x &= \frac{\partial X}{\partial t} = \frac{\partial X}{\partial \phi}\frac{\partial \phi}{\partial t} + \frac{\partial X}{\partial \lambda}\frac{\partial \lambda}{\partial t} + \frac{\partial X}{\partial h}\frac{\partial h}{\partial t} \\
v_y &= \frac{\partial Y}{\partial t} = \frac{\partial Y}{\partial \phi}\frac{\partial \phi}{\partial t} + \frac{\partial Y}{\partial \lambda}\frac{\partial \lambda}{\partial t} + \frac{\partial Y}{\partial h}\frac{\partial h}{\partial t} \\
v_z &= \frac{\partial Z}{\partial t} = \frac{\partial Z}{\partial \phi}\frac{\partial \phi}{\partial t} + \frac{\partial Z}{\partial \lambda}\frac{\partial \lambda}{\partial t} + \frac{\partial Z}{\partial h}\frac{\partial h}{\partial t}
\end{aligned}
\tag{4.14}
$$

where;

$$\frac{\partial X}{\partial \phi} = -(N' + h)\sin\phi\cos\lambda$$

$$\frac{\partial X}{\partial \lambda} = -(N' + h)\cos\phi\sin\lambda$$

$$\frac{\partial X}{\partial h} = \cos\phi\cos\lambda$$

$$\frac{\partial Y}{\partial \phi} = -(N' + h)\sin\phi\sin\lambda$$

$$\frac{\partial Y}{\partial \lambda} = (N' + h)\cos\phi\cos\lambda$$

$$\frac{\partial Y}{\partial h} = \cos\phi\sin\lambda$$

$$\frac{\partial Z}{\partial \phi} = \left(N' - e^2 N' + h\right)\cos\phi$$

$$\frac{\partial Z}{\partial \lambda} = 0$$

$$\frac{\partial Z}{\partial h} = \sin\phi$$

$$\frac{\partial \phi}{\partial t} = \frac{\Delta\phi}{\Delta t} = \frac{\phi_2 - \phi_1}{t_2 - t_1}$$

$$\frac{\partial \lambda}{\partial t} = \frac{\Delta\lambda}{\Delta t} = \frac{\lambda_2 - \lambda_1}{t_2 - t_1}$$

$$\frac{\partial h}{\partial t} = \frac{\Delta h}{\Delta t} = \frac{h_2 - h_1}{t_2 - t_1}$$

t_1 and t_2 are the epoch that the coordinates are measured

The partial derivative equations are derived from the transformation formulae from geodetic coordinates to Cartesian coordinates;

$$\begin{aligned} X &= (N + h)\cos\phi\cos\lambda \\ Y &= (N + h)\cos\phi\sin\lambda \\ Z &= \left(N - e^2 N + h\right)\sin\phi \end{aligned} \tag{4.15}$$

where [34];

X, Y and Z are the geocentric coordinates of the satellite with respect to WGS84 reference frame.

$$N = \frac{a}{\sqrt{1 - e^2\sin^2\phi}}$$

N is ellipsoidal normal [27, p 92]

$$e^2 = \frac{a^2 - b^2}{a^2}$$

In these equations ϕ, λ and h are geodetic coordinates of the satellite and *a* is the semimajor axis and *b* is the semiminor axis of the WGS84 ellipsoid.

Position and velocity vectors of the satellite are shown below

$$r = [\, r_x \quad r_y \quad r_z \,]$$

$$v = [\, v_x \quad v_y \quad v_z \,]$$

where;
r is the position vector
v is the velocity vector.

The next step is rotating these vectors from S_E to S_I. In order to perform this rotation precession, nutation and polar motion corrections should be applied and GAST rotation should be performed. These procedures are explained briefly as;

4.1.4.3.1 Correction Due to Precession

Precession rotation includes 3 Euler rotations, these are;

$R_3(Z_A)R_2(\theta)R_3(\zeta_A)$

$$\begin{aligned}
\zeta_A &= 2306.2181''*T + 0.30188''*T^2 + 0.01800'' * T^3 \\
Z_A &= 2306.2181''*T + 1.09468''*T^2 + 0.01836'' * T^3 \\
\theta_A &= 2004.3109''*T - 0.42665''*T^2 - 0.04176'' * T^3
\end{aligned} \tag{4.16}$$

[24] where;
T is the Julian century computed by the equation

$$T = \frac{d}{36525} \tag{4.17}$$

where;
d is the Julian Day computed by the formula [24]

$$\begin{aligned}
JD &= 367 * Y - \text{floor}\,(7 * (Y + \text{floor}\,((M + 9) / 12)) / 4) + \text{floor}\,(275 * M / 9) \\
&+ D + 1721014 + UT1 / 24 - 0.5
\end{aligned} \tag{4.18}$$

where;
Y is year
M is month
D is date and UT1 is the time in decimal hours in UT1.

4.1.4.3.2 Correction Due to Nutation

After precession correction, nutation correction is applied. The nutation correction includes 3 Euler rotations, these are $R_1(-\varepsilon_0 - \Delta\varepsilon)R_3(-\Delta\psi)R_1(\varepsilon_0)$. Rotation angles are computed by the following formulae [24]

$$\begin{aligned}
&\varepsilon_0 = 84381.448'' - 46.8150'' * T \\
&\Delta\Psi = -0.0048^0 * \sin(f_1) - 0.0004^0 * \sin(f_2) \\
&\Delta\varepsilon = 0.0026^0 * \cos(f_1) + 0.0002^0 * \cos(f_2) \\
&f_1 = 125^0 - 0.05295^0 * d \\
&f_2 = 200.9^0 + 1.97129^0 * d
\end{aligned} \tag{4.19}$$

4.1.4.3.3 Correction Due to Polar Motion

Polar motion is the motion of the rotation axis of the earth relative to the earth's crust as viewed from the earth-fixed reference system. Polar motion directly affects the coordinates of stations on the surface of the earth and the gravity vector. The polar motion effect can be eliminated by two rotations about x and y axes. The rotation angles can be computed from the formula in degrees [35];

$$\begin{aligned}
x &= 0.0417 - 0.0599\cos(A) - 0.0131\sin(A) + 0.0632\cos(C) - 0.1327\sin(C) \\
y &= 0.3475 - 0.0115\cos(A) + 0.0530\sin(A) - 0.1327\cos(C) - 0.0632\sin(C)
\end{aligned} \tag{4.20}$$

where;

$$A = 2\pi\frac{(MJD - 53418)}{365.25}$$

$$C = 2\pi\frac{(MJD - 53418)}{435}$$

MJD = JD - 2400000.5

MJD is the modified Julian Date

4.1.4.3.4 GAST (Greenwich Apparent Sidereal Time)

After the precession and nutation corrections $R_3(GAST)$ rotation is performed[24].

$$\begin{aligned}
GAST &= GMST + (\Delta\Psi * \cos(\varepsilon_0 + \Delta\varepsilon))/15 \\
GMST &= \frac{(UT1 * 3600 + 24110.54841 + 8640184.812866 * T + 0.093104 * T^2 - 6.2 * 10^{-6} * T^3)}{3600} + n * 24
\end{aligned} \tag{4.21}$$

In Equation 4.21 n is an arbitrary integer which satisfies $0 \le GMST < 24$.

where GMST is the Greenwich Mean Sidereal Time.

The rotation from earth fixed reference frame to inertial reference frame can be shown as;

$$ {}^{I}\mathbf{R}_{E} = R_3(\zeta_A)R_2(-\theta_A)R_3(Z_A)R_1(-\varepsilon_0)R_3(\Delta\Psi)R_1(\varepsilon_0+\Delta\varepsilon)R_3(-GAST)R_1(y_p)R_2(x_p) \tag{4.22} $$

$$ {}^{I}r = {}^{I}\mathbf{R}_{E}\,{}^{E}r \tag{4.23} $$

$$ {}^{I}\mathbf{v} = {}^{I}\mathbf{R}_{E}\,{}^{E}\mathbf{v} + {}^{E}\mathbf{r}\times\mathbf{w}_{E} \tag{4.24} $$

When transforming the velocity vector from S_E to S_I, the term ${}^{E}\mathbf{r}\times\mathbf{w}_{E}$ is added to the velocity vector (Equation 4.23). This is because S_E is not an inertial reference frame and velocity measured in this reference system will be different than the velocity measured in inertial reference frame. $\mathbf{w}_{E}$ is the angular velocity of the earth rotation measured in radians and ${}^{\boldsymbol{E}}\mathbf{r}$ is the position vector of the satellite measured in S_E [36].

4.1.4.3.5 Transformation from S_O to S_I

After transforming the position and velocity vectors to S_I, the rotation matrix can be constructed which transforms from S_O to S_I. However, it is easier to construct the rotation matrix from S_I to S_O. This rotation matrix is the attitude of the S_O with respect to S_I and it is represented as [24].

$$ {}^{O}R_{I} = \begin{bmatrix} X_X & X_Y & X_Z \\ Y_X & Y_Y & Y_Z \\ Z_X & Z_Y & Z_Z \end{bmatrix} \tag{4.25} $$

The matrix in Equation 4.25 is constructed in three steps. First the third row is constructed which is the direction of the Z axis of S_O in S_I. By the definition of S_O the Z axis is the opposite direction of the satellite position vector.

$$ Z_{OI} = -\frac{r}{|r|} = \begin{bmatrix} Z_x & Z_y & Z_z \end{bmatrix} \tag{4.26} $$

where;

Z_{OI} is the direction vector of the Z axis of the orbital reference frame with respect to S_I

r is the position vector of the satellite with respect to S_I

Y axis of the S_O with respect to S_I is defined as the perpendicular direction to the both X and Z axes satisfying right hand rule. Since X and Z axes span the orbital plane and velocity vector is always inside the orbital plane, by this definition the direction vector of Y axis in inertial reference system can be computed by the formula;

$$Y_{OI} = -\frac{r \times v}{|r \times v|} = \begin{bmatrix} Y_x & Y_y & Y_z \end{bmatrix} \tag{4.27}$$

where;

Y_{OI} is the direction vector of the Y axis of the S_O with respect to S_I

v is the velocity vector of the satellite with respect to S_I

Since S_O satisfies the right hand rule, the cross product of the Y and Z axes will give the direction of the X axis with respect to S_I. This is shown by;

$$X_{OI} = Y_{OI} \times Z_{OI} = [\, X_x \quad X_y \quad X_z \,] \tag{4.28}$$

Transpose of the rotation matrix shown in Equation 4.25 will be the transformation matrix from S_O to S_I.

$$\overset{I}{R_O} = \begin{bmatrix} X_X & Y_X & Z_X \\ X_Y & Y_Y & Z_Y \\ X_Z & Y_Z & Z_Z \end{bmatrix} \tag{4.29}$$

Direction vector with respect to S_I is transformed to S_E by applying precession and nutation corrections and GAST rotation which can be shown as

$$\overset{E}{r} = \overset{E}{\boldsymbol{R}_I} \overset{I}{r} \tag{4.30}$$

where;

$$\overset{E}{R_I} = R_2(-x_p)R_1(-y_p)R_3(GAST)R_1(-\varepsilon_0 - \Delta\varepsilon)R_3(-\Delta\Psi)R_1(\varepsilon_0)R_3(-Z_A)R_2(\theta_A)R_3(-\zeta_A)$$

Equation of the rotation from S_O to S_E can be written as

$$\overset{E}{D} = \overset{E}{R_I} \overset{I}{R_O} \overset{O}{D} \tag{4.31}$$

where

$\overset{E}{D}$ is the direction vector of the corresponding image point with respect to S_E

Direction vector of corresponding image point with respect to S_E is obtained. The direction vector goes through from satellite's camera focus and passes the corresponding sensing element of the CCD array and intersects the WGS84 ellipsoid. The intersection point of direction vector with the WGS84 ellipsoid surface should be computed in order to complete step 2. Satellite camera's position is known with respect to S_E at the instant of the image acquisiton, if the intersection point on the reference ellipsoid is assumed as P_0 with the coordinates [X_0, Y_0, Z_0] then the following equation can be written [1];

$$\begin{bmatrix} X_0 \\ Y_0 \\ Z_0 \end{bmatrix} = \begin{bmatrix} X_{cam} \\ Y_{cam} \\ Z_{cam} \end{bmatrix} + s * \begin{bmatrix} {}^{E_X}D \\ {}^{E_Y}D \\ {}^{E_Z}D \end{bmatrix} \tag{4.32}$$

where;

X_0, Y_0, Z_0 are the coordinates of the intersection point with respect to S_E

X_{cam}, Y_{cam}, Z_{cam} are the coordinates of the satellite camera with respect to S_E

s is the distance between satellite's camera focus and the intersection point on the reference ellipsoid

${}^{E_X}D$, ${}^{E_Y}D$, ${}^{E_Z}D$ are the components of direction vector from camera focus to image plane with respect to S_E

In Equation 4.32 there are 4 unknowns to be solved which are X_0, Y_0, Z_0 and s. However, Equation 4.32 contains only 3 equations which is inadequate for solving the equation set. One more equation is required for the solution for the intersection point. Since P_0 is on the reference ellipsoid's surface, ellipsoidal surface equation can be written for this point,

$$\frac{X_0 + Y_0}{a^2} + \frac{Z_0}{b^2} = 1 \tag{4.33}$$

where;

a is the semimajor axis

b is the semiminor axis of the WGS84 reference ellipsoid.

This leads to a system of four equations and four unknowns

If Equation 4.32 is substituted into Equation 4.33 the following intersection equation will be obtained,

$$\begin{aligned} &\left[\frac{{}^{E}D_x^2 + {}^{E}D_y^2}{a^2} + \frac{{}^{E}D_z^2}{b^2} \right] * s^2 + 2 * \left[\frac{{}^{E}D_x * X_{cam} + {}^{E}D_y * Y_{cam}}{a^2} + \frac{{}^{E}D_z * Z_{cam}}{b^2} \right] * s \\ &+ \frac{X_{cam}{}^2 + Y_{cam}{}^2}{a^2} + \frac{Z_{cam}{}^2}{b^2} - 1 = 0 \end{aligned} \tag{4.34}$$

Solving Equation 4.34 for s will lead to two solutions for s, which are

$$s_{1,2} = \frac{-\beta \pm \sqrt{\beta^2 - 4\alpha\gamma}}{2\alpha} \tag{4.35}$$

where;

$$\alpha = \frac{{}^{E}D_x^2 + {}^{E}D_y^2}{a^2} + \frac{{}^{E}D_z^2}{b^2}$$

$$\beta = \frac{\overset{E}{D_x} * X_{cam} + \overset{E}{D_y} * Y_{cam}}{a^2} + \frac{\overset{E}{D_z} * Z_{cam}}{b^2}$$

$$\gamma = \frac{{X_{cam}}^2 + {Y_{cam}}^2}{a^2} + \frac{{Z_{cam}}^2}{b^2} - 1$$

Among the two s values the shorter one is the proper solution because the bigger distance gives the other side of the ellipsoidal surface [1]. The smaller root is substituted into the intersection equation and intersection point's coordinates X_0, Y_0, Z_0 are computed. Solution for the smaller root is as following

$$s = \frac{-\beta - \sqrt{\beta^2 - 4\alpha\gamma}}{2\alpha} \tag{4.36}$$

If s is substituted into Equation 4.32 Cartesian coordinates of the intersection point can be computed. This may be thought as the end of Step 2 but this is not the case. Since the light ray passes through the atmosphere which is a dispersive medium, it is refracted and its path is not a straight line anymore. For this reason, computed cartesian coordinates of the ground point should be corrected. The correction is performed by the zenith angle of the direction vector. In order to compute zenith angle the direction vector should be transformed from S_E to S_L. The rotation matrix of this transformation is computed by means of the geodetic coordinates of the corresponding ground point. For this reason, cartesian coordinates should be transformed into geodetic coordinates. Cartesian coordinates are converted to ellipsoidal coordinates by an iterative method [25, p. 100].

$$\phi_i = \tan^{-1}\left(\frac{Z}{\sqrt{X^2 + Y^2}} \left(1 - e^2 \frac{N_i}{N_i + h_i} \right)^{-1} \right) \tag{4.37}$$

$$\lambda = \tan^{-1}\left(\frac{Y}{X} \right)$$

$$\mathrm{h_i} = \frac{\sqrt{\mathrm{X}^2 + Y^2}}{\cos \phi_i} - N_i$$

The algorithm shown in Equation 4.37 is an iterative method, in order to start iteration, it is a good approximation to take initial value of h as 0 and compute ϕ and correct the h. This iteration continues until the difference in h is less than a predefined threshold value.

4.1.5 Atmospheric Refraction Correction

According to the Snell's law light rays are bended while traveling through a medium of changing refraction index (Figure 4.5). Besides the refractivity of the medium, change in direction is proportional to the entrance angle also. The relation between the entrance and exit angles to the boundary is given as;

$$n_1 \sin\theta_1 = n_2 \sin\theta_2 \tag{4.38}$$

where

n_1 is the refractivity index of the first medium

n_2 is the refractivity of the second medium

θ_1 is the entrance angle of the light ray to the boundary

θ_2 is the exit angle of the light from the boundary

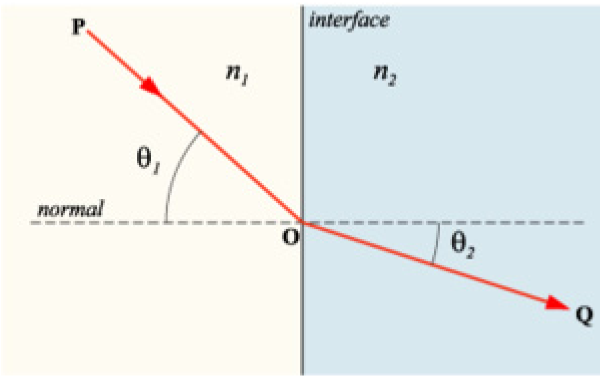

Figure 4.5 Refraction of a light ray in a dispersive medium [37].

Entrance angle of the light ray will be equal to its zenith angle. Computation of zenith and azimuth angles is explained in chapter 4.1.6.

$$N = (n-1)10^6 \tag{4.39}$$

[27, p.120] where

N is the refractivity and computed for visible light by the formula [25 p. 126]

$$\frac{\partial N}{\partial h} = -78\frac{p}{T^2}\left(0.034 + \frac{\partial T}{\partial h}\right) - \frac{11}{T}\frac{\partial e}{\partial h} \tag{4.40}$$

where

h is the elevation with respect to mean sea level

p is atmospheric pressure in hPa

T is the temperature of the atmosphere in Kelvin

e is humidity measured as the water vapor pressure in hPa

Parameters in the Equation 4.40 are not constant and they should be computed for each atmosphere layer. In order to compute the refractivity, the atmosphere is divided into layer of 1 km thickness. Within each layer refractivity is considered as constant

Atmosphere pressure, p is computed from the barometric formula [38]

$$p = p_0 e^{\frac{-Mgh}{RT}} \tag{4.41}$$

where;

h is the height in meter

P_0 is pressure at ground level in hPa

M is the mass of 1 mole of air 0.029 kg mol^{-1}

R is the gas constant (8.314 J K^{-1} mol^{-1})

g_0 is the acceleration due to gravity (9.81 m s^{-2})

By taking the initial values for temperature as 300 Kelvin, atmospheric pressure as 1023 hPa and water vapor pressure as 16 hPa the following values are obtained for the atmospheric conditions for the first 85 km.

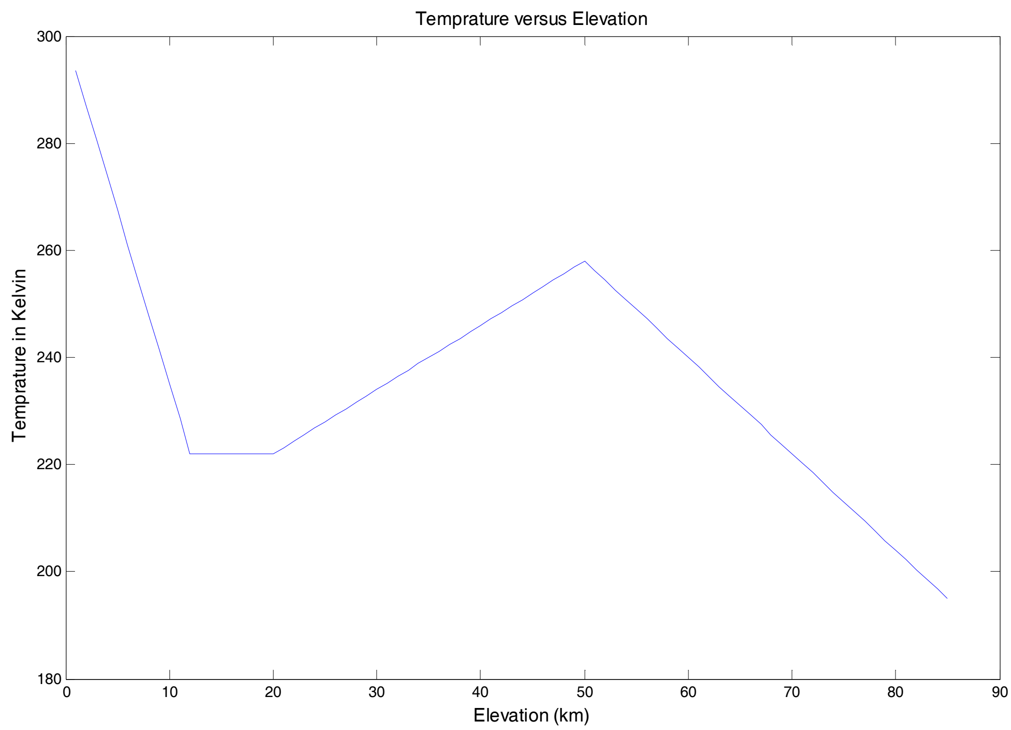

Figure 4.6 Variation of temperature in the atmosphere when ground temperature is 300 Kelvin.

By using the temperature at the corresponding elevation, air pressure is computed for each layer. The graph of the pressure variation with increasing elevation is shown in Figure 4.7,

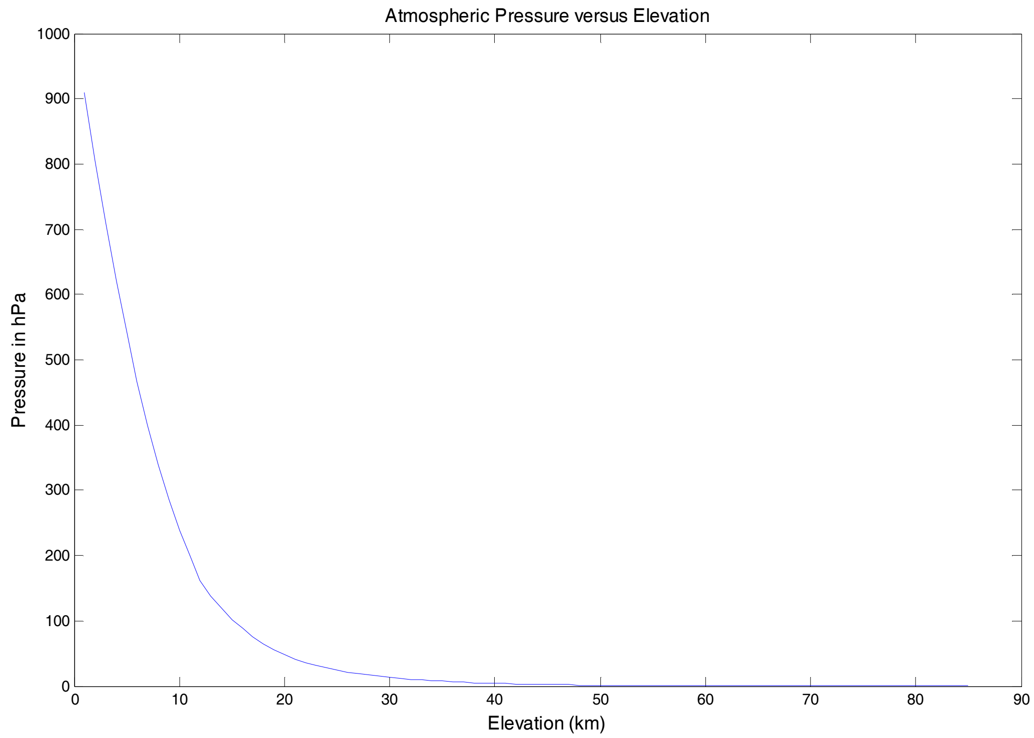

Figure 4.7 Variation of pressure in the atmosphere when ground pressure is 1023 Hpa.

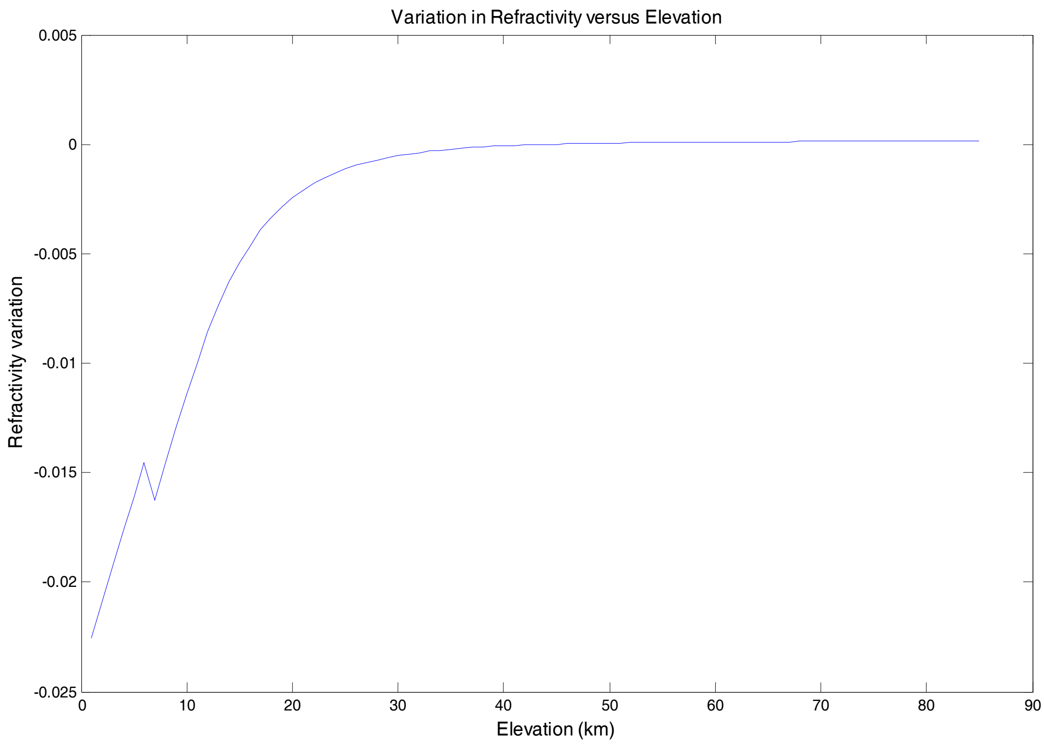

Figure 4.8 Variation of refractivity of the atmosphere.

By using the computed atmospheric parameters, refractivity of each layer can be computed. Graph of refractivity is shown in the Figure 4.8

Finally, refraction index is computed for each layer by using refractivity assuming refraction index is equal to 1 at the top layer (Figure 4.9).

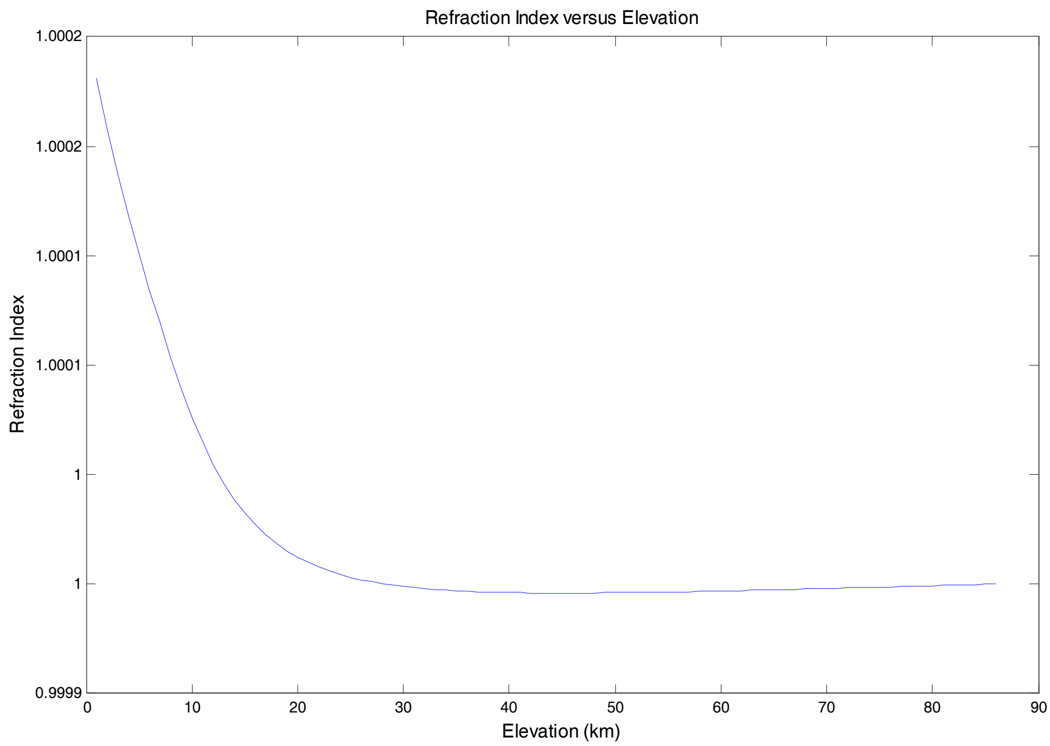

Figure 4.9 Variation of refraction index with respect to elevation

4.1.6 Transformation from S_E to S_L

To perform atmospheric corrections, zenith angle of the direction vector should be computed. To compute zenith and azimuth angles, direction vector in S_E should be transformed to S_L.

In order to transform from S_E to S_L first from the third axis (Z-axis) the frame is rotated by λ degrees and from the second axis (Y-axis) the frame is rotated by 90 – φ degrees. To convert the local system to left hand system the first axis is multiplied by -1. The total rotation is [25, p43]

$$\mathbf{R}_E^L = \mathbf{Q}_1\mathbf{R}_2(90 - \varphi)\mathbf{R}_3(\lambda) \tag{4.42}$$

where

ϕ is the latitude of the point on the ground

λ is the longitude of the point on the ground

If the matrix multiplications represented in Equation 4.42 are performed, the following matrix will be obtained,

$$\overset{L}{\mathbf{R}}_E = \begin{bmatrix} -\sin\phi\cos\lambda & -\sin\phi\sin\lambda & \cos\phi \\ -\sin\lambda & \cos\lambda & 0 \\ \cos\phi\cos\lambda & \cos\phi\sin\lambda & \sin\phi \end{bmatrix} \tag{4.43}$$

In this matrix *sin(90 – φ)* is substituted by *cos(φ)* and *cos(90 – φ)* is substituted by *sin(φ)*.

$$\overset{L}{D} = \overset{L}{\mathbf{R}}_E \overset{E}{D}$$

This can be written in matrix form as;

$$\begin{bmatrix} \overset{L}{D}_x \\ \overset{L}{D}_y \\ \overset{L}{D}_z \end{bmatrix} = \begin{bmatrix} -\sin\phi\cos\lambda & -\sin\phi\sin\lambda & \cos\phi \\ -\sin\lambda & \cos\lambda & 0 \\ \cos\phi\cos\lambda & \cos\phi\sin\lambda & \sin\phi \end{bmatrix} \begin{bmatrix} \overset{E}{D}_x \\ \overset{E}{D}_y \\ \overset{E}{D}_z \end{bmatrix} \tag{4.44}$$

By using the direction vector with respect to S_L, azimuth and zenith angles of the direction line can be computed by the following formulae:

$$\alpha = \tan^{-1}\left(\frac{\overset{L}{D}_y}{\overset{L}{D}_x}\right) \tag{4.45}$$

$$z = \tan^{-1}\left(\frac{\sqrt{\overset{L}{D}{}_x^2 + \overset{L}{D}{}_y^2}}{\overset{L}{D}_z}\right) \tag{4.46}$$

where

α is the azimuth angle

z is the zenith angle

4.1.7 Relief Displacement Correction

The intersection point of the direction vector with the WGS84 ellipsoid is exactly on the reference ellipsoid, in other words its ellipsoidal height is zero which is usually not the real case. Height differences of the objects with respect to datum cause relief displacements which alter the place of the objects in the image. In order to eliminate relief displacements, exact elevation of ground objects should be known. While studying with mono images to eliminate relief displacements a DEM is required. First at the position of intersection, elevation of that point is read from DEM and a correction for relief displacement for the geodetic position is done on reference ellipsoid, then height value of the corrected position is read from DEM and another correction is performed considering the elevation differences between two successive height values obtained from DEM. The iterative procedure continues until the elevation difference between two successive elevation values reduces to a predetermined threshold value [1].

The iteration algorithm is shown in Figure 4.10. The intersection point of direction vector with WGS84 ellipsoid is shown as P_0 in the figure. From its geodetic coordinates an elevation value is obtained from DEM. By using azimuth & zenith angles and ellipsoidal parameters geodetic coordinates of the intersection point is corrected [1]. The correction formulae are shown in Equation 4.47. After the first iteration the present point is called P_1 which has different geodetic coordinates from the previous points, this will cause a different ellipsoidal normal as shown in the Figure 4.10. The direction vector is again transformed from S_E to S_L in order to compute the correct zenith and azimuth angles, after correcting the zenith and azimuth a new height value obtained from DEM, h_1, and geodetic coordinates are corrected if the difference between two height values, $|h_1 - h_0|$, is greater than the pre-defined threshold value, ε. Magnitude of the correction is computed by the elevation differences obtained at current and previous iteration steps. This is the modification for the DRM which was using only the previous elevation data. Iteration procedure continues until the difference between two successive height values are below the threshold value.

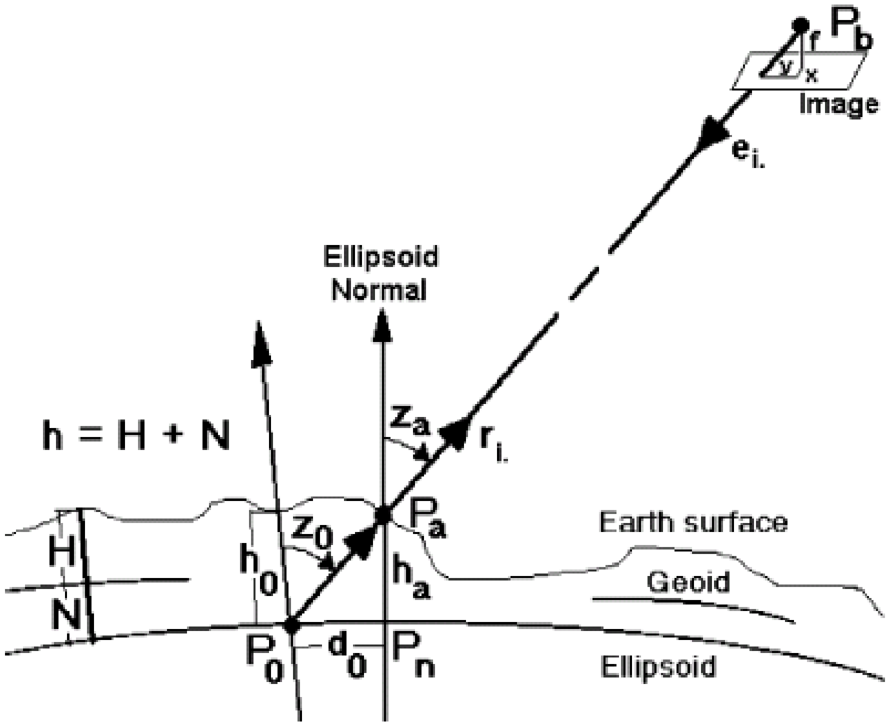

Figure 4.10 Illustration of relief displacement correction algorithm [1]

The procedure can be formulated as;

$$\Delta h_n = h_n(\lambda_{n-1}, \phi_{n-1}) - h_{n-1}(\lambda_{n-1}, \phi_{n-1}) \tag{4.47}$$
$$d_n = \Delta h_n \tan(z)$$

$$\lambda_n = \lambda_{n-1} + d_n \sin(\alpha) * \left(\frac{V}{c}\right)_{n-1} \left(\frac{1}{\cos(\phi_{n-1})}\right)$$

$$\phi_n = \phi_{n-1} + d_n \cos(\alpha_{n-1}) * \left(\frac{V^3}{c}\right)_{n-1}$$

where;

$$c = \frac{a^2}{b}, \qquad V_n = \sqrt{1 - \frac{a^2 - b^2}{b^2} \cos^2(\phi_0)_n}$$

The threshold value to be satisfied is $|\Delta h_n| < \varepsilon$, finally

$\lambda_a = \lambda_n$, $\quad \phi_a = \phi_n$, $\quad h_a = h_n$.

After n iterations final position of the point becomes λ_n, ϕ_n and h_n

Geodetic coordinates of the intersection points and the corrected points are not expected to be exactly on the DEM grids. For this reason, elevation of the point can not be obtained directly. Interpolation is required to predict the elevation of the point. Because of this four nearest grid point's elevation are obtained from DEM and a linear interpolation is applied if P_i is not exactly on the DEM grids.

4.1.8 Transformation from S_G to S_M

After computing the geodetic coordinates for each pixel position, the geodetic coordinates are converted to Universal Transverse Mercator (UTM) coordinates. Conversion of coordinates between the geodetic system of latitude and longitude and the UTM map projection involves complex mathematics. A UTM zone has a number of defining constants in addition to the required standard ellipsoid parameters. These defining constants are;

k_0 is scale factor along the central meridian

ϕ_0 is latitude of the grid origin

λ_0 is longitude of the grid origin

E_0: is false easting

N_0: is false northing

The longitude of the gird origin λ_0 is conventionally referred to as the longitude of the central meridian.

UTM conversion equations involve series expansion which is truncated to a limited number of terms. For this reason, the accuracy of the transformation is limited not only to the number of significant figures in the computations; but also the truncation of the series. When the following formulae are used, the accuracy should be satisfactory as long as the points are limited to the defined region of the particular UTM zone.

A key parameter involved in UTM conversions is the meridional distance M from the equator to a specific latitude ϕ. Calculation of M can be performed by a truncated series expansion which is given in the following equation [2, p.582].

$$M = a\begin{bmatrix} \left(1-\frac{e^2}{4}-\frac{3e^4}{64}-\frac{5e^6}{256}\right)\phi-\left(\frac{3e^2}{8}+\frac{3e^4}{32}+\frac{45e^6}{1024}\right)\sin(2\phi)+\left(\frac{15e^4}{256}+\frac{45e^6}{1024}\right)\sin(4\phi) \\ -\frac{35e^6}{3072}\sin(6\phi) \end{bmatrix} \tag{4.48}$$

where;

M is the meridian distance from the equator to a specific latitude φ,

a is the semimajor axis,

e is the eccentricity,

ϕ is the latitude.

The value of latitude ϕ in the first term must be in radian. This equation is accurate to 1 mm in any latitude.

A forward procedure that can convert latitude ϕ and longitude λ of a point to X and Y Transverse Mercator coordinates begins by computing the following preliminary quantities T, C, A [2, p.582].

$$T = \tan^2\phi \tag{4.49}$$

$$C = e'^2\cos^2\phi \tag{4.50}$$

$$A = (\lambda-\lambda_0)\cos\phi \tag{4.51}$$

where

λ and λ_0 are in radians

e' is second eccentricity

λ_0 is the longitude of the grid origin (central meridian)

The following equations complete the forward conversion to X and Y.

$$X = k_0N\left[A+(1-T+C)\frac{A^3}{6}+(5-18T+T^2+72C-58e'^2)\frac{A^5}{120}\right]+E_0 \tag{4.52}$$

$$Y = k_0 \left\{ \begin{array}{l} M - M_0 + \\ N \tan\phi \left[\begin{array}{l} \dfrac{A^2}{2} + (5 - T + 9C + 4C^2)\dfrac{A^4}{24} \\ + (61 - 58T + T^2 + 600C - 330e'^2)\dfrac{A^6}{720} \end{array} \right] \end{array} \right\} + N_0 \tag{4.53}$$

[2, p. 583] where;

k_0 is a scale factor at central meridian

e' is the second eccentricity

E_0, N_0 are false easting and false northing respectively

M is the meridianal distance at latitude ϕ computed from Eq. 46

M_0 is the meridianal distance at latitude ϕ_0 computed from Eq. 46

N is the length of ellipsoid normal at latitude ϕ expressed in page 35

4.1.9 Resampling

After transforming the geodetic coordinates of the ground point to UTM coordinates, next step is to produce the image map. The computed UTM coordinates will be irregularly spaced and placed. To obtain a regular shaped and spaced UTM grids, a mapping algorithm should be defined that maps Brightness Values of the image with irregular UTM grids to image with regular UTM grids.

When a digital image is acquired, no attempt is made to have the pixels line up with any particular map projection coordinates. It is therefore necessary to perform resampling to obtain a digital sample at an intermediate row, column location. Resampling involves interpolation between existing pixels' brightness value (BV) to synthesize pixels that correspond to fractional locations. Determination of the appropriate fractional locations is often the result of a coordinate transformation.

There are several techniques available for resampling digital images. Among these methods three of them are widely used which are nearest-neighborhood interpolation, bilinear interpolation and bicubic convolution. In this thesis nearest-neighborhood interpolation is used for resampling procedure because of its simplicity. As the methods name implies the BV chosen will be that of the image pixel whose center is closest to the center of the grid cell. From a computational standpoint, all that is required is to round off the fractional row and column values to the nearest integer value [2, p. 563]. After performing the resampling all requirements of the algorithm illustrated in Figure 4.2 will be accomplished.

4.2 DRM Algorithm For Pushbroom Scanners

DRM developed for CCD cameras is adopted for the pushbroom cameras. DRM produces an orthoimage from the raw satellite images by directly intersecting the image to ellipsoidal coordinates avoiding corrections for the projected image. Furthermore the image is transformed into UTM coordinates and by nearest neighborhood resampling algorithm the image pixel positions are computed for the UTM coordinates and the orthoimage is produced from the raw pushbroom satellite image. Since the image accusation is not immediate in pushbroom cameras; position, attitude and time parameters are not constant as in the CCD cameras. Unfortunately these parameters are not available in telemetry for small time intervals. To have continuous data for position and attitude, the position data obtained from GPS receiver and attitude information obtained from gyroscope or star tracker at a constant time interval is interpolated by polynomial functions. Time of the image acquisition is computed by using the time of starting the image acquisition and the acquisition frequency of the pushbroom camera.

Since almost all imaging satellites have pushbroom scanner onboard, there are many articles about rectification of pushbroom imagery in literature [39-51].

4.2.1 Input Data

To implement the method some assumptions are made about the telemetry data related with the position and attitude of the camera. Attitude and position data may vary from satellite to satellite, based on the satellite mission requirements. The method is proposed for a certain type of position and attitude data but no matter the format of the data, the method can be implemented for all pushbroom satellites. The proposed telemetry file data format is given as following;

- Camera position with respect to S_E is available in 3 seconds interval.
- Attitude of the body fixed reference system with respect to the orbital reference system is available in Euler angles in the order of x, y and z axes respectively.
- Time of starting and ending of the image acquisition is given with respect to UT1 time.

4.2.2 Computational Procedure

The registration process will be pixel by pixel. But to register whole image, first one row of the image will be registered and then the position and attitude of the camera will be updated. This requires the computation of the time of acquisition of the image strip. In order to compute the acquisition time of the strip the acquisition frequency f_0, should be known. f_0 can be computed by the following formula;

$$f_0 = \frac{height}{t_e - t_s} \tag{4.54}$$

In this equation t_e is the ending time t_s is the starting time of image acquisition. $height$ is the total number of strips in the image, and f_0 is the acquisition frequency. Acquisition time of i^{th} strip is computed by the formula,

$$t_i = t_s + \frac{i}{f_0} \tag{4.55}$$

in Equation 4.55 i is the strip number.

Position and attitude of the satellite at time t_i is computed by interpolation. A curve is fitted to the position and attitude data of the camera during image acquisition. A second order polynomial interpolation method whose parameters are computed by least squares is used for the satellite position and s-pline method is used for the interpolation of attitude angles.

4.2.2.1 Interpolation of Attitude by Spline Method

Spline interpolation method is preferred for the interpolation of attitude angles because spline provides smooth curves which pass from the data points. However, spline requires boundary conditions for the generation of curves, the rate of change of angles at the start and end of image acquisition is difficult to predict. This difficulty can be easily achieved by the property of splines that the effect of boundary conditions diminishes after two nodes before or after the boundary. In order to get the advantage of this property, data acquisition of the attitude angles starts two epochs before the starting of image acquisition and ends two epochs after the ending of the image acquisition.

If there are n+1 epochs during the image acquisition then the spline interpolation method will produce n different polynomial functions for the interpolation of the attitude angles at the intermediate time values. Characteristics of splines are the two successive spline functions give same value at the boundary node and have same slope. For this reason they produce a continuous and smooth curves that fits the data [52].

General form of spline functions are;

i	Interval	$g_i(x)$	
0	$[t_0, t_1]$	$a_0(t-t_0)^3 + b_0(t-t_0)^2 + c_0(t-t_0) + d_0$	(4.56)
1	$[t_1, t_2]$	$a_1(t-t_1)^3 + b_1(t-t_1)^2 + c_1(t-t_1) + d_1$	
:	:	:	
n	$[t_n, t_{n+1}]$	$a_n(t-t_n)^3 + b_n(t-t_n)^2 + c_n(t-t_n) + d_n$	

where

n is the number of epochs

t_i is the time at the i^{th} epoch

t is the time that interpolation will be performed

a, b, c, d are the coefficients of the polynomials

Computation of a_i, b_i, c_i and d_i is performed by the following formulae

$$a_i = \frac{S_{i+1} - S_i}{6h_i} \tag{4.57}$$

$$b_i = \frac{S_i}{2} \tag{4.58}$$

$$c_i = \frac{y_{i+1} - y_i}{h_i} - \frac{2h_i S_i + h_i S_{i+1}}{6} \tag{4.59}$$

$$d_i = y_i \tag{4.60}$$

In equations 4.57 to 4.60;

y is the value of the function at the corresponding epoch (radian)

h is the difference between two successive epoch (second)

S are the coefficients to be computed by using the data as following

$$\begin{bmatrix} \frac{(h_0 + h_1)(h_0 + 2h_1)}{h_1} & \frac{h_1^2 - h_0^2}{h_1} & & & \\ h_1 & 2(h_1 + h_2) & h_2 & & \\ & h_2 & 2(h_2 + h_3) & h_3 & \\ & & \ddots & \ddots & \ddots \\ & & & \frac{h_{n-2}^2 - h_{n-1}^2}{h_{n-2}} & \frac{(h_{n-1} + h_{n-2})(h_{n-1} + 2h_{n-2})}{h_{n-2}} \end{bmatrix} \begin{bmatrix} S_1 \\ S_2 \\ S_3 \\ \vdots \\ S_{n-1} \end{bmatrix} = 6 \begin{bmatrix} f[x_2, x_3] - f[x_1, x_2] \\ f[x_3, x_4] - f[x_2, x_3] \\ f[x_4, x_5] - f[x_3, x_4] \\ \vdots \\ f[x_{n-2}, x_{n-1}] - f[x_{n-3}, x_{n-2}] \end{bmatrix} \tag{4.61}$$

where;

$f[x_{n-1}, x_n]$ is equal to $f(x_n) - f(x_{n-1})$

If S is solved and substituted into Eq. 4.57, 4.58 and 4.59 the required values of attitude angles can be obtained.

4.2.2.2 Interpolation of Camera Position by Least Squares

Position of the push broom camera is interpolated by a 2^{nd} order polynomial in the form of;

$$a_i t^2 + b_i t + c_i \tag{4.62}$$

where;
a_i, b_i and c_i are the coefficients of the polynomial
t is the time that the camera position is required
i = 1,2,3 for x,y and z coordinates respectively

Computation of the coefficients of the polynomial will be performed by Least Squares (LS) algorithm. LS computes the coefficients of the polynomial which minimizes the sum of the squares of the residuals. This will cause a contradiction that the camera position calculated by interpolation and obtained from telemetry will not be same for the time when position data is available. This is not an important drawback unless the residuals are very large, moreover it is known that observations are prone to error and the LS fit can be considered as the camera position that is corrected from the errors. The solution of parameters will be in the following form [53];

$$\boldsymbol{\beta} = (\boldsymbol{X'}\boldsymbol{X})^{-1}\boldsymbol{X'}\boldsymbol{y} \tag{4.63}$$

where;
i = 1,2,3.

$$\boldsymbol{\beta} = \begin{bmatrix} a_i \\ b_i \\ c_i \end{bmatrix} \qquad \boldsymbol{X} = \begin{bmatrix} \frac{\partial f_1}{\partial a_i} & \frac{\partial f_1}{\partial b_i} & \frac{\partial f_1}{\partial c_i} \\ \vdots & \vdots & \vdots \\ \frac{\partial f_n}{\partial a_i} & \frac{\partial f_n}{\partial b_i} & \frac{\partial f_n}{\partial c_i} \end{bmatrix}$$, if derivatives are substituted

$$\boldsymbol{X} = \begin{bmatrix} \Delta t_1^2 & \Delta t_1 & 1 \\ \vdots & \vdots & \vdots \\ \Delta t_n^2 & \Delta t_n & 1 \end{bmatrix}$$

$$\boldsymbol{y} = \begin{bmatrix} p_1 \\ \vdots \\ p_n \end{bmatrix}$$

in this matrix x, y and z coordinates will be substituted for p

4.2.2.3 Rectification of the Image with DRM

After interpolating the position and attitude of the camera, the image strip can be registered by DRM.

First, the image strip is transformed from S_I to S_P by the following formula;

$$y' = \left(y'' - \frac{width}{2} \right) * c - \Delta y \tag{4.64}$$

In Equation 4.64;
y" is the image coordinate with respect to the raw satellite image (pixel)
width is the width of the image (pixel)
c is the size of the sensing element (mm/pixel)
Δy is the coordinate of the principal point (mm)

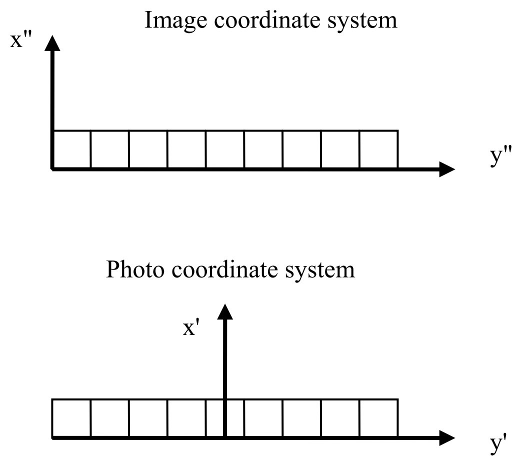

Figure 4.11 Orientation of image and photo coordinate system with respect to scanner.

Lens distortion of the camera is eliminated by the following formula

$$y = y'\left(1 - k_1 y'^2 - k_2 y'^4 - 3py'\right) \tag{4.65}$$

In Equation 4.65,

k_1 and k_2 are the symmetric lens distortion parameters ($1/mm^2$, $1/mm^4$ respectively)
p is the asymmetric lens distortion parameter (1/mm)
y is the corrected photo coordinate (mm)

Camera coordinate system of the pushbroom camera is defined as z axis points through camera direction, x axis points through the satellite flight direction and y axis completes a right hand coordinate system. Camera coordinate system is shown in Figure 4.12.

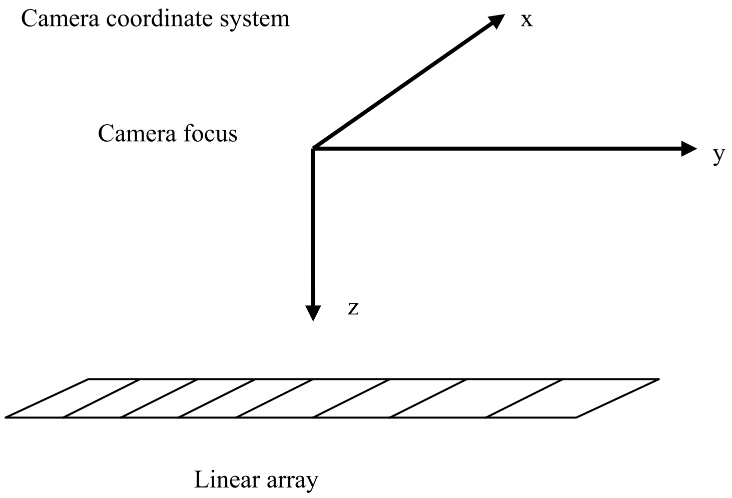

Figure 4.12 Orientation of camera coordinate system with respect to scanner

Direction vector of the line from the camera focus to the center of a certain pixel element in camera coordinate system can be written as;

$$S_C = \frac{[0, y, f]}{\sqrt{y^2 + f^2}} \tag{4.66}$$

where

S_C is the direction vector with respect to the camera coordinate system

f is the focal length of the camera

y is position of the image point in the corresponding strip with respect to S_P

Camera may shot an oblique image by an angle μ according to the flight direction. As a result the camera coordinate system makes an angle μ with respect to body fixed reference system. In order to transform from camera coordinate system to body fixed reference system an $R_1(-\mu)$ rotation is necessary. $R_1(-\mu)$ rotation matrix can be written as;

$$R_1(\mu) = \begin{bmatrix} 1 & 0 & 0 \\ 0 & \cos\mu & -\sin\mu \\ 0 & \sin\mu & \cos\mu \end{bmatrix} \tag{4.67}$$

Transformation from

$$S_B = R_1(\mu) S_C \tag{4.68}$$

In the next step direction vector with respect to S_B is transformed to S_O by using the computed attitude angles interpolated by spline method at the epoch of acquisition of corresponding strip. The transformation from S_B to S_O is performed by 3 Euler rotation in the order of y, x and z axes with the rotation angles for each axis is φ, ω and κ respectively. The transformation from S_B to S_O is written in Equation 4.7.

By using the position and velocity of the camera and the time of the acquisition of the strip, direction vector with respect to S_O is converted to S_E. The following steps are explained at the rectification algorithm of the CCD frame cameras.

- Image strip is intersected with the WGS84 ellipsoid.
- Atmospheric refraction corrections are applied to the intersection coordinates.
- Relief displacements are removed by elevation data obtained from DEM.
- Ellipsoidal coordinates are converted into UTM coordinates.
- Orthoimage with respect to UTM coordinates is produced from the raw pushbroom scanner image by nearest neighboring resampling algorithm.

CHAPTER 5

PARAMETER ESTIMATION

Photogrammetry is an art and science of determining the position and shape of objects from photographs [32]. To be able to make accurate measurements from images camera calibration and rectification of the image must be done. These tasks are performed with the analytical relationship between image points and ground points. As mentioned previously the analytical relationship is given by the colinearity equations. To possess precise parameters a parameter estimation procedure has to be performed.

5.1 Method of Parameter Estimation

A sensible method of estimating unknown parameters is given by minimizing the sum of the squares of the deviations of the observations $\boldsymbol{y}$ from the squares of the deviations of the observations y from the estimators s[E($\boldsymbol{y}$)] of their expected values E($\boldsymbol{y}$), which are functions of the unknown parameters. Hence, the sum of squares ($\boldsymbol{y}$ – s[E($\boldsymbol{y}$)])' ($\boldsymbol{y}$ – s[E($\boldsymbol{y}$)]) shall be minimized. By means of the positive definite covariance matrix D($\boldsymbol{y}$) = $\boldsymbol{\Sigma}$ of the observations, this method can be generalized by the requirement to minimize the quadratic form ($\boldsymbol{y}$ – s[E($\boldsymbol{y}$)])' $\boldsymbol{\Sigma}^{-1}$ ($\boldsymbol{y}$ – s[E($\boldsymbol{y}$)]), since small variances of the observations correspond to large elements of the inverse $\boldsymbol{\Sigma}^{-1}$ of the covariance matrix corresponding to large weights of the observations.

Gauss Markoff model can be represented as

$$X\beta = y + e \qquad \text{with} \qquad D(y) = \sigma^2 \boldsymbol{P}^{-1} \tag{5.1}$$

where;

X_{n*u} (rank X = u)

u is number of parameters

n is number of observations

P_{n*n} is weight matrix with size $n \times n$

$D(y)_{n*n}$ variance covariance matrix of the observations

$$X = \begin{bmatrix} \left.\frac{\partial f_1}{\partial \beta_1}\right|_0 & \left.\frac{\partial f_1}{\partial \beta_2}\right|_0 & \cdots & \left.\frac{\partial f_1}{\partial \beta_u}\right|_0 \\ \vdots & \vdots & \cdots & \vdots \\ \left.\frac{\partial f_n}{\partial \beta_1}\right|_0 & \left.\frac{\partial f_n}{\partial \beta_2}\right|_0 & \cdots & \left.\frac{\partial f_n}{\partial \beta_u}\right|_0 \end{bmatrix}_{n*u} \tag{5.2}$$

$$\Sigma_{yy} = \begin{bmatrix} \sigma_1^2 & \sigma_1\sigma_2 & \cdots & \sigma_1\sigma_n \\ \sigma_2\sigma_1 & \sigma_2^2 & \cdots & \sigma_2\sigma_n \\ \vdots & \vdots & \vdots & \vdots \\ \sigma_n\sigma_1 & \sigma_n\sigma_2 & \cdots & \sigma_n^2 \end{bmatrix}_{n*n} \tag{5.3}$$

Solution for the fixed parameters will be by the following equation [53]

$$\beta = \left(X'PX\right)^{-1} X'Py \qquad \text{with} \qquad D\left(\hat{\beta}\right) = \left(X'PX\right)^{-1} \tag{5.4}$$

Replacing the error vector $\boldsymbol{e}$ in the Gauss-Markoff Model, by a linear combination $-\mathbf{Z}\boldsymbol{\gamma}$ of the unknown random parameters $\boldsymbol{\gamma}$, a mixed model on the basis of fixed and random parameters is obtained by

$$y = \mathbf{X}\boldsymbol{\beta} + \mathbf{Z}\boldsymbol{\gamma} \qquad \text{with } E(\boldsymbol{\gamma}) = 0 \quad \text{and } D(\boldsymbol{\gamma}) = \sigma^2 \Sigma_{\gamma\gamma} \tag{5.5}$$

where

$\boldsymbol{X}$ is $n \times u$ and $\boldsymbol{Z}$ is $n \times r$ matrix of unknown coefficients with rank$\boldsymbol{Z}$ = n. $\boldsymbol{\beta}$ is $u \times 1$ vector of unknown fixed parameters, $\boldsymbol{\gamma}$ is an $r \times 1$ vector of unknown random parameters as measurements with expected value, $E(\boldsymbol{\gamma}) = 0$ and variance covariance matrix, $D(\boldsymbol{\gamma}) = \sigma^2 \Sigma_{\gamma\gamma}$ with unknown positive factor σ^2. $\Sigma_{\gamma\gamma}$ is $r \times r$ given positive definite cofactor matrix, y $n \times 1$ observation vector. The best linear unbiased estimator of the fixed parameter $\hat{\boldsymbol{\beta}}$ of $\boldsymbol{\beta}$ is given by,

$$\hat{\boldsymbol{\beta}} = \left(\mathbf{X}'\boldsymbol{\Sigma}_{yy}^{-1}\mathbf{X}\right)^{-1} \mathbf{X}'\boldsymbol{\Sigma}_{yy}^{-1}\mathbf{y} \tag{5.6}$$

with covariance matrix of the observations $D(y) = D(\mathbf{X}\boldsymbol{\beta} + \mathbf{Z}\boldsymbol{\gamma}) = \sigma^2 \mathbf{Z}\Sigma_{\gamma\gamma}\mathbf{Z}' = \sigma^2 \Sigma_{yy}$

Σ_{yy} is the variance covariance matrix of the observations.

The estimator $\hat{\boldsymbol{\gamma}}$ of $\boldsymbol{\gamma}$ follows with,

$$\hat{\boldsymbol{\gamma}} = \boldsymbol{\Sigma}_{\gamma y}\boldsymbol{\Sigma}_{yy}^{-1}\left(\boldsymbol{y} - \mathbf{X}\hat{\boldsymbol{\beta}}\right) \tag{5.7}$$

where $\Sigma_{\gamma y}$ is covariance of $\boldsymbol{\gamma}$ and $\boldsymbol{y}$ C(γ, y) =C($\boldsymbol{\gamma}$, $\mathbf{X}\boldsymbol{\beta}+\mathbf{Z}\boldsymbol{\gamma}$) = σ^2 $\Sigma_{\gamma\gamma}$ $\mathbf{Z}$'= $\sigma^2 \Sigma_{\gamma y}$

In the algorithm represented, $\boldsymbol{y}$ will be the observations, in other words the geodetic coordinates of the measured ground control points.

$\boldsymbol{\beta}$ is the vector of satellite's inner and outer parameters, which is shown as

$$\boldsymbol{\beta}=\begin{bmatrix} f & \Delta x & \Delta y & c & k_1 & k_2 & p_1 & p_2 & \omega & \phi & \kappa & X_{cam} & Y_{cam} & Z_{cam} \end{bmatrix}' \tag{5.8}$$

where,

f is the focal length of the camera

Δx is the x value of the principal point coordinate of the camera

Δy is the y value of the principal point coordinate of the camera

c is the size of a sensor on the CCD array

k_1 and k_2 are the radial lens distortion parameters

p_1 and p_2 are the asymmetric lens distortion parameters

ω, φ, κ are the attitude angles between S_B and S_O

X_{cam}, Y_{cam}, Z_{cam} are the cartesian coordinates of the camera with respect to S_E.

$2n \times 14$ $\boldsymbol{X}$ matrix includes the partial derivatives of the geodetic coordinates with respect to fixed parameters where the geodetic coordinates are calculated from the rectification equations.

$$\boldsymbol{X}=\begin{bmatrix}
\frac{\partial\phi_1}{\partial f} & \frac{\partial\phi_1}{\partial\Delta x} & \frac{\partial\phi_1}{\partial\Delta y} & \frac{\partial\phi_1}{\partial c} & \frac{\partial\phi_1}{\partial k_1} & \frac{\partial\phi_1}{\partial k_2} & \frac{\partial\phi_1}{\partial p_1} & \frac{\partial\phi_1}{\partial p_2} & \frac{\partial\phi_1}{\partial\omega} & \frac{\partial\phi_1}{\partial\phi} & \frac{\partial\phi_1}{\partial\kappa} & \frac{\partial\phi_1}{\partial X_{cam}} & \frac{\partial\phi_1}{\partial Y_{cam}} & \frac{\partial\phi_1}{\partial Z_{cam}} \\
\frac{\partial\lambda_1}{\partial f} & \frac{\partial\lambda_1}{\partial\Delta x} & \frac{\partial\lambda_1}{\partial\Delta y} & \frac{\partial\lambda_1}{\partial c} & \frac{\partial\lambda_1}{\partial k_1} & \frac{\partial\lambda_1}{\partial k_2} & \frac{\partial\lambda_1}{\partial p_1} & \frac{\partial\lambda_1}{\partial p_2} & \frac{\partial\lambda_1}{\partial\omega} & \frac{\partial\lambda_1}{\partial\phi} & \frac{\partial\lambda_1}{\partial\kappa} & \frac{\partial\lambda_1}{\partial X_{cam}} & \frac{\partial\lambda_1}{\partial Y_{cam}} & \frac{\partial\lambda_1}{\partial Z_{cam}} \\
\vdots & \vdots & \vdots & \vdots & \vdots & \vdots & \vdots & \vdots & \vdots & \vdots & \vdots & \vdots & \vdots & \vdots \\
\frac{\partial\phi_n}{\partial f} & \frac{\partial\phi_n}{\partial\Delta x} & \frac{\partial\phi_n}{\partial\Delta y} & \frac{\partial\phi_n}{\partial c} & \frac{\partial\phi_n}{\partial k_1} & \frac{\partial\phi_n}{\partial k_2} & \frac{\partial\phi_n}{\partial p_1} & \frac{\partial\phi_n}{\partial p_2} & \frac{\partial\phi_n}{\partial\omega} & \frac{\partial\phi_n}{\partial\phi} & \frac{\partial\phi_n}{\partial\kappa} & \frac{\partial\phi_n}{\partial X_{cam}} & \frac{\partial\phi_n}{\partial Y_{cam}} & \frac{\partial\phi_n}{\partial Z_{cam}} \\
\frac{\partial\lambda_n}{\partial f} & \frac{\partial\lambda_n}{\partial\Delta x} & \frac{\partial\lambda_n}{\partial\Delta y} & \frac{\partial\lambda_n}{\partial c} & \frac{\partial\lambda_n}{\partial k_1} & \frac{\partial\lambda_n}{\partial k_2} & \frac{\partial\lambda_n}{\partial p_1} & \frac{\partial\lambda_n}{\partial p_2} & \frac{\partial\lambda_n}{\partial\omega} & \frac{\partial\lambda_n}{\partial\phi} & \frac{\partial\lambda_n}{\partial\kappa} & \frac{\partial\lambda_n}{\partial X_{cam}} & \frac{\partial\lambda_n}{\partial Y_{cam}} & \frac{\partial\lambda_n}{\partial Z_{cam}}
\end{bmatrix}_{2n\times 14} \tag{5.9}$$

Colinearity equations are not linear equations so they should be linearized by first order Taylor expansion. First order Taylor expansion requires the initial approximation values for the parameters and the first derivatives of them.

$$\begin{aligned} y &= y_0\left(f,\Delta x,\Delta y,c,k_1,k_2,p_1,p_2,\omega,\phi,\kappa,X_{cam},Y_{cam},Z_{cam}\right) \\ &+\frac{\partial y}{\partial f}\Delta f+\frac{\partial y}{\partial \Delta x}\Delta\Delta x+\cdots+\frac{\partial y}{\partial Z_{cam}}\Delta Z_{cam} \end{aligned} \tag{5.10}$$

So the equation can be written as

$$\Delta y = X\Delta\beta + Z\gamma \tag{5.11}$$

$$\Delta\hat{\beta}=\left(X\Sigma_{yy}^{-1}X\right)^{-1}X\Sigma_{yy}^{-1}\Delta y \tag{5.12}$$

$$\hat{\beta} = \beta_0 + \Delta\hat{\beta} \tag{5.13}$$

Estimated parameters $\hat{\beta}$ are substituted into the Equation 5.7 in order to compute estimated random parameters. $\boldsymbol{\gamma}$ vector includes the parameters that are the corrections to pixel coordinates and elevation, in other words random errors resulted from the recording of pixel coordinates of digital image and elevation of ground point obtained from DEM. $\boldsymbol{\gamma}$ is given by,

$$\boldsymbol{\gamma} = \begin{bmatrix} \xi x'' & \xi y'' & \xi h \end{bmatrix}'_{1x3n} \tag{5.14}$$

Z matrix can be constituted as follows,

$$\boldsymbol{Z} = \begin{bmatrix} \frac{\partial\phi_1}{\partial x''_1} & \frac{\partial\phi_1}{\partial y''_1} & \frac{\partial\phi_1}{\partial h_1} & \cdots & \frac{\partial\phi_1}{\partial x''_n} & \frac{\partial\phi_1}{\partial y''_n} & \frac{\partial\phi_1}{\partial h_n} \\ \frac{\partial\lambda_1}{\partial x''_1} & \frac{\partial\lambda_1}{\partial y''_1} & \frac{\partial\lambda_1}{\partial h_1} & \cdots & \frac{\partial\lambda_1}{\partial x''_n} & \frac{\partial\lambda_1}{\partial y''_n} & \frac{\partial\lambda_1}{\partial h_n} \\ \vdots & \vdots & \vdots & \ddots & \vdots & \vdots & \vdots \\ \frac{\partial\phi_n}{\partial x''_1} & \frac{\partial\phi_n}{\partial y''_1} & \frac{\partial\phi_n}{\partial h_1} & \cdots & \frac{\partial\phi_n}{\partial x''_n} & \frac{\partial\phi_n}{\partial y''_n} & \frac{\partial\phi_n}{\partial h_n} \\ \frac{\partial\lambda_n}{\partial x''_1} & \frac{\partial\lambda_n}{\partial y''_1} & \frac{\partial\lambda_n}{\partial h_1} & \cdots & \frac{\partial\lambda_n}{\partial x''_n} & \frac{\partial\lambda_n}{\partial y''_n} & \frac{\partial\lambda_n}{\partial h_n} \end{bmatrix}_{2n\times 3n} \tag{5.15}$$

To compute the random parameters a priori information about the correlation of random parameters is needed. The variance covariance matrix of random parameters $\Sigma_{\gamma\gamma}$ should be introduced. A reasonable assumption is made when constructing the variance covariance matrix of the random parameters, that there is no correlation between the random parameters, not only between the random parameters but also between the parameters at measurement sites. This is because obtaining the pixel coordinates from the digital image is prone to random errors. It is not expected to make systematic errors. However, elevation values of the DEM may have bias and the plus or minus systematic error may be present which can not be predicted without a detailed error analysis of DEM.

As a result of these assumptions variance covariance matrix of the random parameters becomes a diagonal matrix. Then the variance covariance matrix of random parameters is multiplied by Z matrix and $\Sigma_{\gamma y}$ is computed. The second unknown for the solution of the random parameters is the variance covariance matrix of the measurements, Σ_{yy} which can be computed as $\boldsymbol{Z\Sigma_{\gamma\gamma}Z'}$.

Parameter estimation is performed usually for fixed parameters in articles [54-72]. In other words, fixed parameters are corrected by Gauss Markov model and the random part in the model is represented with the residuals. However, by using mixed model pixel coordinates are corrected by Fritsch [73].

The matrix inverse in Equation 5.6 can not be computed because of the rank deficiency in the X matrix. However, to compute fixed parameters the matrix inverse is had to be taken, for this reason some regularization methods are applied to achieve this task.

5.2 Regularization Methods

In order to stabilize the system 3 regularization methods are applied and their performances are compared. The regularization methods are fictitious observations, Tikhonov regularization and Singular Value Decomposition (SVD).

5.2.1 Fictitious Observations

A set of fictitious observations, μ , as unknown parameters is added to the system. The system with zero fictitious observations can be written as [74, 75]

$$\begin{bmatrix} \boldsymbol{y} \\ \boldsymbol{\mu} \end{bmatrix} = \begin{bmatrix} \boldsymbol{X} \\ \boldsymbol{I} \end{bmatrix} \boldsymbol{\beta} + \begin{bmatrix} \boldsymbol{Z} & 0 \\ 0 & \boldsymbol{I} \end{bmatrix} \begin{bmatrix} \boldsymbol{\gamma} \\ \boldsymbol{v} \end{bmatrix} \tag{5.16}$$

$$\text{With } D\left(\begin{bmatrix} \mathbf{y} \\ \boldsymbol{\mu} \end{bmatrix} \right) = \sigma^2 \begin{bmatrix} \boldsymbol{I} & 0 \\ 0 & \boldsymbol{V} \end{bmatrix} \tag{5.17}$$

where;

$\boldsymbol{y}$	observation vector
$\boldsymbol{\mu}$	fictitious observations ($\boldsymbol{\mu}=0$)
$\boldsymbol{I}$	unit matrix
$\mathbf{v}$	error vector
$\boldsymbol{V}$	variance covariance matrix of the fixed parameters
σ^2	variance of unit weight.

Solution of Eq.70 for the fixed parameters is performed by the solution

$$\hat{\boldsymbol{\beta}} = \left(\boldsymbol{X'} \left(\boldsymbol{Z\Sigma}_{\gamma\gamma} \boldsymbol{Z'} \right)^{-1} \boldsymbol{X} + \boldsymbol{P} \right)^{-1} \left(\boldsymbol{X'} \left(\boldsymbol{Z\Sigma}_{\gamma\gamma} \boldsymbol{Z'} \right)^{-1} \boldsymbol{y} \right) \tag{5.18}$$

where

$\boldsymbol{P}$	weight matrix for fictitious observations

5.2.2 Tikhonov Regularization

Tikhonov regularization which is the most commonly used method of regularization of ill posed problems is applied also. Its simplest form is an ill conditioned system of linear equations is as follows;

$$\boldsymbol{X}\beta = y \tag{5.19}$$

where;
X is an mxn matrix
β is a column vector of n unknown parameters
y is a column vector of m entries

Minimization of sum of the squares of the residuals is replaced by the problem of seeking an X to minimize [76]

$$\left\|\boldsymbol{X}\beta - y\right\|^2 + \alpha^2\left\|\beta\right\|^2 \tag{5.20}$$

for some suitably chosen Tikhonov factor α >0. The new form of the problem improves the conditioning of the problem, thus enabling a numerical solution. An explicit solution, denoted by $\hat{\beta}$ is given by;

$$\hat{\beta} = \left(\boldsymbol{X}^T\boldsymbol{X} + \alpha^2 I\right)^{-1}\boldsymbol{X}^T y \tag{5.21}$$

where;
I is an nxn identity matrix.

If α is taken as 0 in the Eq. it reduces to the least squares solution of an overdetermined problem (m > n).

Although at first, the choice of the solution to this regularized problem may look artificial, and indeed the parameter α seems rather arbitrarily, the process can be justified in a Bayesian point of view. For an ill posed problem one must necessarily introduce some additional assumptions in order to get a stable solution. Statistically it might be assumed that a priori multivariate normal distribution of $\hat{\beta}$ with errors of zero mean with a standard deviation of σ_x. Moreover, the observations are also subject to errors with zero mean and standard deviation of σ_y. Under these assumptions the Tikhonov regularized solution is the most probable solution given the data and the a priori distribution of β, according to Bayes' theorem. The Tikhonov parameter is then $\alpha = \dfrac{\sigma_y}{\sigma_\beta}$.

For general multivariate normal distributions for β and the data error, a transformation of the variables can be applied to reduce to the case as having zero mean. Equivalently, the equation takes the form

$$\|\boldsymbol{X}\beta - y\|_P^2 + \alpha^2\|\beta - \beta_0\|_Q^2 \tag{5.22}$$

where;

$\|\beta\|_P$ stands for the weighted norm $\beta^T P\beta$.

In the Bayesian interpretation, P is the inverse covariance matrix of y, β_0 is the expected value of β , and αQ is the inverse covariance matrix of β .

This can be solved explicitly by the formula;

$$\beta_0 + \left(\boldsymbol{X}^T\boldsymbol{PX} + \alpha^2\boldsymbol{P}\right)^{-1}\boldsymbol{X}^T\boldsymbol{P}(y - \boldsymbol{X}\beta_0) \tag{5.23}$$

5.2.3 Singular Value Decomposition

Ill conditioned problems can be solved by using singular value decomposition method which is shown above [77];

$$X = U\Sigma V^T \tag{5.24}$$

where

Σ is the diagonal matrix of singular values σ_i augmented with zeros so as to be mxn

U and V are left and right singular vectors respectively.

Tikhonov regularized solution can be expressed as

$$\hat{\beta} = VDU^T y \tag{5.25}$$

where;

D is an mxn matrix equal to $\dfrac{\sigma_i}{\sigma_i + \alpha^2}$ on the diagonal and zero elsewhere. This demonstrates the effect of Tikhonov parameter on the condition number of the regularized problem.

5.3 Effect of Regularization

A study has been performed on the condition number of the design matrix with the position of the control points on the CCD array. In the first case narrowly distributed GCPs are selected and the condition number of the design matrix is computed. In the second run the widely distributed GCPs are selected and the condition number of the design matrix is computed.

Pixel positions used in the narrower distribution;

Table 5.1 Coordinates of narrow distributed pixel positions

950,950	1000,950	1050,950
950,1000	1000,1000	1050,1000
950, 1050	1000,1050	1050,1050

Pixel positions used in the wider distribution;

Table 5.2 Coordinates of wide distributed pixel positions

1,1	1024,1	2048,1
1, 1024	1024,1024	2048,1024
1, 2048	1024,2048	2048,2048

The condition number of a matrix measures the sensitivity of the solution of a system of linear equations to errors in the data. It gives an indication of the accuracy of the results from matrix inversion and the linear equation solution. Values close to 1 indicate a well-conditioned matrix.

Condition number of the design matrix is computed from the fallowing formula;

$$\|X'X\| * \left\|(X'X)^{-1}\right\| \tag{5.26}$$

Where the norm is the Frobenius norm and computed as [78];

$$\|A\| = \sqrt{\sum_{i=1}^{n}\sum_{j=1}^{n} a_{ij}^{2}} \tag{5.27}$$

In the first case condition number is computed by using narrower GCP distribution is computed as;

6.33073e+038

Which is an extremely large number that implies obtaining an accurate solution is impossible.

In the second trial by using the same parameters and same analytical equation but choosing widely distributed pixel positions the condition number is computed as;

3.37508e+030

When two numbers are compared it is seen that choosing widely distributed GCP improves the accuracy of the solution but the improvement in geometry is not adequate since the condition number is again too high to obtain an accurate solution. To conclude it can be said that, significant improvement in accuracy is obtained by choosing GCP widely distributed but brushing up the geometry is not adequate to obtain accurate solution.

This is because the rank deficiency was caused not only from the weak geometry but also the correlation between the parameters. Improving the geometry can help up to a certain case. In order to reach further improvement, mathematical methods should be used. For this reason fictitious observations are added into observations and the solution for the equation became as in the Equation 5.18. The condition number of the matrix to be inversed for the narrow case is computed as;

8.51589e+014

This means that the improvement is significant compared by the improvement gained from strengthening the geometry. Same procedure is applied for the widely distributed pixel positions and the following condition number is obtained;

8.51593e+014

This is a surprising solution that widely distributed solution has slightly weak accuracy compared with narrowly distributed solution. But the condition numbers of the two different geometries are almost the same, because of this it can be said that when fictitious observations are used the effect of geometry fades out. However, the improved condition number is not adequate for accurate solution, it still needs improvement.

Ill conditioned situation has occurred not only from the weak geometry but also the correlation between the parameters used for the camera calibration. Effect of weak geometry has been eliminated by fictitious observations, in order to eliminate the effect of correlation between camera calibration parameters some modification has been done on camera parameters. First of all, camera position is represented by geodetic coordinates instead of cartesian coordinates. In this model, altitude of the camera, size of the sensing element on CCD frame and focal length are correlated. For this reason altitude of the camera and size of the sensing element are eliminated from the equation system.

The parameters of the model is as follows

$$\beta = \begin{bmatrix} f & \Delta x & \Delta y & k_1 & k_2 & p_1 & p_2 & \omega & \phi & \kappa & \phi_{cam} & \lambda_{cam} \end{bmatrix}'_{1\times 12} \qquad (5.28)$$

By using this system with the narrower GCP distribution, condition number of the system is computed as

2.1533e+033

Second mathematical model is slightly better than the first model, but the result is quite bad for a solution of a desired accuracy.

Second method's computational accuracy is examined with widely distributed pixel positions. The condition number computed for this situation is,

1.3246e+024

Obtained result has a considerable improvement compared with the narrow distributed pixel positions. However current situation is still bad for an accurate solution. The improvement gained by choosing widely distributed GCPs is not adequate for obtaining an accurate solution. In order to improve the solution accuracy fictitious observations are introduced and for the narrow distributed pixel positions the following condition number is obtained as,

2.8356383e+010

Condition number computed for narrow model is adequate for solution with computer using 8 byte double, variables. When compared with the first model it is seen that higher improvement in the accuracy of the solution is obtained when a regularization method is applied. The regularization method is also applied to the widely distributed pixel positions and the following result is obtained,

2.8356389e+010

The result is very similar to the first mathematical model in a way that, the condition number computed for the widely distributed pixel positions is slightly worse than the narrower pixel positions.

To conclude the analysis, the distribution of the pixel position has direct impact on the solution accuracy if a regularization method had not been applied. For this type of rectification procedures, the pixel positions should be selected in a way that they should be distributed as wide as possible. However, not an adequate improvement is obtained by selecting widely distributed GCPs in both models. To obtain a solution a regularization method should be applied, when a regularization technique is applied the effect of GCP distribution on the solution accuracy diminishes. Although, narrower distributed GCPs had given slightly better results in both models, since the difference between wide and narrow distributed points is very small there is no contradiction in the comment. Furthermore, regularization improves the accuracy of the solution considerably more than the improvement gained by modifying the imaging geometry. However, when a regularization method is applied the convergence of the problem slows down and more iterations are required.

CHAPTER 6

IMPLEMENTATION OF PARAMETER ESTIMATION AND DRM

In this chapter DRM whose theory was explained in chapter 4 will be implemented. However, initial values obtained for the parameters were not precise enough for the implementation. For this reason, in the beginning a parameter estimation procedure will be applied to correct the parameters that will be used in the implementation of DRM. For the parameter estimation process, Gauss Markoff method explained in chapter 5 will be performed.

6.1 Implementation of Parameter Estimation for CCD Frame Cameras

The parameter estimation will be implemented by using the collected GCPs and Bilsat image presented in Chapter 3. Three regularization methods are implemented for parameter estimation procedure of the CCD frame camera and the results of the methods are compared at the end. Since regularization methods slow down the convergence of the parameter estimation an iterative procedure is applied which continues until the residuals become smaller than a predefined threshold value.

6.1.1 Implementation of Parameter Estimation with Fictitious Observations

Solution of this regularization method requires the cofactor matrix of the parameters. To regularize the equation, cofactor matrix of the parameters (Equation 5.28) shown below is used.

$$D=\begin{bmatrix}
1{,}0E-6 &&&&&&&&&&&& \\
& 1{,}0E-6 &&&&&&&&&&& \\
&& 1{,}0E-7 & 1{,}9E-7 & 3{,}6E-7 &&&&&&&& \\
&& 1{,}9E-7 & 1{,}0E-7 & 6{,}3E-7 &&&&&&&& \\
&& 3{,}6E-7 & 6{,}3E-7 & 1{,}0E-7 &&&&&&&& \\
&&&&& 5{,}0E-7 &&&&&&& \\
&&&&&& 5{,}0E-7 &&&&&& \\
&&&&&&& 5{,}0E-7 &&&&& \\
&&&&&&&& 100 &&&& \\
&&&&&&&&& 1{,}0E-4 &&& \\
&&&&&&&&&& 5{,}0E-4 && \\
&&&&&&&&&&& 5{,}0E-4 &
\end{bmatrix}$$

To satisfy the convergence criteria 552 iteration were performed. The residuals of each GCP computed with the fictitious observations are given in Appendix B. 3D Scatterplots of the corrections for the pixel values and corrections for elevation are presented in Figures 6.1 to 6.3 (Table B.1 and Table B.4,5,6),

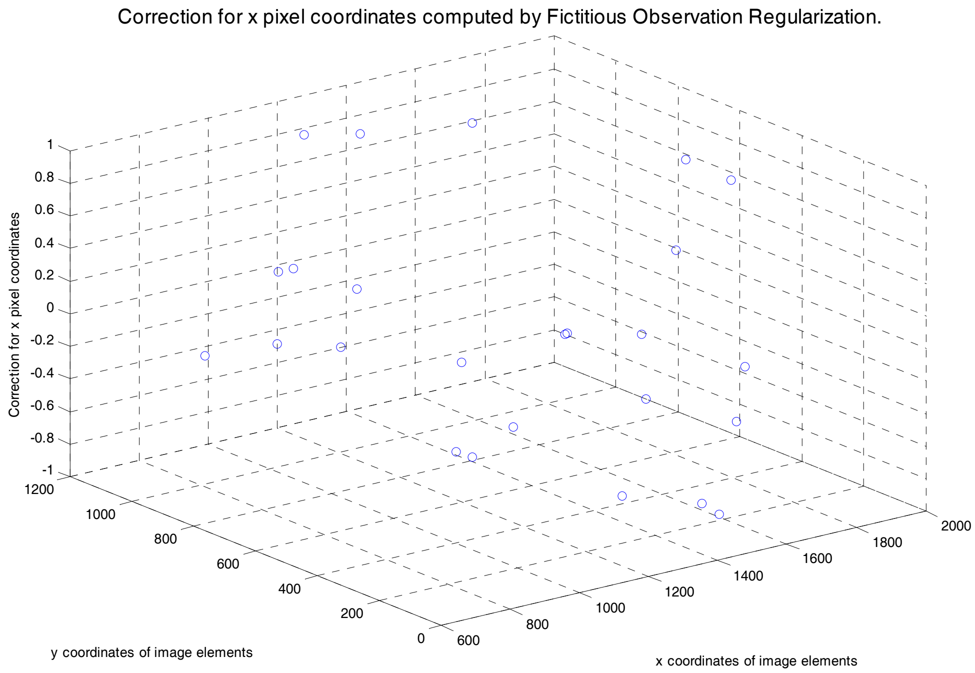

Figure 6.1 x pixel corrections computed by fictitious observation

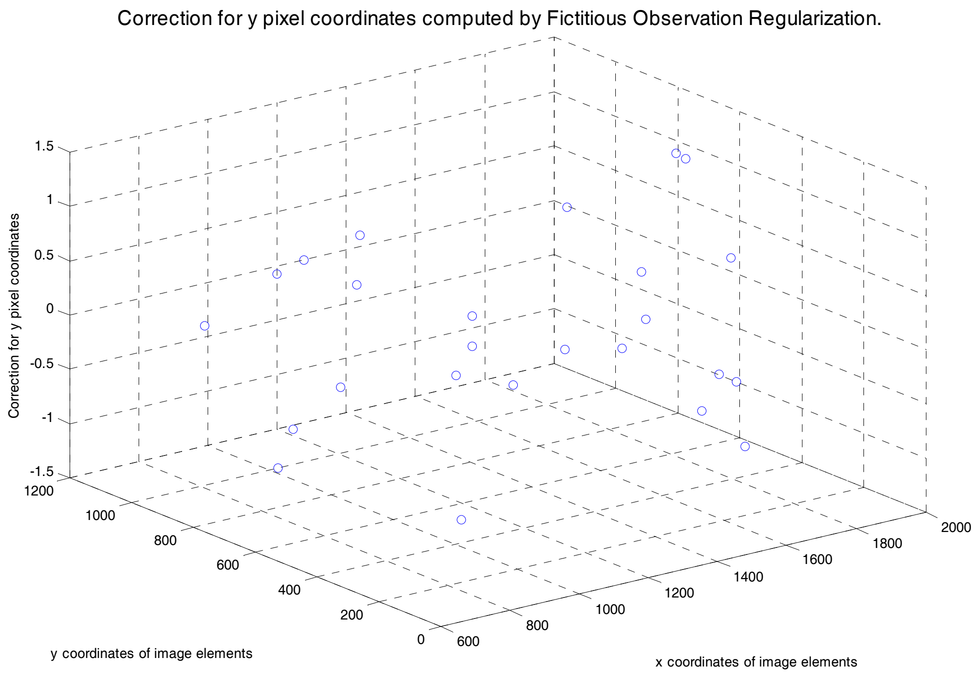

Figure 6.2 y pixel corrections computed by fictitious observation

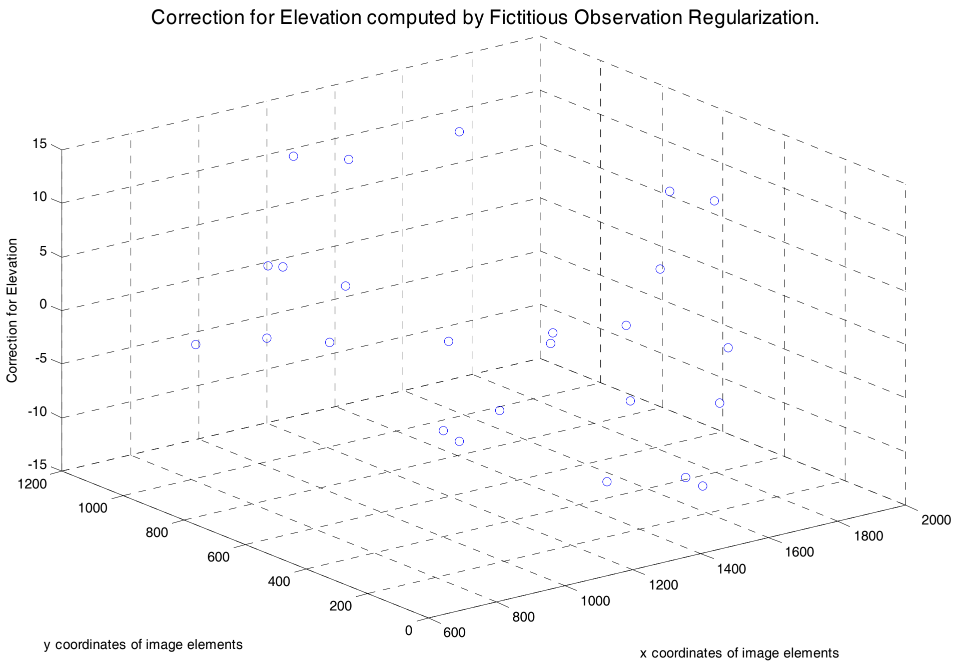

Figure 6.3 Elevation corrections computed by fictitious observation

6.1.2 Implementation of Parameter Estimation with Tikhonov Regularization

For the implementation of Tikhonov regularization 12x12 identity matrix is used to regularize the equation. For the Tikhonov parameter α , 0.0003 is assigned. The selection of Tikhonov parameter has considerable effect on the solution. Selection of too small Tikhonov parameter can not reqularize the solution properly on the other hand selection of too large Tikhonov parameter will slow down the solution and the iteration may not converge.

The assigned Tikhonov parameter can be accepted as a proper value since it reduced the condition number significantly and the problem converged at the end of 487 iterations. Residuals of parameter estimation with Tikhonov regularization is presented in Figure 6.4 to 6.6 (Table B2 and Table B7,8,9).

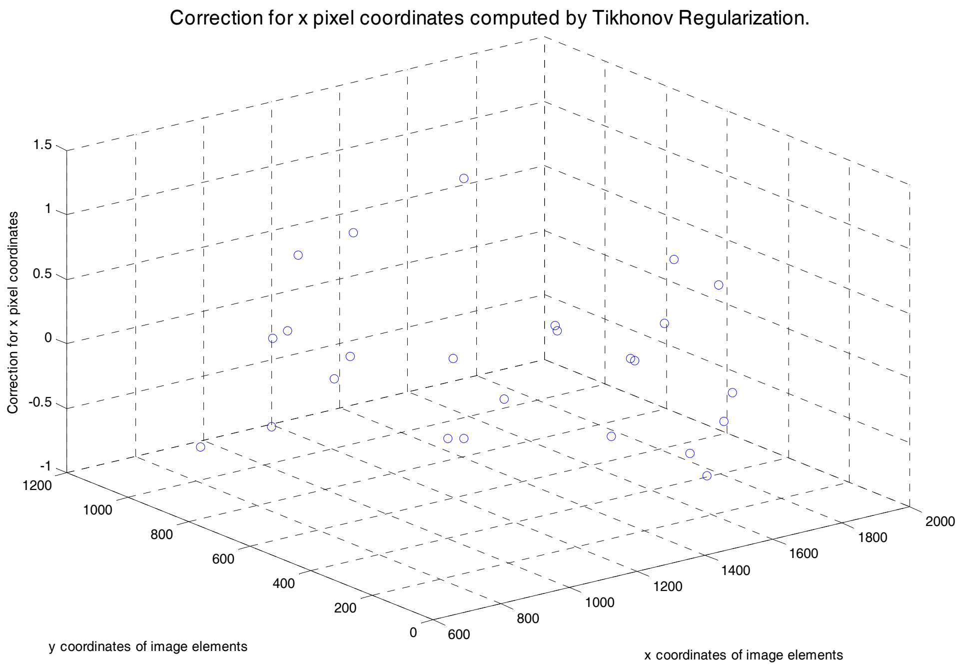

Figure 6.4 x pixel coordinate corrections computed by Tikhonov regularization

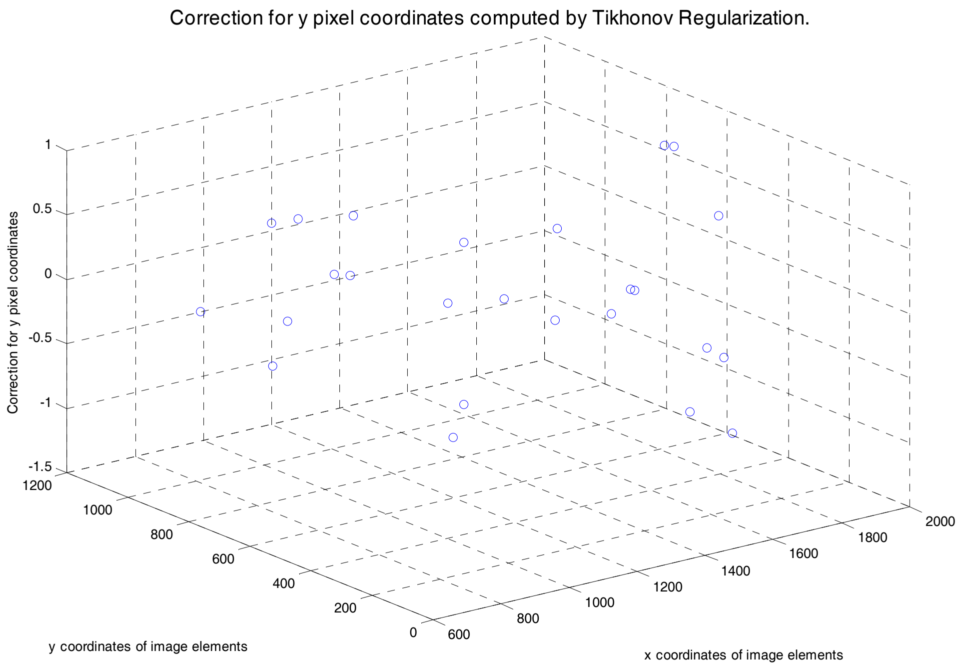

Figure 6.5 y pixel coordinate corrections computed by Tikhonov regularization

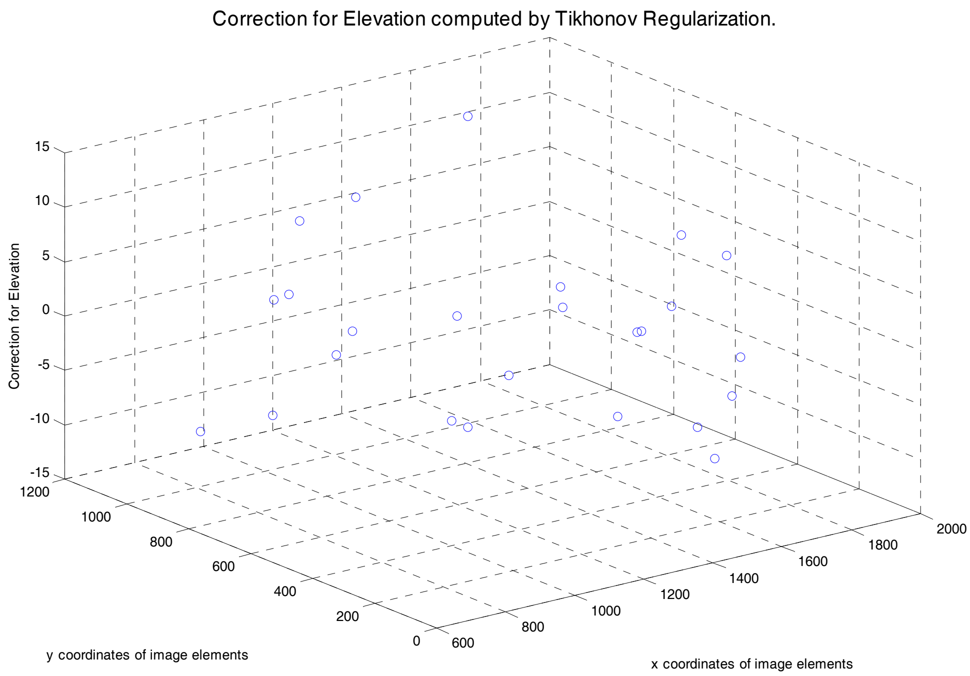

Figure 6.6 Elevation corrections computed by Tikhonov regularization

6.1.3 Implementation of Parameter Estimation with SVD

For the implementation of SVD Tikhonov parameter is assigned as 0.0003 which is same with the Tikhonov regularization. For the standard values of the parameters the variances assigned in fictitious observation regularization are used. Convergence of SVD was very fast at the end of 2 iterations the equation converged. Residuals of parameter estimation with SVD is presented in Figure 6.7 to 6.9 (Table B3 and B10,11,12).

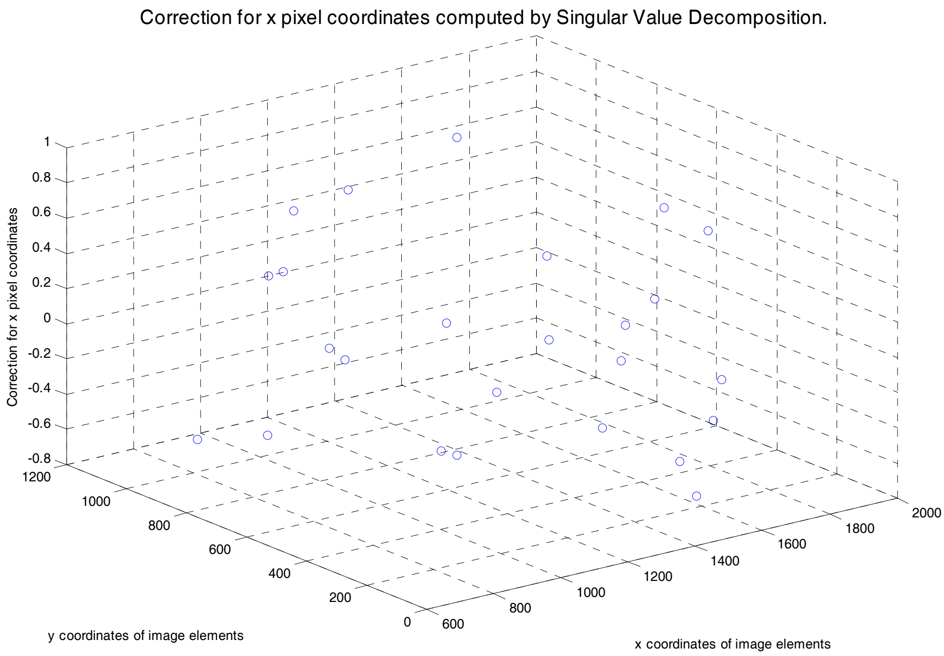

Figure 6.7 x pixel coordinate corrections computed by SVD

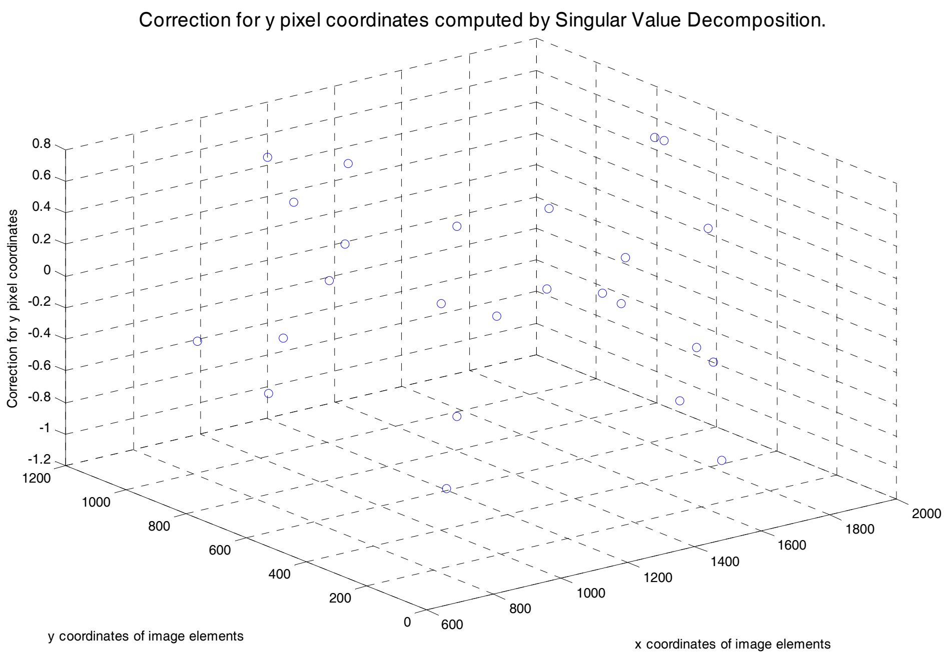

Figure 6.8 y pixel coordinate corrections computed by SVD

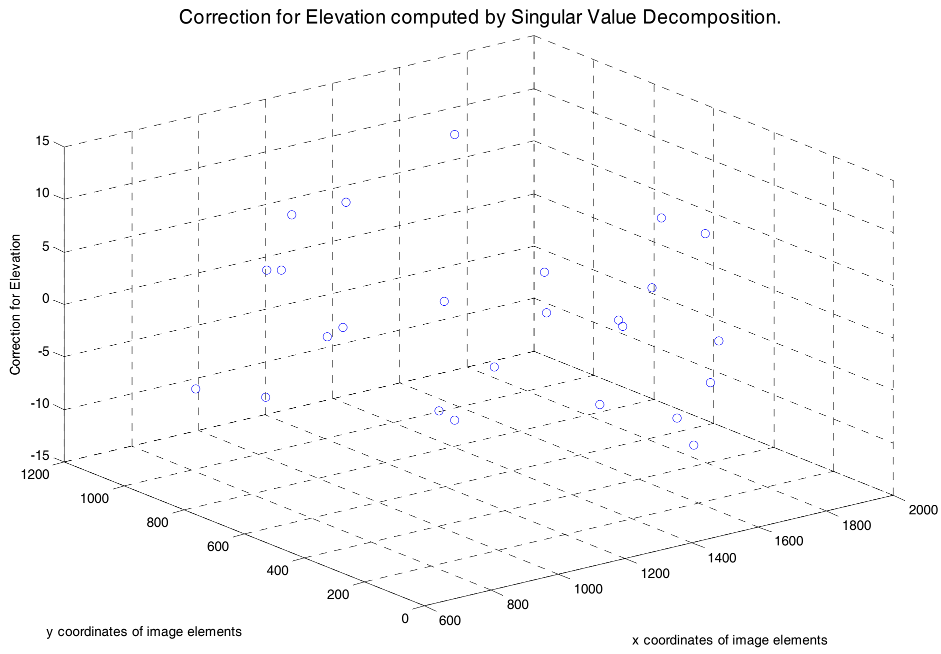

Figure 6.9 Elevation corrections computed by SVD

When the residuals obtained at the end of the three different regularization procedures are examined it is seen that the most pleasing results are obtained with Tikhonov regularization. When the theory behind the regularization methods is examined it is seen that the Tikhonov regularization and fictitious observations are very similar to each other but Tikhonov regularization has no restriction on the corrections of parameters. However, the fictitious observation method requires cofactor matrix of the parameters while Tikhonov regularization requires only an identity matrix whose size is same with the parameter number. For this reason it can be thought that the computed corrections to parameters are weighted according to the variances of the parameters in fictitious observations while there is no weight applied to parameters in Tikhonov regularization.

By considering this it can be easily predicted that, Tikhonov regularization will converge to a minimum in the error space much faster than fictitious observation method. However, since the corrections to parameters are computed without considering the variance of the parameters, the resulting corrections may not be realistic. At least it can be said that fictitious observations can correct the initial values of the parameters better although the residuals are higher. For the implementation of the new orthorectification, parameter estimation results of Tikhonov regularization is used since the initial values of the parameters were very far from their true values so that obtaining their true value were almost impossible.

Singular Value Decomposition (SVD) is the most complicated method among the three. The convergence of SVD is faster than both Tikhonov regularization and fictitious observations. However, in SVD α and variance of the parameters must be determined very carefully if this is ignored the method may diverge. This can be considered as the drawback of the method since the remaining methods always converge unless α is selected too small. While faster convergence of SVD can be considered as its advantage. In order to assure the convergence of SVD solution, α is chosen a little larger, thus the convergence of the method slowed down and residuals increased. Smallest residuals are obtained by SVD regularization, but estimated parameter values were not pleasing compared with other two regularization methods.

Not all of the parameters obtained at the end of the parameter estimation procedure were realistic. To acquire the true value for parameters some restrictions are applied to the parameters. It is known that the average ground resolution of Bilsat image is 27.6 meter. By using this information a relationship is established in between focal length, size of the sensing element and satellite altitude. Because of this restriction camera position and focal length were not allowed to change freely and at the end of the parameter estimation more realistic results are obtained. As expected, residuals of the parameter estimation at the end of the parameter estimation with restriction were higher than the estimation without restriction. This does not mean that the parameter estimation is unsuccessful. It means, the parameter estimation performed by using Tikhonov regularization has converged to a minima which is not the true minima.

6.2 Gauss Markoff Model not of full rank with constraints

Besides using regularization, restrictions to parameters are applied to solve the system correctly. Apart from the effort to prevent the rank deficiency, because of the correlations between the parameters, equation system has rank deficiency and the equation system is named as, "Gauss-Markoff Model not of full rank with constraints". In this system

$$\mathbf{X}\boldsymbol{\beta} = E(y) \qquad \text{with rank X = q < u,} \tag{6.1}$$

$\boldsymbol{H}\,\boldsymbol{\beta} = w$ and D(y) = σ^2 $\boldsymbol{I}$

where

$\boldsymbol{\beta}$ is 12x1 matrix including the parameters

$$\boldsymbol{\beta} = \left[\phi_s \quad \lambda_s \quad \omega \quad \phi \quad \kappa \quad f \quad \Delta x \quad \Delta y \quad k_1 \quad k_2 \quad p_1 \quad p_2\right]'_{12\times 1} \tag{6.2}$$

$$X=\begin{bmatrix} \frac{\partial\phi_1}{\partial\phi_s} & \frac{\partial\phi_1}{\partial\lambda_s} & \frac{\partial\phi_1}{\partial\omega} & \frac{\partial\phi_1}{\partial\phi} & \frac{\partial\phi_1}{\partial\kappa} & \frac{\partial\phi_1}{\partial f} & \frac{\partial\phi_1}{\partial\Delta x} & \frac{\partial\phi_1}{\partial\Delta y} & \frac{\partial\phi_1}{\partial k_1} & \frac{\partial\phi_1}{\partial k_2} & \frac{\partial\phi_1}{\partial p_1} & \frac{\partial\phi_1}{\partial p_2} \\ \frac{\partial\lambda_1}{\partial\phi_s} & \frac{\partial\lambda_1}{\partial\lambda_s} & \frac{\partial\lambda_1}{\partial\omega} & \frac{\partial\lambda_1}{\partial\phi} & \frac{\partial\lambda_1}{\partial\kappa} & \frac{\partial\lambda_1}{\partial f} & \frac{\partial\lambda_1}{\partial\Delta x} & \frac{\partial\lambda_1}{\partial\Delta y} & \frac{\partial\lambda_1}{\partial k_1} & \frac{\partial\lambda_1}{\partial k_2} & \frac{\partial\lambda_1}{\partial p_1} & \frac{\partial\lambda_1}{\partial p_2} \\ \vdots & \vdots & \vdots & \vdots & \vdots & \vdots & \vdots & \vdots & \vdots & \vdots & \vdots & \vdots \\ \frac{\partial\phi_n}{\partial\phi_s} & \frac{\partial\phi_n}{\partial\lambda_s} & \frac{\partial\phi_n}{\partial\omega} & \frac{\partial\phi_n}{\partial\phi} & \frac{\partial\phi_n}{\partial\kappa} & \frac{\partial\phi_n}{\partial f} & \frac{\partial\phi_n}{\partial\Delta x} & \frac{\partial\phi_n}{\partial\Delta y} & \frac{\partial\phi_n}{\partial k_1} & \frac{\partial\phi_n}{\partial k_2} & \frac{\partial\phi_n}{\partial p_1} & \frac{\partial\phi_n}{\partial p_2} \\ \frac{\partial\lambda_n}{\partial\phi_s} & \frac{\partial\lambda_n}{\partial\lambda_s} & \frac{\partial\lambda_n}{\partial\omega} & \frac{\partial\lambda_n}{\partial\phi} & \frac{\partial\lambda_n}{\partial\kappa} & \frac{\partial\lambda_n}{\partial f} & \frac{\partial\lambda_n}{\partial\Delta x} & \frac{\partial\lambda_n}{\partial\Delta y} & \frac{\partial\lambda_n}{\partial k_1} & \frac{\partial\lambda_n}{\partial k_2} & \frac{\partial\lambda_n}{\partial p_1} & \frac{\partial\lambda_n}{\partial p_2} \end{bmatrix}$$

Biased estimator $\tilde{\tilde{\beta}}$ of β is obtained by [53]

$$\tilde{\tilde{\beta}}=(\boldsymbol{X'X})^{-}\left[\boldsymbol{X'y}+\boldsymbol{H'}\left(\boldsymbol{H}(\boldsymbol{X'X})^{-}\boldsymbol{H'}\right)^{-1}\left(w-\boldsymbol{H}(\boldsymbol{X'X})^{-}\boldsymbol{X'y}\right)\right] \tag{6.3}$$

or by

$$\tilde{\tilde{\beta}}=\overline{\beta}-(\boldsymbol{X'X})^{-}\boldsymbol{H'}\left(\boldsymbol{H}(\boldsymbol{X'X})^{-}\boldsymbol{H'}\right)^{-1}\left(\boldsymbol{H}\overline{\beta}-w\right) \tag{6.4}$$

where

$$\overline{\beta}=(\boldsymbol{X'X})^{-}\boldsymbol{X'y} \tag{6.5}$$

$(\boldsymbol{X'X})^{-}$ is the pseudo inverse of $\boldsymbol{X'X}$

Residuals are defined by

$$\tilde{\boldsymbol{e}}=\boldsymbol{X}\tilde{\tilde{\beta}}-y \tag{6.6}$$

$$D(\tilde{\boldsymbol{e}})=\sigma^2\left[\boldsymbol{I}-\boldsymbol{X}(\boldsymbol{X'X})^{-}\boldsymbol{X'}+\boldsymbol{X}(\boldsymbol{X'X})^{-}\boldsymbol{H'}\left(\boldsymbol{H}(\boldsymbol{X'X})^{-}\boldsymbol{H'}\right)^{-1}\boldsymbol{H}(\boldsymbol{X'X})^{-}\boldsymbol{X'}\right] \tag{6.7}$$

where

$$\sigma^2=\frac{1}{n}\left(y-\boldsymbol{X}\tilde{\tilde{\beta}}\right)'\left(y-\boldsymbol{X}\tilde{\tilde{\beta}}\right)=\frac{1}{n}\Omega_H \tag{6.8}$$

$$\Omega_H=\left(y-\boldsymbol{X}\tilde{\tilde{\beta}}\right)'\left(y-\boldsymbol{X}\tilde{\tilde{\beta}}\right)+\left(\tilde{\tilde{\beta}}-\overline{\beta}\right)'\boldsymbol{X'X}\left(\tilde{\tilde{\beta}}-\overline{\beta}\right) \tag{6.9}$$

$$\sigma^2=\frac{\Omega_H}{(n-q+r)} \tag{6.10}$$

is an unbiased estimator of the variance of unit weight.

As a restriction equation, with the help of the Bilsat geometry a relationship between the satellite altitude, focal length, size of the sensor on the CCD array and ground resolution of the Bilsat is derived.

$$G=\frac{f_o H}{c} \tag{6.11}$$

where

G is the ground resolution of Bilsat
f_o is the focal length computed from the restriction equation
H is the altitude of the satellite
c is the size of the sensing element on the CCD camera

In this equation G is assigned as a fixed value equal to 28.8 meter. H is computed by the corrected position at the current step of the parameter estimation procedure, c is also a constant value equal to 0.0074 mm. Restriction equation (See Equation 6.1) is written as

$$H\beta = w = f_o - f \tag{6.12}$$

The restriction equation w represents the required value to be added to the focal length to satisfy the restriction equation while, the linearized Gauss Helmert model computes the corrections to be added to the initial values of the parameters. So the restriction equation has the correction amount to be added to focal length to satisfy the restriction equation.

Solution results of the Gauss-Markoff Model not of full rank with constraints are given in Appendix B in Table B.13 and Table B14. Results of the Gauss Markoff Model with constraint were worse than unconstrained solution. This is an expected result since in order to satisfy the constraint the solution of the model will shift from the minimum sum of the square of residuals.

6.3 Test for Outliers

A test for outliers ε has been performed to make sure that there is not any blunder in the measured ground coordinates or image coordinates. The outlier test procedure is as follows

$$N = X^T PX \tag{6.13}$$

$$Q_{xx} = N^{-1} \tag{6.14}$$

$$Q_{ll} = XQ_{xx}X^T \tag{6.15}$$

$$r_i = 1 - P_i \overline{Q}_{ll} \tag{6.16}$$

$$\nabla l_i = \frac{-e_i}{r_i} \tag{6.17}$$

$$\nabla_0 l_i = \frac{\sigma_i \delta_0}{\sqrt{r_i}} \tag{6.18}$$

$$\sigma_i = \sigma_0 \sqrt{P_i} \tag{6.19}$$

$$\sigma_0 = \sqrt{\frac{e^T Pe}{n-u}} \tag{6.20}$$

$$\delta_{0i} = \delta_0 \sqrt{\frac{1-r_i}{r_i}} \tag{6.21}$$

where

Q_{xx} is the cofactor matrix of parameters

Q_{ll} is the cofactor matrix of the observations

r_i is the redundancy of the i^{th} observation

∇l_i is the probable error of the i^{th} observation

$\nabla_0 l_i$ is the internal reliability of the i^{th} observation

σ_0 is the variance

σ_i is the variance of the i^{th} observation

δ_{0i} is the network anomaly

δ_0 is equal to 4.13 for $\alpha_0 = 0.001$ $\quad \gamma_0 = 0.80$ *test power*

$$\nabla_0 x_i = Q_{xx} x_i^T P_i \nabla_0 l_i \tag{6.22}$$

where

x_i^T is the i^{th} row of the X matrix

P_i is the weight of the i^{th} observation

$$\overline{v}_i = \frac{|v_i|}{\sigma_0 \sqrt{Qv_i v_i}} \tag{6.23}$$

$$Qv_i v_i = \frac{1}{P_i} - \overline{Q}_{ii} \tag{6.24}$$

$$\overline{v}_i = \frac{|v_i|}{\sigma_0 \sqrt{Qv_i v_i}} \tag{6.25}$$

Results of outlier test are given in Appendix B. The outlier test covers 25 ground points. Since each point is represented as latitude and longitude the test is performed for 50 ground coordinates. As explained in Chapter 3 ground points are measured by means of a hand GPS receiver and the expected accuracy of the ground coordinates are 15 meters. Each point is measured by the same method and there was not any obstruction on the terrain for the GPS signal, same weights are assigned for the ground points.

By using the Equations 6.13 to 6.15 corrected measurements' weight matrix is computed. $\overline{Q}_{ii}$ contains the diagonal elements of this matrix. Degree of freedom of each measurement, r_i is computed by $\overline{Q}_{ii}$ and weight of the measurement. With the r_i values of each measurement, condition of each measurement can be commented. It is required that each measurement has r_i value greater than 0.3 to 0.5, fortunately every measurements' r_i values satisfy the requirements. Probable error of each measurement ∇l_i, are computed by the Equation 6.17 and the lowest error limit of each measurement $\nabla_0 l_i$, is computed by the Equation 6.18. $\nabla_0 l_i$ represents the internal reliability of the measurements. These numbers are required to be smaller and have close values. When the error limits of the measurements are examined (Table B.32), it is seen that the values and range are very small. This shows that the measurements are reliable. Finally by using Equation 6.21 δ_{0i}, network anomaly is computed. δ_{0i} is used for the prediction of the maximum effect of error ($\nabla_0 l_i$), on the function. For this reason, the smaller the δ_{0i} values, the better the parameter estimation results. When the δ_{0i} values are examined in Table B.32, it is seen that they are relatively large. This can be explained as the errors in the measurements are small but their effects on the parameter estimation results are significant. This can be explained by the very sensitive analytic relationship between the parameters and the observation. For this reason condition number of the variance covariance matrix is very high.

Additionally, conformity of the measurements is examined by using Equations 6.23 to Equation 6.25. The analysis results are presented in Table B.33. Since all standardized residuals are smaller than 1.96 it can be said that all measurements are concordant. The analyses are performed for $\alpha_0 = 0.001$ and test power as $\gamma_0 = 0.80$.

6.4 Implementation of Tikhonov Regularization for Pushbroom Scanner

ASTER image obtained for the implementation and accuracy assessment of the algorithm had no position and orientation data. For this reason the camera position and the camera attitude were to be determined by a parameter estimation procedure. Some of the parameters mentioned in Chapter 4 have been changed in this procedure since there were no initial data for position and attitude of the camera. Position of the camera has been determined by means of Kepler parameters instead of a second order polynomial. 3 of the 6 Kepler parameters were known for ASTER orbit these are;

Semimajor axis a
Eccentricity e
Inclination i

The remaining 3 parameters are determined by the following procedure;

The raw image is registered by affine transformation. For initial approximation the satellite's attitude angles are assumed to be zero and an initial position of the camera is obtained from the first and second lines, then the satellites velocity is predicted assuming that the time difference of the acquisition of one line is 0.0022 second. The obtained velocity and position is in S_E in order to compute Kepler parameters they should be transformed into S_I.

After obtaining camera position and velocity in S_I, the Kepler parameters are computed by the following formulae [80];

$$H = r \times v \tag{6.26}$$

where;

r is the position vector with respect to S_I

v is the velocity vector with respect to S_I

$$\Omega = \tan^{-1}\left(\frac{H_x}{-H_y}\right) \tag{6.27}$$

where;

H_x is the first element of H

H_y is the second element of H

Ω is the right ascension of the ascending node of the orbit

$$i = \tan^{-1}\left(\frac{\sqrt{H_x^2 + H_y^2}}{H_z}\right) \tag{6.28}$$

where;

i is the inclination

H_x is the third element of H

Inclination angle of ASTER orbit is known as 98.88° and inclination angle is not computed but it is taken as equal to 98.88° [81].

$$P = R_1(i) R_3(\Omega) r \tag{6.29}$$

where;

$$R_1(i) = \begin{bmatrix} 1 & 0 & 0 \\ 0 & \cos i & \sin i \\ 0 & -\sin i & \cos i \end{bmatrix}$$

$$R_3(\Omega) = \begin{bmatrix} \cos\Omega & \sin\Omega & 0 \\ -\sin\Omega & \cos\Omega & 0 \\ 0 & 0 & 1 \end{bmatrix}$$

$$\omega + \nu = \tan^{-1}\left(\frac{P_2}{P_1}\right) \tag{6.30}$$

where

ω argument of perigee

ν is true anomaly

P_2 is second element of P

P_1 is first element of P

Semimajor axis and eccentricity is computed by the following formulae;

$$a = \frac{\|r\|}{2 - \left(\|r\|\|v\|^2 / \mu\right)} \tag{6.31}$$

$$e = \sqrt{1 - \|H\|^2 / \mu a} \tag{6.32}$$

where

μ is GM which is equal to 3.986005e14

However a and e are known a priori and 7078000 meter and 0.0012 are assigned for semimajor axis and eccentricity respectively [81].

E is computed from the formulae

$$\sin E = \frac{r \bullet v}{e\sqrt{\mu a}} \tag{6.33}$$

$$\cos E = \frac{a - \|r\|}{ae} \tag{6.34}$$

$$E = \tan^{-1}\left(\frac{\sin E}{\cos E}\right) \tag{6.35}$$

True anomaly can be computed as

$$f = \tan^{-1}\left(\frac{\sqrt{1-e^2}\,\sin E}{\cos E - e}\right) \tag{6.36}$$

Finally ω can be computed as

$$\omega = (\omega + \nu) - \nu \tag{6.37}$$

This completes the six Kepler elements. However, the computed Kepler parameters do not represent the true orbit because the velocity estimation was not proper so the computed three Kepler parameters are corrected by a parameter estimation procedure. In order to simplify the parameter estimation procedure only right ascension and true anomaly is corrected in an iterative manner.

$$\Delta\beta = \left(X^T X\right)^{-1} X^T \Delta y \tag{6.38}$$

where;

$$\Delta\beta = \begin{bmatrix} \Delta f \\ \Delta\Omega \end{bmatrix}$$

$$X = \begin{bmatrix} \dfrac{\partial\phi_{1sat}}{\partial f} & \dfrac{\partial\phi_{1sat}}{\partial\Omega} \\ \dfrac{\partial\lambda_{1sat}}{\partial f} & \dfrac{\partial\lambda_{1sat}}{\partial\Omega} \\ \dfrac{\partial\phi_{2sat}}{\partial f} & \dfrac{\partial\phi_{2sat}}{\partial\Omega} \\ \dfrac{\partial\lambda_{2sat}}{\partial f} & \dfrac{\partial\lambda_{2sat}}{\partial\Omega} \end{bmatrix}$$

$$\Delta y = \begin{bmatrix} \phi_1 - \phi_{1c} \\ \lambda_1 - \lambda_{1c} \\ \phi_2 - \phi_{2c} \\ \lambda_2 - \lambda_{2c} \end{bmatrix}$$

subscript c in λ_{ic} and ϕ_{ic} indicates ith computed coordinate.

The iteration continues until changes in true anomaly and right ascension becomes smaller than a specified threshold value. The relation between the Kepler parameters and satellite coordinates are set by the following relationship;

Cartesian camera coordinates are obtained by the following relationship

$$\overset{E}{\mathbf{r}} = \overset{E}{\mathbf{R}}_{\mathbf{I}} \overset{I}{\mathbf{r}} \tag{6.39}$$

where;

$\overset{E}{\mathbf{r}}$ is the position vector with respect to S_E

$\overset{E}{\mathbf{R}}_{\mathbf{I}}$ is the rotation matrix transforms the position vector from S_I to S_E computation of $\overset{E}{\mathbf{R}}_{\mathbf{I}}$ is explained in Chapter 4.

$\overset{I}{\mathbf{r}}$ is the position vector with respect to S_I computed by the following equation

$$\overset{I}{\mathbf{r}} = \begin{bmatrix} \overset{I}{X} \\ \overset{I}{Y} \\ \overset{I}{Z} \end{bmatrix} = \overset{I}{\mathbf{R}}_{\mathbf{B}} \overset{B}{\mathbf{r}} \tag{6.40}$$

where;

$\overset{I}{\mathbf{R}}_{\mathbf{B}}$ is the rotation matrix that transforms from S_B to S_I

Construction of $\overset{I}{\mathbf{R}}_{\mathbf{B}}$ is as following

$$\overset{I}{\mathbf{R}}_{\mathbf{B}} = \mathbf{R}_2(\omega + j + \pi/2)\mathbf{R}_1(i + \pi/2)\mathbf{R}_3(\Omega)$$

where;

$$\mathbf{R}_2(\omega + j + \pi/2) = \begin{bmatrix} \cos(\omega + j + \pi/2) & 0 & -\sin(\omega + j + \pi/2) \\ 0 & 1 & 0 \\ \sin(\omega + j + \pi/2) & 0 & \cos(\omega + j + \pi/2) \end{bmatrix}$$

$$\mathbf{R}_1(i + \pi/2) = \begin{bmatrix} 1 & 0 & 0 \\ 0 & \cos(i + \pi/2) & \sin(i + \pi/2) \\ 0 & -\sin(i + \pi/2) & \cos(i + \pi/2) \end{bmatrix}$$

$$\mathbf{R}_3(\Omega) = \begin{bmatrix} \cos\Omega & \sin\Omega & 0 \\ -\sin\Omega & \cos\Omega & 0 \\ 0 & 0 & 1 \end{bmatrix}$$

$\overset{B}{\mathbf{r}}$ is the satellite position vector with respect to S_B derivation of $\overset{B}{\mathbf{r}}$ is as following

$$\overset{B}{\mathbf{r}} = \begin{bmatrix} 0 \\ 0 \\ S \end{bmatrix} \tag{6.41}$$

where;

S is the distance from earth center to satellite and computed as

$$S = a(1 - e\cos E) \tag{6.42}$$

At the end of the parameter estimation Kepler orbit parameters are estimated more accurately. However, it is very rare that the satellite's attitude and camera have no inclination. So the computed Kepler parameters are still needs to be corrected. By using the GCPs; satellite attitude, attitude change rate, camera attitude and camera attitude change rate, camera focus, principle point and satellite position will be estimated by a parameter estimation procedure.

In the parameter estimation procedure the following parameters will be estimated.

$$\beta = \left[\nu\ \Omega\ a_1'\ a_2'\ a_3'\ a_4'\ \dot{a}_1\ \ddot{a}_1\ \dot{a}_2\ \ddot{a}_2\ \dot{a}_3\ \ddot{a}_3\ \dot{a}_4\ \ddot{a}_4\ \phi_s\ \dot{\phi}_s\ \ddot{\phi}_s\ \lambda_s\ \dot{\lambda}_s\ \ddot{\lambda}_s\ f\ \Delta y\ k_1\right]$$

where

ν is the true anomaly

Ω is the right ascension of the ascending node
a'_1 is the roll angle between S_O and S_B
a'_2 is the pitch angle between S_O and S_B
a'_3 is the yaw angle between S_O and S_B
a'_4 is the attitude angle of the camera between S_B and S_C
$\dot{a}_1$ is the change in roll angle with time
$\dot{a}_2$ is the change in pitch angle with time
$\dot{a}_3$ is the change in yaw angle with time
$\dot{a}_4$ is the change in attitude angle of the camera
$\ddot{a}_1$ is the change rate in roll angle with time
$\ddot{a}_2$ is the change rate in pitch angle with time
$\ddot{a}_3$ is the change rate in yaw angle with time
$\ddot{a}_4$ is the change rate in attitude angle of the camera
ϕ_s is position correction for the camera latitude
$\dot{\phi}_s$ is the position correction rate for the camera latitude
$\ddot{\phi}_s$ is the position correction change rate for the camera latitude
λ_s is position correction for the camera longitude
$\dot{\lambda}_s$ is the position correction rate for the camera longitude
$\ddot{\lambda}_s$ is the position correction change rate for the camera longitude
f is the focal length of the camera (mm)
Δy is the principal point coordinate on the pushbroom scanner
k_1 is the radial lens distortion parameter

In the parameter estimation procedure, since GCPs are not imaged at the same time satellite position should be recomputed for each GCP. To compute mean anomaly, time difference between the perigee passage and the image acquisition should be computed. Mean anomaly at the beginning of the image acquisition is estimated by the following formula

$$M = E - e\sin E \tag{6.43}$$

where
M is the mean anomaly
E is eccentric anomaly
e is the eccentricity of the orbit

Time difference between the beginning of the image acquisition and time of the imaging of the GCP is computed as

$$\Delta t = 0.0022 * y \tag{6.44}$$

where;
y is the row number of the image

Change in mean anomaly is computed by the formula

$$\Delta M = \frac{2\pi\Delta t}{\tau} \tag{6.45}$$

where;

$$\tau = 2\pi\sqrt{\frac{a^3}{\mu}} \tag{6.46}$$

where;
τ is the orbit period
a is the semimajor axis of the orbit
μ is GMe 3.986005e14m^3/s^2

Mean anomaly at the time of the acquisition of the GCP is computed as

$$M_i = M + \Delta M \tag{6.47}$$

At this step Eccentric anomaly should be computed. But this requires a solution of nonlinear equation. The eccentric anomaly is computed iteratively by Newton method. Iterative method can be represented as [81];

$$E_{i+1} = E_i - \frac{E_i - e\sin E_i - M}{1 - e\cos E_i} \tag{6.48}$$

In this problem an initial value is required for eccentric anomaly; to start the iteration eccentric anomaly at the beginning of the image acquisition is taken.

True anomaly and distance between satellite and Earth center is computed from the Equation 6.36 and 6.41. Then the Equation 6.38 and 6.39 are applied to compute satellite position in S_E. Cartesian camera position is converted to geodetic coordinates by means of the iterative method and correction to camera position is applied by the following formulae

$$\begin{aligned} \phi_s &= \phi_s + \phi_0 + \dot{\phi}_0\Delta t + \ddot{\phi}_0\Delta t^2 \\ \lambda_s &= \lambda_s + \lambda_0 + \dot{\lambda}_0\Delta t + \ddot{\lambda}_0\Delta t^2 \end{aligned} \tag{6.49}$$

After computing the corrected satellite position, the next step is to compute the intersection point of the image direction vector and WGS84 reference ellipsoid. Direction vector of the line between camera focus and corresponding sensing element with respect to S_C can be written as;

$$\overset{C}{D} = \begin{bmatrix} 0 \\ (x - width/2) * c \\ -f \end{bmatrix} / \sqrt{((x - width/2) * c)^2 + f^2} \tag{6.50}$$

where;

x is the x coordinate of the corresponding picture element in S_{IM}

width is the number columns in the image

c is the size of the sensing element 0.007 mm

f is the focal length of the camera

Transformation from S_C to S_B is performed in two steps; at first step camera system is rotated 180° with respect to x axis and then rotated a_4°. The transformation can be shown as

$$\overset{B}{D} = \overset{B}{R}_C \overset{C}{D} \tag{6.51}$$

where;

$\overset{B}{R}_C$ is the rotation matrix for the transformation from S_C to S_B which can be written as

$$\overset{B}{R}_C = R_1(a_4) R_1(\pi) \tag{6.52}$$

$$a_4 = a_4' + \dot{a}_4 \Delta t + \ddot{a}_4 \Delta t^2$$

The next transformation is from S_B to S_O. This transformation is performed by three successive rotations in the order of y, x and z axes respectively. The transformation can be written as

$$\overset{O}{D} = \overset{O}{R}_B \overset{B}{D} \tag{6.53}$$

where;

$\overset{O}{R}_B$ is the rotation matrix for the transformation from S_B to S_O. The rotation matrix can be written as;

$$\overset{O}{R}_B = R_3(a_3) R_1(a_1) R_2(a_2) \tag{6.54}$$

$$a_1 = a_1' + \dot{a}_1 \Delta t + \ddot{a}_1 \Delta t$$

$$a_2 = a_2' + \dot{a}_2 \Delta t + \ddot{a}_2 \Delta t$$

$$a_3 = a_3' + \dot{a}_3 \Delta t + \ddot{a}_3 \Delta t$$

Rotation from S_O to S_E and intersection of the direction vector with WGS84 ellipsoid and relief displacement corrections are same with the CCD camera model and procedure is explained in

Chapter 4.2. Finally, a mathematical model is established between image points and corresponding ground point.

The parameters in the model are not known, since there is no attitude information or any a priori information about the interior camera parameters. In order to start the parameter estimation procedure initial values for the unknown parameters is assumed as "0". Then all parameters are corrected after the parameter estimation procedure. The general equation for the parameter estimation can be written as;

$$\Delta\beta = (X'X)^{-1} X\Delta y \tag{6.55}$$

where;

$\Delta\beta$ is the corrections for the parameters

Δy is the array of the difference between measured coordinates and computed coordinates of the GCPs.

$$X = \begin{bmatrix} \frac{\partial\phi_1}{\partial v} & \frac{\partial\phi_1}{\partial\Omega} & \cdots & \frac{\partial\phi_1}{\partial\Delta y} & \frac{\partial\phi_1}{\partial k_1} \\ \frac{\partial\lambda_1}{\partial v} & \frac{\partial\lambda_1}{\partial\Omega} & \cdots & \frac{\partial\lambda_1}{\partial\Delta y} & \frac{\partial\lambda_1}{\partial k_1} \\ \vdots & \vdots & \ddots & \vdots & \vdots \\ \frac{\partial\phi_n}{\partial v} & \frac{\partial\phi_n}{\partial\Omega} & \cdots & \frac{\partial\phi_n}{\partial\Delta y} & \frac{\partial\phi_n}{\partial k_1} \\ \frac{\partial\lambda_n}{\partial v} & \frac{\partial\lambda_n}{\partial\Omega} & \cdots & \frac{\partial\lambda_n}{\partial\Delta y} & \frac{\partial\lambda_n}{\partial k_1} \end{bmatrix}_{2n\times 23}$$

Solution for the least square estimation requires computing the matrix inverse. Because of the correlation between parameters and weak geometry of the camera the condition number of the matrix is very high meaning that an accurate solution is impossible. For this reason Tikhonov regularization method is applied to the model and Equation 6.55 becomes

$$\Delta\beta = (X'X + \alpha I)^{-1} X\Delta y \tag{6.56}$$

where;

α is the Tikhonov regularization number

I is the identity matrix of size 23x23

Convergence of the algorithm was very slow because of the regularization procedure. Furthermore, because of the correlations between parameters, all parameters are not estimated at the same time. Attitude parameters and orbit parameters are estimated separately. This was the second factor that slows down the convergence. In order to reduce Δy below the threshold value, 2500 iterations are performed. The computation amount for the algorithm is very demanding. At the of the parameter estimation, following values for the parameters are computed;

Table 6.1 Estimated values of the parameters of the pushbroom model.

Parameter	Estimated Value
True Anomaly	1,54258
Right Ascension	-1,30976
Roll	-0,12800
Pitch	-0,18933
Yaw	-0,09060
Theta	0,13727
Roll Rate	9,711E-08
Roll Rate Change	-1,559E-08
Pitch Rate	8,338E-10
Pitch Rate Change	-1,160E-06
Yaw Rate	2,753E-07
Yaw Rate Change	-2,491E-08
Theta Rate	-0,00369
Theta Rate Change	0,00141
Phi Anomaly	0,00069
Phi A. Rate	-2,082E-04
Phi A. Rate Change	0,00374
Lambda Anomaly	-6,333E-04
L. A. Rate	-0,00262
L. A. Rate Change	0,00126
Focal Length	330,00003
Principle Point	-1,525E-05
Lens Par	-7,112E-05

Residuals of the GCPs and corrected GCP coordinates are presented in Appendix B.

6.5 Implementation of DRM for CCD Frame Cameras

To implement DRM software is written on Matlab. For the rectification procedure the required data: raw image, telemetry and DEM should be supplied to the folder that the software runs. The software gets the image acquisition time, raw image name and telemetry name from the user. Then the software converts the entered UTC time to unix time, opens the telemetry and finds the proper line by using the unix time. The position, velocity and attitude angles of the satellite are obtained from telemetry.

After obtaining necessary data for rectification, the pixel by pixel transformation is performed. The method starts with a double loop of 2048 repetitions for the image to be rectified. First the pixel coordinates are transformed to S_P and the lens distortion corrections are applied. By using focal length of the camera corrected image coordinates are transformed to S_C. The direction vector measured in camera coordinate system is transformed to orbital reference system by the attitude angles obtained from telemetry. By the position and velocity with respect to S_I, the orientation of orbital reference frame is computed and direction vector is transformed to S_I. By using image acquisition time GAST angle is computed and by applying precession, nutation and polar motion correction and GAST rotation direction vector is transformed to S_E.

Intersection pointy of the direction vector with WGS84 ellipsoid is computed by solving the quadratic equation. At this stage the cartesian coordinates are converted to geodetic coordinates and the direction vector is transformed to local coordinate system and its zenith and azimuth angles are computed. By using the zenith angle and atmospheric parameters, atmospheric refraction coefficients are computed for 85 layers and the initial intersection position is corrected.

After the atmospheric refraction correction, relief displacement corrections are performed by iterative method. At this stage the elevation information is obtained from DEM. SRTM DEM is used for the elevation data in this thesis. This file contains elevation data at each 3 arc second interval for both latitude and longitude. A DEM file covers an area of 1 degree latitude to 1 degree longitude thus in a SRTM DEM file there are 1201x1201 numbers. Elevation data is stored in binary format in order to reduce the storage requirement. Elevation data is stored beginning with the top row for the latitude and after completing the whole columns for the longitude going from west to east, the next row for latitude starts which is 3 arc seconds south of the previous row Figure 6.11 [82].

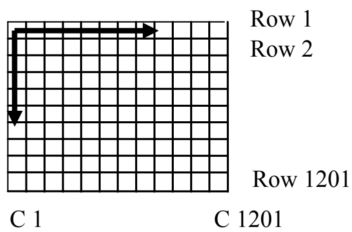

Figure 6.10 Illustration of elevation storage order in SRTM DEM.

Binary DEM could not be retrieved correctly, for this reason software is written in C++ which reads the binary DEM and writes the elevation data to a text file. Elevation data is obtained from this text file in ASCII format.

Bilsat image covers approximately 60x60 km^2 area. Since it is a very wide area, most of the case the image intersects more than one region that a DEM file cover. The possibilities of DEM file requirements are shown in Figures 6.11 to 6.14.

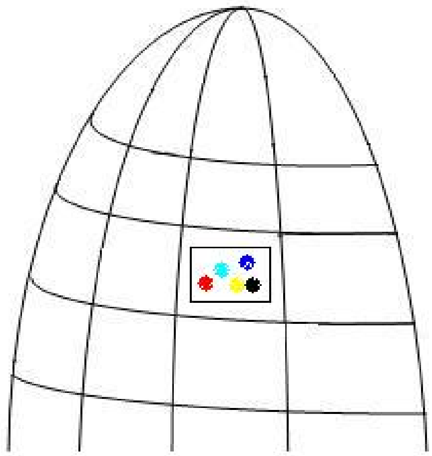

Figure 6.11 Intersection with only one DEM region.

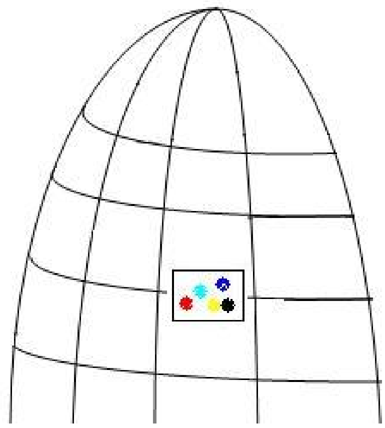

Figure 6.12 Intersection with two DEM regions vertically.

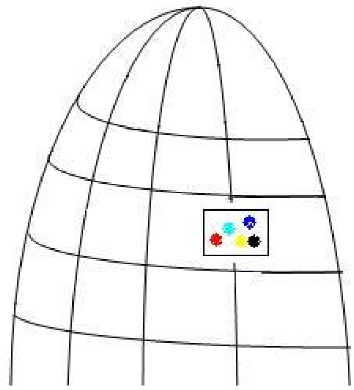

Figure 6.13 Intersection with two DEM regions horizontally.

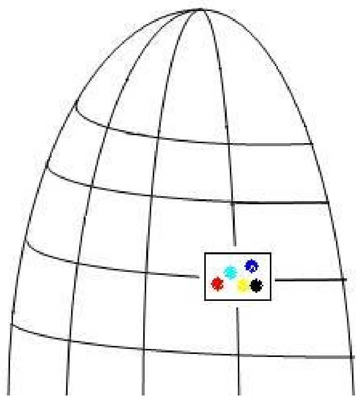

Figure 6.14 Intersection with four DEM regions.

The first possibility is that the image intersects only with one DEM region. This is the easiest situation to handle. In this case only one DEM file is read and no additional procedure is required (Figure 6.11). In the second case, the image intersects with two DEM regions in which one region is at northern of the other (Figure 6.12). In this case two DEM regions are read from two different files and they are embedded to one DEM file. DEM file covering the northern region is kept at upper portion and the file covering the southern region is embedded to the below of that matrix. The top row of the southern matrix is deleted, since it is repeated in the bottom row of the northern matrix. The resulting DEM file consists of 2401x1201 numbers.

The third possibility is that the image intersects with again two DEM regions however; the latter one is at eastern region of the first DEM region. Considering Figure 6.13 the DEM file covering the eastern region is embedded to the left side of the file covering the western region. In this case the matrix consists of the elevation values of the region is 1201x2401 matrix. The last possibility is that the image intersects with four DEM regions. In this case four different DEM file are read and the elevation values are embedded into each other in the following order (Figure 6.14). At first the western side of the northern and southern DEM regions is embedded into each other and 2401x1201 sized matrix is obtained. Next, at the eastern side of the northern and southern DEM regions are embedded and again a 2401x1201 sized matrix is obtained. The two matrixes are embedded into each other by deleting the intersecting column from one of the two matrixes. At the end 2401x2401 sized matrix is obtained.

In the final case, the resulting matrix is considerably large and requires consisting amount of memory. Since, SRTM DEM contains only integer numbers the matrix is converted from double to long integer whose one element contains only two bytes. By this transformation, important amount of memory is saved. However, long integers can not be multiplied by double type numbers, for this reason the elevation value extracted from the matrix is reconverted to double type variable before the multiplication operation. This procedure reduces the memory requirement but increases the computational demand.

To extract the elevation of a ground point, its position in the matrix that stores elevation should be computed. North West corner of the matrix is defined as the origin of the matrix and the coordinate system of the matrix is same with the Figure 6.10. Both latitude and longitude of the North West corner are integers. The difference between North West corner coordinates and the ground points' coordinates are computed. Since SRTM DEM has 3 arc second interval the difference is multiplied by 1200 and increased by 1 to obtain the required position of elevation data. The final number will not be integers in most of the case. For this reason, nearest elevation positions are obtained by computing ceil and floor of the number. Then, elevation of the ground point is estimated by using the neighboring elevation data by linear interpolation. Weights of the elevation data are assigned which are inversely proportional with the distance to the ground point.

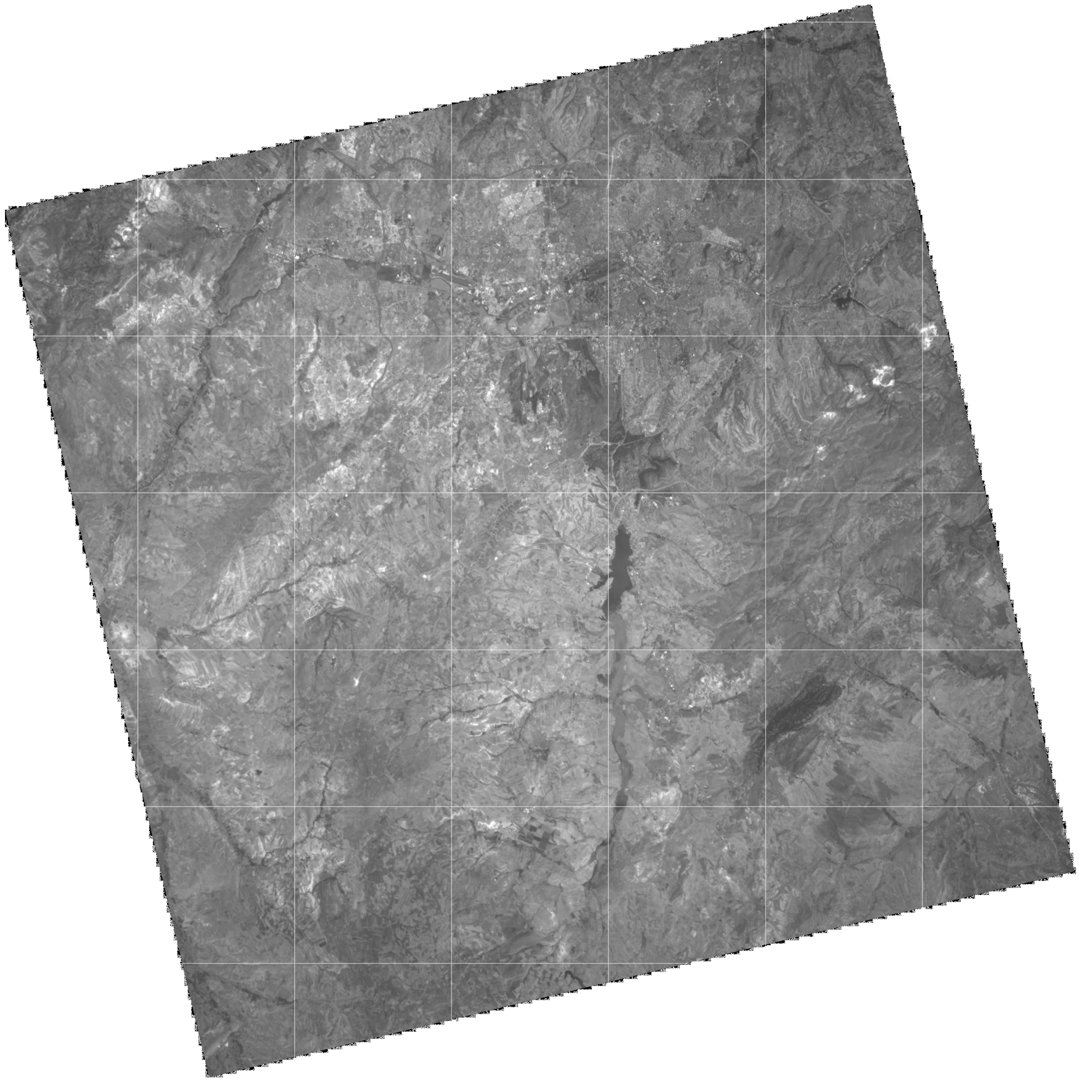

Figure 6.15 Resampled image of orthorectified Bilsat image by using Nearest Neighborhood algorithm

In Figure 6.15 resampled image of the Bilsat is shown. Vertical direction of the image is North direction. Grid lines are drawn at 10 km intervals. Nearest Neighborhood resampling algorithm is preferred for resampling in order to protect original pixel values. Since this map has same scale at every pixel and the north direction is same everywhere, this image can be called as image map.

Rectification is performed by using a DEM, in other words not only the horizontal coordinates but also the elevation of the each pixel is computed. However, the image map shown in Figure 6.15 can not represent the elevation information, except for the shadow and illumination effect on the terrain. To represent the elevation information on the image directly, a 3-D image is produced by using Matlab software. Because of the long processing time and the large storage requirement, only a small portion of the image is transformed to 3-D. The product is shown in Figure 6.16.

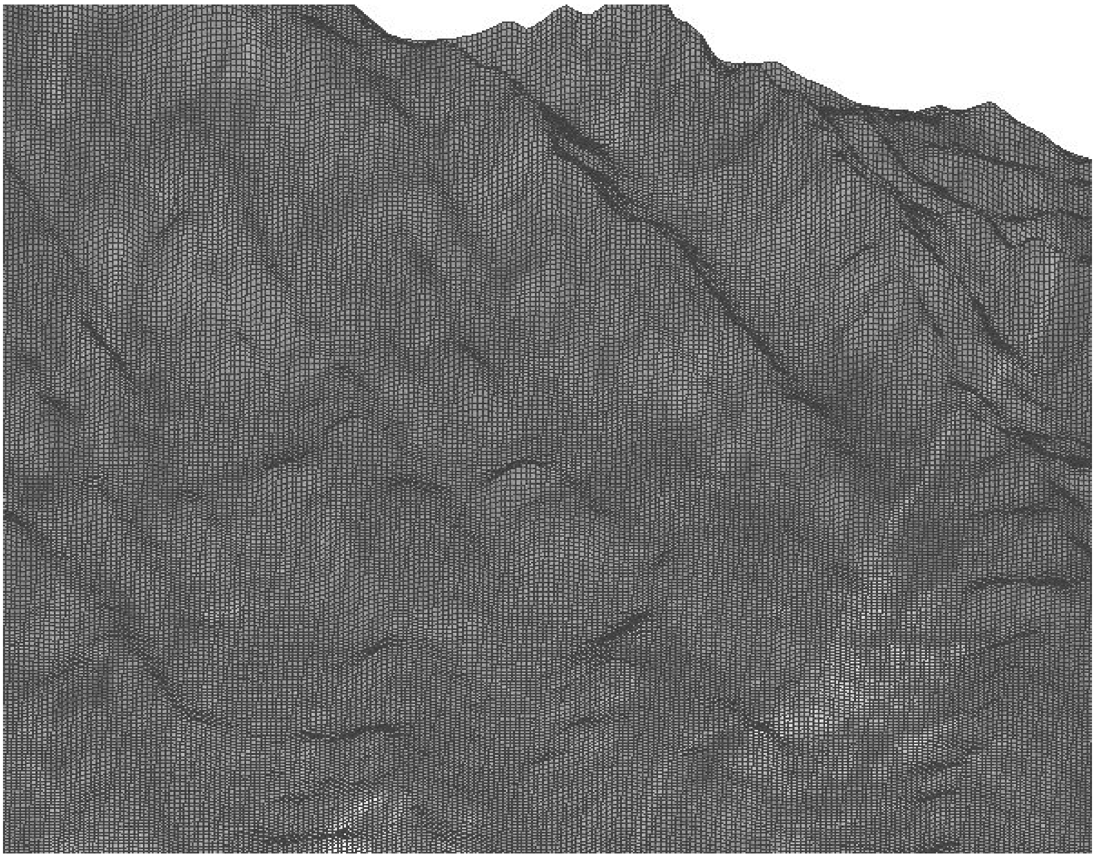

Figure 6.16 3D terrain model of a small portion of the Bilsat Image.

The 3D surface model is generated for a small portion of the whole image since, the construction of the 3D surface model requires very high memory and computation time. In order to represent the 3D surface after the orthorectification a small portion, 250x250 pixel size, of a rectified image is copied and the 3D surface model is generated from that portion.

Since 3 arc second SRTM DEM is used during orthorectification a linear interpolation is performed in order to find pixel’s elevation assuming a constant slope at that location. Because of this, elevation information assigned to pixels is not adequate for regions that have irregular slopes. Moreover for urban areas, a detailed and accurate surface model such as LIDAR data is required to produce a correct 3D urban image.

6.5.1 Convergence Analysis of DRM

The iterative procedure is investigated by changing the threshold value and the number of iterations observed at each pixel is examined. For the analysis threshold values of 1m 0.1 m and 0.01 meter is chosen. For Bilsat images which have approximately 30 meter spatial resolution, error propagation which occurred by even using 1 meter threshold is unimportant which causes roughly ± 0.1 meter position error for almost nadir images and ± 1 meter elevation error.

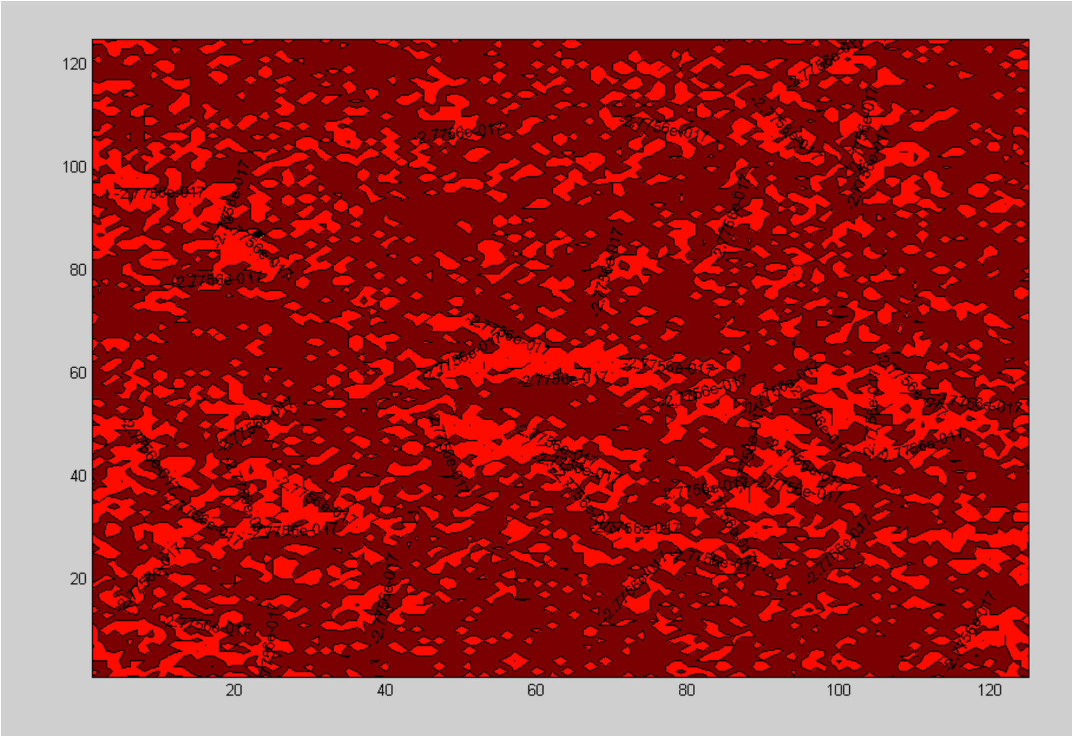

Figure 6.17 Difference between 1 meter threshold and 0.1 meter threshold values.

By examining the Figure 6.17 it will be easily seen that at most of the regions there is no difference namely, no additional iteration occurred by reducing the threshold value from 1 to 0.1 meter. These regions correspond to dark red colored portions in the Figure 6.17. At the remaining portion additional iteration is performed due to stricter threshold value and the difference between 1 meter value and 0.1 meter value is calculated as ± 0.0001 meter. The values can be seen in the d_phi.mat file.

In Figure 6.18 the difference in longitude can be predicted which is resulted by reducing threshold value from 1 meter to 0.1 meter. The contours are same with the latitude but the scale is different. Average difference observed in longitude is around ± 0.001 meter.

Similarly elevation values are compared and it is seen that the difference is about ± 0.006 meters. The elevation difference values are stored in d_h.mat file.

Threshold value is reduced from 0.1 meter to 0.01 meter and the difference between two rectification results is examined. Contour plot that shows the difference can be seen in Figure 6.18.

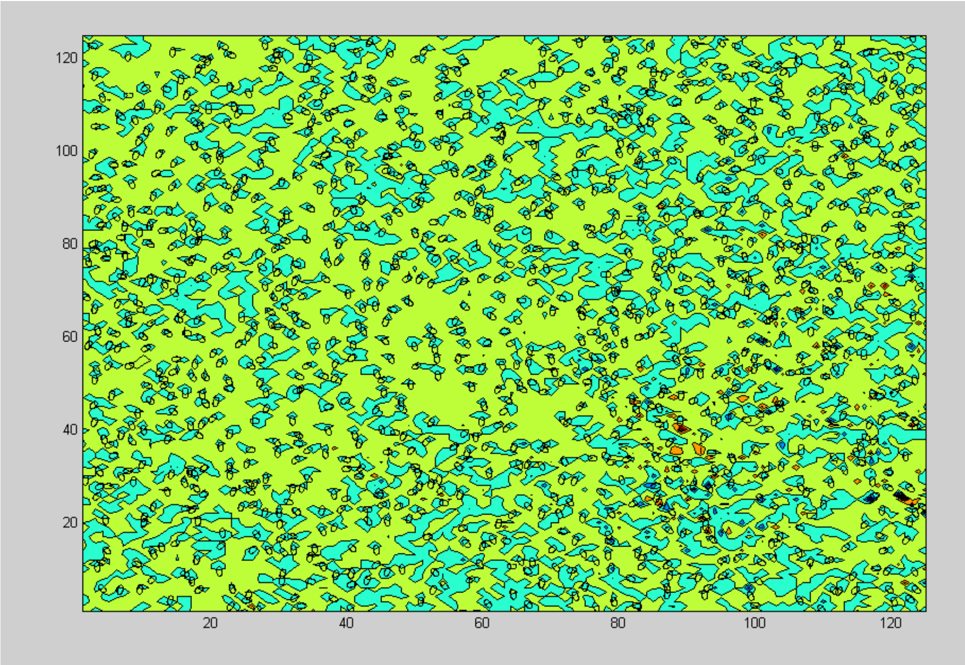

Figure 6.18 Contour map of difference in iteration number caused by changing the threshold value from 0.1 to 0.01 meter.

Threshold value for the stopping criteria is reduced from 0.1 to 0.01 meter and the results are compared. The difference of the analysis results are presented in a contour map as in Figure 6.18. The Blue regions in the figure are the zones where no additional iteration step is occurred; because of this geodetic coordinates of this region did not change by reducing the threshold value.

Average difference for the latitude is computed as $\pm$2.4e-5 meter and for the longitude is $\pm$ 6.0e-5 meter. These differences can be considered as negligible for an image which has approximately 30 meters spatial resolution. It can be concluded that, there is no reason to reduce the threshold value from 0.1 meter to 0.01 meter to increase the accuracy. These changes are negligible because the image was shot almost in nadir direction. Maximum rotation was about 8^{o} around x axis between S_O and S_B, so horizontal coordinates are not affected much by the changes in elevation. Average difference in elevation occurred due to change in the threshold value is computed as $\pm$4.1e-4 meter, which is a negligible value for a map which has a scale 1/250000.

Decreasing the threshold value for stopping criteria for the relief displacement correction stage increases the computation demand. If the threshold value is selected as 1 meter average iteration number for each pixel size is 2.93. This means at the end of 3^{rd} iteration most of the pixels converges and the height difference between previous and next DEM readings becomes less than 1 meter. If the threshold value is selected as 0.1 meter than the average iteration number becomes 3.05. This is slightly more than the previous iteration number. 0.12 increase in average iteration number causes some 500.000 more iteration for the rectification. This is not an unachievable demand for current computer technology but as mentioned the increase in the rectification accuracy is not much and necessary for a coarse resolution image. In the next step the iteration size is selected as 0.01 meter and the average iteration number is computed as 3.64. Increase in computation demand becomes influential and increase in registration accuracy is not satisfactory. However, if the registration algorithm were running on a powerful computer, the increase in computation demand would not cause any problem. Furthermore, increase in iteration number does not require additional memory or storage demand.

The effect of re-computing the ellipsoidal normal or using the first computed ellipsoidal normal has also been examined. In first trial, the ellipsoidal normal has been recomputed for each iteration step and at the second trial the ellipsoidal normal which is computed at the first iteration step is used for the remaining iterations. Difference between the two approaches for latitude is computed as $\pm$ 3.5e-4 meter in average. The contour plot gives the distribution for the each pixel as in Figure 6.19.

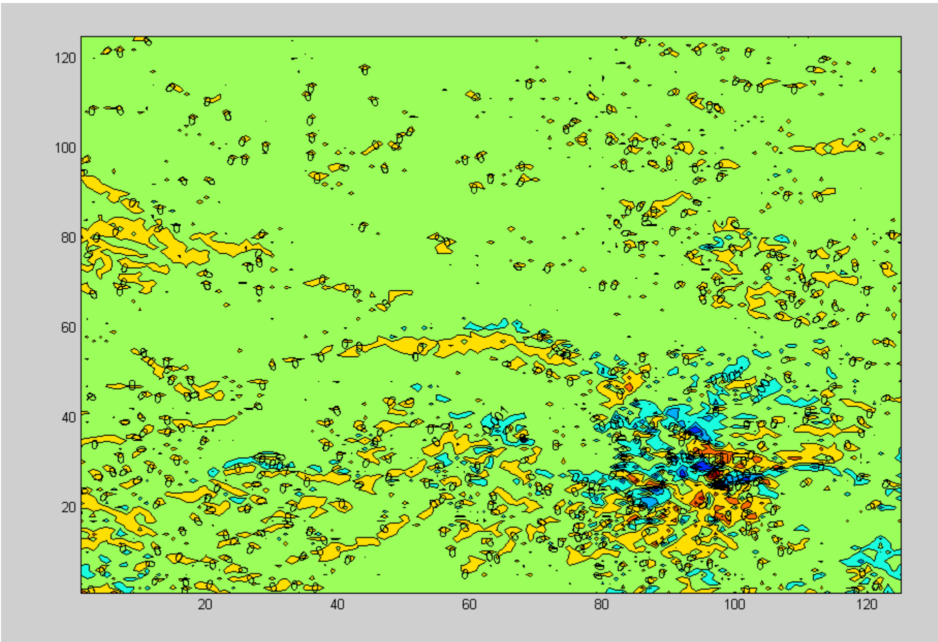

Figure 6.19 Change in latitude due to changing ellipsoidal normal at each iteration.

In Figure 6.19 green portions are labeled as no change or change occurred less than 0.001 meter. Blue portions are the regions that have changed less than – 0.001 meter and orange portions indicate more than 0.001 meter change in direction of latitude. “–” sign indicates shift to the south. It is seen from the contour graph that considerable part of the pixels are affected more than 1 millimeter in direction of latitude due to not re-computing the ellipsoidal normal.

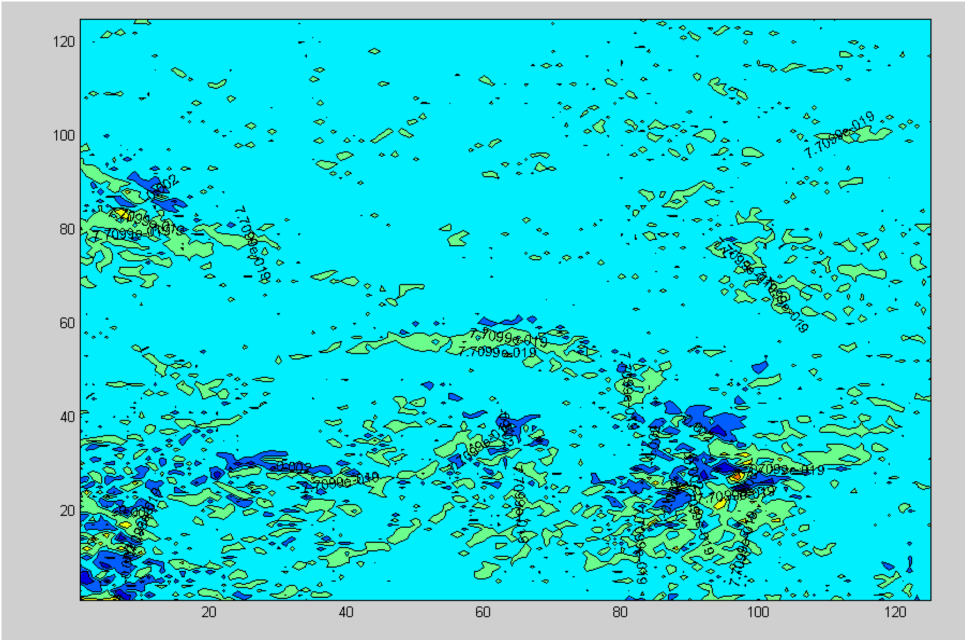

Figure 6.20 Change in longitude at final step due to not recomputing ellipsoidal.

In Figure 6.20 blue portions are regions where no change occurred or changes less than 0.002 meter in absolute value are observed. Green portions indicate shift to the east. On the other hand, dark blue portions indicates shift to the west. Absolute value of average shift of one pixel is computed as ± 6.4e-4 meter which is slightly larger than the shift observed in the direction of latitude.

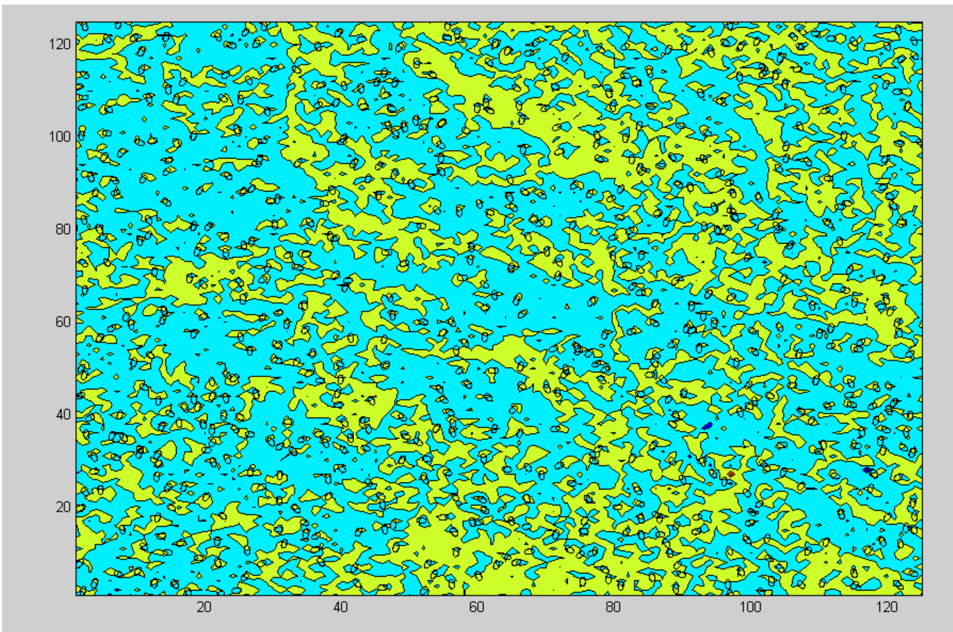

Figure 6.21 Change in elevation at final step due to not updating ellipsoidal normal

Differences between elevations are computed as ± 9.6e-5 meter. This is slightly less than horizontal coordinates because this is the error occurred because of miscomputing the correct position and obtaining wrong elevation from DEM. When the error magnitudes are examined it is seen that, recomputing ellipsoidal normal at each iteration step or keeping it constant for all iterations will not affect the registration accuracy of Bilsat images.

It can be easily predicted that if the inclination of the direction line increases the convergence of the iteration procedure becomes more difficult. In order to examine the convergence of the method high attitude angles are assigned for the attitude angle of the camera. For the first trial 15 degrees are assigned to omega and phi attitude angles, for the second trial 20 degrees are assigned and for the third trial 25 degrees are assigned. The number of iterations for the iterative procedure to converge is plotted in figures 6.22 to 6.24.

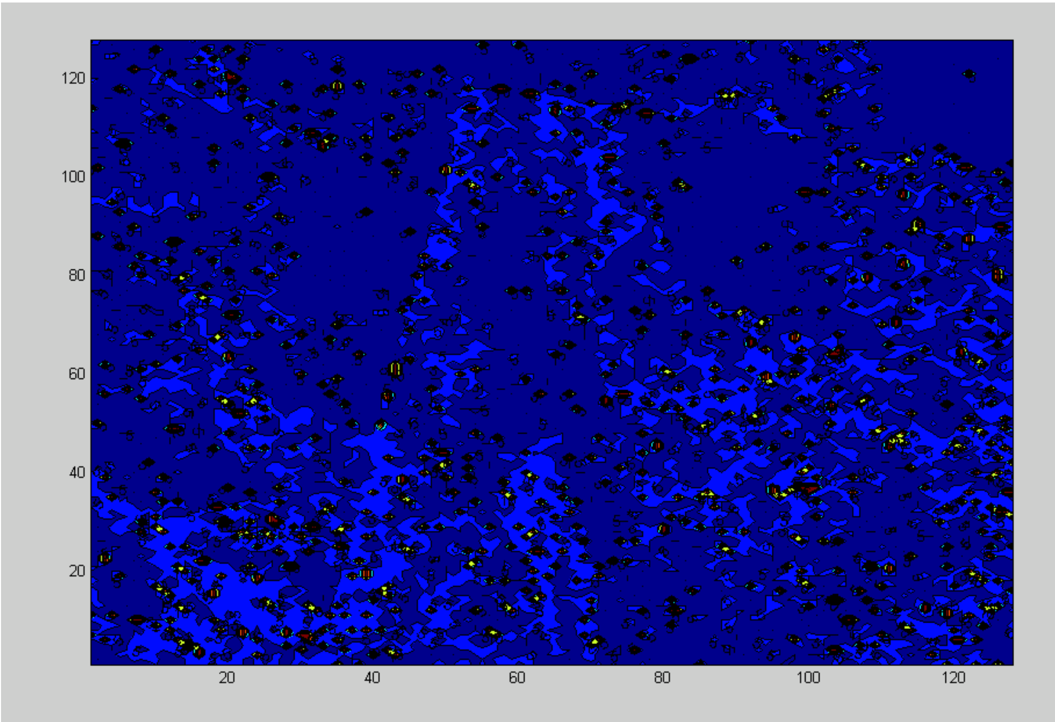

Figure 6.22 Contour map of iteration number for 15^o of attitude angles

Contour map of iteration number is shown in Figure 6.22 for 15^o of attitude angles for roll and pitch. In light blue regions iteration number is less than 5 and in dark blue regions iteration number is between 5 and 10. Light and dark blue regions covers the most of the image, in other words in most of the region iteration number is less than 10. In the remaining parts which are local areas, the iteration continued until 20 or 25 times, these are the places where the slopes changed suddenly i.e. top of a hill or a valley. Average number of iteration for the whole area is computed as 5.6 for 0.1 cm threshold value which is considerably higher than the previous analysis.

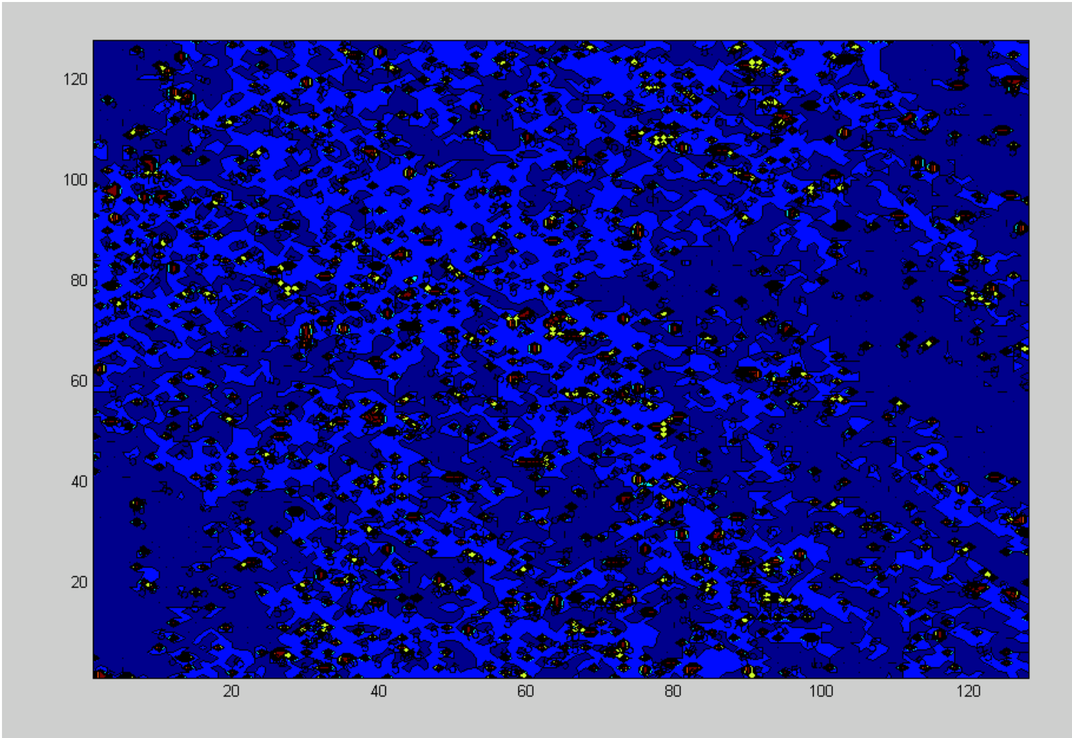

Figure 6.23 Contour map of iteration number for 20^{o} of attitude angles

In Figure 6.23 contour map of iteration number for 20^{o} of attitude angles are shown. In the figure similar to Figure 6.22 light blue area indicates iteration number less than 5 and dark blue area indicates iteration number between 5 and 10. When contour map is examined it is seen that there is a considerable increase in the size of dark blue areas compared with the previous analysis. This indicates that convergence of the relief displacement correction algorithm slows down when roll and pitch angles increase. Average value for the iteration number is computed as 6.4 more than the previous analysis as expected.

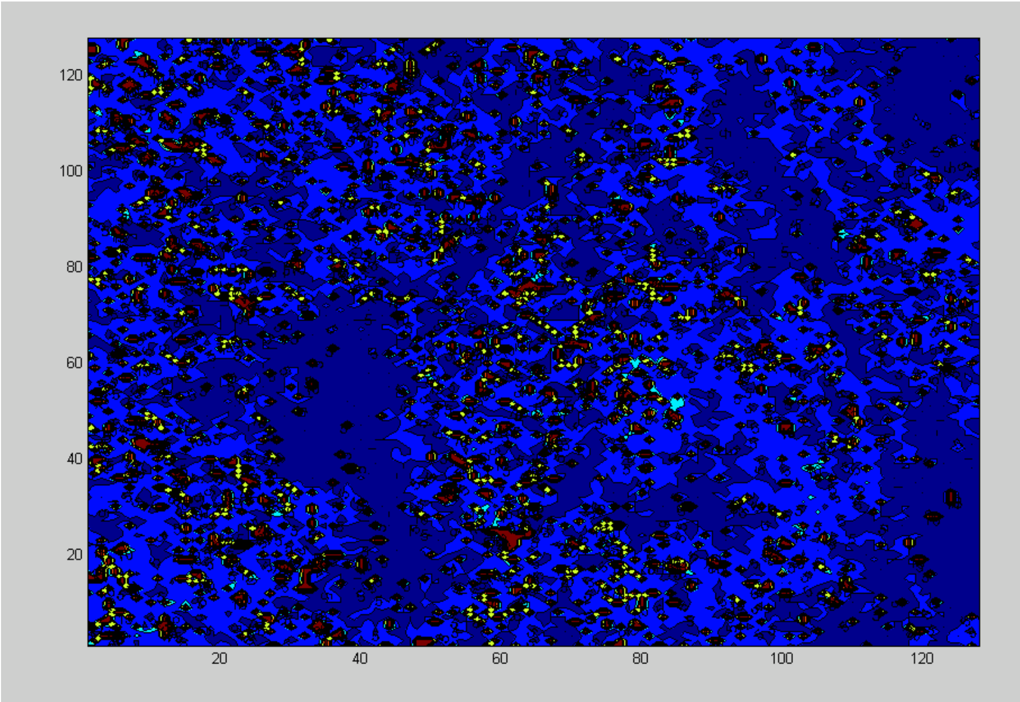

Figure 6.24 Contour map of iteration number for 25^{o} of attitude angles

Figure 6.24 shows the contour map of number of iterations for 25^{o} roll and pitch angles. Contour interval is same with the previous two figures. In this analysis it seen that the iterative relief displacement correction algorithm has converged in smooth regions in less than 10 iterations. On the other hand, in mountainous regions the algorithm did not converged as successfully as the images taken in nadir direction. Red portions show the iteration numbers between 25 and 30. Most of the red portions have iteration number as 30 which is the maximum iteration number in the analysis. It is seen that for highly oblique images the iteration still converges for smooth and gently sloped regions, and the algorithm fails in steep slopes. However, elevation error is not more than one meter; since the image is oblique horizontal coordinates are registered with a considerable error. Average iteration number is computed as 8.1 which is a considerable increase in iteration number and computation demand.

6.6 Implementation of DRM for Pushbroom Scanners

The implementation of DRM adopted for pushbroom scanners will be implemented by the corrected parameters obtained at the end of the parameter estimation procedure. In the parameter estimation procedure, additional parameters are adopted for the orbital perturbation to reduce the residuals. For this reason, there will be small differences in the implementation when compared with the model explained in Chapter 4.

The rectification process first detects the time from the current image line. Then computes the camera position and then computes the attitude of the camera. After performing necessary precession, nutation and polar motion corrections, the image line is intersected with reference ellipsoid. By the algorithm explained in the rectification process for the images taken by CCD frame cameras, atmospheric refraction and relief displacement effects are removed, and geodetic coordinates are transformed to UTM coordinates. By nearest neighbor resampling method an image map shown in Figure 6.25 is produced from the raw ASTER image.

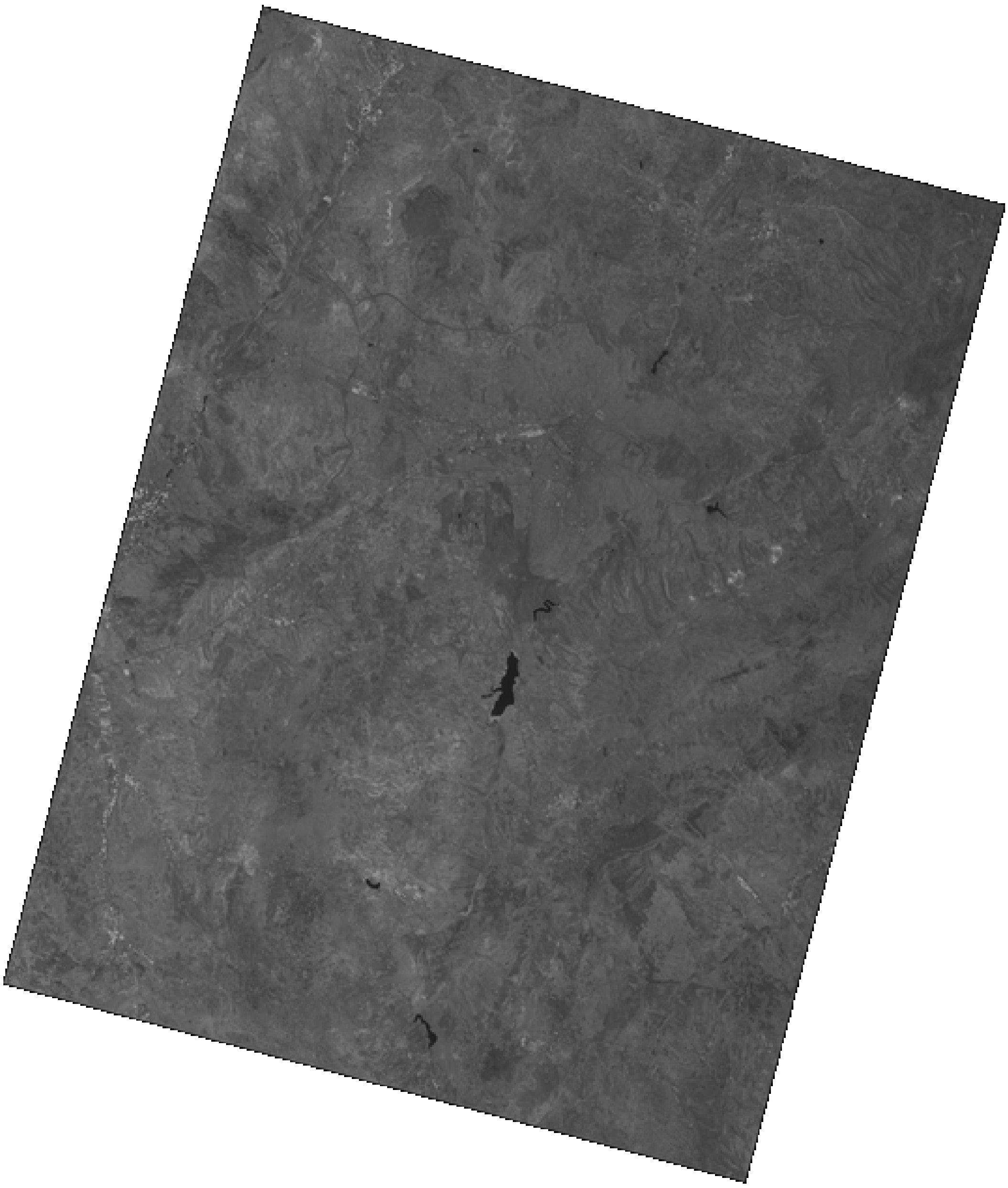

Figure 6.25 Image map produced from the raw ASTER image.

CHAPTER 7

ERROR ANALYSIS OF DRM

7.1 Comparison of DRM for CCD camera with Existing Methods

To measure the accuracy of DRM, rectification results are compared with four rectification methods being currently used. The rectification methods selected for comparison is shown below;

7.1.1 Affine Transformation

$$\begin{aligned} \lambda &= ax + by + c \\ \phi &= dx + ey + f \end{aligned} \tag{7.1}$$

where;

Φ and λ are geodetic coordinates of the GCPs

x and y are the pixel coordinates of the image point

a, b, c, d, e and f are parameters of the rectification method

After the parameter estimation procedure the coefficients are computed and the residuals of the GCPs are given in appendix B Table B.15 to B.17.

Affine Transformation is a simple rectification method that has moderate accuracy; this method is selected because of its simplicity. This method does not take into account of the elevation of the GCPs. Furthermore, the method can not model the earth curvature properly because of inadequate number of parameters used.

7.1.2 3-D Affine Transformation

$$\begin{aligned} x &= a_1 + a_2\phi + a_3\lambda + a_4 h + a_5\phi h + a_6\lambda h \\ y &= b_1 + b_2\phi + b_3\lambda + b_4 h + b_5\phi h + b_6\lambda h \end{aligned} \tag{7.2}$$

where;

x and y are pixel coordinates image point

a and b are coefficients of the model

Φ, λ and h are geodetic coordinates of the GCPs

The second model takes into account of the elevation of GCPs. Furthermore since more parameters are used, this method can model the earth curvature better. The rectification accuracy of the 3D affine transform is compared with DRM.

Residuals of the GCP computed with 3D polynomial model are given in appendix B in Table B.18 to Table B.20.

7.1.3 Projective Transformation

$$\phi = \frac{a_1 x + b_1 y + c_1}{a_3 x + b_3 y + 1} \qquad (7.3)$$

$$\lambda = \frac{a_2 x + b_2 y + c_2}{a_3 x + b_3 y + 1}$$

In this model ϕ and λ are geodetic coordinates of the image. After a linearized least square adjustment the parameters of the projective transformation can be computed.

Residuals of the GCP computed with projective transformation are given in appendix B in Table B.21 to Table B.23.

7.1.4 Pinhole Camera Model

Colinearity equations for the camera can be written as;

$$x = \frac{1}{1 + k_1 r^2 + k_2 r^4}\left[\Delta x - \frac{f}{c}\frac{R_{11}(X - X_L) + R_{12}(Y - Y_L) + R_{13}(Z - Z_L)}{R_{31}(X - X_L) + R_{32}(Y - Y_L) + R_{33}(Z - Z_L)}\right]$$

$$y = \frac{1}{1 + k_1 r^2 + k_2 r^4}\left[\Delta y - \frac{f}{c}\frac{R_{21}(X - X_L) + R_{22}(Y - Y_L) + R_{23}(Z - Z_L)}{R_{31}(X - X_L) + R_{32}(Y - Y_L) + R_{33}(Z - Z_L)}\right] \qquad (7.4)$$

where

$$R = \begin{bmatrix} \cos\phi\cos\kappa & -\cos\phi\sin\kappa & \sin\phi \\ \sin\omega\sin\phi\cos\kappa + \cos\omega\sin\kappa & -\sin\omega\sin\phi\sin\kappa + \cos\omega\cos\kappa & -\sin\omega\cos\phi \\ -\cos\omega\sin\phi\cos\kappa + \sin\omega\sin\kappa & \cos\omega\sin\phi\sin\kappa + \sin\omega\cos\kappa & \cos\omega\cos\phi \end{bmatrix}$$

The solution of this equation set is performed by a least squares solution as

$$\beta = (X'X)^{-1} X'y \qquad (7.5)$$

where;

$$\beta = \begin{bmatrix} X_L & Y_L & Z_L & \omega & \phi & \kappa & f & \Delta x & \Delta y & k_1 & k_2 \end{bmatrix}'$$

$$X = \begin{bmatrix} \frac{\partial x_1}{\partial X_L} & \frac{\partial x_1}{\partial Y_L} & \frac{\partial x_1}{\partial Z_L} & \frac{\partial x_1}{\partial \omega} & \frac{\partial x_1}{\partial \phi} & \frac{\partial x_1}{\partial \kappa} & \frac{\partial x_1}{\partial f} & \frac{\partial x_1}{\partial \Delta x} & \frac{\partial x_1}{\partial \Delta y} & \frac{\partial x_1}{\partial k_1} & \frac{\partial x_1}{\partial k_2} \\ \frac{\partial y_1}{\partial X_L} & \frac{\partial y_1}{\partial Y_L} & \frac{\partial y_1}{\partial Z_L} & \frac{\partial y_1}{\partial \omega} & \frac{\partial y_1}{\partial \phi} & \frac{\partial y_1}{\partial \kappa} & \frac{\partial y_1}{\partial f} & \frac{\partial y_1}{\partial \Delta x} & \frac{\partial y_1}{\partial \Delta y} & \frac{\partial y_1}{\partial k_1} & \frac{\partial y_1}{\partial k_2} \\ \vdots & \vdots & \vdots & \vdots & \vdots & \vdots & \vdots & \vdots & \vdots & \vdots & \vdots \\ \frac{\partial x_n}{\partial X_L} & \frac{\partial x_n}{\partial Y_L} & \frac{\partial x_n}{\partial Z_L} & \frac{\partial x_n}{\partial \omega} & \frac{\partial x_n}{\partial \phi} & \frac{\partial x_n}{\partial \kappa} & \frac{\partial x_n}{\partial f} & \frac{\partial x_n}{\partial \Delta x} & \frac{\partial x_n}{\partial \Delta y} & \frac{\partial x_n}{\partial k_1} & \frac{\partial x_n}{\partial k_2} \\ \frac{\partial y_n}{\partial X_L} & \frac{\partial y_n}{\partial Y_L} & \frac{\partial y_n}{\partial Z_L} & \frac{\partial y_n}{\partial \omega} & \frac{\partial y_n}{\partial \phi} & \frac{\partial y_n}{\partial \kappa} & \frac{\partial y_n}{\partial f} & \frac{\partial y_n}{\partial \Delta x} & \frac{\partial y_n}{\partial \Delta y} & \frac{\partial y_n}{\partial k_1} & \frac{\partial y_n}{\partial k_2} \end{bmatrix}_{2n \times 11}$$

Residuals and the parameters of pinhole camera model is presented in Appendix B.

Pin hole camera model directly maps the pixel coordinates to ground coordinates by colinearity equations. For this reason, it is computationally the most demanding model among the methods chosen for the comparison. Results of pin hole camera model analysis are given in Table B.24 and Table B.25.

7.1.5 Comparison of Rectification Methods

When the residuals of the Ground Control and Ground Check points are examined it is seen that if the complexity of the model increases, accuracy of the results increases too. However, to achieve an accurate solution with a complex model requires demanding mathematical and numerical procedures for satellite images. For this reason, DRM has the most demanding computation and regularization methods to reach the desired accuracy.

Although both DRM and pinhole rectification method are based on the colinearity equations, they end up with different solution and accuracy. DRM has slightly better accuracy which may be because of the better initial values for the parameters and the more complex lens model for imaging camera. Initial values of DRM for attitude are obtained from magnetometer & sun sensor while zero is assigned for the pinhole camera model. Furthermore, camera position was available for DRM by means of a GPS receiver while, the coordinates of the image center is assigned for initial camera position in pinhole camera model. As a result of these, the iteration procedure may converge to local minima and stuck into that local minimum. However, since better initial values are provided for DRM it was able to converge into global minimum.

To compare the overall effectiveness of the model in terms of accuracy, computational cost and complexity; the simpler models becomes more advantageous. Because rectification of the whole Bilsat images with affine transformations and projective transformations are completed in a very short time, similarly with the pinhole camera model rectification takes slightly longer but not very long.

However, rectification of the whole Bilsat image with DRM takes more than 2 hours, which is considerably longer than the other methods. The rectification is performed by using software developed by Matlab and the software run on 1 GHz AMD processor with 256 MB ram. The computation time will be much smaller if the algorithm were run on executable software format and with more powerful computer such as 3 GHz processor and 1 GB ram which is the configuration that can easily be purchased. For this reason the computational demand becomes less important with the improvement in computer technology.

The second drawback is the computational complexity of DRM. If the initial values for the parameters are not accurate enough for a desired accuracy then it is required to improve the initial values by a parameter estimation procedure. Partial derivatives of DRM with respect to parameters are very demanding and the solution of parameter estimation procedure requires regularization. Once the partial derivatives are computed analytically or they can be computed as numerically it will not be a problem but the finding an optimum regularization method may be difficult in some situations. This can be made easier by reducing the number of lens distortion parameters in order to reduce the condition number.

As a conclusion, DRM presents better results when compared with the other existing rectification methods. If the algorithm is run on a powerful computer the computational demand can be easily handled and by applying the proper regularization method optimum results can be achieved. Consequently, it can be suggested that DRM should be preferred if high accuracy is required for rectification process.

7.2 Comparison of DRM for Pushbroom Scanners with Existing Methods

In this section rectification results and performance of DRM adopted for pushbroom scanners will be compared with the existing methods. Rectification results are presented in Appendix B in Table B.27 to Table B.31.

When the rectification results are examined it is seen that the rectification accuracy of DRM is not much better than 3D affine transformation. Actually the low performance of DRM can be explained as assigning improper initial values for the parameter estimation. Neither satellite orbit nor attitude angles were available as initial values for the parameter estimation. For this reason, as explained in Chapter 6 very rough orbit model is assigned for the camera position and perturbation parameters are added to the model in order to decrease residuals at the end of the parameter estimation. However, additional parameters increase the correlation between the parameters and the equation system became highly “ill-conditioned”. For this reason, performance of the DRM is not good as expected. However, if initial parameters for the position and attitude are available, it is certain that the DRM will present much better results.

When the elevations of the ground control points are examined, it is seen that there are moderate elevation changes. To compare the rectification accuracy of the methods, a simulation data is prepared by exaggerating the elevation of the GCPs. Simulation data is prepared by increasing the elevation differences twice of the present situation. Comparison procedure is repeated by simulation data and analysis results are presented in Table B.30 and Table 31. In this case, rectification accuracy of the DRM did not change significantly, but accuracy of 3D affine transformation decreased significantly. From this analysis it can be concluded that the rectification accuracy of DRM does not decrease considerably in steep slopes. This property of DRM makes it an attractive method for the rectification of mountainous images.

Computation time of DRM for pushbroom cameras is much higher than not only the affine transformation but also DRM for CCD frame cameras. In the comparison part of the DRM for frame cameras computation demand of the method was commented as a drawback of the method. Because of the additional parameters added for the orbit and attitude perturbations, computational cost is increased significantly. Additionally, it is expected that pushbroom scanners have higher spatial resolution than CCD frame cameras installed on the same platform. This results larger images for pushbroom scanned terrain of the same area. Because of these reasons, rectification of ASTER images with DRM took considerably long time. Full rectification of one ASTER image took almost 16 hours with 1 GHz AMD processor. However, 3D affine transformation rectified whole image slightly more than half an hour. For the pushbroom scanners, computation cost becomes an important factor even for powerful computers.

7.3 Testing the Parameter Estimation Results

Different regularization methods end up with different estimations to the parameters at the end of the parameter estimation process while the residuals were in acceptable limits. This makes the analyzer suspicious about finding the true global minima that is the closest values of the parameters. The estimation result may converge to local minima with a different combination of estimations to parameters that somehow minimizes the residuals. It may not be always possible to know every parameter exactly and with improper initial value estimation to unknown parameters, the parameter estimation process may converge to irrelevant local minima. In this part, it is desired to see how the improper initial value assignments affect the parameter estimation result. To implement this task, initial values of the parameters are blundered by adding noise. Parameter estimation results are tested for the improper initial values of; velocity, position, focal length, principal coordinates, radial and asymmetric lens parameters. At each analysis one component of velocity and position are blundered so totally 16 analyses were run to complete the test.

In the first run x component of the velocity were blundered by adding 1000 in S_E coordinate system. Velocity is required to establish the orbital reference system, blundering the x component will affect the attitude of the camera. When the estimated parameters are compared with the original results it is seen that camera position is affected about 20 km in x and 10 km in y and z coordinates. Roll and pitch angles are also affected by not as much as the kappa angle. It is seen that the kappa angle is very sensitive to x component of the velocity. Focal length is estimated 3 mm shorter and x coordinate of the principal point is estimated 1 mm further from the origin which is an important amount for the interior camera parameter. The other lens parameters are not affected considerably.

In the second run y component of the velocity is blundered by adding 1000. At the end of the parameter estimation, camera position is affected in similar amounts with the previous analysis but the sign of the displacement is reverse. Similarly attitude angles are effected by almost the same magnitude but in different sign. Kappa angle is again the most affected parameter. Focal length is not affected much while principle coordinates are affected slightly more than half a millimeter. Radial lens distortion parameters are considerably changed but, there is slightly change in asymmetric lens distortion parameters.

In the third run z component of the velocity is blundered by adding 1000. At the end of the parameter estimation camera position is affected only by 5 km in x and y coordinates and surprisingly not affected in z coordinate. Attitude angles are also affected less when compared with the previous analyses and kappa angle is still the most sensitive one. Focal length and principal coordinates are slightly affected and lens distortion parameters are changed very little.

In the fourth run x component of the camera position is blundered by adding 50000. At the end of the analysis it is seen that error in x coordinate of the position had propagated to other components of the position. It is seen that all position components are affected about 20 km. Attitude of the camera is affected very little, even the kappa angle changed about 0.2 degree. However focal length is affected enormously. Remaining parameters show very little change both in magnitude and sign.

In the fifth and sixth run y and z components of the camera is blundered by adding 50000 respectively. Similar to the previous analysis all position components are affected about 20 km in magnitude while there is very little change in attitude angles. Similarly focal length of the camera is estimated more than 5 mm longer than it is. Finally interior camera parameters are not affected considerably.

In the seventh run roll angle is blundered by adding 1 degree. Camera position is affected about 10 km in x and y and 3 km in z components. Only the roll angle is affected by the blundering of the roll angle. Focal length is estimated 1 mm longer than it is and the other camera parameters are not affected considerably.

In the eight run pitch angle is blundered by adding 1 degree. z component of the camera position is affected about 10 km while x and y components are affected by about 5 km. For the attitude angles only pitch angle is affected considerably, the remaining angles are affected slightly. Focal length is estimated 0.5 mm longer and y coordinate of the principle point is estimated about 0.3 mm further. Lens distortion parameters are not affected considerably.

In the ninth run yaw angle is blundered by adding 1 degree. In this analysis camera position is not affected considerably when compared with the previous analysis only x component is displaced by 3 km. Similarly attitude angles are not affected considerably. Surprisingly kappa angle is the least affected parameter in the analysis of blundering the kappa angle. Focal length is estimated a little longer and x coordinate of the principle point is displaced a little and remaining interior camera parameters are not affected much.

In the tenth run focal length is blundered by adding 5 mm. In this analysis camera position and attitude angles are not affected much. Focal length is estimated a little longer and there are slight changes in principle coordinates. Radial lens distortion parameters are affected considerably while asymmetric lens distortion parameters are not.

In the eleventh and twelfth run x and y coordinates of the principle coordinates are blundered. In these analyses, camera position is affected about 1 km and only roll and pitch angles are changed notably. Blundering x coordinate elongates the focal length while y coordinate shortens the focal length. Furthermore, all interior camera parameters are affected significantly in these analyses.

In the thirteenth to sixteenth analyses interior camera parameters are blundered. Camera position and attitude angles are not affected notably but interior camera parameters are affected considerably. Estimated parameters at the end of the test are presented in Table B.34.

CHAPTER 8

SENSITIVITY AND UNCERTAINTY ANALYSIS

In this Chapter sensitivity and uncertainty analysis of DRM is performed. In the analysis three methods are used; first one is differential analysis, the second one is Monte Carlo and third one is the Fourier Amplitude Sensitivity Test (FAST). In three methods the sensitivity of the parameters to the model are examined and uncertainty in the results are computed. Some of the studies about the Sensitivity Analysis methods can be obtained from [83-102].

In the analysis it is aimed to compute the uncertainty of the model, where the parameters have some amount of errors. The errors are assigned by an expert opinion [33] that the uncertainties of the parameters are determined by the possible error ranges that can be observed based on the instrument characteristics which measures the quantity. Star tracker and the GPS receiver on board can be given as the example for this. The remaining error ranges are assigned by the prediction of the precision of the camera calibration performed before the launch of the satellite. Interior camera parameters can be given as example.

The objective of the analysis is to mention the uncertainty in the ground coordinates computed by the DRM with the possible error ranges in the methods. Moreover, it is aimed to compare the performance of the sensitivity analysis methods and list the advantages and disadvantages of the methods.

8.1 Methods of Sensitivity Analysis

8.1.1 Differential Analysis (Covariance Analysis)

Differential analysis is based on Taylor series expansion to approximate the model under consideration. Differential analysis involves four steps;

<u>Step 1:</u>

Base values, ranges and distributions are selected for the input variables. The model including the input variables and the output is written as [88];

$$\boldsymbol{y} = f(x) \tag{8.1}$$

Base value represents the most probable value that the parameter can be assigned. Base values of the interior camera parameters are calculated after the camera calibration procedure and exterior camera parameters are obtained from the telemetry. Finally base value of elevation is provided from DEM. Ranges of the variables are obtained by the Variance Covariance matrix of the parameters, as a result distribution of the parameters are considered as normal.

Step 2:

Taylor series that approximate output variable, $\boldsymbol{y}$ are developed. In this study first order Taylor series approximation is used. First order Taylor Series expansion approximating function y can be written as [88];

$$y(\boldsymbol{x}) = y(\boldsymbol{x}_o) + \sum_{i=1}^{n} \left[\frac{\partial f(\boldsymbol{x}_o)}{\partial x_i} \right] (x_i - x_{io}) \tag{8.2}$$

where

$\boldsymbol{x}_o$ is the vector of input parameters with the corresponding base values

x_i is the value of the i^{th} input parameter within its range

Evaluation of the partial derivatives is the most demanding part of the differential analysis. For this reason, second order Taylor series expansion is avoided.

Step 3:

Variance propagation techniques are used to estimate the uncertainty in y. If first order Taylor series is used the following results will be obtained [88];

$$E(y) \doteq y(\boldsymbol{x}_o) + \sum_{i=1}^{n} \left[\frac{\partial f(\boldsymbol{x}_o)}{\partial x_i} \right] E(x_i - x_{io}) \tag{8.3}$$

$$E(y) = y(\boldsymbol{x}_o) \tag{8.4}$$

where

E denotes the expected value,

Variance is computed from the formula [88];

$$V(y) \doteq y(\boldsymbol{x}_o) + \sum_{i=1}^{n} \left[\frac{\partial f(\boldsymbol{x}_o)}{\partial x_i} \right]^2 V(x_j) + 2 \sum_{i=1}^{n} \sum_{j=i+k}^{n} \left[\frac{\partial f(\boldsymbol{x}_o)}{\partial x_i} \right] \left[\frac{\partial f(\boldsymbol{x}_o)}{\partial x_j} \right] Cov(x_i, x_j) \tag{8.5}$$

where

V is variance of the output variable

Cov is variance covariance matrix of the parameters

Step 4:

Taylor series approximations are used to estimate the importance of each parameter. If first order Taylor series expansion is used for the estimation of y, the contribution of parameters to the variance of y can be estimated with the ratio shown below [88];

$$\sum_{i=1}^{n}\left[\frac{\partial f(\boldsymbol{x}_o)}{\partial x_i}\right]^2 \frac{V(x_j)}{V(\boldsymbol{y})} \tag{8.6}$$

The fractional contributions to variance can be used to order the parameters with respect to their contribution to the uncertainty in ***y***. This ordering depends on both the absolute effect of the parameter, as measured with their partial derivatives, and the effect of distributions assigned to the parameter, as measured by $V(x_i)$.

8.1.2 Monte Carlo Analysis

Monte Carlo analysis is based on performing multiple model evaluations with probabilistically selected model input, and using the results of these evaluations to determine both the uncertainty in model predictions and the input variables that give rise to the determined uncertainty. Monte Carlo analysis consists of five steps;

Step 1:

Range and distribution of each parameter are determined. This can either be obtained by an expert opinion or by a parameter estimation procedure. These ranges and distributions will be used in the next step in the generation of a sample from the corresponding parameters.

Step 2:

A sample set is generated based on the ranges and distributions specified in the first step. Common used sample generation techniques are; random sampling, stratified sampling and Latin hypercube sampling. Among the three methods Latin hypercube sampling method is used because Latin hypercube sampling has a number of desirable properties which can be explained as; full stratification across the range of each variable, relatively small sample size requirement, direct estimation of means, variances and distribution functions and the availability of a variety of techniques for sensitivity analysis [88].

In Latin hypercube sampling method, range of each parameter (i.e. x_i) is divided into m intervals of equal probability and one value is selected from each interval. The m values thus obtained for the first parameter (x_1) are paired at random with the m values obtained for the second parameter

(x_2). These m pairs are combined in a random manner with the m values of the third parameter (x_3) to form m triples. This process is continued until a set of m n-tuples is formed which can be represented as

$$\boldsymbol{x}_i = [x_{i1}, \ldots\ldots, x_{in}], \qquad i = 1, \ldots, m \tag{8.7}$$

where;
m is the sample size
n is the number of parameters

Latin hypercube sampling operates to ensure full coverage (stratification) over the range of each variable. In the case of n sample size, the range of each variable is divided into n equal probability intervals and one value is selected from each interval.

Control of correlation within a sample used in a Monte Carlo analysis is very important. If two or more variables are correlated, then it is necessary that the appropriate correlation structure be incorporated into the sample if meaningful results are to be obtained from the uncertainty and sensitivity analysis. In response to this situation, Iman & Conover have proposed a method of controlling the correlation structure in random and Latin hypercube samples that is based on rank correlation rather than sample correlation [18]. In other words, correlation structures will be controlled on rank-transformed data rather than the original data. The advantages of this method are its simplicity and being distribution free.

The controlling the correlation of the sample set is performed as follows;

The sample set of size m from n input variables is represented in a $m \times n$ matrix named as X. The procedure is based on rearranging the values in the individual columns of X so that a desired rank correlation structure results between the individual variables. Let C is the correlation matrix of the parameters, the aim is to generate a sample set that has same correlation with C.

Although the procedure is based on rearranging the values in the individual columns of X to obtain a new matrix X* that has a rank correlation structure close to that described by C, it is not possible to work directly with X. For this reason, it is necessary to define a new matrix [88];

$$\boldsymbol{S} = \begin{bmatrix} s_{11} & s_{12} & s_{1n} \\ s_{21} & s_{22} & s_{2n} \\ & & \\ s_{m1} & s_{m2} & s_{mn} \end{bmatrix}$$

Matrix **S** has the same dimension as **X**, but it is independent of **X**. Each column of **S** contains a random permutation of the m van der Waerden scores.

$$\Phi^{-1}\left(\frac{i}{m+1}\right), \text{ i} = 1, 2, \ldots, \text{m} \tag{8.8}$$

where Φ^{-1} is the inverse of the standard normal distribution.

The matrix **S** is then rearranged to obtain the correlation structure defined by **C**. This rearrangement is based on the Cholesky factorization of **C**.

$$\boldsymbol{C} = \boldsymbol{PP}^T \tag{8.9}$$

where

P is a lower triangular matrix

Cholesky factorization is possible because C is a symmetric positive definite matrix. The condition that the correlation matrix associated with S be close to the identity matrix should be considered also. Unfortunately the correlation matrix of S will not always be the identity matrix. However, it is possible to make a correction for this situation. The starting point for this correction is the Cholesky factorization for the variance covariance matrix of S [88];

$$\boldsymbol{E} = \boldsymbol{QQ}^{\boldsymbol{T}} \tag{8.10}$$

where

E is the variance covariance matrix of **S**

The matrix **S*** is defined by

$$\boldsymbol{S}^* = \boldsymbol{S}(\boldsymbol{Q}^{-1})^T\boldsymbol{P}^T \tag{8.11}$$

S*** has **C** as its correlation matrix. By rearranging the values in the individual columns of **X** to have same rank order with **S*** will construct the matrix **X*** which has rank correlation matrix close to **C**.

After constructing the sample set, each element of the sample is supplied to the model as input, and the corresponding model predictions leads to sequence of results of the form

Step 3:

Model is evaluated for each sample element shown in Equation 8.7. Creating a sequence of results of the form;

$$\boldsymbol{y}_i = f(x_{i1}, x_{i2}, \ldots, x_{in}) = f(\boldsymbol{x}_i), \qquad \text{i} = 1,2,\ldots,\text{m} \tag{8.12}$$

Model evaluations described in Equation 8.11 create a mapping from the parameters to the results of analysis y_i, which can be studied in subsequent uncertainty and sensitivity analysis.

Step 4:

Results obtained from the analysis are used as the basis for an uncertainty analysis. One way to represent the uncertainty in y can be by means of mean and variable. When random or Latin hypercube sampling is used to generate the sample, the expected value and variance of y can be estimated by the following formula [88].

$$E(y) \doteq \sum_{i=1}^{m} \frac{y_i}{m} \tag{8.13}$$

$$V(y) \doteq \frac{\sum_{i=1}^{m} \left[y_i - E(y) \right]^2}{m-1} \tag{8.14}$$

Use of expected value and variance to characterize uncertainty reduces all of the information in the sample set about the variability in y to two numbers. Clearly, information is lost in this process. Another way to summarize the variability in y is through the use of an estimated distribution function. In particular, this function is given by the step function *F* defined by

$$F(y) = \begin{cases} 0 & \text{if } y < y_i \\ \dfrac{i}{m} & \text{if } y_i \le y < y_{i+1}, \qquad i = 1,2,....,m-1 \\ 1 & \text{otherwise} \end{cases} \tag{8.15}$$

where

y have been ordered so that $y_i \le y_{i+1}$ creating a plot that displays all the information contained about the uncertainty in y in the sample set.

Step 5:

In this step sensitivity analysis, based on an exploration of the mapping from analysis input to analysis results. One of the simplest but also most useful techniques is the generation of scatterplots. A scatterplot for input variable x_j and the output variable y_i is a plot of the points

$$(x_{ij}, y_i), \qquad i=1, 2 ,. . . . ,m \tag{8.16}$$

Sensitivity analysis performed as a part of Monte Carlo studies are often based on regression analysis. In this approach, a model of the form in Equation 8.17 is developed from the mapping between analysis inputs and analysis results [88].

$$y = b_0 + \sum_j b_j x_j \tag{8.17}$$

where

x_j are the parameters under consideration

b_j are the coefficients that must be determined

The coefficients b_j can be used to indicate the importance of the individual variables x_j with respect to the uncertainty in y.

Computation of bj in Equation 8.17, is based on the minimization of sum of the misfits to the model of each equation [64].

In order to measure the extend to which the regression model can match the observed data R^2 value is used. R^2 is computed from the formula [88];

$$R^2 = \frac{\sum_i (\hat{y}_i - \bar{y}_i)}{\sum_i (y_i - \bar{y}_i)} \tag{8.18}$$

where

y_i is the actual value computed from the sample set

$\hat{y}_i$ is the estimate of y_i obtained from the regression model

$\bar{y}_i$ is the mean of y_i

When the variation about the regression line is small, the corresponding R^2 value will be close to 1. Conversely, if variation about the regression line is large, then the corresponding R^2 will be close to 0.

The coefficients of the variables do not represent the importance of variables in the model. Because the unit of variable directly affects the coefficient, in order to obtain an idea about the importance of the variables, parameters and the output values are normalized by subtracting the mean and dividing by standard deviation. After this process, the coefficients are computed again, and the computed coefficients after the standardization is called standardized regression coefficients. The standardization formulae can be shown as [88];

$$Y = \left(\frac{y_i - \bar{y}}{\sigma_y} \right) \tag{8.19}$$

$$x_i = \left(\frac{x_{ij} - \bar{x}_i}{\sigma_{xi}} \right) \tag{8.20}$$

where;

Y is the standardized output

Xi is the standardized parameters

$$\bar{y} = \frac{1}{m} \sum_{i=1}^{m} y_i$$

$$\bar{x}_i = \frac{1}{m}\sum_{j=1}^{m} x_{ij}$$

$$\sigma_y = \sqrt{\frac{\sum_{i=1}^{m}(y_i - \bar{y})^2}{m-1}}$$

$$\sigma_{xi} = \sqrt{\frac{\sum_{i=1}^{m}(x_{ij} - \bar{x}_i)^2}{m-1}}$$

When more than one parameter is under consideration, partial correlation coefficients can be used to provide a measure of the linear relationships between the output variable y and the individual parameters x_p. The partial correlation coefficient between y and an individual variable x_p is obtained from the use of a sequence of regression models. To compute partial correlation coefficient two regression models are constructed [88];

$$\hat{y} = b_0 + \sum_{j \neq p} b_j x_j \tag{8.21}$$

where

$$\hat{x}_p = c_0 + \sum_{j \neq p} c_j x_j$$

The results of the two preceding regressions are used to define the new variables y - $\hat{y}$ and $x_p - \hat{x}_p$. The partial correlation coefficient between y and x_p is the correlation coefficient between y - $\hat{y}$ and $x_p - \hat{x}_p$. Thus, the partial correlation coefficient provides a measure of linear relationship between y and x_p with the linear effects of the other variables removed. The partial correlation coefficient provides a measure of the strength of the linear relationship between two variables after a correction has been made for the linear effects of the other variables in the analysis, and the standard regression coefficient measures the effect on the output variable that results from perturbing an input variable by a fixed fraction of its standard deviation. Thus, partial correlation coefficients and standardized regression coefficients provide related, but not identical measures of variable importance. In particular, the partial correlation coefficient provides a measure of variable importance that tends to exclude the effects of other variables, the assumed distribution for the particular input variable under consideration, and the magnitude of the impact of an input variable on an output variable.

8.1.3 Fourier Amplitude Sensitivity Test (FAST)

FAST is based on performing a numerical calculation to obtain the expected value and variance of a model prediction. Basis of this calculation is a transformation that converts a multidimensional integral over all the uncertain model inputs to a one dimensional integral. Further, a decomposition of the Fourier series representation of the model is used to obtain the fractional contribution of the individual input variables to the variance of the model prediction. FAST method involves the following procedure;

The output y is linked through the model f to a set of n parameters $\mathbf{x} = [x_1, x_2, ..., x_n]$ which can be represented as $y = f(\mathbf{x})$. It is possible to state the expressions for the expected value and variance of y as [88];

$$E(y) = \int_{\Omega} f(\mathbf{x}) p(\mathbf{x}) d\mathbf{x} \tag{8.22}$$

$$V(y) = \int [f(\mathbf{x}) - E(y)]^2 p(\mathbf{x}) d\mathbf{x} \tag{8.23}$$

where;

p(**x**) is the probability distribution function of **x**.

Ω is the set of all possible values that **x** can take.

The multidimensional integrals are difficult to evaluate and this difficult is overcome by applying a procedure that convert the multidimensional integral to one dimensional integral. This is done along a curve exploring the n dimensional domain Ω. The curve is defined by a set of parametric equations [88],

$$x_i(s) = G_i(\sin \omega_i s), \qquad \forall\, i = 1, ..., n \tag{8.24}$$

where;

s is a scalar variable over the range $-\infty < s < +\infty$

G_i are transformation functions

ω_i is a set of different frequencies associated with each parameter.

So the integral in Equation 8.18 becomes

$$E(y) = \frac{1}{2\pi} \int_{-\pi}^{\pi} f[G_1(\sin \omega_1 s), G_2(\sin \omega_2 s), \ldots, G_n(\sin \omega_n s)] ds \tag{8.25}$$

In the second model, as s varies all the factors change simultaneously along a curve that systematically explores Ω. Each x_i oscillates periodically at the corresponding frequency ω_i. The output y shows different periodicities combined with the different frequencies ω_i, whatever the model f is. If the i^{th} factor has strong influence on the output, the oscillations of y at frequency ω_i shall be of high amplitude. This is the basis for computing a sensitivity measure, which is based for factor x_i, on the coefficients of the corresponding frequency ω_i and its harmonics. None of the frequency must be obtainable as a linear combination of the others with integer coefficients, so;

$$\sum_{i=1}^{n} r_i \omega_i \neq 0, \qquad -\infty < r_i < +\infty \tag{8.26}$$

If the condition mentioned in Equation 8.26 is satisfied, the curve is space filling and according to the ergodic theorem the rth moment can be computed by evaluating the model along the curve

$$\bar{y}^{(r)} = \lim_{T\to\infty} \frac{1}{2T} \int_{-T}^{T} f^r\left(x_1(s), x_2(s), \ldots x_n(s)\right) ds \tag{8.27}$$

Cukier showed that if ω_i 's are positive integers, then $T = 2\pi$. By considering *f(s)* within the finite interval (- π; π) Equation 8.22 and Equation 8.23 become [23]

$$E(y) = \frac{1}{2\pi} \int_{-\pi}^{\pi} f(s) ds \tag{8.28}$$

$$V(y) = \frac{1}{2\pi} \int_{-\pi}^{\pi} f^2(s) ds - \left[\frac{1}{2\pi} \int_{-\pi}^{\pi} f(s) ds\right]^2 \tag{8.29}$$

If the function *f(s)* is expanded in a Fourier series, the following equation is obtained;

$$y = f(s) = \sum_{j=-\infty}^{+\infty} \left\{A_j \cos js + B_j \sin js\right\} \tag{8.30}$$

where;

$$A_j = \frac{1}{2\pi} \int_{-\pi}^{\pi} f(s) \cos(js) ds \tag{8.31}$$

$$B_j = \frac{1}{2\pi} \int_{-\pi}^{\pi} f(s) \sin(js) ds \tag{8.32}$$

$$j \in \mathrm{Z} = \{-\infty, \ldots, -1, 0, 1, \ldots, +\infty\}$$

The spectrum of the Fourier series expansion is defined as $\Lambda_j = A_j^2 + B_j^2$ with $j \in Z$ .Since *f(s)* is a real valued function, A_j, B_j, and Λ_j have the following properties;

$A_{-j} = A_j \quad B_{-j} = -B_j \quad \Lambda_{-j} = \Lambda_j$.

By evaluating the spectrum for the fundamental frequency ω_i and its higher harmonics $p\omega_i$, D_i , portion of the output variance D arising from the uncertainty of parameter *i* can be estimated as:

$$\hat{D}_i = \sum_{p \in Z^o} \Lambda_{p\omega_i} = 2\sum_{p=1}^{+\infty} \Lambda_{p\omega_i} \tag{8.33}$$

where;

$$Z^0 = Z - \{0\}$$

By summing all Λ_j, $j \in Z^0$ total variance can be estimated as [23];

$$\hat{D} = \sum_{j \in Z^0} \Lambda_j = 2\sum_{j=1}^{+\infty} \Lambda_j \qquad (8.34)$$

The ratio $\hat{D}_i / \hat{D}$ is the estimate of the main effect of x_i on y. This ratio can be used to computer the rank of the importance of the individual parameters with respect to their impact on the uncertainty in ***y***. In practice, the integrals that define A_j and B_j, must be approximated numerically also the series in Equation 8.33 must be truncated. In principle, its magnitude does not depend on the choice of the frequencies used in computations.

8.2 Implementation of Sensitivity Analysis Methods for CCD Cameras

In this subchapter the sensitivity analysis algorithms explained in chapter 8.1 will be implemented by DRM for CCD frame cameras. Differential analysis and Monte Carlo methods are implemented by 15 parameters. On the other hand, FAST is implemented with only 11 parameters. The reason of this is explained in the implementation part. Moreover the performance and the results of the sensitivity analysis methods are compared at the end of this subchapter.

8.2.1 Implementation of Differential Analysis (Covariance Analysis)

Since y array includes both ϕ and λ, the sensitivity analysis will be performed for each output variables separately. Sensitivity analysis of the new rectification method with Differential Analysis is implemented to 9 different pixel positions on the CCD array of the Bilsat. The pixel positions are given as

Table 8.1 Image Coordinates of analysis locations

	1	2	3	4	5	6	7	8	9
x	1	1	1	1024	1024	1024	2048	2048	2048
y	1	1024	2048	1	1024	2048	1	1024	2048

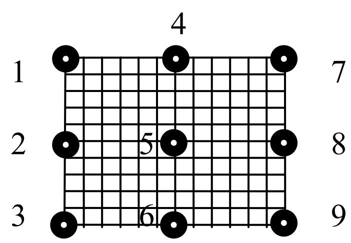

Figure 8.1 Illustration of analysis locations.

The relationship between the parameters and the function can be written as;

$$\boldsymbol{y} = f\left(f, \Delta X, \Delta Y, k_1, k_2, p_1, p_2, c, \omega, \phi, \kappa, X, Y, Z, h\right) \tag{8.35}$$

where

$\boldsymbol{y}$ is the ground coordinates of the corresponding pixel

h is the elevation of ground point obtained from DEM

the remaining are the interior and exterior camera parameters explained at chapter 4.

Variance of the rectification is estimated by the following equation

$$\sigma_\phi^2 = \boldsymbol{X}_\phi \boldsymbol{D} \boldsymbol{X}_\phi^T \tag{8.36}$$

$$\sigma_\lambda^2 = \boldsymbol{X}_\lambda \boldsymbol{D} \boldsymbol{X}_\lambda^T \tag{8.37}$$

where;

$$\boldsymbol{X}_\phi = \begin{bmatrix} \frac{\partial \phi_1}{\partial f} & \frac{\partial \phi_1}{\partial \Delta x} & \cdots & \frac{\partial \phi_1}{\partial Z} & \frac{\partial \phi_1}{\partial h} \\ \vdots & \vdots & \ddots & \vdots & \vdots \\ \frac{\partial \phi_9}{\partial f} & \frac{\partial \phi_9}{\partial \Delta x} & \cdots & \frac{\partial \phi_9}{\partial Z} & \frac{\partial \phi_9}{\partial h} \end{bmatrix}$$

$$\boldsymbol{X}_\lambda = \begin{bmatrix} \frac{\partial \lambda_1}{\partial f} & \frac{\partial \lambda_1}{\partial \Delta x} & \cdots & \frac{\partial \lambda_1}{\partial Z} & \frac{\partial \lambda_1}{\partial h} \\ \vdots & \vdots & \ddots & \vdots & \vdots \\ \frac{\partial \lambda_9}{\partial f} & \frac{\partial \lambda_9}{\partial \Delta x} & \cdots & \frac{\partial \lambda_9}{\partial Z} & \frac{\partial \lambda_9}{\partial h} \end{bmatrix}$$

$$\boldsymbol{D} = \begin{bmatrix} \sigma_f^2 & & & & & & & & \\ & \ddots & & & & & & & \\ & & \sigma_\omega^2 & \sigma_\omega \sigma_\phi & \sigma_\omega \sigma_\kappa & & & & \\ & & \sigma_\phi \sigma_\omega & \sigma_\phi^2 & \sigma_\phi \sigma_\kappa & & & & \\ & & \sigma_\kappa \sigma_\omega & \sigma_\kappa \sigma_\phi & \sigma_\kappa^2 & & & & \\ & & & & & \sigma_X^2 & \sigma_X \sigma_Y & \sigma_X \sigma_Z & \\ & & & & & \sigma_Y \sigma_X & \sigma_Y^2 & \sigma_Y \sigma_Z & \\ & & & & & \sigma_Z \sigma_X & \sigma_Z \sigma_Y & \sigma_Z^2 & \\ & & & & & & & & \sigma_h^2 \end{bmatrix}$$

The variance of inner orientation parameters are obtained by camera calibration procedure performed by F. Jurgen [33]. The variance covariance of the position is obtained from the output of the GPS receiver and accuracy of the attitude parameters are obtained at the end of star tracker calibration procedure.

After computing the estimated variance of the rectification, fractional contribution to variance is obtained by applying the Equation 8.6. The analysis results are given below.

Table 8.2 Variance of the latitude computed by the differential uncertainty analysis

1,57E-10	1,56E-10	1,63E-10
1,59E-10	1,53E-10	1,61E-10
1,96E-10	1,52E-10	1,69E-10

Table 8.3 Variance of the longitude computed by the differential uncertainty analysis

2,63E-10	2,62E-10	2,62E-10
2,52E-10	2,52E-10	2,54E-10
2,96E-10	3,03E-10	2,88E-10

Uncertainty of both latitude and longitude can be represented in UTM coordinates which is a meaningful result. This is performed by applying the formulae:

$$\sigma_x = \sqrt{\left(\frac{\partial x}{\partial \phi}\sigma_\phi\right)^2 + \left(\frac{\partial x}{\partial \lambda}\sigma_\lambda\right)^2} \tag{8.38}$$

$$\sigma_y = \sqrt{\left(\frac{\partial y}{\partial \phi}\sigma_\phi\right)^2 + \left(\frac{\partial y}{\partial \lambda}\sigma_\lambda\right)^2} \tag{8.39}$$

Table 8.4 Variance of the x coordinate in meters

79,771	79,688	81,374
80,264	78,696	80,847
89,249	78,558	82,778

Table 8.5 Variance of the y coordinate in meters

79,151	78,949	78,957
77,422	77,423	77,795
83,896	84,896	82,779

Fractional contribution of the parameters to the uncertainty with different pixel positions is given in Table B.26.

Sensitivity indexes of the parameters with respect to latitude computed for the pixel location (1024, 1024) are presented as Bar Chart in Figure 8.2. Bar Chart is a proper way of visualization of quantities.

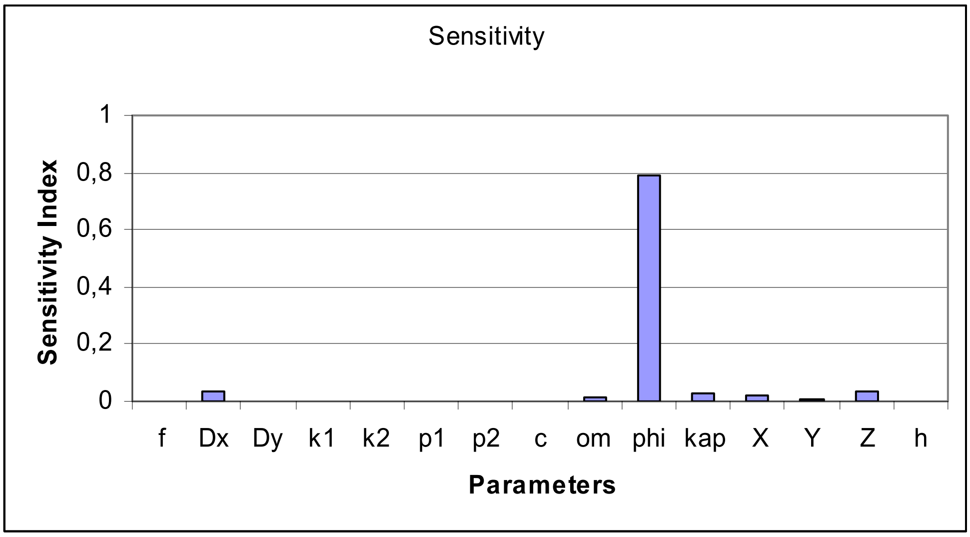

Figure 8.2 Illustration sensitivity indexes of the parameters for latitude.

When sensitivity of the parameters are examined it is seen that lens distortion parameters of the camera including k_1, k_2, p_1 and p_2 and size of the sensing element of the CCD array has smallest contribution to the uncertainty in the rectified image's coordinates. Sensitivity of these parameters is minimum at the middle and increases at the edges and corners of the image. At the middle part of the image c does not contribute any uncertainty to the total uncertainty. This is because size of the sensing element does not have any effect on the rectified coordinates at the middle of the image.

Uncertainty of the elevation obtained from DEM has very small contribution to the total uncertainty. The reason for this result can be explained as the almost nadir imaging of the satellite camera. Therefore, uncertainty in the elevation did not contribute to the total uncertainty considerably. However, in case of a oblique imaging it will be obvious that the contribution of the uncertainty of elevation will be much higher.

The remaining inner orientation parameters and cartesian position of the camera are the parameters that contributes to the total uncertainty moderately. The effect of camera position slightly decreases at the corners of the image. At first glance it can be thought as the effect of camera position decreases at the corners of the image but it is not the case. Since the effect of the other parameters to the uncertainty increases and the contribution of the uncertainty in the camera position to the total uncertainty decreases. In the case of principal coordinates (pc) of the CCD frame, x coordinate of pc contributes more to the uncertainty in the latitude and y coordinate of pc contributes more to the uncertainty in the longitude. Both x and y coordinates of the pc contributes more to the total uncertainty at the lower part of the image.

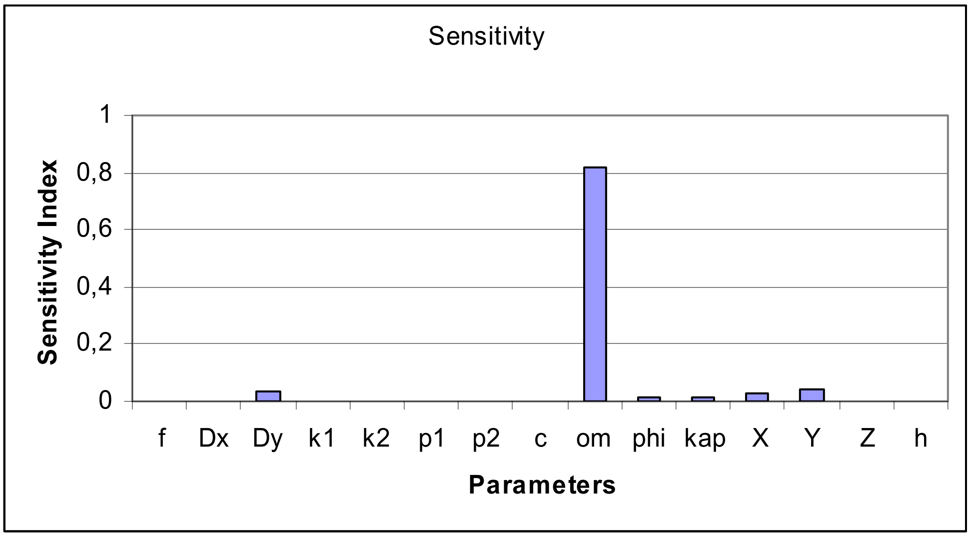

Figure 8.3 Illustration sensitivity indexes of the parameters for longitude

Uncertainty in the attitude angles had contributed to the total uncertainty the most. This is an expected result since the model is very sensitive to the attitude angles which can easily be obtained by examining the partial derivatives. Among the 3 attitude angles κ angle, rotation in z axis, contributes least for both uncertainty in latitude and longitude. Uncertainty in pitch angle, rotation with respect to y axis, has the highest contribution to the uncertainty in the latitude, similarly uncertainty in roll, rotation with respect to x axis, has the highest contribution to the uncertainty in longitude.

8.2.2 Implementation of the Monte Carlo Method

The first step of the Monte Carlo analysis involves the selection of variable ranges and distributions. This step has a significant importance because both the range and distribution of parameters will affect the output of the sensitivity analysis.

In this analysis, distribution of the parameters is accepted as normally distributed and the range is restricted by $\pm 3\sigma$ which covers the 99.9% of the possible range. After the determination of the distributions and ranges, generation of samples representing the determined distribution and ranges are concerned.

Sample size is taken as 1000 and the Monte Carlo analysis is performed for 9 different pixel positions on the CCD array. The results of the 9 analysis each containing 1000 output result is stored in an array shown below.

$$\boldsymbol{X} = \begin{bmatrix} f_1 & \Delta x_1 & \Delta y_1 & \cdots & \omega_1 & \phi_1 & \kappa_1 & X_1 & Y_1 & Z_1 & h_1 \\ f_2 & \Delta x_2 & \Delta y_2 & \cdots & \omega_2 & \phi_2 & \kappa_2 & X_2 & Y_2 & Z_2 & h_2 \\ \vdots & \vdots & \vdots & \cdots & \vdots & \vdots & \vdots & \vdots & \vdots & \vdots & \vdots \\ f_{1000} & \Delta x_{1000} & \Delta y_{1000} & \cdots & \omega_{1000} & \phi_{1000} & \kappa_{1000} & X_{1000} & Y_{1000} & Z_{1000} & h_{1000} \end{bmatrix}_{1000\times 15}$$

After performing the model computations by using the sample set, the expected value and variance for the output value can be estimated.

Table 8.6 Expected values of the corresponding pixel positions for latitude

40,0315	39,7544	39,4745
40,0548	39,7899	39,5175
40,0948	39,8213	39,5465

Table 8.7 Expected values of the corresponding pixel positions for longitude

32,3217	32,3767	32,4080
32,6910	32,7290	32,7704
33,0501	33,0825	33,1311

Table 8.8 Standard deviation of the corresponding pixel values for latitude

1,034E-04	9,618E-05	1,056E-04
9,674E-05	9,569E-05	9,919E-05
1,020E-04	9,453E-05	1,004E-04

Table 8.9 Standard deviation of the corresponding pixel values for longitude

1,564E-04	1,339E-04	1,356E-04
1,272E-04	1,280E-04	1,281E-04
1,359E-04	1,308E-04	1,358E-04

An estimated distribution function gives a better characterization of the uncertainty in an output variable than a mean and variance. Distribution functions can be estimated from the relationship given in Equation 8.15. Abscissa displays the values for the output variable, and the ordinate displays the cumulative probability, which is the probability of obtaining a value equal to or less than a value on the abscissa. The step height is equal to the probability associated with the individual sample elements.

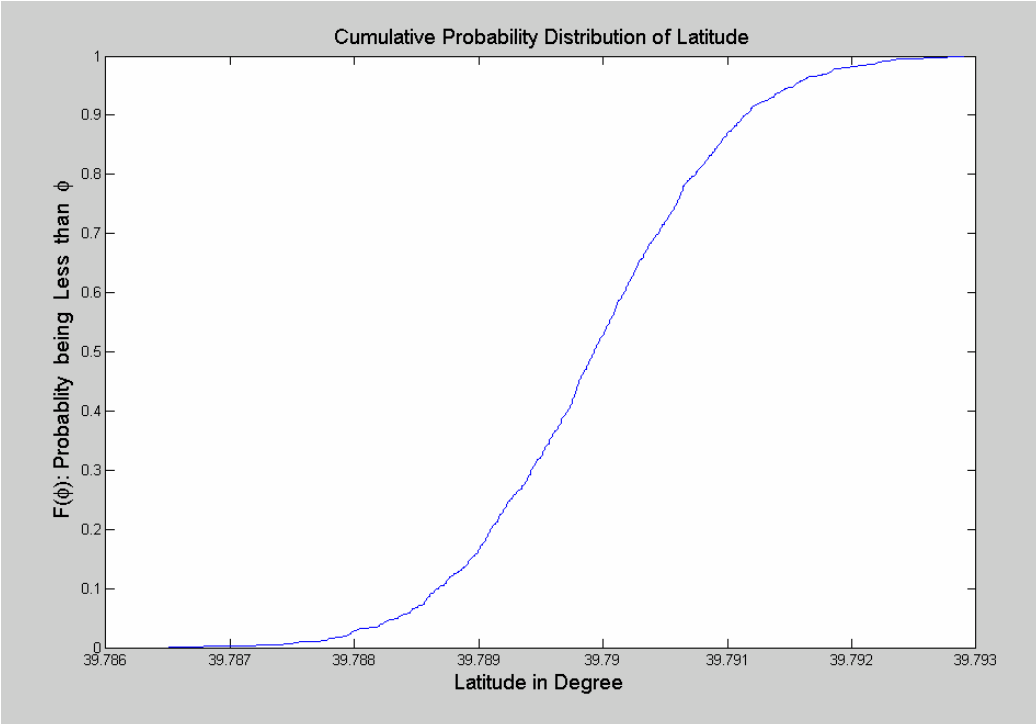

Figure 8.4 Distribution function for the latitude of the camera for the pixel position (1024, 1024)

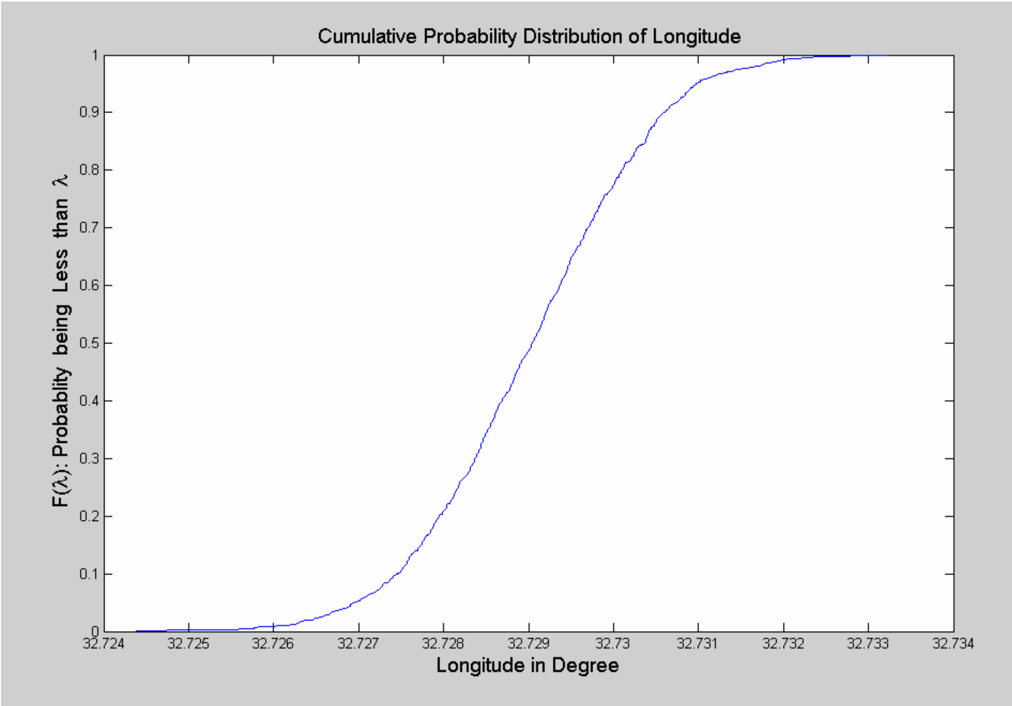

Figure 8.5 Distribution function for the longitude of the camera for the pixel position (1024, 1024)

Cumulative Distribution plots of the Latitude and Longitude of the ground coordinates give considerably precious information. By examining these plots the range of the computed ground coordinates can be obtained and the ranges for any probability ration can easily be computed. The advantage of cumulative distribution plots are, they store all information obtained in the analysis. On the other hand, computing mean and variance gets rid of the information obtained by the analysis and it reduces the information to only two numbers. However, if the two cumulative distribution functions are examined, it will be seen that they are very close to Normal Distribution, so it can be said that there will not be considerable amount of data loss if the data is reduced to mean and variance. But it is certain that original data is always more precise.

Scatterplots are a common way of examining the relationship and sensitivity between the parameters and observations. For this reason by examining the scatterplots the sensitivity of the parameter is tried to be revealed. The generation of scatterplots is undoubtedly the simplest sensitivity analysis technique. This approach consists of generating plots of the (x_{ij}, y_i), $i = 1,. . . ,m$, for each input variable x_j.

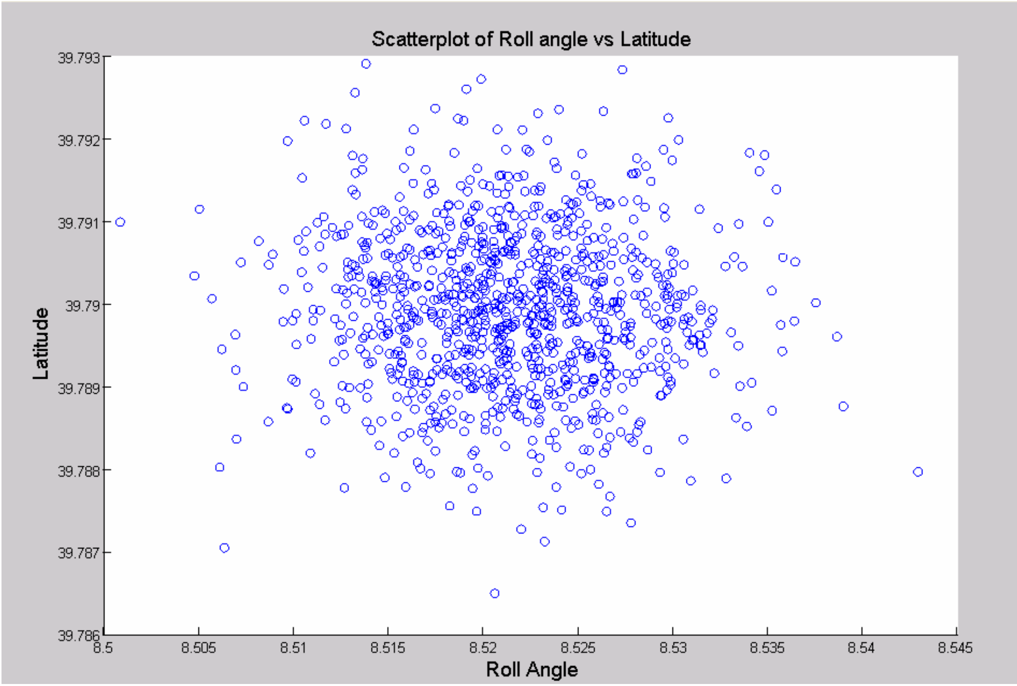

Figure 8.6 Scatterplot of the latitude and roll angle

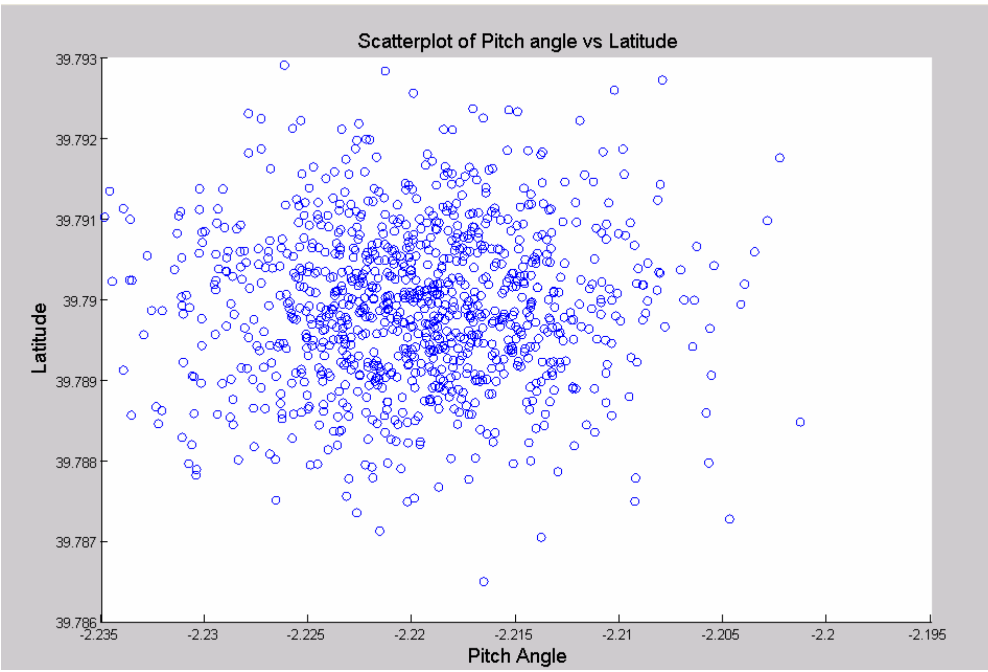

Figure 8.7 Scatterplot of the latitude and pitch angle

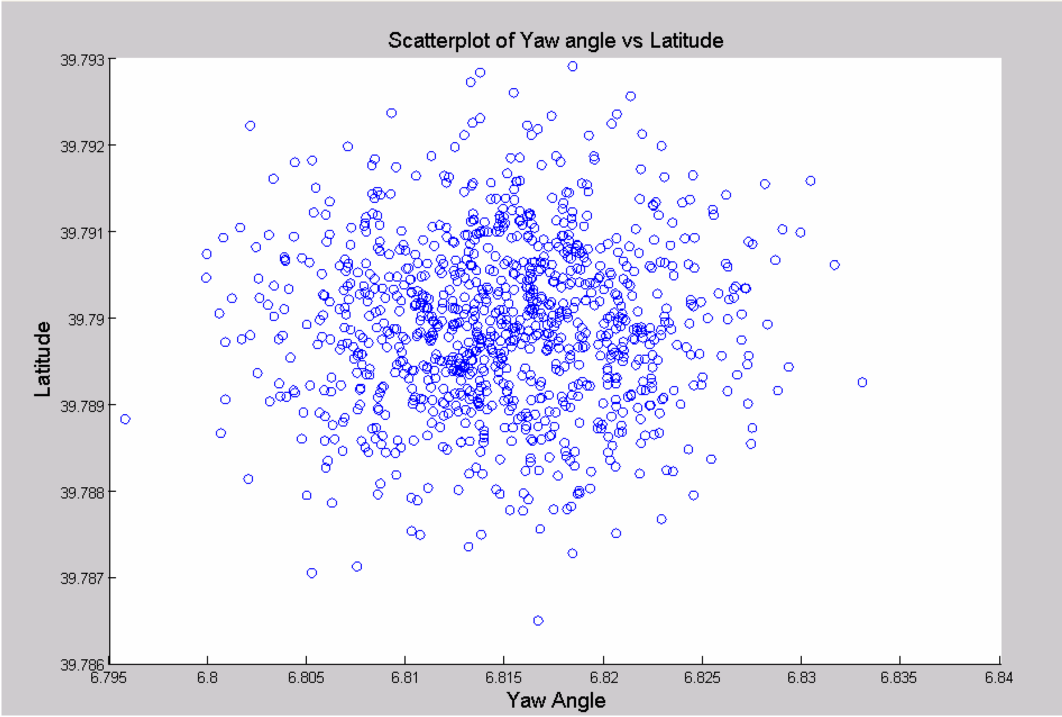

Figure 8.8 Scatterplot of the latitude and yaw angle

When the scatterplot of latitude vs roll angle (Figure 8.6) is examined at first glance it is difficult to see a trend; it seems that the distribution is completely random. Meanwhile, it is not expected to see a trend between roll angle and latitude also.

When the scatterplot represented in Figure 8.7 is examined a slight correlation can be observed between the latitude and pitch angle. The regression line that minimizes the sum of the squares will have a negative slope meaning that if pitch angle is increased the latitude will decrease.

In the scatterplot of the latitude and yaw angle (Figure 8.8) is investigated, it is difficult to see any trend. However, for the central pixel (1024, 1024) it is not expected to see any trend between yaw angle and latitude. So for this pixel location it can be said that latitude is not sensitive to yaw angle.

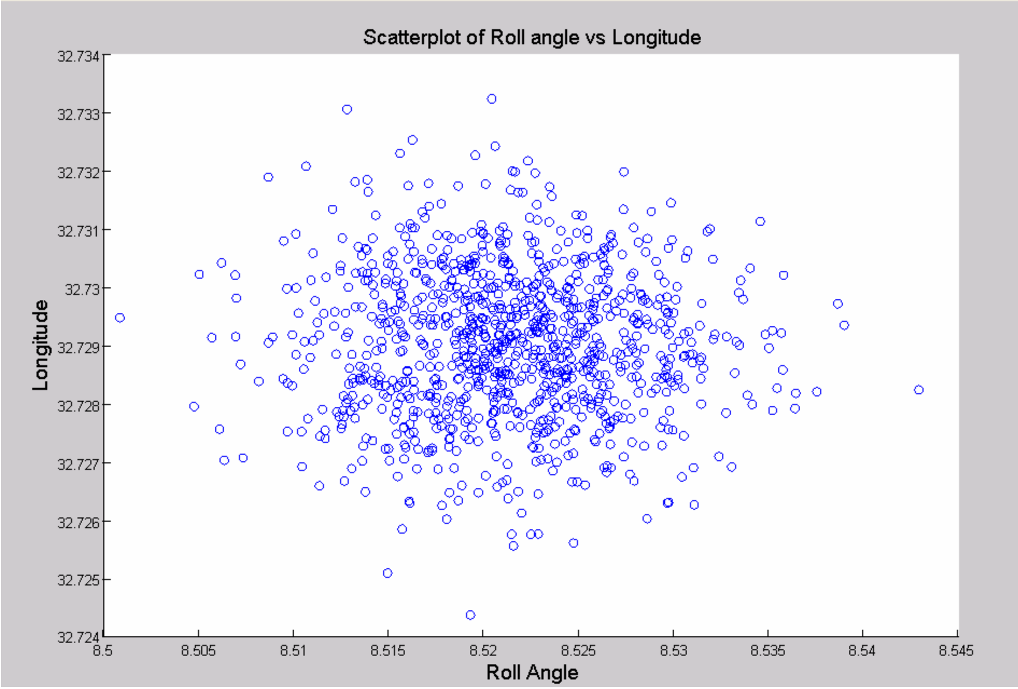

Figure 8.9 Scatterplot of the longitude and roll angle

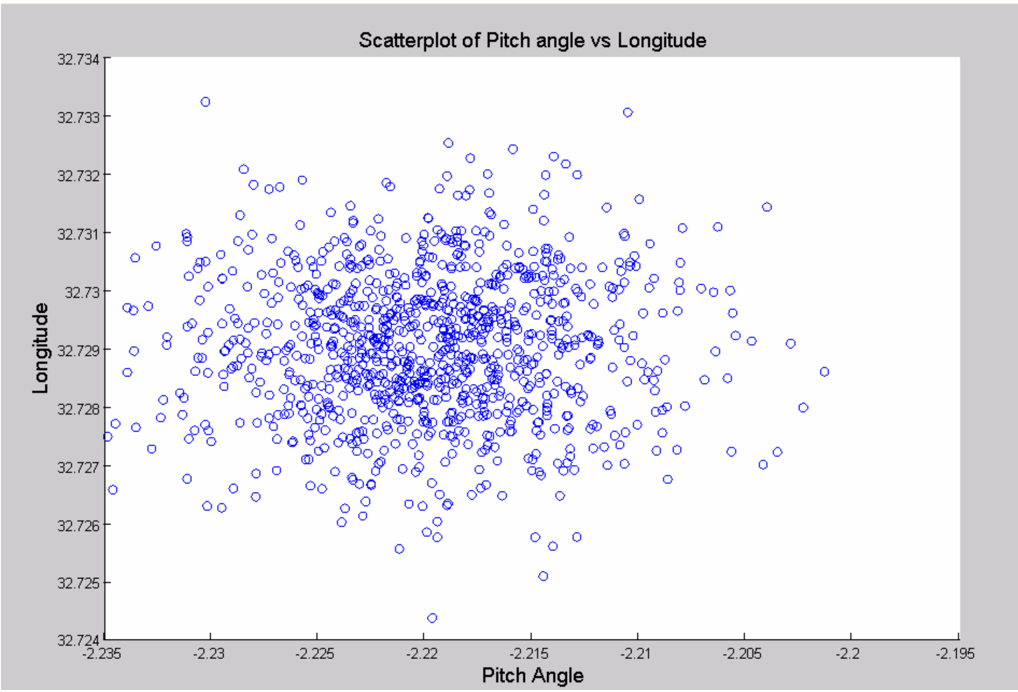

Figure 8.10 Scatterplot of the longitude and pitch angle

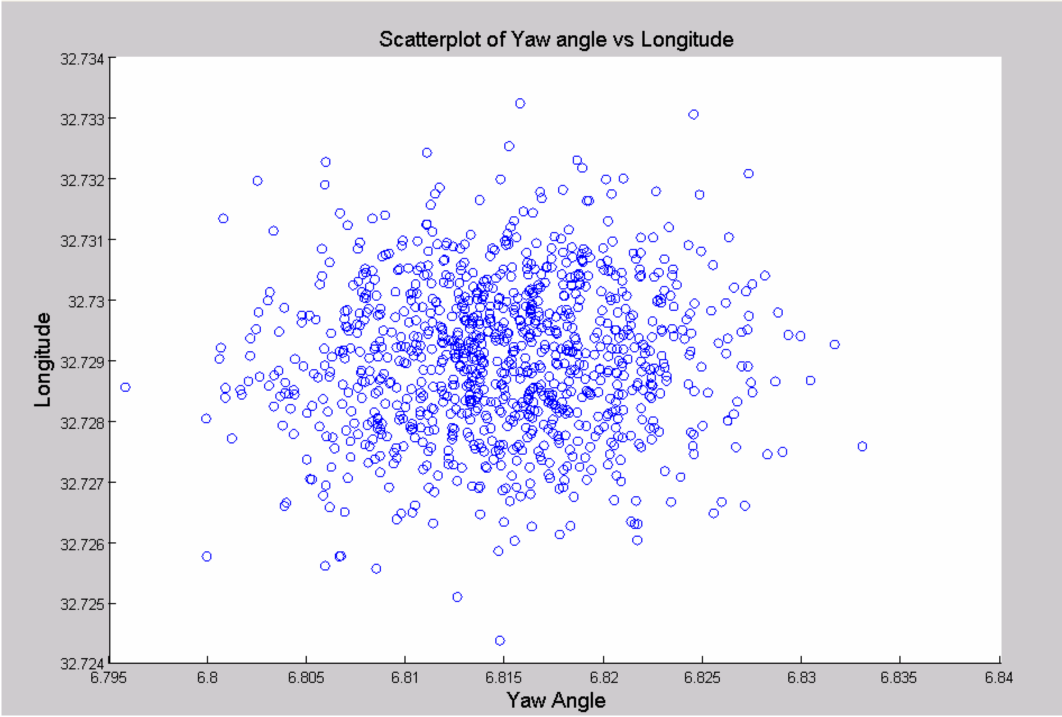

Figure 8.11 Scatterplot of the longitude and yaw angle is shown

Although there is not a sharp trend when the scatterplot is examined carefully it is seen that when roll angle increases longitude decreases (Figure 8.9). This is an expected trend that there is a correlation between longitude and roll angle.

When the scatterplot of pitch angle versus longitude is investigated it is difficult to see a trend (Figure 8.10). The distribution seems to be completely random. This is also an expected result that longitude and pitch angle is not correlated.

When the scatterplot of the yaw angle versus longitude is examined, it can be said that it is difficult to see a trend between yaw angle and longitude (Figure 8.11). This is an expected result since for the pixel position (1024, 1024) it is expected not to see any correlation between yaw angle and longitude. However for the pixel positions located close to the edges of the sensor, changes in yaw angle affect longitude of the ground point considerably.

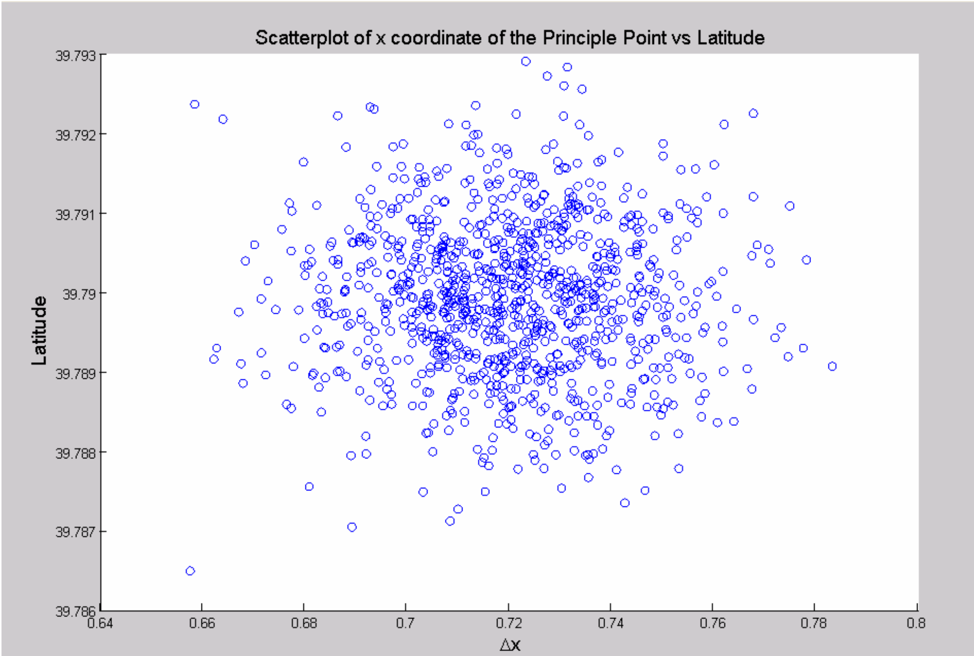

Figure 8.12 Scatterplot of the latitude and x coordinate of the principle point

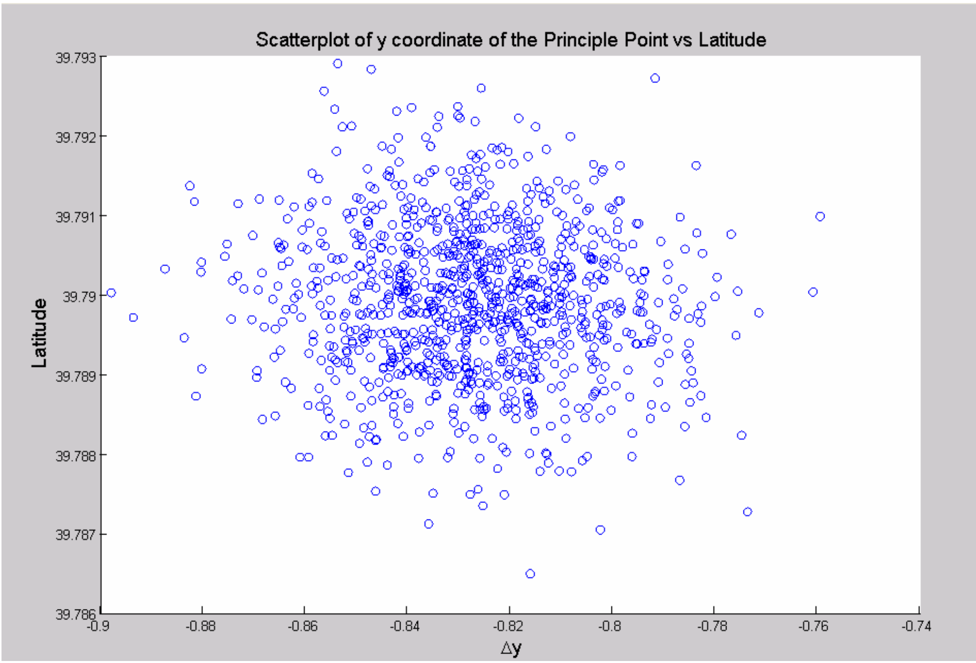

Figure 8.13 Scatterplot of the latitude and y coordinate of the principle point

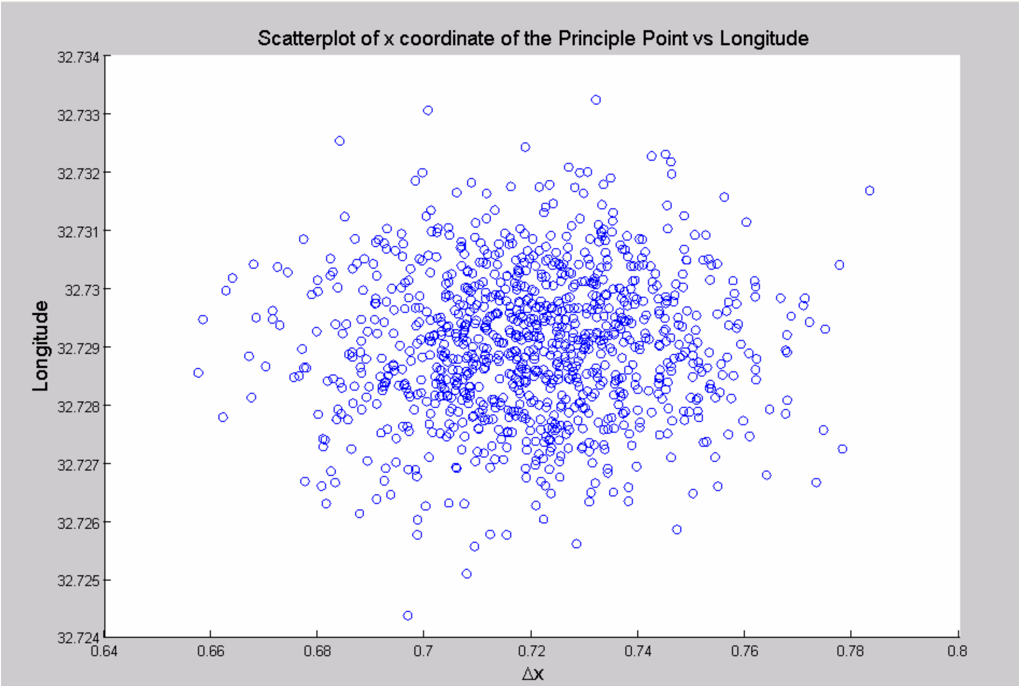

Figure 8.14 Scatterplot of the longitude and x coordinate of the principle point

When the scatterplot of the x coordinate of the principle point, Δx , and latitude of the ground point is examined, it is difficult to see any correlation (Figure 8.12). Additionally, it is not expected to detect a significant correlation between Δx and latitude.

When the scatterplot of the y coordinate of the principle axis Δy , versus latitude of the ground point is investigated it is seen that there is a slight correlation between two parameters (Figure 8.13). It can be concluded that while Δy increases, Latitude decreases. This is also an expected result since the latitude and Δy is expected to be correlated.

When the scatterplot of the x coordinate of the principle point versus longitude is examined, it is seen that there is a weak correlation that when Δx increases, longitude increases as well (Figure 8.14).

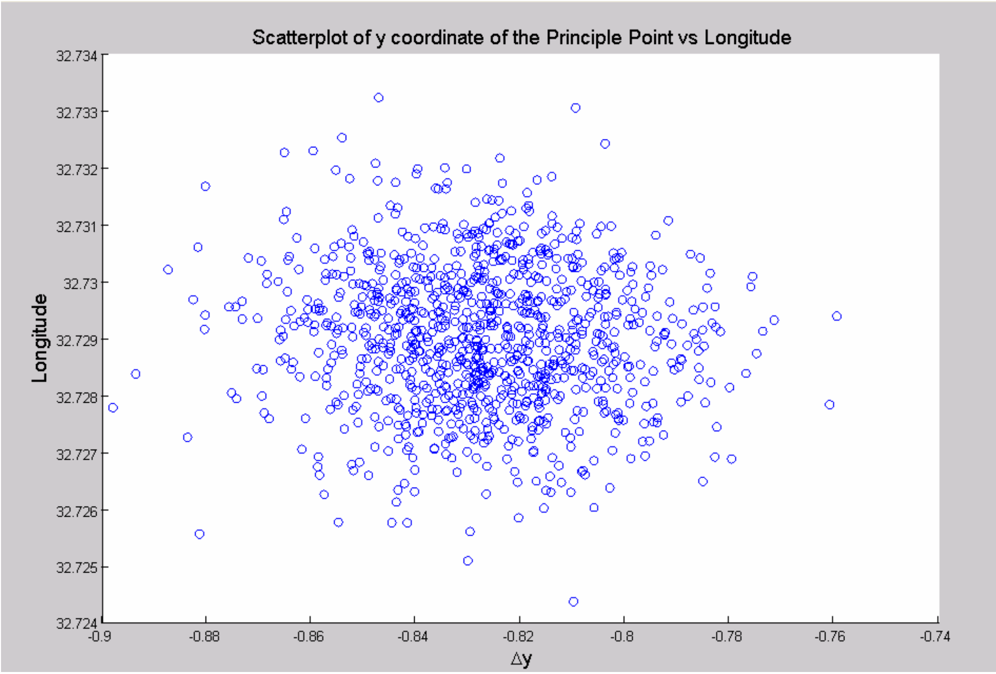

Figure 8.15 Scatterplot of the longitude and y coordinate of the principle point

When the scatterplot of the y coordinate of the principle point, Δy, versus longitude is examined, it is difficult to detect any correlation.

Whole scatterplots are not printed since it is not practical, but when all scatterplots are examined it was not possible to observe a strong trend between the parameters and the ground point's coordinates. However this does not mean that there is not any correlation between the ground point's coordinates and remaining parameters.

When all scatterplots are examined it is seen that lens distortion parameters have almost no correlation with the ground coordinates, this means that lens distortion parameters do not have much sensitivity on ground coordinates. Similarly Elevation of ground coordinates does not have considerable impact on rectified coordinates.

It should be strictly mentioned that the results obtained by examining the scatterplots are valid for the pixel positions next to (1024, 1024) if different pixel positions are examined it should not be expected to end up with similar results. However the result may be similar but it will not be the same. Additionally, correlations detected between attitude and ground point and between principal point and ground point are valid for the current orbit characteristics and attitude angles. If the inclination of the Bilsat changes considerably or any significant change in the attitude angles of the satellite will change the obtained correlations and sensitivity relationships considerably.

After the regression analysis for the geodetic latitude and longitude the following regression coefficients are obtained for the pixel position (1024, 1024).

$$\phi = 1.90e-5+3.38e-6*f-1.22e-5*\Delta x-4.91e-5*\Delta y+6.39e-8*k_1+1.54e-8*k_2$$
$$+9.70e-6*p_1-3.28e-6*p_2+2.54e-7*c-1.58e-3*\omega+9.77e-4*\phi+1.10e-3*\kappa$$
$$+7.01e-8*X_{cam}+4.60e-8*Y_{cam}+5.29e-8*Z_{cam}-1.03e-7*\xi h$$

$$\lambda = 1.16e-5+1.41e-5*f+6.24e-5*\Delta x-7.44e-5*\Delta y-1.40e-7*k_1-2.06e-9*k_2$$
$$-1.31e-5*p_1-2.47e-6*p_2+3.00e-7*c-1.01e-3*\omega+1.09e-3*\phi+3.35e-3*\kappa$$
$$+7.10e-8*X_{cam}+3.33e-8*Y_{cam}+3.27e-8*Z_{cam}-3.35e-8*\xi h$$

Unit of geodetic coordinates for the given coefficients is degree. In this model the coefficients of the parameters are determined in a way which minimizes the sum of the square of the residuals. The higher coefficient does not mean that the variable is more important than the others; it is related with the unit of the variable. For example, coefficients of the camera position are very small when compared with the other parameters coefficients, this is because the satellite position is indicated in millions which is much larger than the other parameters so the coefficients of the camera position is computed to be smaller than the other parameters.

The goodness of fit is measured by the R^2 coefficient, for this regression analysis R^2 is computed as;

0.5156 for the geodetic latitude
0.5018 for the geodetic longitude

This indicates a moderate fit for the nonlinear model with linear regression model.

The solution for the standardized coefficients will be performed by least squares method. The regression model obtained by using standardized coefficients can be seen below;

$$\phi = -2.20e-6*f+2.33e-9*\Delta x-1.54e-8*\Delta y-5.00e-14*k_1+1.84e-12*k_2$$
$$+4.71e-8*p_1+3.95-e-10*p_2-1.23e-14*c-5.59e-7*\omega+1.93e-2*\phi$$
$$+4.54e-4*\kappa+1.31e-6*X_{cam}-1.23e-4*Y_{cam}+8.81e-7*Z_{cam}+3.89e-7*\xi h$$

$$\lambda = -4.75e-6*f+1.28e-8*\Delta x+5.78e-8*\Delta y-7.88e-14*k_1-4.57e-12*k_2$$
$$-9.98e-9*p_1-2.73e-10*p_2-8.60e-15*c-3.11e-2*\omega-3.21e-7*\phi$$
$$+5.53e-7*\kappa-1.97e-4*X_{cam}+1.36e-6*Y_{cam}+7.18e-7*Z_{cam}+1.82e-7*\xi h$$

R^2 value for geodetic latitude is 0.5221
R^2 value for geodetic longitude is 0.5108

Standardized regression coefficients give relationship between the model output and parameters by eliminating the effects of unit of the parameters. This property of standardized regression coefficients makes the comparison between the parameters possible. To begin with latitude, the most important parameter is computed to be pitch angle. Considering the geometry of the satellite, this is not surprising. The second important parameter is Y coordinate of the camera. However size of the sensing element on CCD array is computed to be least important parameter. This is because of the position of the pixel, which the analysis is performed. Just as in the case of differential analysis where the derivative of latitude with respect to c vanishes, the effect of c in Monte Carlo analysis vanishes at the pixel position (1024, 1024). Similar result is observed for yaw angle. Again the importance of yaw angle vanishes at the centre of the image. It seen that focal length is an important parameter both at the centre and at the edges.

When the coefficients of the parameters for the longitude are examined it is seen that roll angle is the most important parameter for the longitude. The second important parameter is the X coordinate of the camera. This result is not surprising when the satellite geometry is considered; these two parameters are expected to be correlated with the longitude. When the remaining parameters are examined besides the camera attitude and camera position, focal length of the camera and anomaly of DEM can be considered as important parameters. Importance of DEM anomaly is computed lower for the longitude than latitude. This is because of the imaging geometry, for a different pixel position or attitude angles a reverse case may be observed. The lens distortion parameters are computed as the least important parameters. Since their coefficients are very small, it is difficult to compare them within each other. A small error in computation procedure may affect the coefficient of the parameter considerably. Since the system was ill conditioned and Tikhonov regularization method is applied, this can easily happen.

Regression analysis often performs poorly when the relationships between the input and output variables are nonlinear. This is an expected result since regression analysis is based on developing linear relationships between variables. The problems associated with poor linear fits to nonlinear data can often be avoided with the technique of rank regression.

In rank regression analysis, original data are replaced with their corresponding ranks and the usual regression procedures are performed on these ranks. Specifically the smallest value of each variable is assigned the rank 1 and the largest value is assigned as rank m where m is the size of the sample set.

The rank correlation data shows that there is no significant correlation between the ranks of the parameters and the output.

Ranked regression coefficients

$$\phi = 8.70e-5*f + 8.86e-5*\Delta x + 8.19e-5*\Delta y + 9.58e-5*k_1 + 9.26e-5*k_2$$
$$+7.32e-5*p_1 + 1.02e-4*p_2 + 9.63e-5*c + 8.92e-5*\omega + 9.80e-5*\phi + 9.97e-5*\kappa$$
$$8.43e-5*X_{cam} + 8.75e-5*Y_{cam} + 7.84e-5*Z_{cam} + 1.03e-4*\xi h$$

$$\lambda = 7.15\text{e-}5*f + 7.29\text{e-}5*\Delta x + 6.74\text{e-}5*\Delta y + 7.88\text{e-}5*k_1 + 7.62\text{e-}5*k_2$$
$$+6.02\text{e-}5*p_1 + 8.38\text{e-}5*p_2 + 7.92\text{e-}5*c + 7.34\text{e-}5*\omega + 8.06\text{e-}5*\phi + 8.20\text{e-}5*\kappa$$
$$+6.93\text{e-}5*X_{cam} + 7.20\text{e-}5*Y_{cam} + 6.45\text{e-}5*Z_{cam} + 8.46\text{e-}5*\xi h$$

R^2 value for geodetic latitude is 0.4905
R^2 value for geodetic longitude is 0.4908

For the solution of the ranked regression coefficients again Tikhonov regularization method is applied. When the coefficients of the ranked transformed data are observed it is seen that the lens distortion parameters are the most important ones. This is really an unexpected result. The reason for this result may be explained by the rank of the lens distortion parameters somehow coincided with each other and the correlation of the rank transformed data of the lens distortion parameters become larger. On the other hand, it is known that the effect of the lens distortion parameters on the ground point's coordinates are very small. When the other parameters are examined it is seen that the x coordinate of the principle point is less important than the y coordinate of the principle point.

When the coefficients of the regression model computed for the longitude are examined, it is seen that their magnitudes are almost same. There are slight differences between the coefficients of parameters which indicates that the rank transformed data did not provide valuable solutions.

Furthermore, the ranked coefficients are standardized and the regression analysis is repeated with the standardized rank coefficients in order to compare the parameter importance with the coefficients of the standardized rank coefficient data results with the other data results. At the end of the analysis the following result is obtained.

$$\phi = 68.22*f + 65.93*\Delta x - 172.04*\Delta y - 113.72*k_1 + 88.25*k_2$$
$$-62.62*p_1 + 212.25*p_2 + 105.29*c - 145.47*\omega + 170.32*\phi - 7.62*\kappa$$
$$91.82*X_{cam} - 13.84*Y_{cam} + 107.26*Z_{cam} + 90.74*\xi h$$

$$\lambda = 58.30*f - 144.75*\Delta x + 15.40*\Delta y + 73.42*k_1 - 59.49*k_2$$
$$-230.03*p_1 - 24.57*p_2 - 63.72*c + 3.13*\omega - 36.05*\phi + 127.80*\kappa$$
$$-66.22*X_{cam} - 104.66*Y_{cam} - 29.70*Z_{cam} - 101.50*\xi h$$

R^2 value for latitude is 0.4356
R^2 value for longitude is 0.4377

When the coefficients of the standardized rank transformed data for latitude are examined, it is seen that attitude angles except for yaw angle have significant effect on the output. Furthermore, pitch angle has the most importance among the attitude angles. It is surprising that asymmetric lens distortion parameter p_1 has the highest coefficient. It is sure that this parameter can not be the most important parameter but its rank transformed form is highly correlated with the rank transformed form of the output variable.

For the coefficients of the longitude, the highest coefficient is again the asymmetric lens distortion parameter. For the longitude asymmetric lens distortion for the x direction has the highest coefficient, while asymmetric lens distortion parameter for the y direction has the highest coefficient for the latitude. x coordinate of the principal point has significant importance also. For position parameters; Y coordinate of the camera position has the highest correlation among the other parameters. Additionally, radial lens distortion parameters have significant importance for both latitude and longitude. Consequently, it can be said that standardized rank transformed data increases the importance of the intrinsic camera parameters.

Table 8.10 Correlation coefficients of latitude computed by original data

Parameter	**Correlation Coefficient**
f	0.019814
Δx	-0.015475
Δy	-0.059639
k1	0.011546
k2	0.030562
p1	0.018968
p2	-0.0069374
c	0.02393
ω	-0.037016
ϕ	0.023234
κ	0.025821
X	0.075037
Y	0.04826
Z	0.055268
ξh	-0.062685

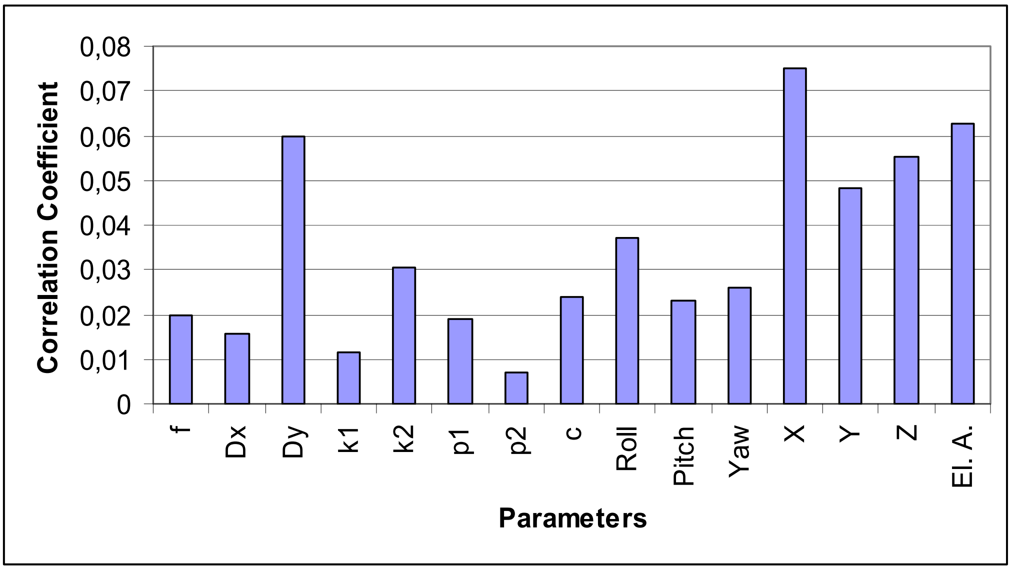

Figure 8.16 Bar chart of the correlation coefficients for latitude

In Figure 8.16 absolute values of the correlation coefficients are plotted in order to represent the magnitude of correlation.

When the partial correlation coefficients of the parameters computed for the latitude are examined, it is seen that the lens distortion parameters have slightly lower importance than the position and attitude of the camera. To begin with focal length of the camera, it has very low correlation with the latitude; this is probably because of the image coordinates of the analysis location. As the previous analysis had shown, at the center of the image effect of focal length on the ground coordinates decreases. As expected latitude is correlated with the y coordinate of the principle point. In the analysis it is seen that there is a strong relationship between Δy and latitude. As computed in the regression analysis second radial lens distortion parameter k_2 has stronger correlation than first radial lens distortion parameter k_1. Additionally, asymmetric lens distortion parameters have comparably less effect on latitude but first asymmetric lens distortion parameter has stronger correlation. Size of the sensor of the CCD frame has considerably stronger correlation with the latitude. Although for the center of the image it is expected to see no correlation with ground coordinates, c has important correlation with latitude.

Position and attitude are the parameters that strong correlations are expected to be observed. On the contrary, slightly larger correlation than the interior camera parameters are found out. Especially the attitude angles have very weak correlation. Roll and yaw angles are not expected to have strong correlation with latitude, however pitch angle is thought to be the most important parameter for the latitude has very weak correlation. This can be explained as the relationship between pitch angle and latitude can be expressed in terms of other parameters such as; camera position and principle point coordinates. Because of this, partial correlation coefficient of pitch is lower than the expected value.

For the camera position, X and Y coordinates have strong correlation which is an expected result. However Z coordinate of the camera position has the highest correlation coefficient among all parameters which is not expected. Furthermore, elevation anomaly has very strong correlation between latitude, which is not an expected result also.

Correlation coefficients of parameters for longitude for the pixel coordinate (1024, 1024) are given as;

Table 8.11 Correlation coefficients of longitude computed by original data

Parameter	**Correlation Coefficient**
f	0.062596
Δx	0.059495
Δy	-0.069782
k1	-0.022712
k2	-0.0030084
p1	-0.019923
p2	-0.0040983
c	0.034977
ω	-0.018621
ϕ	0.019947
κ	0.060504
X	0.061843
Y	0.027501
Z	0.02658
ξh	-0.016636

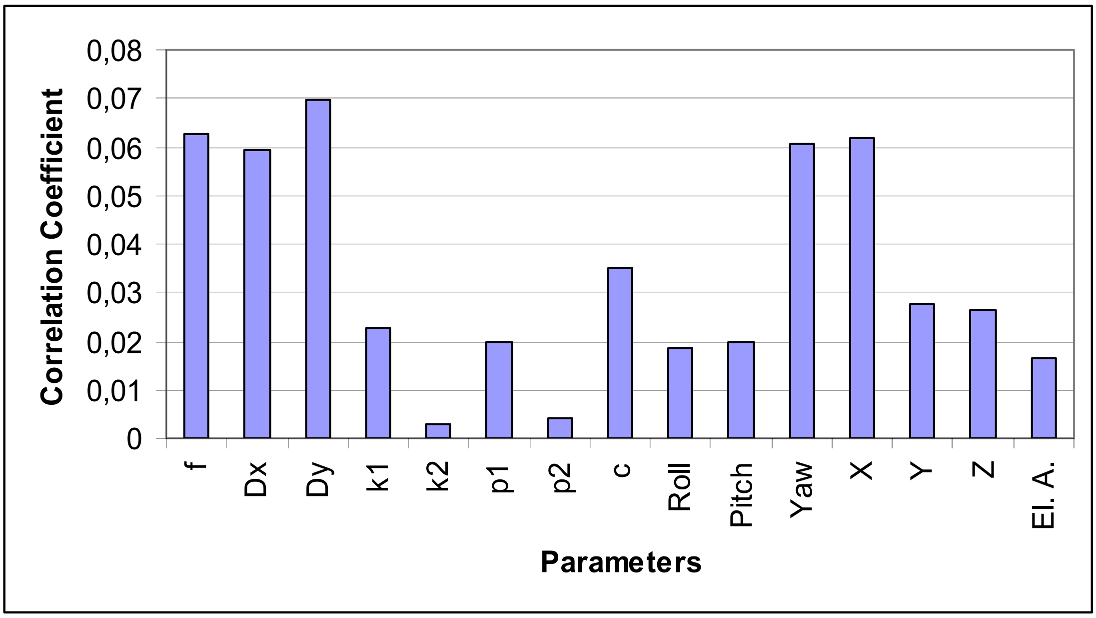

Figure 8.17 Bar chart of the correlation coefficients for longitude

In Figure 8.17 absolute values of the correlation coefficients are plotted in order to represent the magnitude of correlation.

When the correlation coefficients for the longitude are examined it is seen that focal length of the camera has strong correlation with the longitude. In the previous analysis weak correlation with the latitude has been observed. Principle coordinates of the sensor have stronger correlation with the longitude. In the previous analysis y coordinate was computed to have stronger correlation with latitude, similarly for this analysis it is expected to observe strong correlation with x coordinate. Although x coordinate has strong correlation, y coordinate has stronger correlation than x, which is not expected. Radial lens distortion parameters have slightly weak correlation, first radial lens distortion parameter has stronger correlation than the second parameter as expected. Same situation is observed in asymmetric lens distortion parameters also. Similar to the previous analysis, size of the sensor of the CCD frame has strong correlation with ground coordinates. This correlation is not expected for that pixel coordinates where the analysis was performed.

For the attitude and position of the camera, the correlation observed is below the expectations. Especially roll angle has very little correlation with longitude. On the other hand, roll angle is expected to have the strongest correlation with the longitude. Pitch angle has weak correlation which is expected to be observed but yaw angle has very strong correlation which is not expected to be observed. Among the three attitude angles yaw angle is the most correlated parameter, which is certainly an unexpected result leads to the conclusion; the relationship between the yaw angle and longitude can not be represented by the other parameters. For the camera position X coordinate of the camera has very strong correlation, after the focal length of the camera it has the strongest correlation with longitude.

Longitude is expected to be correlated with X and Y coordinates of the camera position, both parameters have direct effect on longitude however correlation of Y coordinate of the camera is weaker than the expected result. Anomaly of the elevation has weak correlation with the longitude. This result was observed at the previous regression analysis also; however ground coordinates are not expected to be highly correlated with elevation anomaly.

Besides partial correlation coefficients of parameters, partial rank correlation coefficients are computed by replacing the original data with rank transformed data. Partial correlation coefficients are presented below.

Table 8.12 Correlation coefficients of latitude computed by rank transformed data

Parameter	**Correlation Coefficient**
f	3.0961
Δx	3.0343
Δy	3.0735
k1	3.084
k2	2.9767
p1	3.049
p2	3.0728
c	3.1129
ω	3.0284
ϕ	3.0216
κ	3.0011
X	3.0317
Y	3.0398
Z	3.0434
ξh	3.0444

When the correlation coefficients computed by the rank transformed data are examined, it is seen that the results are very close to each other. This situation makes commenting on the results difficult because in the computation procedure of the coefficients, Tikhonov regularization is applied for the stabilization of the equation. Accordingly a small error caused by the regularization method may change the variable importance significantly.

Focal length of the camera has slightly stronger correlation with the latitude. Analysis with the original data led to a very weak correlation between focal length and latitude. So it can be said that rank transformation has increased the importance of focal length. Principal point's coordinates have correlation also, especially y coordinate has strong correlation with latitude. This result was observed in the previous analysis also and it is an expected result. First radial lens distortion parameter has strong correlation with the latitude while second lens distortion parameter has weaker correlation. This result was also an expected situation. Additionally, second order lens distortion parameter has the weakest correlation with latitude. Asymmetric lens distortion coefficients have moderate correlation and the second parameter has slightly stronger correlation. This result was observed in the previous analysis also. Size of the sensing element has the strongest correlation. It is known that *c* is an important parameter but its importance is not expected to be stronger than attitude angles.

When the attitude angles are considered, it is seen that roll and pitch angles have moderate importance and Kappa angle has weak correlation. For the latitude it is expected to have strong correlation with pitch angle. However, observing weak correlation with yaw angle is an expected result. For the camera position Z coordinate has the strongest correlation. It is known that all components of camera position influences ground coordinates. However, it is expected to observe higher correlations for X and Y components of the camera position. Elevation anomaly of DEM has moderate correlation with latitude. To conclude the analysis, size of the sensing element has the strong correlation which is an expected result however importance of the Pitch angle is found out to be lower than the expectations.

Next analysis is performed with the rank transformed data to compute the correlation between geodetic longitude and the parameters.

Table 8.13 Correlation coefficients of longitude computed by rank transformed data

Parameter	Correlation Coefficient
f	3.1034
Δx	3.0472
Δy	3.0346
k1	3.0744
k2	3.0353
p1	3.0879
p2	3.0578
c	3.0298
ω	3.0088
ϕ	3.0823
κ	3.0614
X	3.0829
Y	3.0912
Z	3.1195
ξh	3.1131

When the coefficients of the correlation analysis for the longitude with rank transformed data are examined, it is seen that they are close to each other. This is similar to the previous analysis of rank transformed data of latitude. It can be concluded that rank transformed data gives correlation coefficients which are close to each other. So this makes the interpretation of the results of the analysis difficult.

Focal length of the camera has strong correlation with longitude. This was observed in the previous analysis also. However, rank transformed data has slightly decreased its correlation. Principle point coordinates have moderate importance on longitude. Both coordinates have very similar correlation on longitude which is not an expected result. When the imaging geometry of the camera is considered it is expected that the x coordinate should have considerably higher importance on longitude than y coordinate has. Radial lens distortion parameters have moderate importance on the longitude. First radial lens distortion parameter has considerably higher correlation than the second one, which was observed in the previous analysis also. Asymmetric radial lens distortion parameters have slightly stronger correlations. It can be said that higher importance for asymmetric lens distortion was observed by using rank transformed data. Additionally, first asymmetric lens distortion parameter has stronger correlation than the second one. Size of the sensing element has very weak correlation with the longitude, so this can be interpreted as rank transformation decreased the correlation between longitude and size of the sensing element.

When the attitude angles are considered it is seen that pitch and yaw angles have the strongest correlation with longitude. For the roll angle which has slightly weak correlation with latitude is expected to have strong correlation with longitude. Coordinates of the camera position have very strong correlation with longitude. The highest coefficient among all parameters was Z coordinate of camera position. Apparently, this is not an expected result, because Z coordinate is not expected to be correlated with longitude stronger than X and Y coordinates. Furthermore, its correlation coefficient is higher than camera attitude angles' coefficients which is not an expected result. Elevation anomaly also has very strong correlation with longitude so it can be concluded that rank transformation has increases the correlation between the longitude and camera position and elevation anomaly.

Monte Carlo method is an appropriate model for the sensitivity and uncertainty analysis. Since Monte Carlo techniques are particularly appropriate for analysis problems in which large uncertainties are associated with the input variables. In particular, differential analysis is likely to perform poorly when the relationships between the input and output variables are nonlinear and the input variables have large uncertainties. Moreover, Monte Carlo techniques provide direct estimates for distribution functions [88].

Monte Carlo techniques do not require large amount of sophistication that goes beyond the analysis problem of interest. In contrast, differential analysis require a large amount of specialized knowledge to make them work which can be very costly in terms of analyst time as in the case of taking partial derivatives in differential analysis method. Conceptually Monte Carlo techniques are simpler and do not require modifications to the original model or additional numerical procedures [88].

However, in this analysis better results are obtained at the end of the differential analysis. Since sensitivity analysis of Monte Carlo is based on regression analysis, it did not present proper results for a non linear model.

8.2.3 Implementation of FAST

To start the sensitivity analysis range and distribution of the parameters should be determined. To compare the performance of the methods same range and distributions are defined for the parameters;

To compute one dimensional integral in Equation 8.25 frequencies which is not a linear combination of the others should be assigned for each parameter. Unfortunately only 11 linear independent frequencies can be obtained. For this reason, number of parameters is reduced from 14 to 11. The parameters, which sensitivity will be analyzed are listed with the assigned frequencies in Table 8.14 as following;

Cartesian Camera Coordinates in S_E : X, Y, Z

Attitude of Camera: ω, ϕ, κ

Focal length of the Camera: f

Principal Coordinates: Δx Δy

Radial lens distortion parameters: k_1, k_2

Table 8.14 Frequencies assigned for the parameters are listed.

Parameter	X	Y	Z	ω	ϕ	κ	f	Δx	Δy	k_1	k_2
Frequency	145	177	199	41	67	105	219	229	235	243	247

The 11 parameter integral is reduced to one parameter integral by the following transformation [23];

$$x_i = \bar{x}_i\left(1 + \bar{v}_i \sin \omega_i s\right) \tag{8.40}$$

where;

$\bar{x}_i$ is the nominal value of the i[th] parameter

$\bar{v}_i$ defines the endpoints of the estimated range for uncertainty for x_i

ω_i is the assigned frequency for the i[th] parameter

s varies in $-\pi/2, \pi/2$

The assigned v_i values can be listed as;

Table 8.15 Assigned v_i values for the parameters

Prm	X	Y	Z	ω	ϕ	κ	f	Δx	Δy	k_1	k_2
v_i	8.89e-6	1.32e-5	8.82e-6	0.678	2.62	0.890	0.0057	0.074	0.074	1.78e-4	2.22e-8

The integrals in Equations 8.25 are evaluated numerically for the 9 pixel locations which are same with the differential and Monte Carlo sensitivity analysis implementations. Sensitivity values of the parameters computed for the pixel location (1024, 1024) are presented in Table 8.16 and Table 8.17;

Table 8.16 Computed sensitivity indexes for latitude by FAST

Parameter	Sensitivity
X	0,00072
Y	0,00016
Z	0,00039
ω	0,00743
ϕ	0,00191
κ	0,00078
f	0,00019
Δx	5,00E-06
Δy	0,00010
$\mathbf{k_1}$	0,00019
$\mathbf{k_2}$	0,00021

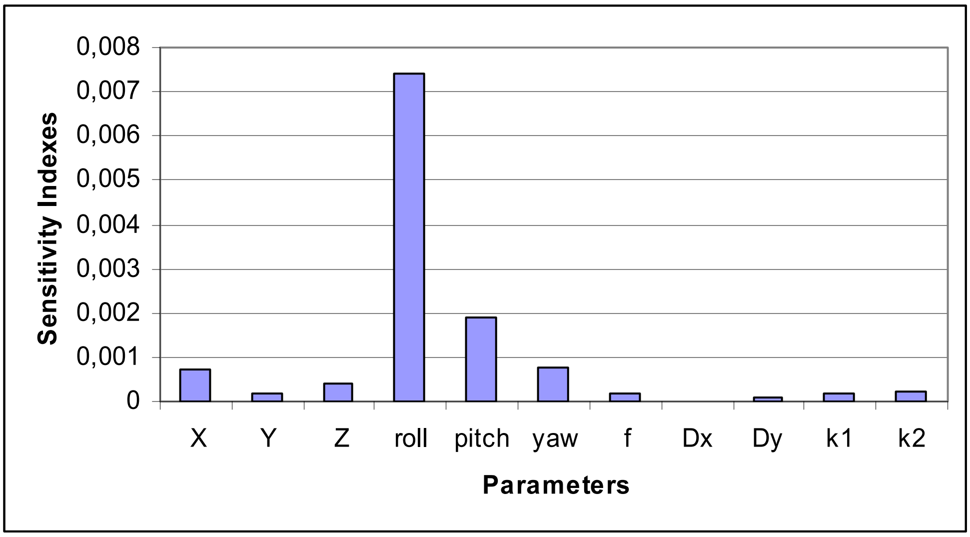

Figure 8.18 Sensitivity Indexes for longitude computed by FAST

When the sensitivity of parameters on the latitude is examined it is seen that the most important parameter is roll angle and the second important one is pitch angle. Least sensitive parameter on the phi coordinate is Δx. As expected Δy has more effect on the latitude than Δx has. Furthermore X cartesian coordinate has significant effect on the latitude.

Table 8.17 Computed sensitivity indexes for longitude by FAST

Parameter	Sensitivity
X	0,00073
Y	0,00015
Z	0,00038
ω	0,00744
ϕ	0,00192
κ	0,00078
f	0,00019
Δx	5,17E-06
Δy	0,00010
k1	0,00019
k2	0,00021

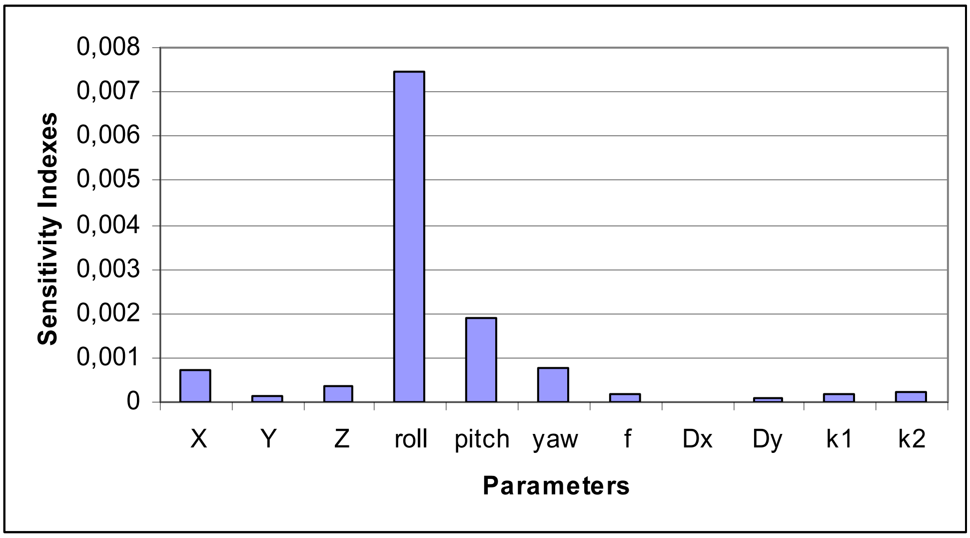

Figure 8.19 Sensitivity Indexes for longitude computed by FAST

When the sensitivity of parameters on the longitude is examined similar results are obtained. Again the most important parameter is roll angle, and then pitch angle is the second important parameter. Least sensitive parameter on the phi coordinate is Δx, however its sensitivity is slightly increased. Furthermore X cartesian coordinate has significant effect on the variance of the lambda coordinate as it effects phi coordinate also. Sensitivity of the parameters on longitude is very similar to their sensitivity on latitude. For the analysis on longitude, it is expected to observe higher sensitivity for Δy and Pitch angle.

Result of the FAST does not depend on the pixel coordinates which is not the case in Differential Analysis and Monte Carlo Simulation. When the analysis results for different pixel locations are examined it is seen that there were almost no differences in sensitivity indexes for the parameters. This is an important advantage of FAST when compared with the other methods since it reduces the number of required model computations significantly.

8.3 Implementation of the Sensitivity Analysis Methods for Pushbroom Scanners

Sensitivity and uncertainty analysis of the DRM is performed by using three methods as in the case for CCD frame camera. Differential analysis, Monte Carlo, and Fourier Amplitude Sensitivity Test (FAST) are implemented respectively. In three methods the sensitivity of the parameters to the model are examined and uncertainty in the results are computed.

For the implementation of Differential Analysis and Monte Carlo Sensitivity analysis 23 parameters are included. However, only 11 parameters are analyzed with FAST. This is because only 11 linearly independent numbers can be obtained [23]. Implementation of Sensitivity Analysis methods are presented below;

8.3.1 Implementation of Differential Analysis (Covariance Analysis)

Differential Analysis method is implemented with 23 parameters, which can be listed as following;

$$\beta = \left[\Omega \; a_1' \; a_2' \; a_3' \; a_4' \; \dot{a}_1 \; \ddot{a}_1 \; \dot{a}_2 \; \ddot{a}_2 \; \dot{a}_3 \; \ddot{a}_3 \; \dot{a}_4 \; \ddot{a}_4 \; \phi_s \; \dot{\phi}_s \; \ddot{\phi}_s \; \lambda_s \; \dot{\lambda}_s \; \ddot{\lambda}_s \; f \; \Delta y \; k_1 \; \xi h \right] \tag{8.41}$$

where

Ω is the right ascension of the ascending node

a'_1 is the roll angle between S_O and S_B

a'_2 is the pitch angle between S_O and S_B

a'_3 is the yaw angle between S_O and S_B

a'_4 is the attitude angle of the camera between S_B and S_C

$\dot{a}_1$ is the change in roll angle with time

$\dot{a}_2$ is the change in pitch angle with time

$\dot{a}_3$ is the change in yaw angle with time

$\dot{a}_4$ is the change in attitude angle of the camera

$\ddot{a}_1$ is the change rate in roll angle with time

$\ddot{a}_2$ is the change rate in pitch angle with time

$\ddot{a}_3$ is the change rate in yaw angle with time

$\ddot{a}_4$ is the change rate in attitude angle of the camera

ϕ_s is position correction for the camera latitude

$\dot{\phi}_s$ is the position correction rate for the camera latitude

$\ddot{\phi}_s$ is the position correction change rate for the camera latitude

λ_s is position correction for the camera longitude

$\dot{\lambda}_s$ is the position correction rate for the camera longitude

$\ddot{\lambda}_s$ is the position correction change rate for the camera longitude

f is the focal length of the camera (mm)

Δy is the principal point coordinate on the pushbroom scanner

k_1 is the radial lens distortion parameter ($1/mm^2$)

ξh is the error of the elevation obtained from DEM.

Differential analysis method is implemented for 15 different pixel locations to examine not only the sensitivity of the parameters but also the change of the sensitivity of the parameters with respect to pixel locations. The pixel locations and distributions are listed below;

Table 8.18 Distribution of analysis locations for pushbroom scanner

1, 1	2500, 1	5000, 1
1, 1000	2500, 1000	5000, 1000
1, 2000	2500, 2000	5000, 2000
1, 3000	2500, 3000	5000, 3000
1, 4000	2500, 4000	5000, 4000

Distribution of the pixel position in the image is shown as;

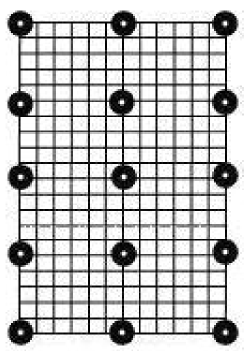

Figure 8.20 Illustration of analysis locations on the image

Similar to the analysis for CCD frame cameras, sensitivity analysis for DRM will be performed for latitude and longitude separately. Variance of the ground positions is computed by Equation 8.4 and Equation 8.5. For the implementation of the differential sensitivity analysis, the variance covariance matrix is assumed to be a diagonal matrix and the order of the parameters will be the same with parameter order in Equation 8.40. Partial derivatives of the parameters with respect to geodetic latitude and longitude of the ground coordinates are represented as;

$$\boldsymbol{X}_{\phi} = \begin{bmatrix} \frac{\partial \phi_1}{\partial \Omega} & \frac{\partial \phi_1}{\partial \omega} & \cdots & \frac{\partial \phi_1}{\partial k_1} & \frac{\partial \phi_1}{\partial \xi h} \\ \vdots & \vdots & \ddots & \vdots & \vdots \\ \frac{\partial \phi_9}{\partial \Omega} & \frac{\partial \phi_9}{\partial \omega} & \cdots & \frac{\partial \phi_9}{\partial k_1} & \frac{\partial \phi_9}{\partial \xi h} \end{bmatrix}_{9\times 23}$$

$$\boldsymbol{X}_{\lambda} = \begin{bmatrix} \frac{\partial \lambda_1}{\partial \Omega} & \frac{\partial \lambda_1}{\partial \omega} & \cdots & \frac{\partial \lambda_1}{\partial k_1} & \frac{\partial \lambda_1}{\partial \xi h} \\ \vdots & \vdots & \ddots & \vdots & \vdots \\ \frac{\partial \lambda_9}{\partial \Omega} & \frac{\partial \lambda_9}{\partial \omega} & \cdots & \frac{\partial \lambda_9}{\partial k_1} & \frac{\partial \lambda_9}{\partial \xi h} \end{bmatrix}_{9\times 23}$$

Variance of the latitude of pixel locations is computed and shown in Table 8.19.

Table 8.19 Variance of latitude computed by differential sensitivity

7,67E-12	8,42E-12	1,14E-11
1,89E-11	3,46E-11	7,64E-12
8,37E-12	1,13E-11	1,87E-11
3,42E-11	7,61E-12	8,32E-12
1,12E-11	1,84E-11	3,38E-11

Variance of the longitude of pixel locations is computed and shown in Table 8.20 as;

Table 8.20 Variance of longitude computed by differential sensitivity

3,82E-11	5,31E-11	1,01E-10
1,89E-10	3,31E-10	3,79E-11
5,27E-11	1,00E-10	1,88E-10
3,29E-10	3,77E-11	5,24E-11
9,94E-11	1,87E-10	3,27E-10

When the variance is transformed from geodetic coordinates to UTM coordinates, the following results shown in Tables 8.21 and 8.22 are obtained.

Table 8.21 Variance of the ground points with respect to UTM x coordinate

311,164	341,491	461,887
766,214	1402,419	310,028
339,523	457,342	757,043
1386,188	308,908	337,596
452,919	748,076	1370,322

Table 8.22 Variance of the ground points with respect to UTM y coordinate

909,385	1263,605	2397,818
4501,326	7889,465	903,623
1255,390	2381,865	4471,800
7838,270	898,027	1247,413
2366,435	4442,750	7788,504

When the sensitivities of the parameters are examined it is seen that the attitude angles have considerable impact on the variance of the ground coordinates (Table 8.23). For the latitude pitch and yaw parameters are very sensitive. Pitch angle is expected to be a sensitive parameter for latitude while yaw angle is not expected to be that much sensitive. Furthermore, change in roll angle with respect to time is very sensitive for latitude. Additionally, latitude is computed to be sensitive to all position anomaly parameters including anomaly in latitude and its rate of change. Because of the obliqueness of the image sensitivity of the DEM error is high.

Longitude is sensitive to roll and theta angles (Table 8.24). The roll and theta angles are expected to have high sensitivity on longitude if the camera geometry is considered. Furthermore, change in pitch angle with respect to time has considerable effect on longitude. This is a similar result of the change in roll angle has high sensitivity on latitude. Surprisingly, longitude is more sensitive to position anomaly of the camera than attitude of the camera. Change in latitude anomaly of the camera has the highest sensitivity while, focal length of the camera has the lowest sensitivity. Additionally error in DEM has slightly important sensitivity on longitude. The remaining parameters do not have considerable sensitivity on longitude. Sensitivity indexes of the parameters for latitude and longitude for the 15 analysis locations are given in Table B.35 and B.36.

Table 8.23 Sensitivity Indexes of the parameters with respect to latitude of ground coordinate (See Equation 8.41).

Parameter	Sensitivity Index
Right Ascension	5,602E-08
Roll	2,312E-03
Pitch	1,641E-01
Yaw	1,038E-02
Theta	2,058E-03
Roll Rate	3,614E-02
Roll Rate Change	6,883E-04
Pitch Rate	5,826E-04
Pitch Rate Change	1,501E-05
Yaw Rate	1,270E-07
Yaw Rate Change	1,075E-07
Theta Rate	4,893E-04
Theta Rate Change	6,625E-03
Phi Anomaly	3,472E-02
Phi A. Rate	4,702E-01
Phi A. Rate Change	2,196E-01
Lambda Anomaly	2,974E-02
L. A. Rate	1,935E-02
L. A. Rate Change	2,620E-03
Focal Length	4,201E-13
Principle Coordinate	1,866E-09
Lens D. Parameter	2,139E-09
DEM Error	4,019E-04

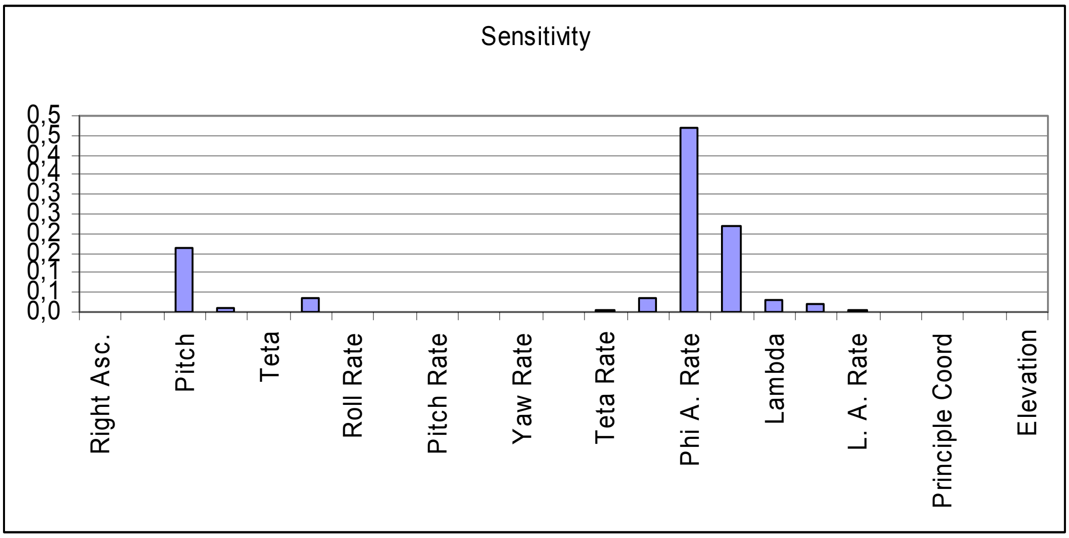

Figure 8.21 Sensitivity indexes of parameters with respect to latitude

Table 8.24 Sensitivity Indexes of the parameters with respect to longitude of ground coordinate.

Parameter	**Sensitivity Index**
Right Ascension	1,203E-04
Roll	3,050E-02
Pitch	1,121E-07
Yaw	1,266E-03
Theta	7,148E-02
Roll Rate	6,497E-06
Roll Rate Change	1,237E-07
Pitch Rate	1,048E-07
Pitch Rate Change	8,883E-03
Yaw Rate	7,519E-05
Yaw Rate Change	6,364E-05
Theta Rate	6,454E-03
Theta Rate Change	8,740E-02
Phi Anomaly	2,375E-08
Phi A. Rate	3,248E-07
Phi A. Rate Change	2,679E-02
Lambda Anomaly	3,628E-03
L. A. Rate	6,722E-01
L. A. Rate Change	9,104E-02
Focal Length	1,458E-11
Principle Coordinate	6,483E-08
Lens D. Parameter	7,430E-08
DEM Error	1,051E-04

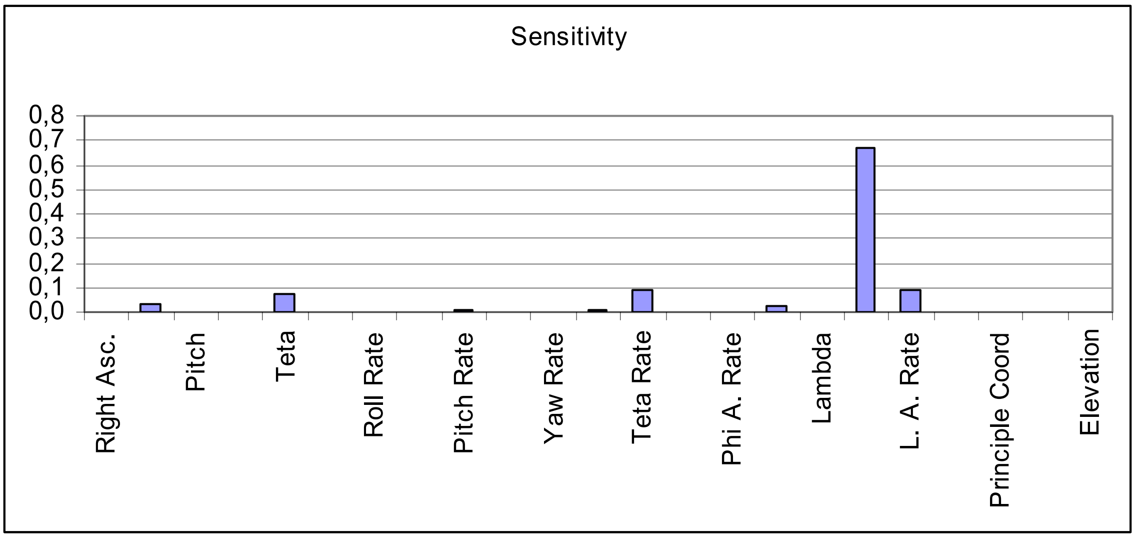

Figure 8.22 Sensitivity indexes of parameters with respect to longitude

8.3.2 Monte Carlo Sensitivity Analysis

For the Monte Carlo Sensitivity Analysis same 23 parameters are selected for the analysis. Distribution of the parameters is accepted as normally distributed and the range is restricted by $\pm 3\sigma$ of its mean value which covers the 99.9% of the possible range. For the sampling Latin Hypercube sampling method is used.

For the sample generation it is assumed that there is no correlation between parameters. Similar to the Monte Carlo analysis for the CCD camera 1000 sample is generated for the model evaluation. Sample size is adequate for the representation of the normal distribution.

After evaluating the model with the generated sample set for the corresponding pixel positions, the fallowing mean and standard deviations are obtained.

Table 8.25 Expected value of the latitude computed by Monte Carlo analysis

40,357	40,220	40,099
39,992	39,900	40,351
40,215	40,093	39,986
39,894	40,346	40,209
40,087	39,981	39,888

Table 8.26 Expected value of the longitude obtained by Monte Carlo analysis

34,16276	34,11499	33,95756
33,68918	33,30595	34,20479
34,15695	33,99966	33,7317
33,34926	34,24678	34,19885
34,04169	33,77413	33,39249

Variance of the ground points' coordinates are given as;

Table 8.27 Variance of the UTM x coordinate in meter

940,432	3517,139	56199,137
84114,023	96757,481	941,369
3517,881	56209,352	84149,282
96798,876	945,873	3518,667
56220,260	84187,716	96845,007

Table 8.28 Variance of the UTM y coordinates in meter

9546,721	24215,459	39155,049
87855,562	64318,090	9546,893
24164,339	38272,615	82581,426
43446,433	9546,904	24115,024
37421,542	77472,673	23053,435

As mentioned before description of the data set by mean value and variance causes considerable amount of data loss. For this reason mean and variance are not adequate for the data analysis in Monte Carlo sensitivity analysis method. For an efficient analysis of the data, probability distribution functions should be generated.

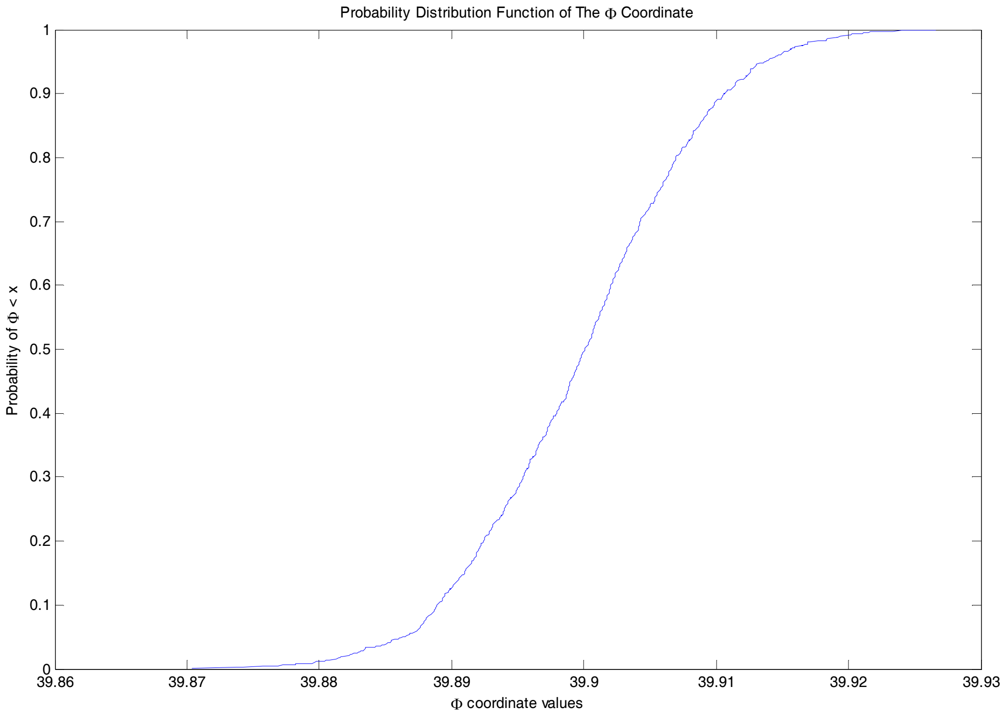

Figure 8.23 Cumulative Distribution Function of Latitude for the pixel coordinates of (2500, 1000).

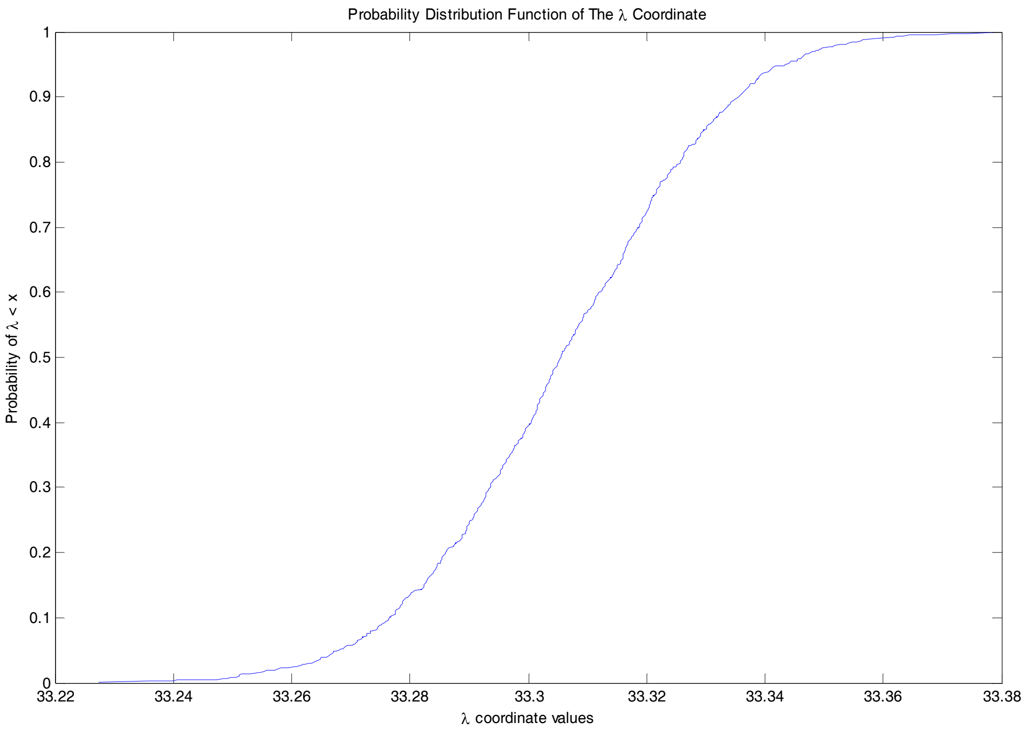

Figure 8.24 Cumulative Distribution function of Longitude for the pixel coordinates of (2500, 1000)

Examining scatterplots is a common way to interpret the relations between the parameters and the output. But since there are 23 parameters for the Pushbroom case, examining the relationships one by one by means of scatterplots will not be feasible. For this reason, scatterplots of the parameters versus the computed ground coordinates will not be printed. The relation between parameters and ground coordinates will be tried to find out by regression analysis.

In the first regression analysis raw data is analyzed and for the pixel position (2500, 2000) following R^2 values are obtained;

0,5298 for the latitude
0,5254 for the longitude

R^2 values are satisfactory for a non linear model. The high R^2 value can be explained as taking 23 parameters for the regression analysis. It should be mentioned that during the computation of the regression parameters, the matrix inverse required for the solution of the coefficients of the parameters could not be computed by ordinary methods and Tikhonov regularization is used for the computation of the regression parameters. At the end of the computation, the following regression parameters are obtained for the phi and lambda coordinates respectively;

$$
\begin{aligned}
\phi = {} & 3.46e-4 + 5.87e-4 * v - 1.94e-3 * \Omega - 1.57e-4 * a_1' - 4.35e-4 * a_2' + 8.24e-3 * a_3' \\
& + 3.27e-4 * a_4' - 1.68e-6 * \phi_s + 1.89e-7 * \dot{\phi}_s + 4.07e-5 * \ddot{\phi}_s - 1.72e-6 * \lambda_s + 3.21e-7 * \dot{\lambda}_s \\
& - 7.90e-5 * \ddot{\lambda}_s - 9.98e-6 * \dot{a}_1' - 1.34e-4 * \ddot{a}_1' + 7.13e-5 * \dot{a}_2' - 1.61e-3 * \ddot{a}_2' + 1.45e-5 * \dot{a}_3' \\
& - 1.12e-3 * \ddot{a}_3' - 7.63e-5 * \dot{a}_4' + 6.18e-3 * \ddot{a}_4' + 1.15e-1 * f + 2.38e-5 * \Delta y - 2.16e-4 * k_1 \\
& - 3.17e-8 * \xi h
\end{aligned}
$$

$$
\begin{aligned}
\lambda = {} & 2.47e-4 + 7.96e-3 * v - 2.10e-1 * \Omega + 4.55e-3 * a_1' - 1.24e-1 * a_2' + 9.98e-1 * a_3' \\
& + 3.30e-2 * a_4' - 2.45e-4 * \phi_s - 2.65e-5 * \dot{\phi}_s - 2.02e-3 * \ddot{\phi}_s + 3.20e-4 * \lambda_s + 4.86e-5 * \dot{\lambda}_s \\
& - 4.10e-3 * \ddot{\lambda}_s - 4.98e-4 * \dot{a}_1' - 1.02e-2 * \ddot{a}_1' + 7.00e-3 * \dot{a}_2' - 1.75e-1 * \ddot{a}_2' + 2.37e-4 * \dot{a}_3' \\
& - 1.45e-1 * \ddot{a}_3' - 1.08e-2 * \dot{a}_4' + 7.15e-1 * \ddot{a}_4' + 9.87e-2 * f + 9.41e-3 * \Delta y - 5.59e-2 * k_1 \\
& + 9.00e-6 * \xi h
\end{aligned}
$$

As mentioned before, coefficients of the parameters do not directly indicate the variable importance because coefficients of the parameters depend on the unit of the parameter. For this reason the parameter with highest coefficient is not the most sensitive parameter. However, coefficients indicate the change in the ground coordinates if a unit change is occurred in the parameter. When the coefficients are examined it is seen that the latitude is very sensitive to the focal length of the camera. Second important parameter is the yaw angle. For longitude, again focal length is an important parameter but right ascension of the ascending node, pitch, yaw and theta angle of the camera are more sensitive. Furthermore, lens parameter k_1 and pitch and yaw change rates are also important for longitude. Their changes effect the ground coordinates considerably.

Standardized regression coefficients are a better way to represent the parameter importance since they do not depend on the unit of the parameter. As performed for the CCD cameras, parameters are standardized by subtracting their mean value and dividing to their standard deviation. After the regression analysis the following coefficients are obtained;

$$\begin{aligned}\phi &= 1.13e-3*\nu + 5.66e-4*\Omega - 8.75e-5*a_1' - 4.51e-5*a_2' - 1.61e-3*a_3' \\ &+ 1.25e-3*a_4' - 3.37e-4*\phi_s + 6.81e-4*\dot{\phi}_s + 9.30e-5*\ddot{\phi}_s - 5.98e-4*\lambda_s + 9.56e-4*\dot{\lambda}_s \\ &- 2.67e-4*\ddot{\lambda}_s - 1.04e-4*\dot{a}_1' - 4.32e-4*\ddot{a}_1' + 4.61e-3*\dot{a}_2' + 1.68e-4*\ddot{a}_2' + 1.37e-3*\dot{a}_3' \\ &+ 3.97e-4*\ddot{a}_3' - 5.76e-3*\dot{a}_4' + 7.86e-5*\ddot{a}_4' - 1.61e-6*f + 8.18e-4*\Delta y + 1.23e-3*k_1 \\ &- 1.36e-25*\xi h\end{aligned}$$

$$\begin{aligned}\lambda &= 2.28e-1*\nu - 6.84e-2*\Omega - 2.34e-2*a_1' - 3.57e-2*a_2' + 2.70e-1*a_3' \\ &+ 2.18e-1*a_4' - 8.00e-2*\phi_s + 1.17e-1*\dot{\phi}_s - 1.39e-2*\ddot{\phi}_s - 1.51e-1*\lambda_s + 2.17e-1*\dot{\lambda}_s \\ &- 1.65e-2*\ddot{\lambda}_s - 5.11e-2*\dot{a}_1' - 5.32e-2*\ddot{a}_1' + 1.04e-1*\dot{a}_2' + 4.35e-3*\ddot{a}_2' + 8.91e-3*\dot{a}_3' \\ &+ 8.24e-3*\ddot{a}_3' - 6.62e-3*\dot{a}_4' + 1.63e-3*\ddot{a}_4' - 2.97e-6*f + 2.00e-2*\Delta y - 2.82e-2*k_1 \\ &+ 1.54e-23*\xi h\end{aligned}$$

with R^2 values of

0,5624 for the latitude

0,5273 for the longitude

When the regression coefficients are analyzed, it is seen that latitude generally depends on the attitude and attitude rates. There is no significant difference between the sensitivities of the attitude angles. Although roll angle is expected to have considerable effect on the latitude, at the end of the analysis it is seen that it does not have significant effect. Ground elevation has least effect on latitude.

For longitude, besides the attitude angles orbital parameters, such as right ascension of the ascending node and argument of perigee have considerable effect on the longitude. Similarly, elevation of ground point has very little effect on the longitude. Longitude is affected more than latitude by the interior camera parameters such as principle coordinate of pushbroom camera and tangential lens distortion parameters.

The coefficients computed after the regression analysis can not be said to be true coefficients of the model. There are several reasons for this proposal, the first one is that the model is not linear and for this reason finding a true relationship by a linear regression analysis is not expected. But the results will give a rough idea about the parameters of the model. However, the results obtained cannot be dependable. Another reason that can reduce the reliability of the analysis results is that in the model there were 24 parameters which are somehow correlated with each other either in the sampling process or in the mathematical model. This situation reduces the accuracy of the solution of the regression model because of the rank deficiency in the model. Analyzing the model with more parameters may give higher R^2 values but the solution of the model may not be accurate because of the rank deficiency. This can be the explanation of the unexpected results.

Besides standardized regression analysis, rank transformed and standardized rank transformed data can be analyzed also. To perform this regression analysis, original data is replaced with its rank value and the rank transformed data is analyzed. Following coefficients are computed after the analysis of rank transformed data;

$$\begin{aligned}\phi &= 1.19e-1*\nu + 6.25e-2*\Omega + 8.15e-2*a_1' + 1.03e-1*a_2' + 2.83e-2*a_3' \\ &+ 7.26e-2*a_4' + 5.02e-2*\phi_s + 6.52e-2*\dot{\phi}_s + 9.32e-2*\ddot{\phi}_s + 1.07e-1*\lambda_s + 1.22e-1*\dot{\lambda}_s \\ &+ 1.40e-1*\ddot{\lambda}_s + 1.56e-1*\dot{a}_1' + 1.01e-1*\ddot{a}_1' + 6.75e-4*\dot{a}_2' + 7.65e-4*\ddot{a}_2' + 1.11e-3*\dot{a}_3' \\ &+ 8.93e-4*\ddot{a}_3' + 8.10e-4*\dot{a}_4' + 8.86e-4*\ddot{a}_4' + 1.09e-3*f + 1.26e-2*\Delta y + 1.03e-2*k_1 \\ &+ 1.64e-1*\xi h\end{aligned}$$

$$\begin{aligned}\lambda &= 3.25e-2*\nu + 9.97e-2*\Omega + 1.42e-2*a_1' + 6.12e-2*a_2' + 3.07e-2*a_3' \\ &+ 1.09e-1*a_4' + 1.16e-1*\phi_s + 2.87e-3*\dot{\phi}_s + 1.49e-1*\ddot{\phi}_s + 1.56e-1*\lambda_s + 1.68e-1*\dot{\lambda}_s \\ &+ 1.92e-1*\ddot{\lambda}_s + 1.36e-1*\dot{a}_1' + 1.58e-1*\ddot{a}_1' - 3.95e-3*\dot{a}_2' - 3.86e-3*\ddot{a}_2' - 3.52e-3*\dot{a}_3' \\ &- 3.73e-3*\ddot{a}_3' - 3.82e-3*\dot{a}_4' - 3.74e-3*\ddot{a}_4' - 3.53e-3*f - 3.37e-3*\Delta y - 3.58e-3*k_1 \\ &+ 7.75e-2*\xi h\end{aligned}$$

with R^2 values of

0,5360 for the latitude

0,5174 for the longitude

Rank transformed data represents the relationship between the parameters and the output variables better than the data itself if the relationship is nonlinear and monotonic. The regression analysis performed with the rank transformed data is expected to give better results than the original data.

When the results of analysis are examined; for latitude, roll and pitch angles have considerable effect on the results. Surprisingly elevation of the ground point has more effect on the output than it has on the previous regression results.

For the longitude orbit perturbation parameters have considerable impact on the output and the inner orientation parameters have lower effect compared with the previous regression results. Furthermore longitude is sensitive to attitude change rates especially the omega angle.

The regression analysis is repeated by standardizing the rank transformed data and following results are obtained;

$$\begin{aligned}\phi &= -121.34*\nu + 50.45*\Omega + 17.39*a_1' - 92.34*a_2' + 118.87*a_3' - 47.36*a_4' + 84.20*\phi_s \\ &+ 52.88*\dot{\phi}_s + 1.13*\ddot{\phi}_s - 26.65*\lambda_s - 107.98*\dot{\lambda}_s - 216.41*\ddot{\lambda}_s - 72.43*\dot{a}_1' + 21.45*\ddot{a}_1' \\ &+ 21.44*\dot{a}_2' + 21.44*\ddot{a}_2' + 21.44*\dot{a}_3' + 21.44*\ddot{a}_3' + 21.44*\dot{a}_4' + 21.44*\ddot{a}_4' + 21.44*f \\ &+ 21.44*\Delta y + 21.44*k_1 - 247.23*\xi h\end{aligned}$$

$$\begin{aligned}\lambda &= 111.96*\nu - 9.62*\Omega + 167.15*a_1' + 44.50*a_2' + 95.07*a_3' - 78.52*a_4' - 42.69*\phi_s \\ &+ 178.91*\dot{\phi}_s - 71.57*\ddot{\phi}_s - 74.35*\lambda_s - 125.46*\dot{\lambda}_s - 165.61*\ddot{\lambda}_s - 72.48*\dot{a}_1' - 124.48*\ddot{a}_1' \\ &+ 25.12*\dot{a}_2' + 25.12*\ddot{a}_2' + 25.12*\dot{a}_3' + 25.12*\ddot{a}_3' + 25.12*\dot{a}_4' + 25.12*\ddot{a}_4' + 25.12*f \\ &+ 25.12*\Delta y + 25.12*k_1 + 32.33*\xi h\end{aligned}$$

with R^2 values of
0,4676 for the latitude
0,4358 for the longitude

In the standardized rank transformed data an unexpected result is obtained. 9 parameters both for the latitude and longitude have the same coefficients. There are little differences at these coefficients that fractional part is same up to six or seven digits. The explanation of this event can be the ill conditioned situation of the solution that every parameter sample set has same values ranging from zero to one. This may cause an inaccurate solution for the last ten parameters. For the other parameters the output result is sensitive for the attitude angles and the orbit perturbation parameters which is an expected result.

Partial correlation coefficient is a good representation of variable importance too. To examine the effect of the parameter on ground coordinate by a different method, partial correlation coefficients are computed.

Table 8.29 Correlation coefficients of the parameters for the latitude (See Equation 8.41).

Parameter	**Correlation Coefficient**
True Anomaly	0,0634
Right Ascension	0,0311
Roll	-0,0017
Pitch	-0,005
Yaw	0,0833
Theta	0,068
Roll Rate	-0,0271
Roll Rate Change	0,0305
Pitch Rate	0,0074
Pitch Rate Change	-0,0276
Yaw Rate	0,053
Yaw Rate Change	-0,0195
Theta Rate	0,0073
Theta Rate Change	-0,031
Phi Anomaly	0,0447
Phi A. Rate	-0,0389
Phi A. Rate Change	0,0089
Lambda Anomaly	-0,0283
L. A. Rate	-0,0495
L. A. Rate Change	0,0604
Focal Length	-0,0036
Principle Coordinate	0,0028
Lens D. Parameter	-0,0248
DEM Error	-0,012

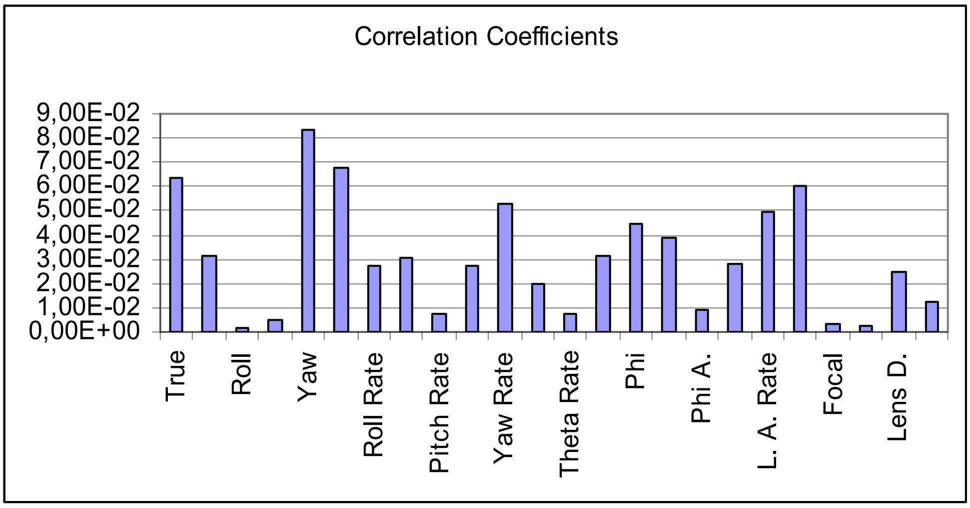

Figure 8.25 Bar chart of the correlation coefficients for latitude

In Figure 8.25 absolute values of the correlation coefficients are plotted in order to represent the magnitude of correlation.

When the correlation coefficients are examined it is seen that true anomaly and right ascension of the ascending node have significant importance on the latitude (Table 8.29). This means that the Kepler Elements are important parameters that they can not be expressed in terms of other parameters. Pitch and Yaw are the important attitude angles of the camera while Roll angle is not as important as Pitch and Yaw angles for latitude. Theta is also an important parameter for the latitude; it is one of the highest correlated parameter. Furthermore, changes of attitude angles and change rates of attitude angles are highly correlated also. They have strong correlation with latitude so they can be considered as important parameters for the rectification.

Position anomalies and their rates are highly correlated also. Although they are not correlated as high as attitude parameters they can still be considered as important parameters. Interior camera parameters have moderate correlation with latitude, especially focal length and principle point coordinate have very little correlation. Radial lens distortion parameter k_1 has strong correlation with latitude. Additionally elevation anomaly can be considered as slightly correlated with latitude.

Table 8.30 Correlation Coefficients of the parameters for the longitude (See Equation 8.41)

Parameter	Correlation Coefficient
True Anomaly	0,0652
Right Ascension	0,0204
Roll	0,0003
Pitch	-0,0118
Yaw	0,0732
Theta	0,0577
Roll Rate	-0,0283
Roll Rate Change	0,0308
Pitch Rate	-0,0016
Pitch Rate Change	-0,0367
Yaw Rate	0,0576
Yaw Rate Change	-0,0073
Theta Rate	-0,0017
Theta Rate Change	-0,0166
Phi Anomaly	0,0316
Phi A. Rate	-0,0304
Phi A. Rate Change	0,0018
Lambda Anomaly	-0,0263
L. A. Rate	-0,0507
L. A. Rate Change	0,0508
Focal Length	-0,0006
Principle Coord	0,0083
Lens D. Parameter	-0,0466
DEM Error	0,023

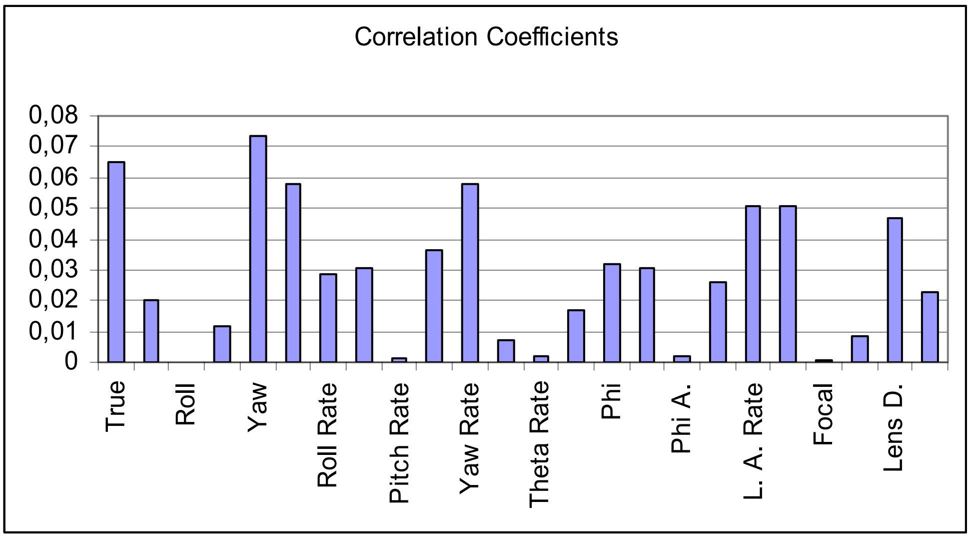

Figure 8.26 Bar chart of the correlation coefficients for longitude

In Figure 8.26 absolute values of the correlation coefficients are plotted in order to represent the magnitude of correlation.

Right ascension of the ascending node and true anomaly have high correlation with longitude also (Table 8.30). However, for the right ascension of the ascending node it is expected to be more strongly correlated with longitude. Pitch and yaw angles are highly correlated, while roll angle has almost no correlation with longitude. For the roll angle it is expected to have higher correlation with longitude. Furthermore theta angle is highly correlated with longitude which was also highly correlated with latitude. Additionally attitude angles' rate and change rate are highly correlated with longitude also. Both anomaly of the camera position for latitude and longitude are correlated with longitude of the ground point. Additionally, rate and change rate of the longitude of the position anomaly are more correlated with longitude of the ground point than the other parameters. For the intrinsic parameters focal length and principle point location have slightly weak correlation with longitude which was observed in the analysis for latitude also. Lens distortion parameter has strong correlation with longitude. Anomaly of elevation has stronger correlation with longitude than it has with latitude.

Table 8.31 Correlation Coefficients of the parameters for the latitude with rank transformed data

Parameter	**Correlation Coefficient**
True Anomaly	0,0332
Right Ascension	0,0309
Roll	-0,0103
Pitch	-0,0028
Yaw	0,0251
Theta	-0,0271
Roll Rate	0,0091
Roll Rate Change	-0,0207
Pitch Rate	-0,0142
Pitch Rate Change	-0,0074
Yaw Rate	0,0014
Yaw Rate Change	0,0228
Theta Rate	0,0374
Theta Rate Change	0,0534
Phi Anomaly	0,0123
Phi A. Rate	0,0123
Phi A. Rate Change	0,0123
Lambda Anomaly	0,0123
L. A. Rate	0,0123
L. A. Rate Change	0,0123
Focal Length	0,0123
Principle Coordinate	0,0123
Lens D. Parameter	0,0123
DEM Error	0,0579

Besides partial correlation coefficients of the original data, correlation coefficients of the rank transformed data are computed as in the case of Monte Carlo Analysis for CCD frame cameras. The reason of this, it is expected that the rank transformed data represent the relationship between the parameters and the model output in non linear monotonic models better than the original data. The computed partial correlation coefficients of the rank transformed data are shown in Table 8.31;

Rank transformed form of the Kepler parameters are highly correlated with latitude. The same relationships were observed in the analysis performed with original data. When attitude angles of the satellite are examined it is seen that roll and yaw angles are highly correlated with latitude. Pitch angle has very weak correlation with latitude of the ground point. Theta angle, which is the attitude of the camera, is strongly correlated with latitude. Rate and change rate of the attitude angles of the camera and satellite also have strong correlation with latitude. Among the rate and change rates of the attitude angles, theta's rate and change rate are observed to be the most correlated ones. Surprisingly anomalies of the satellite position have same correlation with latitude. This unexpected result can be explained as their correlations with the latitude are the same if the portion of the relationship which can be expressed by the remaining parameters are subtracted. Exactly the same correlation coefficients for the position anomalies may be caused by the regularization method that Tikhonov number may not be selected properly for these parameters. When the intrinsic camera parameters are examined it is seen that their importance has increased after the application of rank transformation. Additionally same result can be concluded by examining the correlation coefficient of anomaly of the elevation.

Table 8.32 Correlation Coefficients of the parameters for the longitude with rank transformed data

Parameter	Correlation Coefficient
True Anomaly	0,0393
Right Ascension	-0,0415
Roll	0,009
Pitch	-0,0657
Yaw	-0,0212
Theta	-0,0322
Roll Rate	0,0338
Roll Rate Change	0,0129
Pitch Rate	-0,0713
Pitch Rate Change	0,0273
Yaw Rate	0,0255
Yaw Rate Change	0,0432
Theta Rate	0,0622
Theta Rate Change	0,0281
Phi Anomaly	0,0439
Phi A. Rate	0,0439
Phi A. Rate Change	0,0439
Lambda Anomaly	0,0439
L. A. Rate	0,0439
L. A. Rate Change	0,0439
Focal Length	0,0439
Principle Coordinates	0,0439
Lens D. Parameter	0,0439
DEM Error	-0,0185

True anomaly and right ascension of the ascending node have considerably strong correlation with longitude (Table 8.32). In the analysis with the original data, correlation of right ascension of the ascending node was computed weaker than the expected. However, with the rank transformed data more realistic results are obtained if the Kepler parameters are considered. When the attitude angles of the satellite are considered, it is seen that pitch angle has the highest correlation with the longitude of the ground coordinate. Furthermore, theta angle is highly correlated with longitude also. As in the case of the previous analysis rate and change rate of the attitude angles are highly correlated with longitude. Among these pitch rate and theta rate have the highest correlation coefficients. Similar to the previous analysis camera position anomaly parameters have same correlation coefficients. The result can not be explained as a coincidence. This shows that uncorrelated relationship of the position anomalies for both latitude and longitude are the same for the rank transformed data. Intrinsic camera parameters have slightly stronger correlation in the case of rank transformed data. However, elevation anomaly has weaker correlation coefficients.

8.3.3 Fourier Amplitude Sensitivity Test (FAST)

Besides Differential and Monte Carlo Sensitivity Analysis, the sensitivity of the parameters for the Pushbroom scanner model is tested by FAST. Implementation of FAST is performed by 11 parameters, since the application of the model requires the generation of same amount of linear independent integer numbers. Since only 11 linear independent integer numbers can be obtained, accordingly sensitivity of only 11 parameters is analyzed.

Implementation of the FAST will be the same with the implementation of FAST for CCD cameras. The parameters to be analyzed are;

ν true anomaly
Ω right ascension of the ascending node
f focal length of the camera
Δy Principal coordinate of the camera
ϕ_s position correction for the camera latitude
λ_s position correction for the camera longitude
a'_1 roll angle between S_O and S_B
a'_2 pitch angle between S_O and S_B
a'_3 yaw angle between S_O and S_B
a'_4 attitude angle of the camera between S_B and S_C
k_1 lens distortion parameter

Frequencies assigned for the parameters are as following;

145 177 199 41 67 105 219 229 235 243 247

The 11 parameter integral is reduced to one parameter integral by the transformation explained in Equation 8.31. Assigned v_i values for the transformation are listed in Table 8.33;

Table 8.33 Assigned v_i values to the parameters

Parameter	Value
v_1	4,63E-05
v_2	3,93E-05
v_3	1,4
v_4	3,43E-07
v_5	4,03E-09
v_6	2,50E-08
v_7	1,28E-04
v_8	1,89E-04
v_9	9,06E-05
v_{10}	1,37E-04
v_{11}	1,00E-05

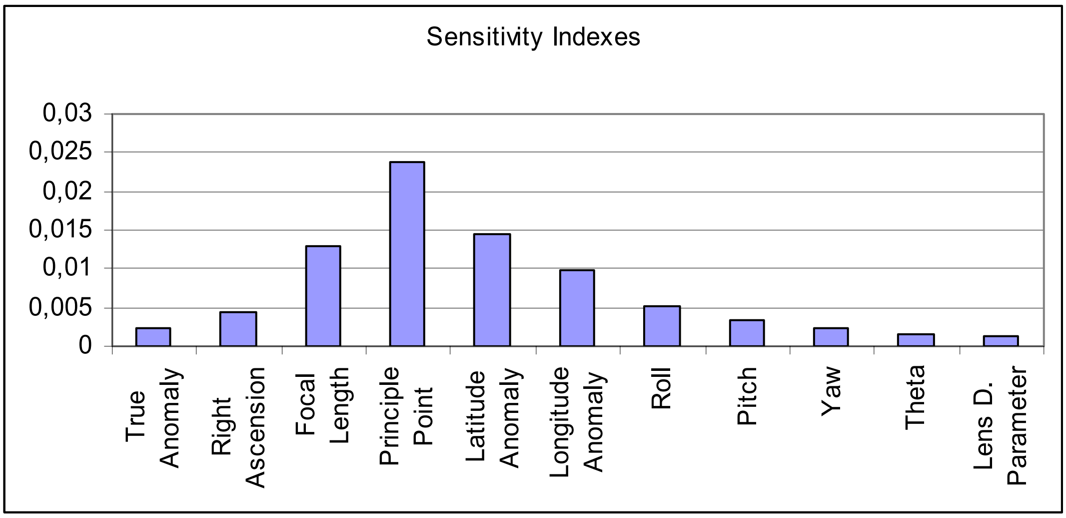

Figure 8.27 Sensitivity Indexes for longitude computed by FAST

Sensitivity analysis with FAST method is performed for 36 image points. Analysis results for the image point (2000,2000) is given in Table 8.34;

Table 8.34 Sensitivity indexes of latitude of pushbroom model (see p. 167)

Parameter	Sensitivity
ν	0,0023091
Ω	0,0043536
f	0,012822
Δy	0,023876
ϕ_s	0,014567
λ_s	0,0098141
a'_1	0,0052627
a'_2	0,0033327
a'_3	0,0023154
a'_4	0,0016547
k_1	0,0014188

When the sensitivity indices computed after the FAST are examined, it is seen that among the orbital parameters right ascension of the ascending node affects the output more than the true anomaly (Table 8.34). Focal length of the camera also has significant effect on the latitude of the rectified ground coordinates. Δy, principle point of the sensor has the highest importance on the latitude. Position anomalies of the satellite influence the latitude of the ground point. Anomaly in the latitude has higher influence than the anomaly in longitude. Among the attitude angles of the satellite and camera roll and pitch angles have the highest effect on the latitude. Lens distortion parameter k_1 has moderate effect on the latitude.

Table 8.35 Sensitivity indexes of longitude of pushbroom model (see p. 167)

Parameter	Sensitivity
ν	0,00137
Ω	0,00079
f	0,00216
Δy	0,00970
ϕ_s	0,00372
λ_s	0,00228
a'_1	0,00101
a'_2	0,00049
a'_3	0,00051
a'_4	0,00043
k_1	0,00038

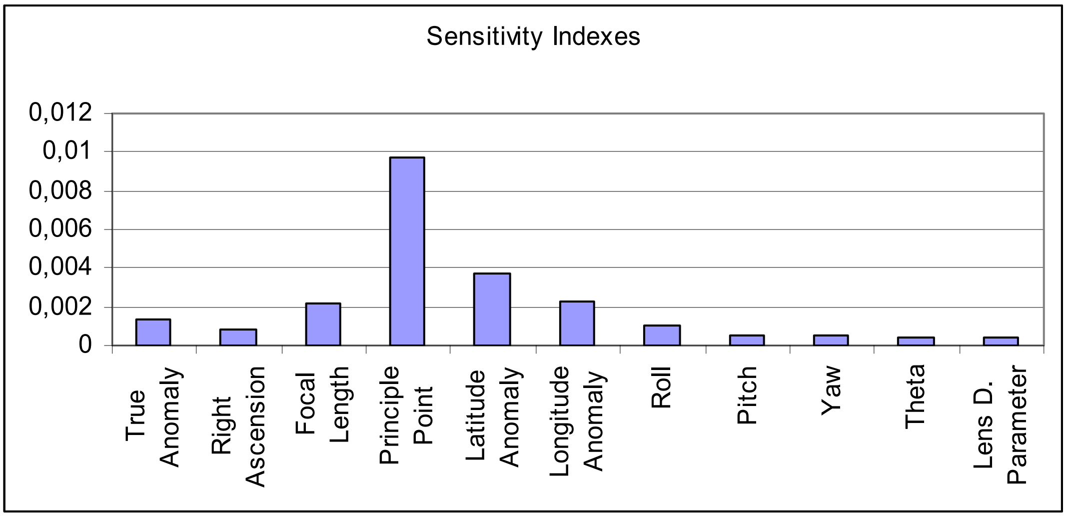

Figure 8.28 Sensitivity Indexes for longitude computed by FAST

When the results in Table 8.35 are examined it is seen that both latitude and longitude are sensitive to focal length, to attitude angles and to orbit perturbation parameters. Longitude is very sensitive to principal point. On the other hand, latitude is not, as expected. Additionally, k_1 which is the lens distortion parameter is thought to be more sensitive to longitude, but the results showed that it has very little sensitivity for both, especially for the longitude.

Roll and theta angles have considerable impact on latitude, however only roll angle have notable effect on longitude. Sensitivity of the parameters do not depend on the pixel position. When the FAST analysis results of the other pixel locations are examined which are presented in Appendix B, it will be seen that sensitivity indexes of the same parameter for different pixel locations are almost the same. This property of FAST reduces the number of model implementations considerably. However, implementation of one model in FAST is computationally more demanding than one implementation of both Differential and Monte Carlo Sensitivity Analysis.

CHAPTER 9

DISCUSSION OF RESULTS AND CONCLUSIONS

In this chapter an overall discussion of the analysis and the thesis will be performed and some recommendations will be made for the future studies. Discussions and suggestions will be made for each chapter separately and an overall conclusion will be written for the thesis study.

In chapter 1, a brief literature survey is given for rectification, error analysis and sensitivity and uncertainty analysis. Apart from literature survey, rectification steps are basically introduced.

In chapter 2, reference systems and time systems used in the thesis is briefly explained. Besides, assumptions while defining reference systems such as; image coordinate system, camera coordinate system, etc. are explained and illustrated by figures. By these explanations, any possible misunderstanding is prevented.

In chapter 3, study area, image and DEM used in the analysis is briefly explained. Furthermore, technical properties of the satellites that take the images are briefly introduced. By the help of this information, imaging geometry can easily be identified and the analysis results of sensitivity and uncertainty can easily be commented.

In chapter 4, algorithm of DRM is explained in detail. Every step of DRM is clearly explained and illustrated that it can easily be implemented. In this work, special effort is spent on the atmospheric refraction correction, which is skipped for coarse spatial resolution satellite images. Additionally relief displacement correction and resampling algorithms are stated clearly. Besides, convergence of the DRM is improved by modifying the relief displacement correction algorithm.

DRM is adopted for pushbroom scanners in Chapter 4. Since rectification of pushbroom images requires continuous camera position and attitude data, interpolation methods are introduced for this purpose. Both rectification methods for CCD frame cameras and pushbroom scanners require position and attitude data from telemetry. If these data are not available, by means of space resection, position and attitude should be estimated.

Algorithm of DRM can be improved by using better lens distortion and atmosphere refraction models. Current algorithm does not check for the possible blunders can be present in position and attitude data. For the future studies, the model can be improved and the telemetry file can be checked for the blunders.

In chapter 5, parameter estimation algorithms used in this thesis are explained. Gauss Helmert (Mixed Model) model is applied for parameter estimation. In this model besides fixed parameters, random parameters are introduced to the system. For random parameters; correction to elevation obtained from SRTM DEM and correction to pixel coordinates of GCPs are assigned. At the end of the parameter estimation corrections for random and fixed parameters are computed. Because of the camera geometry and correlations between the parameters resulting equation system in parameter estimation procedure was “ill-conditioned”. To stabilize the system three regularization algorithms are introduced to the system and their performances are compared. For a detailed analysis, atmospheric refraction parameters can be added to the system as random parameters. Temperature, humidity and air pressure are the parameters which can be considered as “random parameters” for different portion of the satellite image.

Additionally in chapter 5, improvement gained by introducing regularization methods are examined. For this analysis fictitious observation regularization methods is applied. The test includes the not only the effect of regularization but also the effect of GCP distribution and correlations between parameters. The improvement in the solution accuracy is measured by the condition number of the matrix to be inverted. In the first analysis, 14 parameters model is tested and for the second analysis 12 parameters model is tested. By examining the results of analysis, it is concluded that if the GCPs are narrowly distributed it reduces the accuracy of the solution but if a regularization method is introduced to the system this effect diminishes. Regularization methods significantly increase the accuracy of the solution, but it can not completely remove the effect of correlation between the parameters. At the end of the analysis it is seen that there was significant difference between the 14 parameters model and 12 parameters model. For this reason, to obtain an accurate solution at the end of the parameter estimation, uncorrelated analytical model should be derived even regularization methods are implemented. Additionally, for slightly correlated models as in the case of 12 parameter model, if GCPs are widely distributed with the improvement in the computation precision of computers without any regularization algorithm accurate solutions can be obtained in the future.

In chapter 6, parameter estimation and the DRM both for CCD frame camera and pushbroom scanners are implemented. Parameter estimation procedure is implemented three times with different regularization methods to compare the results and performance of the regularization methods. For this reason, scope of the parameter estimation procedure was not only to correct the parameters but also to test the performance of the regularization methods.

Among the three regularization methods introduced, singular value decomposition (SVD) gave the smallest residuals. Furthermore convergence of SVD was the fastest however, estimated parameters with SVD was not realistic. In other words, focal length and satellite position was not properly estimated. This can be caused by improper selection of regularization factor, α or the inaccurate singular value decomposition. This can be possible, because of the very high condition number of the system to be decomposed. Remaining methods; Tikhonov regularization and fictitious observation solutions are similar to each other. Fictitious observation uses cofactor matrix of parameters, while Tikhonov regularization uses identity matrix for stabilizing the system. For this reason, it is expected to end up with smaller residuals for Tikhonov regularization since it estimates the parameters more freely. On the other hand, cofactor matrix of the parameters behaves like a weight matrix and adds restrictions to the parameter estimation procedure. Because of this, error function cannot converge to minima as small as in the case of Tikhonov regularization. However, if initial values of the parameters are precise, then fictitious observation should be selected for regularization. In this thesis, results of Tikhonov regularization method are used because the initial values for the parameters were not precise and it is not necessary to estimate parameters by assigning weights.

Additionally, restriction equations are appended to parameter estimation procedure to obtain better estimations to parameters. For this purpose, by using geometrical relationship between focal length, spatial resolution, satellite altitude and size of the sensing element a restriction equation is generated. It has turned out that, estimated parameters were better than the result of the parameter estimation without restriction, although residuals were larger. This was an expected result since adding restrictions to the system increases the residuals. This can be explained by the restriction equation which prevents the error function (sum of the squares of the residuals) converging to minima if the restriction equation is violated. For this reason, restriction equation put restrictions to the possible values that can be assigned to focal length while preventing the error function to converge to minima.

Furthermore an outlier test is performed to check if there is a blunder in the coordinate measurements of GCPs. When the result of analysis was examined, it was found that there is not any blunder in the measurements. But the equation system was computed to be highly sensitive on the error of the ground coordinates. This means that error in the ground coordinates of the GCPs effect the parameter estimation result significantly which was expected because the equation system is “ill-conditioned”. Contribution of bad satellite geometry to the sensitivity is significant.

Parameter estimation procedure is also applied to DRM for pushbroom scanners. In this case only Tikhonov regularization method is employed. Unfortunately, since initial values for the parameters were not available, initial values are assigned roughly. Additionally parameters of the rectification method were highly correlated i.e. attitude angles and position anomaly parameters were correlated. Because of these two reasons residuals were not pleasing. Ironically additional parameters added to the system can not decrease the residuals, since they reduce the accuracy of the solution considerably.

From the results of the analysis it can be concluded that for DRM for pushbroom scanners, initial values of the parameters must be close to their “true values” to obtain a proper estimation at the end.

At the end of the parameter estimation, with the corrected parameters DRM both for CCD frame cameras and pushbroom scanners are implemented. By Nearest Neighbor resampling algorithm, image maps are produced from the raw satellite images. It is seen that the computational demand and storage requirement of the DRM is very high. Especially for the pushbroom scanners generation of an image map on a 1 GHz computer took almost 16 hours. Additionally, storage of the ground coordinates of the ASTER image requires more than 600 MB. For BilSAT images implementation of the algorithm takes less than 3 hours and the storage requirement is slightly less than 100 MB. Storage amount will not cause any problem when the present storage media is considered. However, computational demand of the DRM, especially for the pushbroom images is very high that even a workstation may be required. The algorithm is implemented by using Matlab, however on executable software, computation time will decrease significantly.

DRM provides valuable information after the rectification. Resulting product has accurate registered coordinates and has 3D position data: horizontal coordinates and elevation. Furthermore, accurate 3D terrain views can be generated with DRM depending on the accuracy of DEM. If the computational cost and the benefits of DRM is compared it is seen that the benefits are highly dominant.

As a final analysis in chapter 6, convergence of DRM is tested. Furthermore differences in result of the rectification are measured with respect to different threshold values. Besides these analyses by assigning highly oblique attitude angles, the convergence performance of DRM is tested for oblique images. To conclude the analysis results, re-computing the ellipsoidal normal does not provide a notable improvement in the rectification accuracy. Also assigning very small threshold values for the convergence criteria does not improve the accuracy. For a reasonable threshold value, 0,1 meter can be proposed.

Convergence of the relief displacement algorithm is relatively fast for attitude angles less than 15 degrees. However, for the attitude angles more than 20 degrees convergence of the algorithm significantly slows down. In the analysis, as a limit case 25 degrees are assigned for roll and pitch angles leading to very slow convergence of DRM. For some points an iterative relief displacement correction was stopped, since it reached the maximum allowable iteration number. However, this analysis proved that DRM can be applied to the rectification of highly oblique images successfully with only a small amount of rectification error for steep sloped portions of the image.

In chapter 7, accuracy of DRM for both CCD frame cameras and pushbroom scanners are compared with some of the existing methods. Results of comparison indicate that DRM has higher accuracy for CCD frame cameras and slightly accurate results for pushbroom images. Unpleasing results of the DRM for pushbroom scanners are probably caused by assigning improper initial values for the parameters. The performance of the method is tested with simulation data in which the elevation differences between ground control points are exaggerated. DRM method performance was very pleasing while affine transformation method showed significant decrease in accuracy. This shows that DRM can be implemented for the rectification of mountainous areas with confidence.

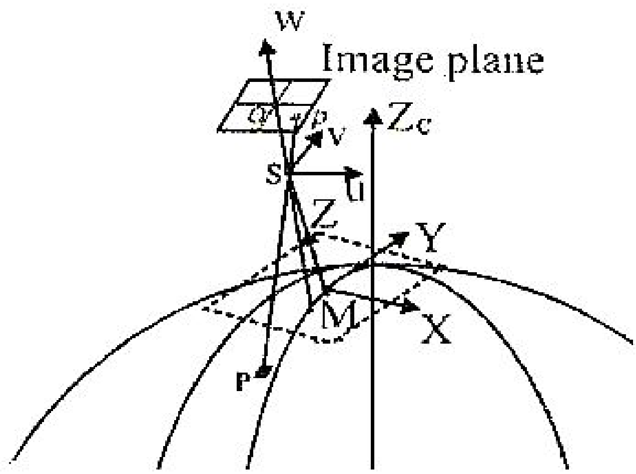

(a) Classical differential rectification procedure

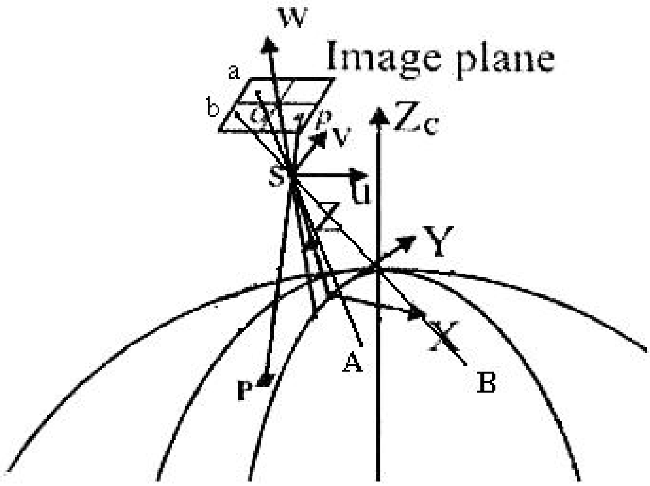

(b) DRM method

Figure 9.1 Comparison of the DRM with classical differential rectification method [4].

As shown in Figure 9.1 DRM maps the image coordinates directly on to the reference ellipsoid while the classical rectification methods project the pixels on a plane. Although earth curvature corrections are applied after the projection, error caused by the assumption can not be completely removed. Furthermore if image is not taken in nadir direction, error caused by the classical rectification methods increase considerably. However, oblique images do not introduce significant errors in DRM, the only error is the effect of elevation anomaly on the horizontal coordinates. This can easily be overcome by using precise DEM.

Besides error analysis, in chapter 7 sensitivity of parameter estimation procedure with respect to blunders in the initial values of the parameters are examined. It is seen that yaw angle is significantly affected by the blunders. It is known that the sensitivity of yaw angle is more than interior camera parameters which are not affected as much as yaw angle. This shows that it can not be said that high sensitive parameters can be estimated accurately and low sensitive parameters can not be estimated as high accurate as high sensitive parameters. Accuracy of parameter estimation depends on the correlation of the parameter with the remaining parameters and the effect of the errors of the initial values assigned to parameters. However, it is expected to estimate high sensitive parameters accurately if it is not highly correlated with the other parameters. This can easily be seen by examining the cofactor matrix of the estimated parameters.

In chapter 8, a detailed sensitivity and uncertainty analysis of the DRM for both CCD frame cameras and pushbroom scanners is performed. In the analysis three sensitivity analysis methods are implemented which can be listed as; Differential Analysis, Monte Carlo Sensitivity Analysis and FAST. Besides sensitivity of the parameters, performances of the methods are compared.

Differential Analysis is a local sensitivity analysis method that one parameter is free to change while the remaining parameters are kept constant. To predict the sensitivity of the parameter, base value (true value) of the parameters should be known accurately. If this can not be known, based on the sensitivity of the remaining parameters the model can behave considerably different and lead to an irrelevant sensitivity index. Furthermore if the model is complex or parameter number is relatively high, computing the partial derivatives analytically will be very demanding. If the partial derivatives are computed numerically, then inaccurate computation of partial derivatives may be faced because of the limitation of the computer. Differential Analysis had shown that uncertainty in the rectified images increases at the pixel positions further from the image center. Furthermore it is seen that Bilsat images can be rectified by DRM method better than 3 pixel accuracy without using any GCP if the exterior camera parameters are obtained from telemetry.

Monte Carlo Sensitivity Analysis does not require computing partial derivatives and it is a global sensitivity analysis method. Furthermore, it requires several implementation of the method based on a random sampling of the domain of the parameters. These properties of the Monte Carlo Sensitivity Analysis present very precious information about uncertainty of the model output. Especially cumulative probability distribution functions of the model output is significantly important information provided by the method. However, sensitivity analysis of the method is not as valuable as uncertainty analysis. Sensitivity analysis is based on regression analysis of the parameters and model output. Linear relationship is derived by means of coefficient at the end of the analysis, and sensitivity of the parameter is assigned by considering the coefficient of the parameter. Since the relationship is nonlinear, linear regression analysis can not model the relationship between the parameters and output variable properly. Low R^2 values obtained at the end of the analysis can be the proof of this comment. Additionally, although the sample set of the parameters are sampled randomly, for the systems having relatively more parameters the coefficients of the parameters can not be computed accurately because of the correlation. Furthermore regularization methods may lead to inaccurate solution for the coefficients of the parameters. To conclude, valuable information about the sensitivity of the parameters could not be obtained by regression analysis.

FAST method requires assigning linearly independent integer number for each parameter which is labeled as the parameters frequency. Then the Fourier transformation of the model is computed and sensitivity of each parameter is obtained by its frequency amplitude. Drawback of FAST can be counted as its complex theory and linearly independent number requirement. Because of the second drawback, parameter number to be analyzed is decreased to 11. If the assigned frequencies of the parameters are somehow correlated, FAST will give completely irrelevant sensitivity indexes. Furthermore, for complex models integral of the Fourier transform is evaluated numerically and this may cause computational errors. On the other hand, FAST gave very similar sensitivity indexes for different pixel locations. This property of FAST reduces the required analysis number, thus reducing the computation amount.

For the overall comparison of the three methods Monte Carlo Sensitivity Analysis, provided valuable information about the uncertainty of the model. Although it is a local sensitivity analysis method, differential analysis presented meaningful and valuable sensitivity indexes for the parameters.

For future studies some recommendations can be made concerning the DRM. The convergence criteria of the method can be increased by adding logical statements. Furthermore, it is possible that for highly oblique images the algorithm may converge to more than one elevation value for a ground coordinate. This may be prevented by checking the neighboring pixels' ground coordinates. The algorithm may be extended and improved for bundle block adjustment. Mosaics can be produced from sequential satellite images after performing a parameter estimation procedure. Additionally DRM provides very accurate results, so this can be especially useful for producing super resolution images especially for the mountainous regions. Furthermore, DRM can be implemented in a GIS software.

REFERENCES

[1] Mahmut O. Karslioglu, Jurgen Friedrich. "A New Differential Geometric Method to Rectify Digital Images of the Earth's Surface Using Isothermal Coordinates", IEEE Transactions on Geoscience and Remote Sensing, Vol. 43, No. 3, March 2005.

[2] Paul R. Wolf, Bon A. Dewitt, "Elements of Photogrammetry with Applications in GIS" Third Edition Mc Graw Hill.

[3] Prof. Emeritus Shunji Murai, The University of Tokyo, JICA Seminars, Remote Sensing Course, 2005 Ankara.

[4] Zhou, NASA Report 2001.

[5] Okamoto, A., Fraser, C., Hattori, S., Hasegawa, H. And Ono, T., 1998. An alternative approach to the triangulation of SPOT imagery. IAPRS, Vol. 32, part4, p. 457 – 462.

[6] El-Manadili, Y. And Novak, K., "Precision rectification of SPOT Imagery using the direct linear transformation model. Photogrammetric Engineering and Remote Sensing 62(1), p. 62 – 72, 1996.

[7] Kornus, W., Lehner, M. And Schroeder, M. "Geometric inflight-calibration by block adjustment using MOMS-2P imagery of the intersecting stereo strips." Veröffentlichungen des Instituts für Photogrammetrie und Ingenieurvermessungen, Universitat Hannover, Nr. 18. Joint Workshop of ISPRS WG I/1, I/3 and IV/4, Sensors and Mapping from Space, Hanover, September 27-30, 1999.

[8] Ebner, H., Kornus, W. And Ohlhof, T. "A simulation study on point determination for the MOMS-02/D2 space project using an extended functional model." IAPRS, Vol. XXIX, part B4, commission IV, p. 458 – 464. ISPRS congress Washington, D. C. 1992.

[9] Gugan, D. "Practical aspects of topographic mapping from SPOT imagery. The photogrammetric record 12 (69), p. 349 – 355.

[10] Valadan Zoej, M. And Javid Foomani, M. "Mathematical modeling and accuracy testing of SPOT level 1B stereo pairs." The Photogrammetric Record 16(91), p. 67 – 82.

[11] Baltsavias, E. and Stallmann, D. “Geometric potential of MOMS-02/D2 data for point positioning, DTM and orthoimage generation.” IAPRS, Vol. XXXI, part B4, commission IV, p. 110 – 116. ISPRS Congress Vienna 1996.

[12] Fritsch, D., Kiefner, M., Stallmann, D. and Hahn, M. “Improvement of the automatic MOMS02-P DTM reconstruction”, IAPRS, Vol. 32, part 4, p 325 – 330 1998.

[13] Baltsavias, E. and Stallmann, D. “Metric information extraction from SPOT images and the role of polynomial mapping functions”, IAPRS, Vol, XXIX, part B4, commission IV, p. 358 – 364. ISPRS congress Washington, D. C. 1992.

[14] A. Ö. OK “Accuracy Assessment of the Dem and Orthoimage Generated From ASTER”, Master Thesis METU, September 2005.

[15] Technical Panel, Michael Firestone (Chair), “Guiding Principles for Monte Carlo Analysis.” Risk Assessment Forum, U.S. Environment Protection Agency Washington, DC, March 1997.

[16] M. Granger Morgan and Max Henrion with a chapter by Mitchell Small, “Uncertainty A Guide to dealing with Uncertainty in Qualitative Risk and Policy Analysis.” Cambridge University Press 1993.

[17] Xiaojin (Jerry) Ji and Panos D. Prevedouros, “Comparison of Methods for Sensitivity and Uncertainty Analysis of Signalized Intersections Analyzed with HCM.”, Accepted for the publication in the Transportation Research Record.

[18] W. J. Conover and Ronald L. Iman, “Analysis of Covariance Using the Rank Transformation”, Biometrics 38, 715 – 724, September 1982.

[19] J.C. Helton “Mathematical and Numerical Approaches in Performance Assessment for Radioactive Waste Disposal: Dealing with Uncertainty” Document 5120.

[20] Victor R. Vasquez and Wallace B. Whiting, “Accounting for Both Random Errors in Uncertainty Propagation Analysis of Computer Models Involving Experimental Measurements with Monte Carlo Methods”, Risk Analysis, Vol. 25, No. 6, 2006.

[21] J.C. Helton, F. J. Davis, J. D. Johnson “A Comparison of uncertainty and sensitivity analysis results obtained with random and Latin hypercube sampling”, Reliability Engineering and System Safety 89 (2005) 305 – 330.

[22] Karen Chan, Andrea Saltelli, Stefano Tarantola, "Sensitivity Analysis of Model Output: Variance-Based Methods Make the Difference", Proceedings of the 1997 winter Simulation Conference ed. S. Andradottir, K. J. Healy, D. H. Withers, and B. L. Nelson.

[23] A. Saltelli, S. Tarantola, and P.S. Chan, "A Quantitative Model-Independent Method for Global Sensitivity Analysis of Model Output"

[24] B. Erbaş and H. Urhan, "Yönelim Belirleme ve Kontrol Sistemi Bilgi Notu Koordinat Sistemleri ve Dönüşümler Üzerine", 09.02.2003, TÜBİTAK-BİLTEN.

[25] Wolfgang Torge "Geodesy" Third Edition. Walter de Gruyter Berlin 2001.

[26] Wikipedia the free encyclopedia. http://en.wikipedia.org/wiki/UTC
Visited on August 2006.

[27] Wikipedia the free encyclopedia. http://en.wikipedia.org/wiki/UT0 visited on August 2006,

[28] Wikipedia the free encyclopedia. http://en.wikipedia.org/wiki/Unix_Time.
Visited on August 2006,

[29] Tübütak Bilten, http://www.bilten.metu.edu.tr/bilsat/tr/about/properties.asp
Visited on August 2006.

[30] Jet Propulsion Laboratory, http://asterweb.jpl.nasa.gov/characteristics.asp
Visited on August 2006.

[31] Jet Propulsion Laboratory, California Institute of Technology
http://www2.jpl.nasa.gov/srtm/srtmBibliography.html visited on September 2006.

[32] Karl Krauss,"Photogrammetry Volume 1 Fundamentals and Standard Processes" Dümmler 1993 Bonn.

[33] J. Friedrich, U. M. Leloğlu, E. Tunalı, "Geometric Camera Calibration of the BilSAT Small Satellite: Preliminary Results", ISPRS Workshop Topographic Mapping from Space (with Special Emphasis on Small Satellites), ISPRS Vol: XXXVI-1/W41, Ankara, Turkey February 14-16, 2006.

[34] R. Rummel and T. Peters "Reference systems in Satellite Geodesy" Technische Universitat München, Institut für Astronomiche und physikalische Geodasie, München 2001.

[35] International Earth Rotation Service (IERS).
http://www.iers.org/products/6/9989/orig/bulletina-xix-029.txt visited on August 2006.

[36] William Tyrrell Thomson "Introduction to Space Dynamics", 1986, Dover Publicatins, INC., New York.

[37] Wikipedia the free encyclopedia, http://en.wikipedia.org/wiki/Snells_law.
Visited on August 2006.

[38] Wikipedia the free encyclopedia. http://en.wikipedia.org/wiki/Barometric_formula
visited on August 2006.

[39] T. Westin and J. Forsgren, "Orthorectification of EROS A1 Images" METRIA, P.O Box 820, SE-981 28 Kiruna, Sweden.

[40] L.C. Chen, T.A. Teo and J.Y. Rau, "Fast Orthorectification for Satellite Images Using Patch Backprojection",0-7803-7929-2/03 2003 IEEE.

[41] M. Ettarid, A.A.M'Hand and R. Aloui, "Digital True Orthophotos Generation", From Pharaohs to Geoinformatics FIG Working week 2005 and GSDI-8 Cairo, Egypt April 16-21, 2005.

[42] F. Amhar, "The Generation of True Orthophotos 3D Building Model in Conjunction With a Conventional DTM", IAPRS, Vol.32, Part 4 "GIS-Between Visions and Applications", Stuttgart, 1998.

[43] Z. Qin, W. Li, M. Li, Z. Chen and G. Zhou, "A methodology for True Orthorectification of Large-Scale Urban Aerial Images and Automatic Detection of Building Occlusions Using Digital Surface Model", 0-7803-7929-2/03 2003 IEEE.

[44] H. B. Hanley and C. S. Fraser, "Geopositioning Accuracy of IKONOS Imagery: Indications from 2D Transformations", Submitted to photogrammetric Record, 5 April 2001.

[45] P. Reinartz, M. Lehner, R. Müller and M. Schroeder, "Accuracy Analysis for DEM and Orthoimages Derived from SPOT HRS Stereo Data Without Using GCP", Commission I/2.

[46] K. Kraus, C. Briese, M. Attwenger, N. Pfeifer, "Quality Measures for Digital Terrain Models", Commission II, WG II/2.

[47] P. Fricker, R. Sandau and A. S. Walker, "Progress in the Development of a High Performance Airborne Digital Sensor", Photogrammetric Record, 16(96): 911 – 927 (October 2000).

[48] L. G. Brown "A survey of Image Registration Techniques", ACM Computing Surveys, Vol. 24, No. 4, December 1992.

[49] D. Poli, "Orientation of Satellite and Airborne Imagery From Multi-Line Pushbroom Sensors with A Rigorous Sensor Model", Commision I, WG I/5.

[50] M. J. V. Zoej, S. Yavari and S. Sadeghian, "Mathematical Modeling of IKONOS Geo Image", ISPRS Workshop in ANKARA.

[51] P. Reinartz, M. Lehner, R. Müller, M. Rentsch and M. Schroeder, "First Results on Accuracy Analysis for DEM and Orthoimages Derived from SPOT HRS Stereo Data over Bavaria".

[52] C. F. Gerald and P. O. Wheatley, "Applied Numerical Analysis" Sixth Edition, Addison-Wesley.

[53] Karl Rudolf Koch "Parameter Estimation and Hypothesis Testing in Linear Models", Second Edition Springer.

[54] C. Dörstel, K. Jacobsen, D. Stallmann, "DMC – Photogrammeteric Accuracy – Calibration Aspects and Generation of Synthetic DMC Images", Technical Session

[55] M. Cramer, D. Stallmann and N. Haala, "Sensor Integration and Calibration of Digital Airborne Three-line Camera Systems", Commission II, Working Group 1.

[56] M. Cramer and D. Stallmann, "On the use of GPS/inertial exterior orientation parameters in airborne photogrammertry", Photogrammetric Week 2001, Fritsch/Spiller (eds.), Wichmann Verlag, Heidelberg, Germany.

[57] N. Haala, D. Stallmann and M. Cramer, "Calibration of Directly Measured Position and Attitude by Aerotriangulation of Three-line Airborne Imagery", Commission III, Working Group 1.Institude of Photogrammetry (ifp) University of Stuttgart, Germany.

[58] R. B. Huseby, O. M. Halck and R. Solberg, "A model-based approach for Geometrical correction of optical satellite Images", International Journal of Remote Sensing, Vol. 26, No. 15, 10 August 2005, 3205 – 3223.

[59] W. Krüger, "Robust and Efficient map-to-image Registration With Line Segments", Machine Vision and Applications (2001) 13 : 38 – 50, Springer – Verlag 2001.

[60] A. P. D. Poz, A. M. G. Tommaselli,“Automatic Absolute Orientation of Scanned Aerial Photographs“, Anais do X SIBGRAPI (1998) 1-8.

[61] M. J. Valadan Zoej and G. Petrie, “Mathematical Modeling and Accuracy Testing of SPOT Level 1B Stereopairs”, Photogrammetric Record, 16(91): 67- 82 (April 1998)

[62] R. Gupta and R. I. Hartley, “Camera Estimation for Orbiting Pushbroom Imaging Systems”

[63] Q. Zheng, V. Klemas, X.-H. Yan, Z. Wang, K. Kagleder,“Digital Orthorectification of Space Shuttle Coastel Ocean Photographs”, Int. J. Remote Sensing, 1997, Vol.18, No.1, 197-211.

[64] P. Grussenmeyer, O.A. Khalil, “Solutions for Exterior Orientation in Photogrammetry: A Review”, Photogrammetry Record, 17(100):615 – 634 (October 2002).

[65] A. M. G. Tommaselli, ”Line Based Camera Calibration in Machine Vision Dynamic Applications”, 100 SBA Controle & Automaçao Vol. 10 no. 02/Maio, Jun., Jul., Agosto 1999.

[66] Q. Ji, M. S. Costa, R. M. Haralick, L. G. Shapiro, “A Robust Linear Least-Squares Estimation of Camera Exterior Orientation Using Multiple Geometric Features”, ISPRS Journal of Photogrammetry & Remote Sensing 55 (2000) 75 – 93.

[67] S. Joseph and C. Yuan, “A General Photogrammetric Method for Determining Object Position and Orientation”, IEEE Transactions on Robotics and Automation, Vol. 5, No, 2, April 1989.

[68] Y. Liu, T. S. Huang and O. D. Faugeras, “Determination of Camera Location from 2-D to 3-D Line and point Correspondences”, IEEE Transactions on Pattern Analysis and Machine Intelligence. Vol. 12, No, 1. January 1990.

[69] G. Zhou, K. Jezek, W. Wright, J. Rand and J. Granger,”Orthorectification of 1960s Satellite Photographs Covering Greenland”, IEEE Transactions on Geoscience and Remote Sensing, Vol.40, No.6, June 2002.

[70] R. Müller, M. Lehner, P. Reinartz, M. Schroeder, “Evaluation of Spaceborne and Airborne Line Scanner Images Using a Generic Ortho Image Processor”, Commission I, WG I/5.

[71] D. Poli, “Georeferencing Of MOMS-02 and MISR Stereoimages with Strict Sensor model”, Commission I.

[72] A. Krupnik, “Accuracy Prediction for Ortho-image Generation”, Photogrammetric Record, 18(101): 41 – 58 (March 2003).

[73] D. Fritsch, D. Stallmann, ”Rigorous Photogtammetric Processing of High Resolution Satellite Imagery”, ISPRS, Vol. XXXIII, Amsterdam, 2000.

[74] W. TORBJORN, “Precision rectification of SPOT imagery” Photogrammetric Engineering and Remote Sensing. Vol. 56, pp. 247-253. Feb. 1990.

[75] M. O. Karslıoğlu, “An Interactive program for GPS-based dynamic orbit determination of small satellites”, Computers & Geosciences 31 (2005) 309 - 317.

[76] Wikipedia the free encyclopedia, http://en.wikipedia.org/wiki/Tikhonov_regularization Visited on August 2006.

[77] Wikipedia the free encyclopedia, http://en.wikipedia.org/wiki/Singular_value_decomposition Visited on August 2006.

[78] E. Kreyszig, “Advanced Engineering Mathematics” 8th edition. John Wiley & Sons, inc. 1999, Singapore.

[79] Hüseyin Demirel, “Dengeleme Hesabı” Yıldız Teknik Üniversitesi Basım-Yayın Merkezi / İstanbul – 05, 2nd Edition.

[80] V.A. Chobotov, “Orbital Mechanics”, American Institute of Aeronautics and Astronautics, c1991, Washington, DC.

[81]O. Montenbruck, E. Gill “Satellite Orbits Models Methods Applications”, Springer, 2000.

[82] G. Sun, K. J. Ranson, V. I. Kharuk, and K. Kovacs, “Validation of surface height from shuttle radar topography mission using shuttle laser altimeter” Remote Sens. Env., vol. 88, p. 401 – 411, 2003.

[83] V. Schwieger, “Variance-based Sensitivity Analysis for Model Evaluation in Engineering Surveys”, INGEO 2004 and FIG Regional Central and Eastern European Conference on Engineering Surveying Bratislava, Slovakia November 11-13, 2004.

[84] S. Fang, G. Z. Gertner, S. Shinkareva, G. Wang and A. Anderson, “Improved Generalized Fourier Amplitude Sensitivity Test (FAST) for model assessment “,Statistics and Computing 13: 221 – 226, 2003, Kluwer Academic Publishers.

[85] J.C. Helton and F.J. Davis “Illustration of Sampling-Based Methods for Uncertainty and Sensitivity Analysis”, Document 0001, Sandia National Laboratories.

[86] J.C. Helton, J.D. Johnson, C.J. Sallabery and C.B. Storlie, “Survey of sampling-based methods for uncertainty and sensitivity analysis”, Reliability Engineering and System Safety, Article in Press.

[87] J.C. Helton and F.J. Davis, “Latin hypercube sampling and the Propagation of Uncertainty in Analyses of Complex Systems”, Reliability Engineering and System Safety 81 (2003) 23 – 69.

[88] J. C. Helton, “Uncertainty and Sensitivity Analysis Techniques for use in Performance assessment for Radioactive Waste Disposal”, Reliability Engineering and System Safety 42 (1993) 000 – 000.

[89] A. Saltelli, M. Ratto, S. Tarantola and F. Campolongo, “Sensitivity Analysis Practices. Strategies for Model-Based Inference”, RESS Review.

[90] M. Gahegan and M. Ehlers, “A framework for the modeling of Uncertainty Between Remote Sensing and Geographic Information Systems”, ISPRS Journal of Photogrammetry & Remote Sensing 55 (2000)176 – 188.

[91] E. Saliby, F. Pacheco, “An Emprical Evaluation of Sampling Methods in Risk Analysis Simulation: Quasi-Monte Carlo, Descriptive Sampling, and Latin Hypercube Sampling.”, Proceedings of the 2002 Winter Simulation Conference, E. Yücesan, C.-H. Chen, J. L. Snowdon and J. M. Charnes, eds.

[92] J. C. Helton, “Sampling-Based Methods for Uncertainty and Sensitivity Analysis”, Sensitivity Analysis of Model Output Kenneth M. Hanson and François M. Hemez, eds. Los Alamos National Laboratory, 2005. http://library.lanl.gov/

[93] M. Liefvendahl, R.Stocki, “A study on Algorithms for Optimization of Latin Hypercubes” submitted for reviews in Journal of Statistical Planning and Inference, 2003.

[94] A. F. M. Smith and G. O. Roberts, “Bayesian Computation via the Gibbs Sampler ans Related Markov Chain Monte Carlo Methods”, J. R. Statist. Soc. B (1993) 55, No. 1, pp. 3 – 23.

[95] M. K. Muleta, J. W. Nicklow, “Sensitivity and Uncertainty Analysis Coupled With Automatic Calibration for a Distributed Watershed Model”, Journal of Hydrology 306 (2005) 127 – 145.

[96] A. Saltelli, “Sensitivity Analysis for Importance Assessment”, Risk Analysis, Vol 22, No. 3, 2002.

[97] R. A. Dandekar, M. Cohen and N. Kirkendall, “Applicability of Latin Hypercube Sampling to Create Multi Variate Synthetic Micro Data”, Exchange of Technology and Know-how New Techniques and Technologies for Statistics, ETK ’2001 – NTTS ’2001, Crete (Greece), pp. 839-847, 2001.

[98] A. Hakami, M. T. Odman and A. G. Russel, “High-Order, Direct Sensitivity Analysis of Multidimensional Air Quality Models” Environmental Science & Technology / Vol. 37, No. 11, 2442 – 2452, 2003.

[99] A. Saltelli and J. Marivoet, “Non-parameteric Statistics in Sensitivity Analysis for Model Output: Acomparison of Selected Techniques”, Reliability Engineering and System Safety 28 (1990) 229 – 253.

[100] H. C. Frey, S. R. Patil, “Identification and Review of Sensitivity Analysis Methods”, Risk Analysis, Vol. 22, No. 3, 2002.

[101] M. Ratto, S. Tarantola and A. Saltelli, “Sensitivity analysis in model calibration: GSA-GLUE approach”, Computer Physics Communications 136 (2001) 212 – 224.

[102] A. Saltelli, “Global Sensitivity Analysis: An Introduction”, Sensitivity Analysis of Model Output Kenneth M. Hanson and François M. Hemez, eds. Los Alamos National Laboratory, 2005, http://library.lanl.gov/ visited on August 2006.

APPENDIX A

TERMINOLOGY

Some of the terms used in the thesis and derivation of some equations are briefly introduced in this appendix.

- **Image Maps:** Rectified images can be used as maps after the rectification, because the rectified images will have same scale and direction at every pixel. Maps produced by this way save time and money compared with the classical map production methods [2, p. 293]. An example of an image map is shown in the Fig 1. Rectified images provide a basis for image maps and can be used as a data source for GIS applications.

Figure A.1 Example of an image map, it has a scale and a legend. Courtesy of *İşlem Şirketler Grubu* "Bosporus and Environ".

In the image map shown in Figure A.1 has same scale at every pixel. In other words each picture element of the image covers same area on ground. Furthermore, north direction is same at every location in the image. This is sustained by rectifying the image. Besides, the map has a legend for specific areas inside the image, such as lakes, forests, urban areas, harbors and etc. for this reason the rectified image can be used as a map and called as image map.

- **DEM (Digital Elevation Model):** DEM is a coordinated elevation data collected at regular grids and stored in a specific format. DEM has certain accuracy which depends on the method it is produced [2, p11].
- **Rectification:** Process of assigning coordinates with respect to a certain datum for all pixels of the image taken from airplane or satellite.. This may be achieved by performing an affine transformation or by differential rectification [2, p.189].
- **Rank Transformation:** Replacement of numeric data with its rank is called rank transformation. In rank transformed data, smallest number is assigned as 1, second smallest data is assigned as 2 and the largest number is assigned as the size of the sample set. Rank transformed data is expected to give better results than original data for non linear models.
- **Base Value:** Most probable value of a parameter.

Derivation of $\mathbf{R}_{213}(-\omega, -\varphi, -\kappa)$ Rotation Matrix

$\mathbf{R}_{213}(-\omega, -\varphi, -\kappa)$ rotation matrix is constructed by rotating the 3 axes in an order 2, 1 and 3. Conventions of the rotation are as follows;

- The coordinate system is Right Handed reference system
- No 1 axis is X, No 2 axis is Y and No 3 axis is Z axis.
- Angles are measured as positive, when looking from the positive side of the principle rotation axis and rotating the axes in counter clockwise direction.

Rotation in X direction, (rotation of 1) by $-\omega$ angle;

$$\begin{aligned} X' &= X \\ Y' &= Y * \cos\omega - Z * \sin\omega \\ Z' &= Y * \sin\omega + Z * \cos\omega \end{aligned} \tag{A.1}$$

In matrix form

$$\begin{bmatrix} 1 & 0 & 0 \\ 0 & \cos\omega & -\sin\omega \\ 0 & \sin\omega & \cos\omega \end{bmatrix} \tag{A.2}$$

Rotation in Y direction, rotation of 2 axis by –φ angle.

$$\begin{aligned} X'' &= X'\cos\phi + Z'\sin\phi \\ Y'' &= Y' \\ Z'' &= -X'\sin\phi + Z'\cos\phi \end{aligned} \tag{A.3}$$

in matrix form

$$\begin{bmatrix} \cos\phi & 0 & \sin\phi \\ 0 & 1 & 0 \\ -\sin\phi & 0 & \cos\phi \end{bmatrix} \tag{A.4}$$

Rotation in Z direction, rotation 3 by –κ angle

$$\begin{aligned} X''' &= X''\cos\kappa - Y''\sin\kappa \\ Y''' &= X''\sin\kappa + Y''\cos\kappa \\ Z''' &= Z'' \end{aligned} \tag{A.5}$$

in matrix form

$$\begin{bmatrix} \cos\kappa & -\sin\kappa & 0 \\ \sin\kappa & \cos\kappa & 0 \\ 0 & 0 & 1 \end{bmatrix} \tag{A.6}$$

Then the multiplication of these three matrixes will form $\boldsymbol{R_{213}}$ rotation matrix;

$$\boldsymbol{R_{213}} = \begin{bmatrix} \cos\kappa & -\sin\kappa & 0 \\ \sin\kappa & \cos\kappa & 0 \\ 0 & 0 & 1 \end{bmatrix} \begin{bmatrix} 1 & 0 & 0 \\ 0 & \cos\omega & -\sin\omega \\ 0 & \sin\omega & \cos\omega \end{bmatrix} \begin{bmatrix} \cos\phi & 0 & \sin\phi \\ 0 & 1 & 0 \\ -\sin\phi & 0 & \cos\phi \end{bmatrix}$$

$$\boldsymbol{R_{213}} = \begin{bmatrix} \cos\kappa\cos\phi - \sin\kappa\sin\omega\sin\phi & -\sin\kappa\cos\omega & \cos\kappa\sin\phi + \sin\kappa\sin\omega\cos\phi \\ \sin\kappa\cos\phi + \cos\kappa\sin\omega\sin\phi & \cos\kappa\cos\omega & \sin\kappa\sin\phi - \cos\kappa\sin\omega\cos\phi \\ -\cos\omega\sin\phi & \sin\omega & \cos\omega * \cos\phi \end{bmatrix} \tag{A.7}$$

Lens Distortion

The mathematical equations for the model of lens distortions typically comprise two components: symmetric radial distortion and decentering distortion [2, p. 64].

Radial Lens Distortion

Symmetric radial lens distortion is the symmetric component of distortion that occurs along radial lines from the principal point (Figure A.2). Although the amount may be negligible, this type of distortion is theoretically always present even if the lens system is perfectly manufactured to design specifications. Distortion occurs in a direction inward toward or outward from the center of the image. In this thesis radial distortions are corrected by a two parameter polynomial considering the distance of the image point with respect to principal point [2].

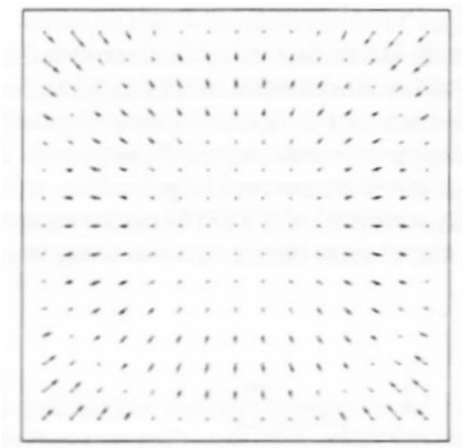

Figure A.2 Symmetric radial lens distortion effects [2, p. 65]

Decentering Lens Distortion

Decentering lens distortion is the lens distortion that remains after compensation for symmetric radial lens distortion (Figure A.3). Decentering distortion can be further broken into asymmetric radial and tangential lens distortion components. These distortions are caused by imperfections in the manufacture and alignment of the lens system. In this thesis decentering lens distortions are modeled with two parameters also.

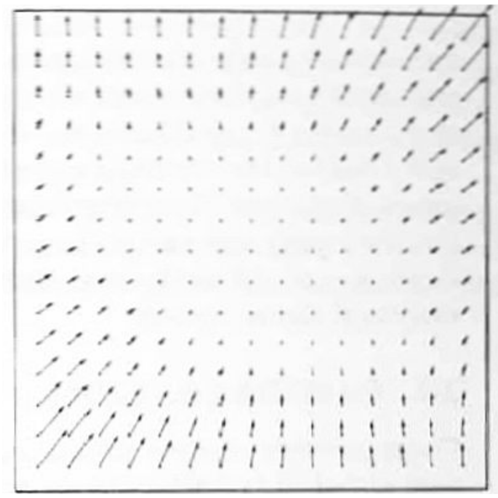

Figure A.3 Decentering lens distortion [2, p. 65]

Symmetric radial lens distortion and decentering lens distortion effects are usually present in every camera and their superposition is shown in Figure A.4. The superposed effect is corrected by means of a polynomial function whose coefficients are determined after a camera calibration procedure.

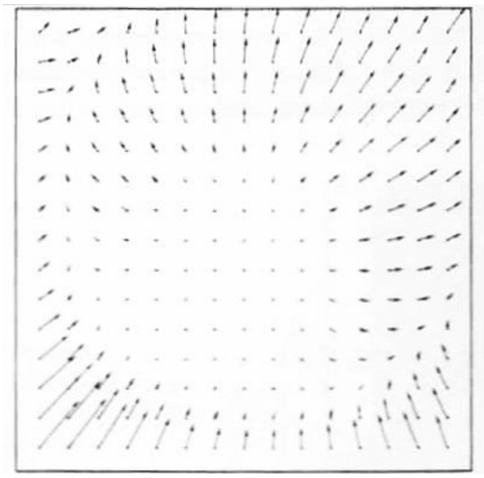

Figure A.4 Combined symmetric radial and decentering lens distortion effect [2, p. 65].

APPENDIX B

RESULTS OF ANALYSES

Analysis results for the Mixed Model with fictitious observations

Table B.1 Corrections to the pixel values obtained after the Mixed Model with fictitious observations

X	Y	Elevation
0,0856	-0,2278	1,4346
0,5668	-0,6219	8,3557
0,5506	-0,9736	8,5932
-0,2730	-0,1243	-3,4418
-0,2904	0,2225	-4,1192
0,9439	0,2746	12,0127
0,9619	0,5150	11,9228
-0,0033	0,0424	-0,1021
0,9441	-0,6274	13,3334
-0,3288	0,6754	-5,3105
-0,3306	0,0960	-4,4644
0,1859	1,1821	0,7741
0,7498	1,1475	8,1578
0,7672	0,4439	9,3579
-0,1529	-0,9531	-0,8435
-0,4502	-0,3045	-5,5091
-0,9727	-0,1679	-12,5532
-0,8157	-0,3565	-10,3112
-0,1069	0,5891	-2,1757
-0,6884	0,3295	-9,5828
0,3825	0,4421	4,5314
0,0730	-1,3223	2,7295
-0,4291	-0,2462	-5,3598
-0,7255	0,2164	-9,9031
-0,6663	-0,2830	-8,4362

Analysis results for the Mixed Model with Tikhonov regularization method

Table B.2 Corrections to pixel coordinates and elevation of GCPs computed after Mixed Model analysis with Tikhonov regularization method

X	Y	Elevation
0,0899	0,4039	0,80487523
0,4628	0,0339	6,29381961
0,4107	-0,3056	5,93652936
-0,8222	-0,2702	-10,845288
-0,7689	0,3086	-10,688376
0,4972	0,2745	6,36043459
0,6772	0,3156	8,72586453
-0,2972	-0,1669	-3,7961352
1,0021	-1,2512	14,9763047
-0,1637	0,1311	-2,363846
-0,3665	-0,3265	-4,5249452
-0,0984	0,7850	-2,2331912
0,4081	0,7851	4,53453508
0,3918	0,4242	4,75688551
-0,1591	-0,9716	-1,1839371
-0,3420	-0,3412	-4,2461055
-0,7077	-0,2147	-9,2971991
-0,4119	-0,5886	-4,9785595
0,3939	0,4326	4,90206592
-0,1864	0,2666	-2,8162941
0,7776	0,3216	10,2841212
0,3508	-0,7585	5,6001475
-0,0899	0,1815	-1,4239973
-0,5455	0,4767	-7,926503
-0,5026	0,0440	-6,860747

Analysis results for the Mixed Model with Singular Value Decomposition.

Table B.3 Corrections to pixel coordinates and elevation of GCPs computed after Mixed Model analysis with Singular Value Decomposition

X	**Y**	**Elevation**
0,1246	0,2629	1,3171
0,5580	-0,1022	7,5648
0,5337	-0,4492	7,6904
-0,6711	-0,4279	-8,2883
-0,7229	0,6486	-10,3725
0,5040	0,3104	6,1836
0,6329	0,5706	7,5171
-0,3447	0,0474	-4,5878
0,8552	-1,1146	12,8482
-0,2818	0,2191	-4,0250
-0,3909	-0,3743	-4,5808
-0,0452	0,6724	-1,5211
0,4796	0,6591	5,3171
0,4793	0,2509	5,8752
-0,1580	-0,9903	-0,8653
-0,3637	-0,3381	-4,3354
-0,7503	-0,1956	-9,5924
-0,4678	-0,4404	-5,6188
0,3653	0,5365	4,1560
-0,2062	0,3171	-3,1517
0,8453	0,4274	10,7210
0,3421	-0,9726	5,8448
-0,1481	0,0141	-1,9840
-0,6097	0,4667	-8,7100
-0,5596	0,0087	-7,4163

Residuals of the parameter estimation with fictitious observation

Table B.4 Residuals of the GCPs with respect to geodetic and UTM coordinates are shown

Latitude	Longitude
1,08E-06	4,10E-07
3,18E-06	3,25E-06
4,77E-06	2,93E-06
3,99E-07	-1,84E-06
-1,20E-06	-1,74E-06
-6,82E-07	6,29E-06
-1,78E-06	6,56E-06
-1,97E-07	5,64E-09
3,42E-06	5,70E-06
-3,26E-06	-1,70E-06
-6,35E-07	-2,09E-06
-5,25E-06	1,92E-06
-4,74E-06	5,59E-06
-1,52E-06	5,28E-06
4,27E-06	-1,51E-06
1,09E-06	-3,10E-06
1,20E-07	-6,40E-06
1,09E-06	-5,47E-06
-2,74E-06	-3,46E-07
-1,93E-06	-4,23E-06
-1,75E-06	2,71E-06
5,98E-06	-3,24E-07
8,41E-07	-2,91E-06
-1,42E-06	-4,54E-06
8,67E-07	-4,46E-06

X	Y
6,9102	2,0029
20,2718	15,8407
30,3574	14,2880
2,5394	-8,9623
-7,6711	-8,4723
-4,3452	30,7018
-11,3188	32,0171
-1,2534	0,0275
21,8087	27,8279
-20,7697	-8,2921
-4,0455	-10,2049
-33,4394	9,3908
-30,2100	27,2815
-9,6964	25,7861
27,1873	-7,3808
6,9531	-15,1161
0,7642	-31,2516
6,9288	-26,6960
-17,4523	-1,6892
-12,2934	-20,6180
-11,1192	13,2005
38,0851	-1,5805
5,3559	-14,1874
-9,0688	-22,1450
5,5213	-21,7872

Table B.5 Estimated parameters after the parameter estimation with fictitious observation

Parameters	**Estimated Value**
X	4496830,4
Y	3021719,0
Z	4534207,9
ω	0,147532
ϕ	-0,038086
κ	0,112314
f	176,153596
Δx	0,001784
Δy	-0,365364
k_1	0,000355
k_2	-0,000004
p_1	-0,000507
p_2	0,000584

Table B.6 Corrected GCP coordinates after the parameter estimation with fictitious observation

X	Y	Z
4126272,656	2645481,229	4068886,962
4128644,784	2644301,205	4067351,983
4129406,774	2643774,527	4066981,403
4132631,257	2650464,290	4059747,586
4128760,341	2654853,979	4060538,708
4127390,933	2657052,192	4060463,680
4124621,792	2658297,927	4062427,989
4124735,636	2658567,385	4062105,210
4119026,068	2663727,719	4064732,366
4114329,127	2665950,876	4067878,960
4110720,994	2667733,116	4070308,206
4108988,665	2668723,875	4071361,420
4108559,218	2668714,475	4071783,984
4106679,985	2666053,549	4075558,864
4106318,780	2660000,084	4079598,212
4106814,376	2658851,938	4079967,429
4107776,273	2657065,044	4080129,215
4108822,447	2654036,046	4081215,130
4111674,443	2650510,834	4080440,152
4112819,465	2649553,487	4079838,383
4115760,192	2645691,402	4079419,512
4120479,837	2646573,865	4073896,908
4117762,702	2650915,543	4073829,649
4119545,667	2652998,066	4070764,588
4120404,334	2651703,569	4070704,864

Table B.7 Residuals of the GCPs with respect to geodetic and UTM coordinates with Tikhonov regularization are shown

Phi	Lambda
-6,759E-07	1,096E-06
1,448E-06	4,103E-06
3,006E-06	3,935E-06
6,176E-07	-4,061E-06
-5,140E-07	-4,840E-06
2,209E-07	3,081E-06
-8,284E-07	3,869E-06
7,905E-07	-2,746E-06
4,663E-06	4,619E-06
-2,161E-06	-1,836E-06
1,205E-07	-2,290E-06
-4,737E-06	1,221E-06
-4,314E-06	4,77E-06
-1,54E-06	4,81E-06
4,59E-06	-4,73E-07
1,49E-06	-1,73E-06
5,71E-07	-4,67E-06
1,86E-06	-3,23E-06
-2,41E-06	1,98E-06
-1,93E-06	-1,97E-06
-2,08E-06	5,00E-06
4,18E-06	1,03E-06
-2,97E-07	-2,14E-06
-2,06E-06	-4,86E-06
3,36E-09	-4,70E-06

X	Y
-4,3057	5,3470
9,2225	20,0222
19,1473	19,2000
3,9341	-19,8145
-3,2743	-23,6159
1,4071	15,0321
-5,2768	18,8779
5,0352	-13,4015
29,7062	22,5403
-13,7672	-8,9606
0,7674	-11,1735
-30,1723	5,9599
-27,4802	23,2956
-9,8360	23,4954
29,2588	-2,3103
9,5086	-8,4191
3,6375	-22,8010
11,8715	-15,7667
-15,3681	9,6566
-12,2773	-9,5949
-13,2744	24,3964
26,5956	5,0206
-1,8940	-10,4544
-13,1157	-23,7110
0,0214	-22,9226

Table B.8 Estimated parameters after the parameter estimation with Tikhonov regularization.

Parameters	Estimated Value
X	4496191,626
Y	3024516,853
Z	4532983,158
ω	0,14746
ϕ	-0,03813
κ	0,11231
f	175,92984
Δx	0,63002
Δy	-0,83923
k_1	0,00036
k_2	-4,44E-06
p_1	-0,00051
p_2	0,00058

Table B.9 Corrected GCP coordinates after the parameter estimation with Tikhonov regularization.

X	Y	Z
4126276,841	2645488,043	4068878,345
4128648,427	2644308,665	4067343,493
4129410,109	2643782,659	4066972,789
4132636,354	2650454,734	4059748,63
4128766,164	2654839,767	4060542,056
4127396,323	2657037,071	4060468,067
4124625,653	2658284,853	4062432,594
4124739,522	2658553,98	4062110,005
4119024,667	2663720,637	4064738,386
4114325,688	2665947,999	4067884,288
4110718,894	2667730,749	4070311,853
4108988,739	2668719,977	4071363,884
4108559,883	2668710,298	4071786,036
4106681,259	2666051,802	4075558,724
4106314,843	2660003,755	4079599,77
4106809,293	2658856,808	4079969,358
4107770,069	2657071,279	4080131,387
4108813,783	2654043,646	4081218,886
4111667,106	2650519,785	4080441,721
4112813,422	2649562,886	4079838,37
4115755,239	2645701,705	4079417,839
4120482,408	2646583,532	4073888,087
4117764,536	2650921,325	4073824,071
4119548,651	2652998,266	4070761,459
4120407,866	2651704,634	4070700,624

Residuals of the parameter estimation process with SVD.

Table B.10 Residuals of the GCPs with respect to geodetic and UTM coordinates are shown

Phi	Lambda
-9,856E-07	3,531E-07
8,542E-07	2,802E-06
2,387E-06	2,398E-06
1,968E-06	-4,471E-06
-4,149E-06	-3,729E-06
-1,337E-06	3,975E-06
-2,523E-06	4,871E-06
-6,534E-07	-1,804E-06
5,744E-06	4,554E-06
-1,301E-06	-2,310E-06
1,317E-06	-3,443E-06
-3,081E-06	-4,558E-07
-2,678E-06	3,051E-06
-7,936E-07	3,532E-06
4,658E-06	-8,276E-07
1,488E-06	-1,854E-06
4,999E-07	-4,384E-06
1,840E-06	-2,711E-06
-2,155E-06	2,923E-06
-1,529E-06	-9,867E-07
-1,320E-06	5,591E-06
4,802E-06	1,208E-06
-1,127E-07	-1,035E-06
-2,554E-06	-3,609E-06
-3,837E-07	-3,638E-06

X	Y
-6,2784	1,7232
5,4413	13,6713
15,2057	11,7030
12,5331	-21,8176
-26,4308	-18,1972
-8,5196	19,3970
-16,0688	23,7709
-4,1621	-8,8034
36,5878	22,2207
-8,2904	-11,2730
8,3894	-16,8025
-19,6237	-2,2243
-17,0589	14,8904
-5,0552	17,2355
29,6689	-4,0386
9,4804	-9,0459
3,1846	-21,3915
11,7222	-13,2292
-13,7301	14,2655
-9,7410	-4,8146
-8,4097	27,2809
30,5865	5,8941
-0,7178	-5,0507
-16,2689	-17,6090
-2,4444	-17,7548

Estimated parameters after the parameter estimation method with SVD

Table B.11 Estimated parameters after the parameter estimation with SVD

Parameters	**Estimated Value**
X	4509500,482
Y	3080868,378
Z	4481833,738
ω	0,188215
ϕ	0,044602
κ	0,114253
f	175,502284
Δx	0,000552
Δy	-0,366332
k_1	0,000355
k_2	-0,000004
p_1	-0,000387
p_2	0,000440

Table B.12 Corrected GCP coordinates after the parameter estimation with SVD

X	Y	Z
4126225,757	2645536,613	4068898,435
4128598,719	2644356,178	4067362,929
4129360,975	2643829,309	4066992,221
4132586,540	2650521,405	4059755,763
4128714,258	2654912,646	4060547,150
4127344,351	2657111,631	4060472,078
4124574,229	2658357,783	4062437,051
4124688,120	2658627,328	4062114,166
4118976,483	2663789,379	4064742,139
4114277,905	2666013,279	4067889,796
4110668,483	2667796,116	4070319,867
4108935,535	2668787,227	4071373,432
4108505,932	2668777,830	4071796,145
4106626,017	2666115,948	4075572,333
4106264,745	2660060,393	4079613,176
4106760,515	2658911,835	4079982,508
4107722,773	2657124,324	4080144,371
4108769,310	2654094,258	4081230,666
4111622,354	2650567,871	4080455,487
4112767,795	2649610,199	4079853,537
4115709,566	2645746,790	4079434,565
4120430,888	2646629,606	4073910,115
4117712,783	2650972,786	4073842,769
4119496,365	2653056,042	4070776,615
4120355,341	2651761,102	4070716,896

Residuals of the parameter estimation process with restriction.

Table B.13 Residuals of the GCPs with respect to geodetic and UTM coordinates are shown

Latitude	Longitude	X	Y
3,07E-06	1,85E-05	19,547	90,3787
7,47E-06	2,46E-05	47,5743	120,0869
9,58E-06	2,56E-05	61,044	124,7898
1,75E-05	1,36E-05	111,158	66,5793
1,52E-05	5,27E-06	96,92	25,7055
1,60E-05	9,64E-06	102,0324	47,0274
1,20E-05	6,65E-06	76,556	32,4686
1,41E-05	-1,18E-07	89,6533	-0,5752
1,39E-05	-3,85E-06	88,5621	-18,7876
2,36E-06	-1,70E-05	15,0592	-82,836
1,22E-06	-2,22E-05	7,7549	-108,2135
-4,99E-06	-2,09E-05	-31,7597	-101,7304
-5,12E-06	-1,75E-05	-32,6131	-85,6165
-7,23E-06	-1,56E-05	-46,0471	-75,8929
-6,72E-06	-1,44E-05	-42,8292	-70,381
-1,03E-05	-1,41E-05	-65,7261	-68,9128
-1,16E-05	-1,45E-05	-74,0448	-70,965
-1,18E-05	-9,04E-06	-75,4655	-44,1355
-1,54E-05	1,98E-06	-97,9489	9,6796
-1,41E-05	-3,07E-08	-90,0623	-0,1497
-1,37E-05	1,35E-05	-87,5489	65,6518
4,31E-07	1,24E-05	2,7482	60,7289
-4,08E-06	2,41E-06	-26,0057	11,7412
-1,41E-06	-8,89E-07	-8,9904	-4,3391
7,71E-07	1,40E-06	4,9134	6,8216

Table B.14 Estimated parameters after the parameter estimation with restriction.

Parameters	**Estimated Value**
X	4496564,668
Y	3022658,349
Z	4533847,454
ω	0,14744
ϕ	-0,03814
κ	0,11231
f	177,22806
Δx	0,62988
Δy	-0,83915
k_1	0,00036
k_2	-4,44E-06
p_1	-0,00051
p_2	0,00058

Registration with Affine Model.

Table B.15 Estimated paramters of the Affine Transformation after the parameter estimation

Parameters	Estimated Value
a	3,181E-05
b	2,592E-04
c	39,7894
d	3,451E-04
e	-3,787E-05
f	32,7307

.

Residuals of the parameter estimation process of Affine Transformation.

Table B.16 Residuals of the GCPs with respect to geodetic and UTM coordinates are shown

Phi	lambda
-8,889E-06	4,336E-06
-2,303E-06	7,626E-06
1,883E-06	5,282E-06
8,455E-06	-9,245E-06
1,847E-06	-8,233E-06
3,598E-06	5,031E-06
-4,795E-06	5,353E-06
-4,556E-07	-7,631E-06
7,424E-06	-1,356E-06
-5,528E-06	-4,173E-07
2,774E-06	-3,546E-06
-5,033E-06	3,617E-06
-4,059E-06	1,082E-05
-1,241E-06	7,319E-06
8,412E-06	4,229E-07
2,226E-06	-3,956E-06
1,586E-06	-8,109E-06
3,700E-06	-1,056E-05
-1,586E-06	3,227E-06
-4,147E-09	-3,678E-06
5,056E-07	4,161E-06
4,554E-06	4,466E-06
-6,538E-06	2,955E-06
2,628E-07	-5,129E-06
-6,795E-06	-2,763E-06

X	Y
-56,625	21,159
-14,667	37,215
11,992	25,774
53,855	-45,112
11,763	-40,175
22,920	24,549
-30,544	26,123
-2,902	-37,237
47,288	-6,614
-35,210	-2,036
17,668	-17,302
-32,057	17,650
-25,857	52,821
-7,904	35,714
53,586	2,064
14,179	-19,302
10,105	-39,569
23,571	-51,529
-10,104	15,749
-0,026	-17,949
3,221	20,302
29,011	21,794
-41,649	14,419
1,674	-25,026
-43,286	-13,480

Residuals of the Ground Check Points of the Affine Model.

Table B.17 Residuals of the Ground Check Points with respect to geodetic and UTM coordinates are shown

Phi	Lambda
2,440E-06	8,795E-07
-1,580E-06	-7,095E-06
8,479E-07	3,791E-06
5,891E-06	4,894E-06
-1,904E-05	-8,373E-06
-1,951E-05	-2,866E-06
-9,689E-06	-6,231E-06
-5,929E-06	-9,396E-06
2,638E-05	5,875E-06
5,153E-06	1,945E-05
-7,752E-06	-1,267E-05

X	Y
15,5420	4,2916
-10,0614	-34,6236
5,4013	18,4997
37,5269	23,8821
-121,2976	-40,8593
-124,2791	-13,9847
-61,7190	-30,4042
-37,7667	-45,8518
168,0590	28,6673
32,8222	94,9173
-49,3827	-61,8198

Registration with 3D Affine Model

Table B.18 Estimated parameters of the 3D Affine Transformation after the parameter estimation procedure of Least Squares.

parameters	Estimated Values
a1	-108583,069
a2	25111,387
a3	161346,701
a4	-561,477
a5	-1244,994
a6	2491,929
b1	143496,402
b2	-221285,498
b3	19629,346
b4	-2331,218
b5	2882,303
b6	555,155

Residuals of the parameter estimation process of 3D Affine Transformation.

Table B.19 Residuals of the GCPs with respect to geodetic and UTM coordinates are shown

x	y
0,0405	-1,2289
-1,0633	-0,2533
-1,0818	0,3682
0,1897	-0,5049
1,1463	0,5036
-0,9796	0,9058
-0,8262	-0,8166
1,1996	0,6375
0,4670	0,9283
0,4030	-1,1635
0,6412	0,8341
-0,4934	-0,9239
-1,7617	-0,8434
-0,7983	-0,4885
-0,6044	1,5512
0,3486	0,3089
1,0095	0,1952
1,0832	0,7028
-0,7715	-0,8658
0,5556	-0,3433
-0,7968	-0,4291
0,0502	1,4940
0,1156	-0,9295
0,9893	0,9046
0,9383	-0,5430

X	Y
1,1743	-35,6375
-30,8348	-7,3460
-31,3727	10,6787
5,5000	-14,6423
33,2422	14,6040
-28,4092	26,2678
-23,9604	-23,6825
34,7885	18,4876
13,5421	26,9199
11,6870	-33,7410
18,5944	24,1880
-14,3082	-26,7935
-51,0898	-24,4574
-23,1512	-14,1653
-17,5281	44,9849
10,1093	8,9580
29,2752	5,6598
31,4130	20,3820
-22,3721	-25,1096
16,1132	-9,9568
-23,1067	-12,4447
1,4547	43,3253
3,3537	-26,9569
28,6900	26,2335
27,2106	-15,7484

Residuals of the Ground Check Points of the 3D Affine Model.

Table B.20 Residuals of the GCPs with respect to geodetic and UTM coordinates are shown

x	y
9,8377	1,2881
12,5121	0,7080
11,3659	1,0180
10,1018	2,1648
5,6651	-3,2643
3,3998	-3,4695
2,3818	-1,3644
0,6542	-0,3904
-6,1486	5,5447
-8,1160	1,3091
-7,6136	-2,5219

X	Y
285,2921	37,3555
362,8505	20,5315
329,6125	29,5224
292,9511	62,7781
164,2886	-94,6655
98,5942	-100,6159
69,0730	-39,5685
18,9726	-11,3221
-178,3103	160,7953
-235,3637	37,9626
-220,7939	-73,1355

Registration with Projective Transformation

Table B.21 Estimated parameters of the projective transformation model with least squares

Parameters	Estimated Value
a1	2,2878E-04
a2	2,0982E-04
a3	39,7893
b1	5,0751E-04
b2	-7,8750E-05
b3	32,7309
c1	4,9349E-06
c2	-1,2413E-06

Residuals of the parameter estimation process of projective transformation

Table B.22 Residuals of the GCPs with respect to geodetic and UTM coordinates are shown

Phi	Lambda
9,164E-06	-9,703E-07
3,441E-06	-2,157E-06
-4,573E-07	1,109E-06
-5,386E-06	1,051E-05
-1,069E-06	5,813E-06
-3,755E-06	-8,423E-06
3,938E-06	-9,066E-06
-4,714E-07	3,879E-06
-9,703E-06	-1,162E-06
3,777E-06	3,695E-07
-3,521E-06	6,222E-06
4,876E-06	7,611E-07
4,160E-06	-6,207E-06
3,225E-06	-3,987E-06
-5,978E-06	-7,463E-07
-1,065E-07	2,989E-06
-8,651E-08	6,327E-06
-3,181E-06	8,127E-06
5,748E-07	-5,516E-06
-1,400E-06	1,693E-06
-3,306E-06	-3,967E-06
-5,987E-06	-3,765E-06
5,694E-06	-5,022E-06
-7,539E-07	2,518E-06
6,312E-06	6,676E-07

X	Y
58,3737	-4,7346
21,9220	-10,5232
-2,9130	5,4112
-34,3060	51,3037
-6,8073	28,3640
-23,9209	-41,1007
25,0827	-44,2399
-3,0027	18,9283
-61,8069	-5,6692
24,0588	1,8031
-22,4267	30,3628
31,0585	3,7140
26,5014	-30,2905
20,5423	-19,4530
-38,0783	-3,6415
-0,6783	14,5857
-0,5510	30,8721
-20,2632	39,6554
3,6616	-26,9161
-8,9211	8,2606
-21,0615	-19,3593
-38,1383	-18,3696
36,2694	-24,5076
-4,8022	12,2879
40,2096	3,2575

Residuals of the Ground Check Points of the Projective transformation

Table B.23 Residuals with respect to geodetic and UTM coordinates are shown

Phi	Lambda
-2,899E-06	-1,670E-06
1,142E-06	7,436E-06
-6,664E-07	-2,335E-06
-5,480E-06	-2,588E-06
1,860E-05	5,665E-06
1,902E-05	-1,657E-07
9,212E-06	3,113E-06
5,487E-06	6,236E-06
-2,670E-05	-8,862E-06
-5,326E-06	-2,219E-05
6,547E-06	9,330E-06

X	Y
-18,4670	-8,1506
7,2767	36,2875
-4,2449	-11,3950
-34,9045	-12,6302
118,4511	27,6440
121,1762	-0,8085
58,6796	15,1911
34,9491	30,4316
-170,0803	-43,2462
-33,9242	-108,2760
41,7033	45,5271

Residuals of the Space Resection Model computed after the parameter estimation procedure

Table B.24 Residuals of the GCPs with respect to geodetic and UTM coordinates are shown

x	y
0,7928	1,0216
1,4957	-0,1766
1,2378	-1,0603
-1,8686	-1,4068
-1,7348	-0,0809
0,5710	-0,0560
0,6205	1,2987
-1,3949	0,1940
0,1733	-1,5290
0,2432	1,0371
0,0132	-0,8267
1,0579	1,0913
2,2401	1,0131
1,0480	0,3611
-0,2743	-1,6358
-1,2504	-0,2225
-1,9062	-0,1753
-2,3093	-0,2204
0,2293	0,9072
-0,7207	0,2216
0,9927	0,3875
1,1849	-1,8133
0,4115	0,4457
-0,8027	-1,3296
-0,5530	0,2369

X	Y
22,9903	29,6264
43,3753	-5,1217
35,8962	-30,7487
-54,1894	-40,7972
-50,3092	-2,3468
16,5576	-1,6244
17,9945	37,6623
-40,4521	5,6266
5,0243	-44,3410
7,0540	30,0759
0,3814	-23,9749
30,6791	31,6477
64,9629	29,3799
30,3920	10,4719
-7,9547	-47,4382
-36,2616	-6,4537
-55,2798	-5,0837
-66,9697	-6,3919
6,6497	26,3091
-20,9000	6,4264
28,7886	11,2372
34,3621	-52,5857
11,9335	12,9256
-23,2792	-38,5584
-16,0379	6,8710

Residuals of the Ground Check Points of the Space Resection model.

Table B.25 Residuals of the GCPs with respect to geodetic and UTM coordinates are shown

x	y
-0,3069	-1,7492
-1,6409	-1,0162
0,1721	-1,2530
0,4872	-2,2883
-2,4492	2,7578
-1,5608	2,9743
-1,8866	0,7905
-2,3041	-0,0821
0,8780	-6,6418
2,6926	-1,8059
-2,9255	0,8839

X	Y
-8,90126	-50,7268
-47,5861	-29,4698
4,98974	-36,337
14,12735	-66,3607
-71,0268	79,9762
-45,2632	86,2547
-54,7114	22,92508
-66,8189	-2,38119
25,46055	-192,6122
78,0854	-52,3711
-84,8395	25,63339

Sensitivity Indexes computed after the differential Sensitivity Analysis

Table B.26a Sensitivity of the parameters for the 9 different pixel locations computed by Differential Sensitivity Analysis for latitude.

Parameter	1	2	3	4	5	6	7	8	9
f	1,361E-02	5,076E-02	2,245E-01	1,299E-03	6,008E-04	4,116E-04	2,707E-02	4,834E-02	1,012E-01
Dx	2,284E-02	3,298E-02	5,978E-02	1,890E-02	3,205E-02	6,224E-02	2,123E-02	2,593E-02	4,709E-02
Dy	4,788E-04	7,584E-04	9,180E-04	4,144E-04	6,555E-04	1,156E-03	3,568E-04	5,880E-04	7,931E-04
k1	8,020E-06	3,160E-06	2,410E-05	3,130E-07	1,980E-11	1,010E-08	2,550E-05	7,460E-06	2,420E-05
k2	1,130E-09	7,550E-11	2,110E-09	1,590E-11	2,410E-19	2,110E-13	4,870E-09	3,460E-10	3,080E-09
p1	6,830E-05	5,860E-05	1,848E-04	9,470E-06	1,220E-08	1,160E-05	1,284E-04	9,730E-05	1,957E-04
p2	1,080E-05	6,270E-08	6,180E-05	3,120E-06	5,840E-09	5,840E-07	4,850E-05	1,350E-06	2,370E-05
c	2,260E-05	3,400E-05	9,010E-05	5,690E-07	0,000E+00	8,330E-07	4,250E-05	3,070E-05	5,600E-05
om	1,585E-02	1,413E-02	1,041E-02	1,791E-02	1,623E-02	1,448E-02	1,939E-02	1,685E-02	1,397E-02
phi	7,697E-01	7,497E-01	5,978E-01	7,780E-01	7,874E-01	7,799E-01	7,485E-01	7,486E-01	7,052E-01
kap	4,070E-02	2,608E-02	1,212E-02	4,274E-02	2,907E-02	1,727E-02	4,393E-02	2,932E-02	1,671E-02
X	1,999E-02	1,912E-02	1,492E-02	2,202E-02	2,187E-02	2,124E-02	2,318E-02	2,265E-02	2,097E-02
Y	8,049E-03	7,911E-03	6,341E-03	8,932E-03	9,104E-03	9,077E-03	9,455E-03	9,491E-03	9,024E-03
Z	3,491E-02	3,510E-02	2,897E-02	3,247E-02	3,395E-02	3,473E-02	2,881E-02	2,988E-02	2,903E-02
h	1,800E-05	7,860E-06	1,150E-06	1,031E-04	7,680E-05	5,230E-05	2,506E-04	2,010E-04	1,562E-04

Table B.26b Sensitivity of the parameters for the 9 different pixel locations computed by Differential Sensitivity Analysis for longitude.

Parameter	1	2	3	4	5	6	7	8	9
f	3,669E-02	3,621E-03	1,416E-01	2,732E-02	6,335E-04	1,588E-01	1,710E-02	5,530E-05	1,184E-01
Dx	1,053E-03	5,901E-04	4,839E-04	3,868E-04	6,055E-04	8,356E-04	4,140E-05	5,320E-04	1,746E-03
Dy	2,119E-02	3,929E-02	5,924E-02	1,959E-02	3,348E-02	5,237E-02	1,862E-02	3,217E-02	4,028E-02
k1	2,240E-05	2,340E-07	1,520E-05	6,350E-06	2,090E-11	4,590E-06	1,620E-05	6,370E-09	2,740E-05
k2	3,170E-09	5,590E-12	1,330E-09	3,210E-10	2,540E-19	9,640E-11	3,080E-09	2,950E-13	3,480E-09
p1	3,850E-05	3,030E-06	2,340E-05	1,630E-09	1,960E-09	1,010E-06	1,630E-05	4,070E-07	7,150E-05
p2	1,388E-04	8,440E-06	1,527E-04	8,080E-05	1,700E-08	8,930E-05	1,082E-04	1,150E-05	1,690E-04
c	3,480E-05	6,110E-07	5,100E-05	1,910E-05	0,000E+00	5,170E-05	1,750E-05	6,230E-07	6,700E-05
om	8,112E-01	8,219E-01	6,847E-01	8,091E-01	8,175E-01	6,658E-01	8,046E-01	8,055E-01	6,972E-01
phi	1,443E-02	1,482E-02	1,241E-02	1,445E-02	1,443E-02	1,151E-02	1,427E-02	1,377E-02	1,135E-02
kap	4,351E-03	5,433E-03	5,183E-03	1,107E-02	1,263E-02	1,138E-02	2,066E-02	2,232E-02	2,119E-02
X	2,863E-02	2,762E-02	2,169E-02	2,798E-02	2,692E-02	2,066E-02	2,733E-02	2,599E-02	2,113E-02
Y	3,637E-02	3,971E-02	3,532E-02	3,666E-02	3,977E-02	3,452E-02	3,666E-02	3,946E-02	3,640E-02
Z	1,156E-03	7,166E-04	3,035E-04	1,002E-03	6,097E-04	2,405E-04	8,844E-04	5,070E-04	1,938E-04
h	6,978E-04	4,311E-04	1,820E-04	6,116E-04	3,709E-04	1,458E-04	5,460E-04	3,120E-04	1,189E-04

Table B.27 Corrected GCP coordinates for pushbroom scanner

Point ID	X	Y	Z
1	4128670	2644278	4067342
2	4129436	2643762	4066960
3	4132622	2650480	4059746
4	4128749	2654871	4060539
5	4127397	2657033	4060470
6	4124552	2658338	4062458
7	4124730	2658578	4062104
8	4119052	2663688	4064732
9	4114304	2665940	4067911
10	4110716	2667729	4070317
11	4108982	2668701	4071383
12	4108555	2668671	4071816
13	4106689	2666030	4075565
14	4106334	2660041	4079557
15	4106805	2658885	4079955
16	4107747	2657105	4080133
17	4108792	2654063	4081228
18	4111660	2650486	4080471
19	4112786	2649578	4079856
20	4115766	2645660	4079434
21	4120502	2646579	4073871
22	4117770	2650925	4073816
23	4119531	2653001	4070777
24	4120394	2651716	4070707
25	4121963	2649512	4070587
26	4122930	2648046	4070530
27	4124024	2647886	4069616
28	4125270	2647335	4068683
29	4126173	2646659	4068208
30	4119923	2653403	4070148
31	4118332	2654569	4070966
32	4117765	2655222	4071138
33	4116878	2656130	4071404
34	4115568	2657810	4071884
35	4114813	2658209	4072077
36	4114385	2658435	4072416
37	4113532	2659086	4072884
38	4113425	2659599	4072715
39	4126996	2660102	4058806
40	4131570	2664174	4051606
41	4133570	2666322	4048141
42	4135090	2669677	4044541
43	4098010	2659316	4088391
44	4095156	2660130	4090743
45	4092969	2665583	4089402
46	4090196	2668612	4090314
47	4111435	2626949	4096021
48	4112732	2634318	4089602
49	4107873	2641445	4090148
50	4118060	2630971	4086372

Table B.28 Residuals of the GCPs with respect to geodetic and UTM coordinates are shown

Point ID	Latitude	Longitude	X	Y
1	-2,21E-06	6,88E-06	-14,099	33,56
2	-5,92E-07	4,97E-06	-3,771	24,243
3	-2,45E-07	-3,65E-06	-1,563	-17,811
4	2,32E-06	-4,62E-06	14,782	-22,539
5	-1,42E-06	-4,61E-06	-9,043	-22,485
6	-3,48E-06	-3,99E-06	-22,151	-19,481
7	7,83E-07	-4,98E-06	4,99	-24,304
8	-6,73E-06	8,07E-06	-42,84	39,386
9	-6,55E-06	1,61E-06	-41,702	7,831
10	-2,16E-06	4,56E-06	-13,759	22,227
11	1,48E-06	2,61E-06	9,451	12,749
12	-3,63E-06	2,79E-06	-23,139	13,594
13	7,11E-07	-4,66E-07	4,526	-2,273
14	8,58E-06	-7,67E-06	54,657	-37,437
15	2,89E-06	-7,22E-06	18,397	-35,237
16	-1,59E-06	-7,21E-06	-10,133	-35,165
17	-7,49E-06	-5,29E-06	-47,699	-25,796
18	-7,09E-06	6,01E-06	-45,166	29,318
19	-3,35E-06	-7,42E-06	-21,318	-36,196
20	-2,55E-06	6,53E-06	-16,262	31,878
21	-1,37E-06	3,75E-06	-8,755	18,317
22	3,90E-06	4,39E-06	24,86	21,443
23	-2,37E-06	5,03E-06	-15,087	24,565
24	-2,64E-06	2,26E-06	-16,801	11,013
25	-6,21E-06	-4,04E-06	-39,553	-19,694
26	-1,06E-06	5,26E-06	-6,739	25,648
27	2,46E-06	6,49E-06	15,668	31,647
28	-1,09E-06	6,25E-06	-6,92	30,473
29	2,83E-06	-2,43E-06	18,012	-11,871
30	4,26E-06	3,10E-06	27,152	15,102
31	1,62E-06	-2,89E-07	10,321	-1,412
32	-3,66E-08	-9,05E-07	-0,233	-4,414
33	-1,24E-06	-4,19E-06	-7,892	-20,431
34	4,76E-06	-6,11E-06	30,342	-29,83
35	6,14E-06	1,05E-06	39,09	5,136
36	5,67E-06	-1,49E-06	36,105	-7,274
37	3,60E-06	-4,38E-06	22,905	-21,368
38	3,05E-06	-3,55E-06	19,446	-17,34
39	2,61E-06	-5,46E-07	16,628	-2,664
40	3,23E-06	-3,23E-06	20,547	-15,765
41	2,89E-06	1,74E-06	18,397	8,513
42	-3,28E-06	9,35E-07	-20,903	4,56
43	-2,36E-07	-9,50E-07	-1,503	-4,637
44	4,20E-06	-1,91E-06	26,743	-9,331
45	4,01E-06	5,46E-06	25,527	26,62
46	-6,15E-06	6,59E-06	-39,176	32,16
47	-2,11E-06	1,41E-06	6,877	6,877
48	5,71E-06	-8,41E-06	-41,014	-41,014
49	-3,65E-06	6,75E-06	32,922	32,922
50	2,82E-06	-4,92E-06	-24,01	-24,01

Table B.29 Residuals of the ASTER image with 3D affine rectification method

Point ID	Latitude	Longitude	X	Y
1	-1,80E-06	6,23E-06	-11,481	30,421
2	-2,62E-07	4,42E-06	-1,672	21,566
3	6,69E-08	-3,17E-06	0,426	-15,456
4	1,90E-06	-4,09E-06	12,135	-19,948
5	-1,05E-06	-4,08E-06	-6,682	-19,897
6	-3,00E-06	-3,49E-06	-19,13	-17,042
7	4,44E-07	-4,43E-06	2,829	-21,627
8	-6,09E-06	7,37E-06	-38,785	35,951
9	-5,92E-06	1,22E-06	-37,708	5,976
10	-1,75E-06	4,03E-06	-11,16	19,652
11	1,11E-06	2,18E-06	7,069	10,649
12	-3,15E-06	2,35E-06	-20,074	11,451
13	3,75E-07	-1,43E-07	2,389	-0,696
14	7,85E-06	-6,99E-06	50,011	-34,101
15	2,44E-06	-6,56E-06	15,566	-32,011
16	-1,21E-06	-6,55E-06	-7,717	-31,941
17	-6,81E-06	-4,72E-06	-43,403	-23,04
18	-6,44E-06	5,41E-06	-40,994	26,387
19	-2,88E-06	-6,75E-06	-18,343	-32,924
20	-2,13E-06	5,91E-06	-13,538	28,821
21	-1,01E-06	3,27E-06	-6,404	15,939
22	3,41E-06	3,87E-06	21,708	18,905
23	-1,95E-06	4,48E-06	-12,425	21,872
24	-2,21E-06	1,84E-06	-14,053	8,999
25	-5,60E-06	-3,53E-06	-35,663	-17,246
26	-7,05E-07	4,69E-06	-4,491	22,901
27	2,04E-06	5,86E-06	12,976	28,603
28	-7,32E-07	5,63E-06	-4,661	27,486
29	2,39E-06	-2,01E-06	15,203	-9,815
30	3,75E-06	2,64E-06	23,887	12,884
31	1,24E-06	2,52E-08	7,892	0,123
32	2,65E-07	-5,59E-07	1,689	-2,729
33	-8,77E-07	-3,68E-06	-5,587	-17,946
34	4,22E-06	-5,51E-06	26,912	-26,874
35	5,53E-06	7,00E-07	35,227	3,418
36	5,08E-06	-1,12E-06	32,389	-5,448
37	3,12E-06	-3,86E-06	19,85	-18,836
38	2,60E-06	-3,08E-06	16,564	-15,011
39	2,18E-06	-2,19E-07	13,883	-1,067
40	2,76E-06	-2,77E-06	17,611	-13,509
41	2,44E-06	1,35E-06	15,566	6,602
42	-2,82E-06	5,88E-07	-17,944	2,87
43	7,58E-08	-6,03E-07	0,483	-2,94
44	3,69E-06	-1,51E-06	23,493	-7,39
45	3,51E-06	4,89E-06	22,337	23,847
46	-5,54E-06	5,96E-06	-35,306	29,085
47	-1,70E-06	1,04E-06	-10,84	5,072
48	5,13E-06	-7,69E-06	32,661	-37,522
49	-3,17E-06	6,11E-06	-20,195	29,827
50	2,38E-06	-4,37E-06	15,13	-21,344

Table B.30 Analysis results of ASTER image rectification by DRM with simulated elevation

Point ID	Latitude	Longitude	X	Y
1	1,40E-06	7,46E-06	8,918	36,403
2	4,48E-06	3,84E-06	28,512	18,738
3	-4,87E-06	-1,34E-06	-30,998	-6,539
4	-1,20E-06	-3,18E-06	-7,644	-15,517
5	2,90E-06	-3,16E-06	18,473	-15,42
6	-1,00E-06	-1,98E-06	-6,37	-9,662
7	-4,11E-06	-3,86E-06	-26,193	-18,836
8	-7,18E-06	9,74E-06	-45,737	47,528
9	-6,84E-06	-2,56E-06	-43,571	-12,492
10	1,50E-06	3,06E-06	9,555	14,932
11	-2,78E-06	-6,40E-07	-17,709	-3,123
12	-1,30E-06	-3,00E-07	-8,281	-1,464
13	-4,25E-06	4,71E-06	-27,073	23,003
14	1,07E-05	-8,98E-06	68,159	-43,82
15	-1,20E-07	-8,12E-06	-0,764	-39,623
16	2,58E-06	-8,10E-06	16,435	-39,526
17	-8,62E-06	-4,44E-06	-54,909	-21,666
18	-7,88E-06	5,82E-06	-50,196	28,4
19	-7,60E-07	-8,50E-06	-4,841	-41,477
20	7,40E-07	6,82E-06	4,714	33,28
21	2,98E-06	1,54E-06	18,983	7,515
22	1,82E-06	2,74E-06	11,593	13,37
23	1,10E-06	3,96E-06	7,007	19,324
24	5,80E-07	-1,32E-06	3,695	-6,441
25	-6,20E-06	-2,06E-06	-39,494	-10,052
26	3,59E-06	4,38E-06	22,868	21,373
27	-9,20E-07	6,72E-06	-5,86	32,792
28	3,54E-06	6,26E-06	22,524	30,547
29	-2,20E-07	9,80E-07	-1,401	4,782
30	2,50E-06	2,80E-07	15,925	1,366
31	-2,52E-06	-4,95E-06	-16,052	-24,153
32	-4,47E-06	3,88E-06	-28,474	18,943
33	3,25E-06	-2,36E-06	20,677	-11,516
34	3,44E-06	-6,02E-06	21,913	-29,376
35	6,06E-06	-3,60E-06	38,602	-17,567
36	5,16E-06	2,76E-06	32,869	13,468
37	1,24E-06	-2,72E-06	7,899	-13,273
38	2,00E-07	-1,16E-06	1,274	-5,66
39	-6,40E-07	4,56E-06	-4,077	22,261
40	5,20E-07	-5,40E-07	3,312	-2,635
41	-1,20E-07	-2,30E-06	-0,764	-11,223
42	-6,40E-07	-3,82E-06	-4,077	-18,66
43	-4,85E-06	3,79E-06	-30,884	18,514
44	2,38E-06	1,98E-06	15,161	9,662
45	2,02E-06	4,78E-06	12,867	23,325
46	-6,08E-06	6,92E-06	-38,73	33,768
47	1,60E-06	-2,92E-06	10,192	-14,249
48	5,26E-06	-1,04E-05	33,506	-50,651
49	-1,34E-06	7,22E-06	-8,536	35,231
50	-2,40E-07	-3,74E-06	-1,529	-18,25

Table B.31 Analysis results rectified by 3D Affine transformation.

Point ID	Latitude	Longitude	X	Y
1	1,95E-06	1,24E-05	12,422	60,74
2	6,95E-06	6,57E-06	44,262	32,035
3	-7,58E-06	-2,50E-06	-48,301	-12,211
4	-1,63E-06	-5,49E-06	-10,351	-26,802
5	4,39E-06	-5,46E-06	27,948	-26,643
6	-1,95E-06	-3,54E-06	-12,422	-17,286
7	-6,36E-06	-6,60E-06	-40,494	-32,194
8	-1,20E-05	1,62E-05	-76,392	78,819
9	-1,14E-05	-3,84E-06	-72,873	-18,714
10	2,11E-06	5,30E-06	13,457	25,85
11	-4,19E-06	-7,15E-07	-26,706	-3,489
12	-2,44E-06	-1,63E-07	-15,527	-0,793
13	-6,58E-06	7,34E-06	-41,923	35,794
14	1,77E-05	-1,49E-05	112,829	-72,793
15	1,30E-07	-1,35E-05	0,828	-65,974
16	3,87E-06	-1,35E-05	24,636	-65,815
17	-1,43E-05	-7,54E-06	-91,298	-36,793
18	-1,31E-05	9,78E-06	-83,638	47,736
19	-1,56E-06	-1,41E-05	-9,937	-68,987
20	8,78E-07	1,14E-05	5,59	55,665
21	4,52E-06	2,83E-06	28,776	13,797
22	3,28E-06	4,78E-06	20,91	23,313
23	1,46E-06	6,76E-06	9,316	32,987
24	6,18E-07	-1,82E-06	3,933	-8,881
25	-1,04E-05	-3,67E-06	-66,248	-17,921
26	5,51E-06	7,44E-06	35,091	36,317
27	-1,17E-06	1,12E-05	-7,453	54,872
28	5,42E-06	1,05E-05	34,532	51,225
29	-3,25E-08	1,27E-06	-0,207	6,185
30	4,39E-06	7,80E-07	27,948	3,806
31	-3,77E-06	-7,72E-06	-24,015	-37,662
32	-6,94E-06	5,98E-06	-44,2	29,196
33	4,95E-06	-4,16E-06	31,53	-20,3
34	5,92E-06	-1,01E-05	37,679	-49,322
35	1,02E-05	-5,53E-06	64,799	-26,96
36	8,71E-06	4,16E-06	55,483	20,3
37	2,34E-06	-4,75E-06	14,906	-23,154
38	6,50E-07	-2,21E-06	4,141	-10,784
39	-7,15E-07	7,09E-06	-4,555	34,589
40	1,17E-06	-1,20E-06	7,453	-5,868
41	1,30E-07	-3,41E-06	0,828	-16,652
42	-1,37E-06	-5,89E-06	-8,695	-28,737
43	-7,55E-06	5,84E-06	-48,117	28,499
44	4,19E-06	2,89E-06	26,706	14,115
45	3,61E-06	8,09E-06	22,98	39,489
46	-1,02E-05	1,16E-05	-65,006	56,458
47	2,28E-06	-4,42E-06	14,492	-21,568
48	8,87E-06	-1,72E-05	56,518	-83,894
49	-2,50E-06	1,21E-05	-15,941	58,837
50	-6,50E-08	-6,40E-06	-0,414	-31,242

Table B.32 Outlier test results

Point ID	Weight	Qii	ri	Comment	Dli	Doli	Doxi
1	1	0,1526	0,8474	Well	7,98E-07	1,54E-05	1,7528
2	1	0,19	0,81	Well	-1,35E-06	1,58E-05	2,0003
3	1	0,2309	0,7691	Well	-1,88E-06	1,62E-05	2,2627
4	1	0,2591	0,7409	Well	-5,54E-06	1,65E-05	2,4425
5	1	0,2895	0,7105	Well	-4,23E-06	1,68E-05	2,6365
6	1	0,3396	0,6604	Well	-5,96E-06	1,75E-05	2,9619
7	1	0,3416	0,6584	Well	-9,38E-07	1,75E-05	2,9746
8	1	0,4553	0,5447	Well	7,46E-06	1,92E-05	3,7761
9	1	0,1944	0,8056	Well	6,38E-07	1,58E-05	2,0289
10	1	0,2623	0,7377	Well	6,56E-06	1,65E-05	2,4629
11	1	0,1862	0,8138	Well	-2,71E-07	1,57E-05	1,9757
12	1	0,2308	0,7692	Well	-4,01E-06	1,62E-05	2,2624
13	1	0,1922	0,8078	Well	1,03E-06	1,58E-05	2,0145
14	1	0,1957	0,8043	Well	-4,81E-06	1,58E-05	2,0375
15	1	0,1874	0,8126	Well	-9,73E-07	1,57E-05	1,9836
16	1	0,2047	0,7953	Well	3,45E-06	1,59E-05	2,0953
17	1	0,341	0,659	Well	-7,08E-06	1,75E-05	2,9708
18	1	0,4483	0,5517	Well	-8,37E-06	1,91E-05	3,7228
19	1	0,1975	0,8025	Well	2,69E-06	1,58E-05	2,0491
20	1	0,2792	0,7208	Well	2,55E-06	1,67E-05	2,5703
21	1	0,1875	0,8125	Well	-1,48E-07	1,57E-05	1,9838
22	1	0,2171	0,7829	Well	2,93E-06	1,60E-05	2,1746
23	1	0,2391	0,7609	Well	6,23E-06	1,63E-05	2,3151
24	1	0,2682	0,7318	Well	-1,67E-06	1,66E-05	2,5003
25	1	0,2461	0,7539	Well	5,72E-06	1,63E-05	2,3594
26	1	0,2773	0,7227	Well	-6,61E-06	1,67E-05	2,5585
27	1	0,2578	0,7422	Well	2,08E-06	1,65E-05	2,434
28	1	0,2573	0,7427	Well	-6,48E-06	1,65E-05	2,4309
29	1	0,2467	0,7533	Well	-6,10E-06	1,64E-05	2,3638
30	1	0,2079	0,7921	Well	5,98E-07	1,59E-05	2,1159
31	1	0,2136	0,7864	Well	-1,90E-06	1,60E-05	2,1523
32	1	0,1771	0,8229	Well	2,10E-06	1,56E-05	1,9162
33	1	0,1558	0,8442	Well	-6,76E-07	1,54E-05	1,7743
34	1	0,1451	0,8549	Well	5,47E-06	1,54E-05	1,7016
35	1	0,2387	0,7613	Well	-2,45E-06	1,63E-05	2,3125
36	1	0,1733	0,8267	Well	3,91E-06	1,56E-05	1,8907
37	1	0,1982	0,8018	Well	3,01E-06	1,59E-05	2,0532
38	1	0,1659	0,8341	Well	-2,37E-06	1,55E-05	1,8416
39	1	0,2042	0,7958	Well	2,42E-06	1,59E-05	2,092
40	1	0,1585	0,8415	Well	2,34E-06	1,55E-05	1,7927
41	1	0,418	0,582	Well	3,58E-06	1,86E-05	3,5004
42	1	0,2428	0,7572	Well	-6,60E-06	1,63E-05	2,3386
43	1	0,2123	0,7877	Well	-5,30E-06	1,60E-05	2,144
44	1	0,1601	0,8399	Well	-1,23E-06	1,55E-05	1,803
45	1	0,2847	0,7153	Well	4,16E-07	1,68E-05	2,6056
46	1	0,2098	0,7902	Well	2,71E-06	1,60E-05	2,1278
47	1	0,266	0,734	Well	2,81E-06	1,66E-05	2,4861
48	1	0,2709	0,7291	Well	6,67E-06	1,66E-05	2,5175
49	1	0,2472	0,7528	Well	-4,46E-09	1,64E-05	2,3669
50	1	0,2743	0,7257	Well	6,47E-06	1,67E-05	2,5394

Table B.33 Conformity test results of the measurements

Point ID	Qvivi	vi	Decision
1	0,8474	0,0734	concordant
2	0,8100	0,1218	concordant
3	0,7691	0,1651	concordant
4	0,7409	0,4767	concordant
5	0,7105	0,3566	concordant
6	0,6604	0,4842	concordant
7	0,6584	0,0761	concordant
8	0,5447	0,5502	concordant
9	0,8056	0,0573	concordant
10	0,7377	0,5635	concordant
11	0,8138	0,0245	concordant
12	0,7692	0,3512	concordant
13	0,8078	0,0922	concordant
14	0,8043	0,4314	concordant
15	0,8126	0,0877	concordant
16	0,7953	0,3080	concordant
17	0,6590	0,5745	concordant
18	0,5517	0,6219	concordant
19	0,8025	0,2413	concordant
20	0,7208	0,2163	concordant
21	0,8125	0,0134	concordant
22	0,7829	0,2588	concordant
23	0,7609	0,5430	concordant
24	0,7318	0,1428	concordant
25	0,7539	0,4968	concordant
26	0,7227	0,5616	concordant
27	0,7422	0,1792	concordant
28	0,7427	0,5587	concordant
29	0,7533	0,5292	concordant
30	0,7921	0,0532	concordant
31	0,7864	0,1683	concordant
32	0,8229	0,1902	concordant
33	0,8442	0,0622	concordant
34	0,8549	0,5054	concordant
35	0,7613	0,2136	concordant
36	0,8267	0,3554	concordant
37	0,8018	0,2694	concordant
38	0,8341	0,2167	concordant
39	0,7958	0,2161	concordant
40	0,8415	0,2144	concordant
41	0,5820	0,2732	concordant
42	0,7572	0,5745	concordant
43	0,7877	0,4704	concordant
44	0,8399	0,1123	concordant
45	0,7153	0,0352	concordant
46	0,7902	0,2410	concordant
47	0,7340	0,2403	concordant
48	0,7291	0,5691	concordant
49	0,7528	0,0004	concordant
50	0,7257	0,5514	concordant

Table B.34 Sensitivity of the Parameter Estimation Procedure to Initial Values

	1	2	3	4	5	6	7	8	9	10	11	12
X	4,48E+06	4,52E+06	4,50E+06	4,51E+06	4,51E+06	4,51E+06	4,49E+06	4,50E+06	4,50E+06	4,50E+06	4,50E+06	4,50E+06
Y	3,03E+06	3,01E+06	3,02E+06	3,04E+06	3,04E+06	3,04E+06	3,04E+06	3,03E+06	3,02E+06	3,02E+06	3,02E+06	3,02E+06
Z	4,55E+06	4,52E+06	4,53E+06	4,56E+06	4,55E+06	4,56E+06	4,54E+06	4,52E+06	4,53E+06	4,53E+06	4,54E+06	4,54E+06
roll	9,64E+00	7,13E+00	8,22E+00	8,47E+00	8,40E+00	8,49E+00	9,57E+00	8,46E+00	8,31E+00	8,30E+00	8,31E+00	8,28E+00
pitch	-3,10E+00	-1,11E+00	-2,00E+00	-2,24E+00	-2,17E+00	-2,21E+00	-2,31E+00	-1,19E+00	-2,09E+00	-2,08E+00	-2,11E+00	-2,09E+00
yaw	1,46E+01	-2,60E+00	4,89E+00	6,70E+00	6,20E+00	6,51E+00	6,60E+00	6,41E+00	6,47E+00	6,49E+00	6,49E+00	6,52E+00
f	1,73E+02	1,75E+02	1,75E+02	1,83E+02	1,81E+02	1,84E+02	1,77E+02	1,76E+02	1,76E+02	1,77E+02	1,76E+02	1,77E+02
Dx	1,63E+00	-8,68E-02	2,71E-01	6,19E-01	5,26E-01	7,25E-01	7,82E-01	6,38E-01	4,01E-01	4,59E-01	1,18E+00	2,40E-01
Dy	-2,55E-01	-1,76E-01	-1,75E-01	-6,98E-01	-7,69E-01	-7,50E-01	-6,15E-01	-1,19E+00	-8,55E-01	-1,76E-01	-1,11E-01	4,23E-01
k1	7,26E-04	-7,75E-05	1,40E-04	6,06E-04	4,80E-04	5,24E-04	3,89E-04	2,57E-04	2,41E-04	1,54E-04	4,84E-04	2,22E-04
k2	-8,61E-06	1,27E-06	-1,80E-06	-6,53E-06	-5,32E-06	-6,07E-06	-4,88E-06	-3,11E-06	-2,99E-06	-2,28E-06	-7,91E-06	-3,09E-06
p1	-1,33E-04	-7,51E-04	-5,82E-04	-5,80E-04	-5,84E-04	-5,12E-04	-3,87E-04	-6,01E-04	-5,62E-04	-5,13E-04	-4,45E-04	-6,25E-04
p2	7,50E-04	5,68E-04	5,66E-04	4,51E-04	4,80E-04	5,37E-04	4,95E-04	4,84E-04	5,58E-04	6,18E-04	7,99E-04	5,70E-04

Table B.35 Sensitivity indexes of the DRM pushbroom parameters for latitude

Analysis	Right Asc.	Roll	Pitch	Yaw	Theta	Roll Rate	Roll Rate Change	Pitch Rate	Pitch Rate Change	Yaw Rate	Yaw Rate Change
1	2,53E-07	1,42E-02	7,54E-01	4,57E-02	2,13E-02	1,63E-01	1,94E-10	1,03E-17	7,20E-05	3,81E-14	2,02E-21
2	2,31E-07	1,39E-02	6,87E-01	4,19E-02	2,12E-02	1,48E-01	1,77E-04	9,34E-06	6,46E-05	3,42E-08	1,81E-09
3	1,70E-07	1,00E-02	5,07E-01	3,12E-02	1,45E-02	1,10E-01	5,22E-04	1,11E-04	4,70E-05	9,94E-08	2,10E-08
4	1,03E-07	5,37E-03	3,04E-01	1,89E-02	6,67E-03	6,62E-02	7,09E-04	3,37E-04	2,79E-05	1,33E-07	6,32E-08
5	5,60E-08	2,31E-03	1,64E-01	1,04E-02	2,06E-03	3,61E-02	6,88E-04	5,83E-04	1,50E-05	1,27E-07	1,08E-07
6	2,54E-07	1,40E-02	7,55E-01	4,40E-02	2,14E-02	1,63E-01	1,95E-10	1,03E-17	6,93E-05	3,67E-14	1,93E-21
7	2,32E-07	1,38E-02	6,90E-01	4,04E-02	2,14E-02	1,49E-01	1,78E-04	9,40E-06	6,24E-05	3,30E-08	1,75E-09
8	1,72E-07	1,00E-02	5,11E-01	3,02E-02	1,47E-02	1,11E-01	5,28E-04	1,12E-04	4,55E-05	9,64E-08	2,04E-08
9	1,04E-07	5,36E-03	3,07E-01	1,83E-02	6,76E-03	6,70E-02	7,17E-04	3,41E-04	2,71E-05	1,29E-07	6,13E-08
10	5,67E-08	2,30E-03	1,66E-01	1,01E-02	2,09E-03	3,66E-02	6,96E-04	5,89E-04	1,46E-05	1,23E-07	1,04E-07
11	2,55E-07	1,39E-02	7,57E-01	4,22E-02	2,15E-02	1,64E-01	1,95E-10	1,03E-17	6,67E-05	3,53E-14	1,87E-21
12	2,33E-07	1,37E-02	6,92E-01	3,89E-02	2,15E-02	1,50E-01	1,79E-04	9,45E-06	6,01E-05	3,18E-08	1,68E-09
13	1,74E-07	9,96E-03	5,15E-01	2,92E-02	1,48E-02	1,12E-01	5,33E-04	1,13E-04	4,41E-05	9,33E-08	1,97E-08
14	1,05E-07	5,34E-03	3,10E-01	1,77E-02	6,85E-03	6,78E-02	7,26E-04	3,46E-04	2,63E-05	1,25E-07	5,95E-08
15	5,74E-08	2,29E-03	1,68E-01	9,75E-03	2,12E-03	3,70E-02	7,04E-04	5,96E-04	1,41E-05	1,20E-07	1,01E-07

Table B.35 Sensitivity indexes of the DRM pushbroom parameters for latitude (continued)

Analysis	Theta Rate	Theta Rate Change	Phi Anomaly	Phi A. Rate	Phi A. Rate Change	Lambda Anomaly	L. A. Rate	L. A. Rate Change	Focal Length	Principle Coord	Lens Par	Elevation
1	1,87E-10	1,59E-16	9,97E-09	8,44E-15	6,05E-08	5,11E-16	1,25E-08	1,06E-16	4,35E-12	1,94E-08	2,22E-08	1,76E-03
2	1,84E-04	1,55E-04	9,09E-03	7,69E-03	5,54E-02	4,69E-04	1,25E-02	1,06E-04	4,32E-12	1,93E-08	2,21E-08	1,62E-03
3	5,31E-04	1,80E-03	2,68E-02	9,08E-02	1,65E-01	5,58E-03	3,41E-02	1,16E-03	2,95E-12	1,32E-08	1,51E-08	1,21E-03
4	6,39E-04	4,87E-03	3,62E-02	2,76E-01	2,25E-01	1,71E-02	3,53E-02	2,69E-03	1,36E-12	6,05E-09	6,93E-09	7,33E-04
5	4,89E-04	6,63E-03	3,47E-02	4,70E-01	2,20E-01	2,97E-02	1,94E-02	2,62E-03	4,20E-13	1,87E-09	2,14E-09	4,02E-04
6	1,86E-10	1,58E-16	9,99E-09	8,46E-15	5,81E-08	4,92E-16	1,26E-08	1,06E-16	0,00E+00	1,94E-08	0,00E+00	1,76E-03
7	1,82E-04	1,54E-04	9,12E-03	7,72E-03	5,34E-02	4,52E-04	1,26E-02	1,06E-04	1,33E-18	1,94E-08	0,00E+00	1,62E-03
8	5,29E-04	1,79E-03	2,70E-02	9,15E-02	1,60E-01	5,40E-03	3,45E-02	1,17E-03	0,00E+00	1,33E-08	0,00E+00	1,21E-03
9	6,38E-04	4,86E-03	3,66E-02	2,79E-01	2,18E-01	1,66E-02	3,58E-02	2,73E-03	0,00E+00	6,13E-09	0,00E+00	7,39E-04
10	4,87E-04	6,60E-03	3,51E-02	4,75E-01	2,13E-01	2,88E-02	1,97E-02	2,66E-03	0,00E+00	1,90E-09	0,00E+00	4,06E-04
11	1,84E-10	1,56E-16	1,00E-08	8,47E-15	5,59E-08	4,72E-16	1,27E-08	1,07E-16	4,39E-12	1,95E-08	2,24E-08	1,76E-03
12	1,81E-04	1,53E-04	9,15E-03	7,75E-03	5,14E-02	4,35E-04	1,26E-02	1,07E-04	4,39E-12	1,95E-08	2,24E-08	1,62E-03
13	5,27E-04	1,78E-03	2,73E-02	9,23E-02	1,54E-01	5,22E-03	3,48E-02	1,18E-03	3,03E-12	1,34E-08	1,54E-08	1,22E-03
14	6,36E-04	4,84E-03	3,69E-02	2,81E-01	2,11E-01	1,61E-02	3,63E-02	2,76E-03	1,40E-12	6,22E-09	7,14E-09	7,45E-04
15	4,85E-04	6,57E-03	3,55E-02	4,80E-01	2,06E-01	2,79E-02	2,00E-02	2,70E-03	4,34E-13	1,93E-09	2,21E-09	4,09E-04

Table B.36 Sensitivity indexes of the DRM pushbroom parameters for longitude

Analysis	Right Asc.	Roll	Pitch	Yaw	Theta	Roll Rate	Roll Rate Change	Pitch Rate	Pitch Rate Change	Yaw Rate	Yaw Rate Change
1	1,04E-03	2,72E-01	4,77E-04	1,11E-02	6,37E-01	6,01E-05	7,15E-14	3,78E-21	7,71E-02	4,08E-11	2,16E-18
2	7,51E-04	1,95E-01	4,17E-04	7,96E-03	4,55E-01	4,26E-05	5,07E-08	2,68E-09	5,55E-02	2,94E-05	1,55E-06
3	3,96E-04	1,02E-01	1,73E-04	4,19E-03	2,38E-01	2,21E-05	1,05E-07	2,23E-08	2,92E-02	6,19E-05	1,31E-05
4	2,11E-04	5,39E-02	3,76E-05	2,23E-03	1,26E-01	1,16E-05	1,24E-07	5,91E-08	1,56E-02	7,42E-05	3,53E-05
5	1,20E-04	3,05E-02	1,12E-07	1,27E-03	7,15E-02	6,50E-06	1,24E-07	1,05E-07	8,88E-03	7,52E-05	6,36E-05
6	1,05E-03	2,72E-01	5,19E-04	1,11E-02	6,37E-01	5,78E-05	6,88E-14	3,64E-21	7,76E-02	4,10E-11	2,17E-18
7	7,56E-04	1,95E-01	4,50E-04	7,97E-03	4,55E-01	4,10E-05	4,88E-08	2,58E-09	5,58E-02	2,95E-05	1,56E-06
8	3,99E-04	1,02E-01	1,88E-04	4,20E-03	2,38E-01	2,13E-05	1,01E-07	2,14E-08	2,94E-02	6,22E-05	1,32E-05
9	2,12E-04	5,38E-02	4,29E-05	2,24E-03	1,26E-01	1,12E-05	1,19E-07	5,69E-08	1,57E-02	7,46E-05	3,55E-05
10	1,21E-04	3,05E-02	4,07E-07	1,27E-03	7,15E-02	6,26E-06	1,19E-07	1,01E-07	8,94E-03	7,56E-05	6,40E-05
11	1,06E-03	2,72E-01	5,62E-04	1,11E-02	6,36E-01	5,56E-05	6,62E-14	3,50E-21	7,80E-02	4,13E-11	2,18E-18
12	7,61E-04	1,94E-01	4,84E-04	7,99E-03	4,55E-01	3,94E-05	4,69E-08	2,48E-09	5,61E-02	2,97E-05	1,57E-06
13	4,01E-04	1,02E-01	2,04E-04	4,21E-03	2,38E-01	2,05E-05	9,74E-08	2,06E-08	2,96E-02	6,26E-05	1,33E-05
14	2,14E-04	5,38E-02	4,84E-05	2,24E-03	1,26E-01	1,07E-05	1,15E-07	5,47E-08	1,58E-02	7,50E-05	3,57E-05
15	1,22E-04	3,05E-02	8,86E-07	1,28E-03	7,15E-02	6,02E-06	1,15E-07	9,71E-08	8,99E-03	7,61E-05	6,44E-05

Table B.36 Sensitivity indexes of the DRM pushbroom parameters for longitude (continued)

Analysis	Theta Rate	Theta Rate Change	Phi Anomaly	Phi A. Rate	Phi A. Rate Change	Lambda Anomaly	L. A. Rate	L. A. Rate Change	Focal Length	Principle Coord	Lens Par	Elevation
1	3,60E-09	3,05E-15	6,31E-12	5,35E-18	1,46E-08	1,24E-16	3,74E-07	3,17E-15	1,30E-10	5,78E-07	6,62E-07	9,07E-04
2	2,57E-03	2,18E-03	5,52E-06	4,67E-06	1,05E-02	8,91E-05	2,67E-01	2,26E-03	9,28E-11	4,13E-07	4,73E-07	6,54E-04
3	5,39E-03	1,82E-02	9,14E-06	3,10E-05	2,22E-02	7,51E-04	5,60E-01	1,90E-02	4,86E-11	2,16E-07	2,48E-07	3,45E-04
4	6,41E-03	4,88E-02	4,48E-06	3,41E-05	2,66E-02	2,02E-03	6,67E-01	5,08E-02	2,57E-11	1,14E-07	1,31E-07	1,84E-04
5	6,45E-03	8,74E-02	2,38E-08	3,25E-07	2,68E-02	3,63E-03	6,72E-01	9,10E-02	1,46E-11	6,48E-08	7,43E-08	1,05E-04
6	3,60E-09	3,05E-15	6,86E-12	5,80E-18	1,47E-08	1,24E-16	3,74E-07	3,17E-15	0,00E+00	5,77E-07	0,00E+00	8,74E-04
7	2,57E-03	2,18E-03	5,95E-06	5,04E-06	1,06E-02	8,93E-05	2,67E-01	2,26E-03	0,00E+00	4,13E-07	0,00E+00	6,30E-04
8	5,38E-03	1,82E-02	9,96E-06	3,37E-05	2,22E-02	7,53E-04	5,60E-01	1,90E-02	0,00E+00	2,16E-07	0,00E+00	3,33E-04
9	6,41E-03	4,88E-02	5,10E-06	3,89E-05	2,66E-02	2,03E-03	6,67E-01	5,08E-02	0,00E+00	1,14E-07	0,00E+00	1,77E-04
10	6,45E-03	8,74E-02	8,61E-08	1,17E-06	2,69E-02	3,64E-03	6,72E-01	9,10E-02	0,00E+00	6,48E-08	0,00E+00	1,01E-04
11	3,60E-09	3,05E-15	7,43E-12	6,30E-18	1,47E-08	1,24E-16	3,74E-07	3,17E-15	1,30E-10	5,77E-07	6,63E-07	8,41E-04
12	2,57E-03	2,18E-03	6,41E-06	5,42E-06	1,06E-02	8,94E-05	2,67E-01	2,26E-03	9,28E-11	4,12E-07	4,74E-07	6,07E-04
13	5,38E-03	1,82E-02	1,08E-05	3,66E-05	2,23E-02	7,55E-04	5,60E-01	1,90E-02	4,86E-11	2,16E-07	2,48E-07	3,20E-04
14	6,41E-03	4,88E-02	5,76E-06	4,39E-05	2,67E-02	2,04E-03	6,67E-01	5,08E-02	2,57E-11	1,14E-07	1,31E-07	1,71E-04
15	6,45E-03	8,73E-02	1,88E-07	2,55E-06	2,70E-02	3,66E-03	6,72E-01	9,10E-02	1,46E-11	6,48E-08	7,45E-08	9,76E-05

APPENDIX C

PARTIAL DERIVATIVES

In this section partial derivatives of DRM for CCD frame cameras with respect to inner and outer camera parameters are given.

C.1 Partial Derivative with respect to f

$$\frac{\partial x'}{\partial f}=0 \qquad \frac{\partial y'}{\partial f}=0 \qquad \frac{\partial z'}{\partial f}=-1 \qquad \frac{\partial r}{\partial f}=0$$

$$\frac{\partial x}{\partial f}=0 \qquad \frac{\partial y}{\partial f}=0 \qquad \frac{\partial z}{\partial f}=\frac{\partial z'}{\partial f}$$

$$\frac{\partial S_{Camerax}}{\partial f}=-\frac{\left(x^2+y^2+z^2\right)^{\frac{-1}{2}}*\left(z*\frac{\partial z}{\partial f}\right)*x}{\left(x^2+y^2+z^2\right)}$$

$$\frac{\partial S_{Cameray}}{\partial f}=-\frac{\left(x^2+y^2+z^2\right)^{\frac{-1}{2}}*\left(z\frac{\partial z}{\partial f}\right)y}{\left(x^2+y^2+z^2\right)}$$

$$\frac{\partial S_{Cameraz}}{\partial f}=\frac{\sqrt{x^2+y^2+z^2}\,\frac{\partial z}{\partial f}-\left(x^2+y^2+z^2\right)^{\frac{-1}{2}}\left(z\frac{\partial z}{\partial f}\right)z}{\left(x^2+y^2+z^2\right)}$$

$$\frac{\partial S_{Bx}}{\partial f}=\frac{\partial S_{Cx}}{\partial f} \qquad \frac{\partial S_{By}}{\partial f}=-\frac{\partial S_{Cy}}{\partial f} \qquad \frac{\partial S_{Bz}}{\partial f}=-\frac{\partial S_{Cz}}{\partial f}$$

$$\frac{\partial S_{Orbitalx}}{\partial f}=\left(\cos\kappa\cos\phi-\sin\kappa\sin\omega\sin\phi\right)\frac{\partial S_{Camerax}}{\partial f}-\sin\kappa\cos\omega\frac{\partial S_{Cameray}}{\partial f}$$
$$+\left(\cos\kappa\sin\phi+\sin\kappa\sin\omega\cos\phi\right)\frac{\partial S_{Cameraz}}{\partial f}$$

$$\frac{\partial S_{Orbitaly}}{\partial f}=\left(\sin\kappa\cos\phi+\cos\kappa\sin\omega\sin\phi\right)\frac{\partial S_{Camerax}}{\partial f}+\cos\kappa\cos\omega\frac{\partial S_{Cameray}}{\partial f}$$
$$+\left(\sin\kappa\sin\phi-\cos\kappa\sin\omega\cos\phi\right)\frac{\partial S_{Cameraz}}{\partial f}$$

$$\frac{\partial S_{Orbitalz}}{\partial f}=-\cos\omega\sin\phi\frac{\partial S_{Camerax}}{\partial f}+\sin\omega\frac{\partial S_{Cameray}}{\partial f}+\cos\omega\cos\phi\frac{\partial S_{Cameraz}}{\partial f}$$

$$\frac{\partial S_{Earthfixedx}}{\partial f} = r_{11}\frac{\partial S_{Orbitalx}}{\partial f} + r_{12}\frac{\partial S_{Orbitaly}}{\partial f} + r_{13}\frac{\partial S_{Orbitalz}}{\partial f}$$

$$\frac{\partial S_{Earthfixedy}}{\partial f} = r_{21}\frac{\partial S_{Orbitalx}}{\partial f} + r_{22}\frac{\partial S_{Orbitaly}}{\partial f} + r_{23}\frac{\partial S_{Orbitalz}}{\partial f}$$

$$\frac{\partial S_{Earthfixedz}}{\partial f} = r_{31}\frac{\partial S_{Orbitalx}}{\partial f} + r_{32}\frac{\partial S_{Orbitaly}}{\partial f} + r_{33}\frac{\partial S_{Orbitalz}}{\partial f}$$

$$\frac{\partial X_0}{\partial f} = \frac{\partial s}{\partial f} S_{Earthfixed\ x} + s\frac{\partial S_{Earthfixed\ x}}{\partial f}$$

$$\frac{\partial Y_0}{\partial f} = \frac{\partial s}{\partial f} S_{Earthfixed\ y} + s\frac{\partial S_{Earthfixed\ y}}{\partial f}$$

$$\frac{\partial Z_0}{\partial f} = \frac{\partial s}{\partial f} S_{Earthfixed\ z} + s\frac{\partial S_{Earthfixed\ z}}{\partial f}$$

$$\frac{\partial s}{\partial f} = \frac{\left(-\frac{\partial \beta}{\partial f} - \frac{1}{2}\left(\beta^2 - 4\alpha\gamma\right)^{\frac{-1}{2}}\left(2\beta\frac{\partial \beta}{\partial f} - 4\alpha\frac{\partial \gamma}{\partial f} - 4\gamma\frac{\partial \alpha}{\partial f}\right)\right) * 2\alpha - 2\frac{\partial \alpha}{\partial f}\left(-\beta - \sqrt{\beta^2 - 4\alpha\gamma}\right)}{4 * \alpha^2}$$

$$\frac{\partial \alpha}{\partial f} = \frac{2 * S_{Earthfixed\ x} * \frac{\partial S_{Earthfixed\ x}}{\partial f} + 2 * S_{Earthfixed\ y} * \frac{\partial S_{earthfixed\ y}}{\partial f}}{a^2} + \frac{2 * S_{Earthfixed\ z} * \frac{\partial S_{earthfixed\ z}}{\partial f}}{b^2}$$

$$\frac{\partial \beta}{\partial f} = \frac{X_{cam} * \frac{\partial S_{Earthfixed\ x}}{\partial f} + Y_{cam} * \frac{\partial S_{earthfixed\ y}}{\partial f}}{a^2} + \frac{Z_{cam} * \frac{\partial S_{earthfixed\ z}}{\partial f}}{b^2}$$

$$\frac{\partial \gamma}{\partial f} = 0$$

$$\frac{\partial \lambda}{\partial f} = \frac{1}{1 + \left(\frac{Y_0}{X_0}\right)^2} * \left(\frac{X_0 * \frac{\partial Y_0}{\partial f} - Y_0 * \frac{\partial X_0}{\partial f}}{X_0^2}\right)$$

$$\frac{\partial \phi}{\partial f} = \frac{\left[\frac{\partial Z_o}{\partial f}\sqrt{X_o^2 + Y_o^2} - \left(X_o\frac{\partial X_o}{\partial f} + Y_o\frac{\partial Y_o}{\partial f}\right) * \left(X_o^2 + Y_o^2\right)^{\frac{-1}{2}} * Z_o\right]}{\left(1 + \frac{Z_o^2}{\left(X_o^2 + Y_o^2\right)\left(1 - \frac{e^2 N}{N + h}\right)}\right) * \left(1 - \frac{e^2 N}{N + h}\right) * \left(X_o^2 + Y_o^2\right)}$$

C.2 Partial Derivative with respect to Δx

$$\frac{\partial x'}{\partial \Delta x} = -1 \qquad \frac{\partial y'}{\partial \Delta x} = 0 \qquad \frac{\partial z'}{\partial \Delta x} = 0$$

$$\frac{\partial r}{\partial \Delta x} = \frac{1}{2}\left(x'^2 + y'^2\right)^{\frac{-1}{2}}\left(2x'\frac{\partial x'}{\partial \Delta x}\right)$$

$$\frac{\partial x}{\partial \Delta x} = \frac{\partial x'}{\partial \Delta x}\left[1 - k_1 r^2 - k_2 r^4 - 2p_1 x' - 2p_2 y' - \frac{p_1 r^2}{x'}\right]$$
$$+ x'\left[-2k_1 r\frac{\partial r}{\partial \Delta x} - 4k_2 r^3\frac{\partial r}{\partial \Delta x} - 2p_1\frac{\partial x'}{\partial \Delta x} - \frac{p_1\left(2r\frac{\partial r}{\partial \Delta x}x' - r^2\frac{\partial x'}{\partial \Delta x}\right)}{x'^2}\right]$$

$$\frac{\partial y}{\partial \Delta x} = y'\left(-2k_1 r\frac{\partial r}{\partial \Delta x} - 4k_2 r^3\frac{\partial r}{\partial \Delta x} - 2p_1\frac{\partial x'}{\partial \Delta x} - \frac{2rp_2}{y'}\frac{\partial r}{\partial \Delta x}\right)$$

$$\frac{\partial z}{\partial \Delta x} = 0$$

$$\frac{\partial S_{Camerax}}{\partial \Delta x} = \frac{\left(x^2+y^2+z^2\right)^{\frac{1}{2}}\frac{\partial x}{\partial \Delta x} - x\left(x^2+y^2+z^2\right)^{\frac{-1}{2}}\left(x\frac{\partial x}{\partial \Delta x} + y\frac{\partial y}{\partial \Delta x}\right)}{\left(x^2+y^2+z^2\right)}$$

$$\frac{\partial S_{Cameray}}{\partial \Delta x} = \frac{\left(x^2+y^2+z^2\right)^{\frac{1}{2}}\frac{\partial y}{\partial \Delta x} - y\left(x^2+y^2+z^2\right)^{\frac{-1}{2}}\left(x\frac{\partial x}{\partial \Delta x} + y\frac{\partial y}{\partial \Delta x}\right)}{\left(x^2+y^2+z^2\right)}$$

$$\frac{\partial S_{Cameraz}}{\partial \Delta x} = -\frac{z\left(x^2+y^2+z^2\right)^{\frac{-1}{2}}\left(x\frac{\partial x}{\partial \Delta x} + y\frac{\partial y}{\partial \Delta x}\right)}{\left(x^2+y^2+z^2\right)}$$

$$\frac{\partial S_{Bx}}{\partial \Delta x} = \frac{\partial S_{Cx}}{\partial \Delta x} \qquad \frac{\partial S_{By}}{\partial \Delta x} = -\frac{\partial S_{Cy}}{\partial \Delta x} \qquad \frac{\partial S_{Bz}}{\partial \Delta x} = -\frac{\partial S_{Cz}}{\partial \Delta x}$$

$$\frac{\partial S_{Orbitalx}}{\partial \Delta x} = \left(\cos\kappa\cos\phi - \sin\kappa\sin\omega\sin\phi\right)\frac{\partial S_{Camerax}}{\partial \Delta x} - \sin\kappa\cos\omega\frac{\partial S_{Cameray}}{\partial \Delta x}$$
$$+ \left(\cos\kappa\sin\phi + \sin\kappa\sin\omega\cos\phi\right)\frac{\partial S_{Cameraz}}{\partial \Delta x}$$

$$\frac{\partial S_{Orbitaly}}{\partial \Delta x} = \left(\sin\kappa\cos\phi + \cos\kappa\sin\omega\sin\phi\right)\frac{\partial S_{Camerax}}{\partial \Delta x} + \cos\kappa\cos\omega\frac{\partial S_{Cameray}}{\partial \Delta x}$$
$$+ \left(\sin\kappa\sin\phi - \cos\kappa\sin\omega\cos\phi\right)\frac{\partial S_{Cameraz}}{\partial \Delta x}$$

$$\frac{\partial S_{Orbitalz}}{\partial \Delta x} = -\cos\omega\sin\phi\frac{\partial S_{Camerax}}{\partial \Delta x} + \sin\omega\frac{\partial S_{Cameray}}{\partial \Delta x} + \cos\omega\cos\phi\frac{\partial S_{Cameraz}}{\partial \Delta x}$$

$$\frac{\partial S_{Earthfixed\ x}}{\partial \Delta x} = r_{11}\frac{\partial S_{Orbitalx}}{\partial \Delta x} + r_{12}\frac{\partial S_{Orbitaly}}{\partial \Delta x} + r_{13}\frac{\partial S_{Orbitalz}}{\partial \Delta x}$$

$$\frac{\partial S_{Earthfixed\ y}}{\partial \Delta x} = r_{21}\frac{\partial S_{Orbitalx}}{\partial \Delta x} + r_{22}\frac{\partial S_{Orbitaly}}{\partial \Delta x} + r_{23}\frac{\partial S_{Orbitalz}}{\partial \Delta x}$$

$$\frac{\partial S_{Earthfixed\ z}}{\partial \Delta x} = r_{31}\frac{\partial S_{Orbitalx}}{\partial \Delta x} + r_{32}\frac{\partial S_{Orbitaly}}{\partial \Delta x} + r_{33}\frac{\partial S_{Orbitalz}}{\partial \Delta x}$$

$$\frac{\partial X_0}{\partial \Delta x} = \frac{\partial s}{\partial \Delta x} S_{Earthfixed\ x} + s\frac{\partial S_{Earthfixed\ x}}{\partial \Delta x}$$

$$\frac{\partial Y_0}{\partial \Delta x} = \frac{\partial s}{\partial \Delta x} S_{Earthfixed\ y} + s\frac{\partial S_{Earthfixed\ y}}{\partial \Delta x}$$

$$\frac{\partial Y_0}{\partial \Delta x} = \frac{\partial s}{\partial \Delta x} S_{Earthfixed\ z} + s\frac{\partial S_{Earthfixed\ z}}{\partial \Delta x}$$

$$\frac{\partial s}{\partial \Delta x} = \frac{\left(-\frac{\partial \beta}{\partial \Delta x} - \frac{1}{2}\left(\beta^2 - 4\alpha\gamma\right)^{\frac{-1}{2}}\left(2\beta\frac{\partial \beta}{\partial \Delta x} - 4\alpha\frac{\partial \gamma}{\partial \Delta x} - 4\gamma\frac{\partial \alpha}{\partial \Delta x}\right)\right) * 2\alpha - 2\frac{\partial \alpha}{\partial \Delta x}\left(-\beta - \sqrt{-\beta^2 - 4\alpha\gamma}\right)}{4 * \alpha^2}$$

$$\frac{\partial \alpha}{\partial \Delta x} = \frac{2 * S_{E\ x} * \frac{\partial S_{Ex}}{\partial \Delta x} + 2 * S_{E\ y} * \frac{\partial S_{Ey}}{\partial \Delta x}}{a^2} + \frac{2 * S_{Ez} * \frac{\partial S_{Ez}}{\partial \Delta x}}{b^2}$$

$$\frac{\partial \beta}{\partial \Delta x} = \frac{X_{cam} * \frac{\partial S_{Earthfixed\ x}}{\partial \Delta x} + Y_{cam} * \frac{\partial S_{earthfixed\ y}}{\partial \Delta x}}{a^2} + \frac{Z_{cam} * \frac{\partial S_{earthfixed\ z}}{\partial \Delta x}}{b^2}$$

$$\frac{\partial \gamma}{\partial \Delta x} = 0$$

$$\frac{\partial \lambda}{\partial \Delta x} = \frac{1}{1 + \left(\frac{Y_0}{X_0}\right)^2} * \left(\frac{X_0 * \frac{\partial Y_0}{\partial \Delta x} - Y_0 * \frac{\partial X_0}{\partial \Delta x}}{X_0^2}\right)$$

$$\frac{\partial \phi}{\partial \Delta x} = \frac{\left[\frac{\partial Z_o}{\partial \Delta x}\sqrt{X_o^2 + Y_o^2} - \left(X_o\frac{\partial X_o}{\partial \Delta x} + Y_o\frac{\partial Y_o}{\partial \Delta x}\right) * \left(X_o^2 + Y_o^2\right)^{\frac{-1}{2}} * Z_o\right]}{\left(1 + \frac{Z_o^2}{\left(X_o^2 + Y_o^2\right)\left(1 - \frac{e^2 N}{N + h}\right)}\right) * \left(1 - \frac{e^2 N}{N + h}\right) * \left(X_o^2 + Y_o^2\right)}$$

C.3 Partial Derivative with respect to Δy

$$\frac{\partial x'}{\partial \Delta y} = 0 \qquad \frac{\partial y'}{\partial \Delta y} = -1 \qquad \frac{\partial z'}{\partial \Delta y} = 0$$

$$\frac{\partial r}{\partial \Delta y} = \frac{1}{2}\left(x'^2 + y'^2\right)^{\frac{-1}{2}}\left(2y'\frac{\partial y'}{\partial \Delta y}\right)$$

$$\frac{\partial x}{\partial \Delta y} = x'\left(-2k_1 r\frac{\partial r}{\partial \Delta y} - 4k_2 r^3\frac{\partial r}{\partial \Delta y} - 2p_2\frac{\partial y'}{\partial \Delta y}\right)$$

$$\frac{\partial y}{\partial \Delta y} = \frac{\partial y'}{\partial \Delta y}\left[1 - k_1 r^2 - k_2 r^4 - 2p_1 x' - 2p_2 y' - \frac{p_1 r^2}{y'}\right] + y'\left[-2k_1 r\frac{\partial r}{\partial \Delta y} - 4k_2 r^3\frac{\partial r}{\partial \Delta y} - 2p_2\frac{\partial y'}{\partial \Delta y} - \frac{p_2\left(2r\frac{\partial r}{\partial \Delta y}y' - r^2\frac{\partial y'}{\partial \Delta y}\right)}{y'^2}\right]$$

$$\frac{\partial z}{\partial \Delta y} = 0$$

$$\frac{\partial S_{Camerax}}{\partial \Delta y} = \frac{\left(x^2 + y^2 + z^2\right)^{\frac{1}{2}}\frac{\partial x}{\partial \Delta y} - x\left(x^2 + y^2 + z^2\right)^{\frac{-1}{2}}\left(x\frac{\partial x}{\partial \Delta y} + y\frac{\partial y}{\partial \Delta y}\right)}{\left(x^2 + y^2 + z^2\right)}$$

$$\frac{\partial S_{Cameray}}{\partial \Delta y} = \frac{\left(x^2 + y^2 + z^2\right)^{\frac{1}{2}}\frac{\partial y}{\partial \Delta y} - y\left(x^2 + y^2 + z^2\right)^{\frac{-1}{2}}\left(x\frac{\partial x}{\partial \Delta y} + y\frac{\partial y}{\partial \Delta y}\right)}{\left(x^2 + y^2 + z^2\right)}$$

$$\frac{\partial S_{Cameraz}}{\partial \Delta y} = -\frac{z\left(x^2 + y^2 + z^2\right)^{\frac{-1}{2}}\left(x\frac{\partial x}{\partial \Delta y} + y\frac{\partial y}{\partial \Delta y}\right)}{\left(x^2 + y^2 + z^2\right)}$$

$$\frac{\partial S_{Bx}}{\partial \Delta y} = \frac{\partial S_{Cx}}{\partial \Delta y} \qquad \frac{\partial S_{By}}{\partial \Delta y} = -\frac{\partial S_{Cy}}{\partial \Delta y} \qquad \frac{\partial S_{Bz}}{\partial \Delta z} = -\frac{\partial S_{Cz}}{\partial \Delta z}$$

$$\frac{\partial S_{Ox}}{\partial \Delta y} = \left(\cos\kappa\cos\phi - \sin\kappa\sin\omega\sin\phi\right)\frac{\partial S_{Bx}}{\partial \Delta y} - \sin\kappa\cos\omega\frac{\partial S_{By}}{\partial \Delta y} + \left(\cos\kappa\sin\phi + \sin\kappa\sin\omega\cos\phi\right)\frac{\partial S_{Bz}}{\partial \Delta y}$$

$$\frac{\partial S_{Oy}}{\partial \Delta y} = \left(\sin\kappa\cos\phi + \cos\kappa\sin\omega\sin\phi\right)\frac{\partial S_{Bx}}{\partial \Delta y} + \cos\kappa\cos\omega\frac{\partial S_{By}}{\partial \Delta y} + \left(\sin\kappa\sin\phi - \cos\kappa\sin\omega\cos\phi\right)\frac{\partial S_{Bz}}{\partial \Delta y}$$

$$\frac{\partial S_{Oz}}{\partial \Delta y} = -\cos\omega\sin\phi\frac{\partial S_{Bx}}{\partial \Delta y} + \sin\omega\frac{\partial S_{By}}{\partial \Delta y} + \cos\omega\cos\phi\frac{\partial S_{Bz}}{\partial \Delta y}$$

$$\frac{\partial S_{Ex}}{\partial \Delta y} = r_{11}\frac{\partial S_{Ox}}{\partial \Delta y} + r_{12}\frac{\partial S_{Oy}}{\partial \Delta y} + r_{13}\frac{\partial S_{Oz}}{\partial \Delta y}$$

$$\frac{\partial S_{Ey}}{\partial \Delta y} = r_{21}\frac{\partial S_{Ox}}{\partial \Delta y} + r_{22}\frac{\partial S_{Oy}}{\partial \Delta y} + r_{23}\frac{\partial S_{Oz}}{\partial \Delta y}$$

$$\frac{\partial S_{Ez}}{\partial \Delta y} = r_{31}\frac{\partial S_{Ox}}{\partial \Delta y} + r_{32}\frac{\partial S_{Oy}}{\partial \Delta y} + r_{33}\frac{\partial S_{Oz}}{\partial \Delta y}$$

$$\frac{\partial X_0}{\partial \Delta y} = \frac{\partial s}{\partial \Delta y} S_{Ex} + s\frac{\partial S_{Ex}}{\partial \Delta y}$$

$$\frac{\partial Y_0}{\partial \Delta y} = \frac{\partial s}{\partial \Delta y} S_{Ey} + s\frac{\partial S_{Ey}}{\partial \Delta y}$$

$$\frac{\partial Y_0}{\partial \Delta y} = \frac{\partial s}{\partial \Delta y} S_{Ez} + s\frac{\partial S_{Ez}}{\partial \Delta y}$$

$$\frac{\partial s}{\partial \Delta y} = \frac{\left(-\frac{\partial \beta}{\partial \Delta y} - \frac{1}{2}\left(\beta^2 - 4\alpha\gamma\right)^{\frac{-1}{2}}\left(2\beta\frac{\partial \beta}{\partial \Delta y} - 4\alpha\frac{\partial \gamma}{\partial \Delta y} - 4\gamma\frac{\partial \alpha}{\partial \Delta y}\right)\right) * 2\alpha - 2\frac{\partial \alpha}{\partial \Delta y}\left(-\beta - \sqrt{-\beta^2 - 4\alpha\gamma}\right)}{4 * \alpha^2}$$

$$\frac{\partial \alpha}{\partial \Delta y} = \frac{2 * S_{Ex} * \frac{\partial S_{Ex}}{\partial \Delta y} + 2 * S_{Ey} * \frac{\partial S_{Ey}}{\partial \Delta y}}{a^2} + \frac{2 * S_{Ez} * \frac{\partial S_{Ez}}{\partial \Delta y}}{b^2}$$

$$\frac{\partial \beta}{\partial \Delta y} = \frac{X_{cam} * \frac{\partial S_{Ex}}{\partial \Delta y} + Y_{cam} * \frac{\partial S_{Ey}}{\partial \Delta y}}{a^2} + \frac{Z_{cam} * \frac{\partial S_{Ez}}{\partial \Delta y}}{b^2}$$

$$\frac{\partial \gamma}{\partial \Delta y} = 0$$

$$\frac{\partial \lambda}{\partial \Delta y} = \frac{1}{1 + \left(\frac{Y_0}{X_0}\right)^2} * \left(\frac{X_0 * \frac{\partial Y_0}{\partial \Delta y} - Y_0 * \frac{\partial X_0}{\partial \Delta y}}{X_0^2}\right)$$

$$\frac{\partial \phi}{\partial \Delta y} = \frac{\left[\frac{\partial Z_o}{\partial \Delta y}\sqrt{X_o^2 + Y_o^2} - \left(X_o\frac{\partial X_o}{\partial \Delta y} + Y_o\frac{\partial Y_o}{\partial \Delta y}\right) * \left(X_o^2 + Y_o^2\right)^{\frac{-1}{2}} * Z_o\right]}{\left(1 + \frac{Z_o^2}{\left(X_o^2 + Y_o^2\right)\left(1 - \frac{e^2 N}{N + h}\right)}\right) * \left(1 - \frac{e^2 N}{N + h}\right) * \left(X_o^2 + Y_o^2\right)}$$

C.4 Partial Derivative with respect to k_1

$$\frac{\partial x'}{\partial k_1} = 0 \qquad \frac{\partial y'}{\partial k_1} = 0 \qquad \frac{\partial z'}{\partial k_1} = 0$$

$$\frac{\partial r}{\partial k_1} = 0 \qquad \frac{\partial x}{\partial k_1} = -r^2 x' \qquad \frac{\partial y}{\partial k_1} = -r^2 y' \qquad \frac{\partial z}{\partial k_1} = 0$$

$$\frac{\partial S_{Camerax}}{\partial k_1} = \frac{\left(x^2+y^2+z^2\right)^{\frac{1}{2}} \frac{\partial x}{\partial k_1} - x\left(x^2+y^2+z^2\right)^{\frac{-1}{2}}\left(x\frac{\partial x}{\partial k_1} + y\frac{\partial y}{\partial k_1}\right)}{\left(x^2+y^2+z^2\right)}$$

$$\frac{\partial S_{Cameray}}{\partial k_1} = \frac{\left(x^2+y^2+z^2\right)^{\frac{1}{2}} \frac{\partial y}{\partial k_1} - y\left(x^2+y^2+z^2\right)^{\frac{-1}{2}}\left(x\frac{\partial x}{\partial k_1} + y\frac{\partial y}{\partial k_1}\right)}{\left(x^2+y^2+z^2\right)}$$

$$\frac{\partial S_{Cameraz}}{\partial k_1} = -\frac{z\left(x^2+y^2+z^2\right)^{\frac{-1}{2}}\left(x\frac{\partial x}{\partial k_1} + y\frac{\partial y}{\partial k_1}\right)}{\left(x^2+y^2+z^2\right)}$$

$$\frac{\partial S_{Bx}}{\partial k_1} = \frac{\partial S_{Cx}}{\partial k_1} \qquad \frac{\partial S_{By}}{\partial k_1} = -\frac{\partial S_{Cy}}{\partial k_1} \qquad \frac{\partial S_{Bz}}{\partial k_1} = -\frac{\partial S_{Cz}}{\partial k_1}$$

$$\frac{\partial S_{Orbitalx}}{\partial k_1} = \left(\cos\kappa\cos\phi - \sin\kappa\sin\omega\sin\phi\right)\frac{\partial S_{Bx}}{\partial k_1} - \sin\kappa\cos\omega\frac{\partial S_{By}}{\partial k_1}$$
$$+\left(\cos\kappa\sin\phi + \sin\kappa\sin\omega\cos\phi\right)\frac{\partial S_{Bz}}{\partial k_1}$$

$$\frac{\partial S_{Orbitaly}}{\partial k_1} = \left(\sin\kappa\cos\phi + \cos\kappa\sin\omega\sin\phi\right)\frac{\partial S_{Bx}}{\partial k_1} + \cos\kappa\cos\omega\frac{\partial S_{By}}{\partial k_1}$$
$$+\left(\sin\kappa\sin\phi - \cos\kappa\sin\omega\cos\phi\right)\frac{\partial S_{Bz}}{\partial k_1}$$

$$\frac{\partial S_{Orbitalz}}{\partial k_1} = -\cos\omega\sin\phi\frac{\partial S_{Bx}}{\partial k_1} + \sin\omega\frac{\partial S_{By}}{\partial k_1} + \cos\omega\cos\phi\frac{\partial S_{Bz}}{\partial k_1}$$

$$\frac{\partial S_{Ex}}{\partial k_1} = r_{11}\frac{\partial S_{Ox}}{\partial k_1} + r_{12}\frac{\partial S_{Oy}}{\partial k_1} + r_{13}\frac{\partial S_{Oz}}{\partial k_1}$$

$$\frac{\partial S_{Ey}}{\partial k_1} = r_{21}\frac{\partial S_{Ox}}{\partial k_1} + r_{22}\frac{\partial S_{Oy}}{\partial k_1} + r_{23}\frac{\partial S_{Oz}}{\partial k_1}$$

$$\frac{\partial S_{Ez}}{\partial k_1} = r_{31}\frac{\partial S_{Ox}}{\partial k_1} + r_{32}\frac{\partial S_{Oy}}{\partial k_1} + r_{33}\frac{\partial S_{Oz}}{\partial k_1}$$

$$\frac{\partial X_0}{\partial k_1} = \frac{\partial s}{\partial k_1}S_{Ex} + s\frac{\partial S_{Ex}}{\partial k_1}$$

$$\frac{\partial Y_0}{\partial k_1} = \frac{\partial s}{\partial k_1}S_{Ey} + s\frac{\partial S_{Ey}}{\partial k_1}$$

$$\frac{\partial Y_0}{\partial k_1} = \frac{\partial s}{\partial k_1} S_{Ez} + s \frac{\partial S_{Ez}}{\partial k_1}$$

$$\frac{\partial s}{\partial k_1} = \frac{\left(-\frac{\partial \beta}{\partial k_1} - \frac{1}{2}\left(\beta^2 - 4\alpha\gamma\right)^{\frac{-1}{2}}\left(2\beta \frac{\partial \beta}{\partial k_1} - 4\alpha \frac{\partial \gamma}{\partial k_1} - 4\gamma \frac{\partial \alpha}{\partial k_1}\right)\right) * 2\alpha - 2\frac{\partial \alpha}{\partial k_1}\left(-\beta - \sqrt{-\beta^2 - 4\alpha\gamma}\right)}{4 * \alpha^2}$$

$$\frac{\partial \alpha}{\partial k_1} = \frac{2 * S_{Ex} * \frac{\partial S_{Ex}}{\partial k_1} + 2 * S_{Ey} * \frac{\partial S_{Ey}}{\partial k_1}}{a^2} + \frac{2 * S_{Ez} * \frac{\partial S_{Ez}}{\partial k_1}}{b^2}$$

$$\frac{\partial \beta}{\partial k_1} = \frac{X_{cam} * \frac{\partial S_{Ex}}{\partial k_1} + Y_{cam} * \frac{\partial S_{Ey}}{\partial k_1}}{a^2} + \frac{Z_{cam} * \frac{\partial S_{Ez}}{\partial k_1}}{b^2}$$

$$\frac{\partial \gamma}{\partial k_1} = 0$$

$$\frac{\partial \lambda}{\partial k_1} = \frac{1}{1 + \left(\frac{Y_0}{X_0}\right)^2} * \left(\frac{X_0 * \frac{\partial Y_0}{\partial k_1} - Y_0 * \frac{\partial X_0}{\partial k_1}}{X_0^2}\right)$$

$$\frac{\partial \phi}{\partial k_1} = \frac{\left[\frac{\partial Z_o}{\partial k_1}\sqrt{X_o^2 + Y_o^2} - \left(X_o \frac{\partial X_o}{\partial k_1} + Y_o \frac{\partial Y_o}{\partial k_1}\right) * \left(X_o^2 + Y_o^2\right)^{\frac{-1}{2}} * Z_o\right]}{\left(1 + \frac{Z_o^2}{\left(X_o^2 + Y_o^2\right)\left(1 - \frac{e^2 N}{N + h}\right)}\right) * \left(1 - \frac{e^2 N}{N + h}\right) * \left(X_o^2 + Y_o^2\right)}$$

C.5 Partial Derivative with respect to k_2

$$\frac{\partial x'}{\partial k_2} = 0 \qquad \frac{\partial y'}{\partial k_2} = 0 \qquad \frac{\partial z'}{\partial k_2} = 0$$

$$\frac{\partial r}{\partial k_2} = 0 \qquad \frac{\partial x}{\partial k_2} = -r^4 x' \qquad \frac{\partial y}{\partial k_2} = -r^4 y' \qquad \frac{\partial z}{\partial k_2} = 0$$

$$\frac{\partial S_{Cx}}{\partial k_2} = \frac{\left(x^2 + y^2 + z^2\right)^{\frac{1}{2}} \frac{\partial x}{\partial k_2} - x\left(x^2 + y^2 + z^2\right)^{\frac{-1}{2}}\left(x \frac{\partial x}{\partial k_2} + y \frac{\partial y}{\partial k_2}\right)}{\left(x^2 + y^2 + z^2\right)}$$

$$\frac{\partial S_{Cy}}{\partial k_2}=\frac{\left(x^2+y^2+z^2\right)^{\frac{1}{2}}\frac{\partial y}{\partial k_2}-y\left(x^2+y^2+z^2\right)^{\frac{-1}{2}}\left(x\frac{\partial x}{\partial k_2}+y\frac{\partial y}{\partial k_2}\right)}{\left(x^2+y^2+z^2\right)}$$

$$\frac{\partial S_{Cz}}{\partial k_2}=-\frac{z\left(x^2+y^2+z^2\right)^{\frac{-1}{2}}\left(x\frac{\partial x}{\partial k_2}+y\frac{\partial y}{\partial k_2}\right)}{\left(x^2+y^2+z^2\right)}$$

$$\frac{\partial S_{Bx}}{\partial k_2}=\frac{\partial S_{Cx}}{\partial k_2} \qquad \frac{\partial S_{By}}{\partial k_2}=-\frac{\partial S_{Cy}}{\partial k_2} \qquad \frac{\partial S_{Bz}}{\partial k_2}=-\frac{\partial S_{Cz}}{\partial k_2}$$

$$\frac{\partial S_{Orbitalx}}{\partial k_2}=(\cos\kappa\cos\phi-\sin\kappa\sin\omega\sin\phi)\frac{\partial S_{Bx}}{\partial k_2}-\sin\kappa\cos\omega\frac{\partial S_{By}}{\partial k_2}$$

$$+(\cos\kappa\sin\phi+\sin\kappa\sin\omega\cos\phi)\frac{\partial S_{Bz}}{\partial k_2}$$

$$\frac{\partial S_{Orbitaly}}{\partial k_2}=(\sin\kappa\cos\phi+\cos\kappa\sin\omega\sin\phi)\frac{\partial S_{Bx}}{\partial k_2}+\cos\kappa\cos\omega\frac{\partial S_{By}}{\partial k_2}$$

$$+(\sin\kappa\sin\phi-\cos\kappa\sin\omega\cos\phi)\frac{\partial S_{Bz}}{\partial k_2}$$

$$\frac{\partial S_{Orbitalz}}{\partial k_2}=-\cos\omega\sin\phi\frac{\partial S_{Bx}}{\partial k_2}+\sin\omega\frac{\partial S_{By}}{\partial k_2}+\cos\omega\cos\phi\frac{\partial S_{Bz}}{\partial k_2}$$

$$\frac{\partial S_{Ex}}{\partial k_2}=r_{11}\frac{\partial S_{Ox}}{\partial k_2}+r_{12}\frac{\partial S_{Oy}}{\partial k_2}+r_{13}\frac{\partial S_{Oz}}{\partial k_2}$$

$$\frac{\partial S_{Ey}}{\partial k_2}=r_{21}\frac{\partial S_{Ox}}{\partial k_2}+r_{22}\frac{\partial S_{Oy}}{\partial k_2}+r_{23}\frac{\partial S_{Oz}}{\partial k_2}$$

$$\frac{\partial S_{Ez}}{\partial k_2}=r_{31}\frac{\partial S_{Ox}}{\partial k_2}+r_{32}\frac{\partial S_{Oy}}{\partial k_2}+r_{33}\frac{\partial S_{Oz}}{\partial k_2}$$

$$\frac{\partial X_0}{\partial k_2}=\frac{\partial s}{\partial k_2}S_{Ex}+s\frac{\partial S_{Ex}}{\partial k_2}$$

$$\frac{\partial Y_0}{\partial k_2}=\frac{\partial s}{\partial k_2}S_{Ey}+s\frac{\partial S_{Ey}}{\partial k_2}$$

$$\frac{\partial Y_0}{\partial k_2}=\frac{\partial s}{\partial k_2}S_{Ez}+s\frac{\partial S_{Ez}}{\partial k_2}$$

$$\frac{\partial s}{\partial k_2}=\frac{\left(-\frac{\partial\beta}{\partial k_2}-\frac{1}{2}\left(\beta^2-4\alpha\gamma\right)^{\frac{-1}{2}}\left(2\beta\frac{\partial\beta}{\partial k_2}-4\alpha\frac{\partial\gamma}{\partial k_2}-4\gamma\frac{\partial\alpha}{\partial k_2}\right)\right)*2\alpha-2\frac{\partial\alpha}{\partial k_2}\left(-\beta-\sqrt{-\beta^2-4\alpha\gamma}\right)}{4*\alpha^2}$$

$$\frac{\partial\alpha}{\partial k_2}=\frac{2*S_{Ex}*\frac{\partial S_{Ex}}{\partial k_2}+2*S_{Ey}*\frac{\partial S_{Ey}}{\partial k_2}}{a^2}+\frac{2*S_{Ez}*\frac{\partial S_{Ez}}{\partial k_2}}{b^2}$$

$$\frac{\partial \beta}{\partial k_2} = \frac{X_{cam} * \frac{\partial S_{Ex}}{\partial k_2} + Y_{cam} * \frac{\partial S_{Ey}}{\partial k_2}}{a^2} + \frac{Z_{cam} * \frac{\partial S_{Ez}}{\partial k_2}}{b^2}$$

$$\frac{\partial \gamma}{\partial k_2} = 0$$

$$\frac{\partial \lambda}{\partial k_2} = \frac{1}{1 + \left(\frac{Y_0}{X_0}\right)^2} * \left(\frac{X_0 * \frac{\partial Y_0}{\partial k_2} - Y_0 * \frac{\partial X_0}{\partial k_2}}{X_0^2} \right)$$

$$\frac{\partial \phi}{\partial k_2} = \frac{\left[\frac{\partial Z_o}{\partial k_2} \sqrt{X_o^2 + Y_o^2} - \left(X_o \frac{\partial X_o}{\partial k_2} + Y_o \frac{\partial Y_o}{\partial k_2} \right) * \left(X_o^2 + Y_o^2 \right)^{\frac{-1}{2}} * Z_o \right]}{\left(1 + \frac{Z_o^2}{\left(X_o^2 + Y_o^2 \right)\left(1 - \frac{e^2 N}{N+h} \right)} \right) * \left(1 - \frac{e^2 N}{N+h} \right) * \left(X_o^2 + Y_o^2 \right)}$$

C.6 Partial Derivative with respect to p_1

$$\frac{\partial x'}{\partial p_1} = 0 \qquad \frac{\partial y'}{\partial p_1} = 0 \qquad \frac{\partial z'}{\partial p_1} = 0 \qquad \frac{\partial r}{\partial p_1} = 0$$

$$\frac{\partial x}{\partial p_1} = x'\left(-2x' - \frac{r^2}{x'} \right) \qquad \frac{\partial y}{\partial p_1} = -2x'y' \qquad \frac{\partial z}{\partial p_1} = 0$$

$$\frac{\partial S_{Cx}}{\partial p_1} = \frac{\left(x^2 + y^2 + z^2 \right)^{\frac{1}{2}} \frac{\partial x}{\partial p_1} - x\left(x^2 + y^2 + z^2 \right)^{\frac{-1}{2}} \left(x \frac{\partial x}{\partial p_1} + y \frac{\partial y}{\partial p_1} \right)}{\left(x^2 + y^2 + z^2 \right)}$$

$$\frac{\partial S_{Cy}}{\partial p_1} = \frac{\left(x^2 + y^2 + z^2 \right)^{\frac{1}{2}} \frac{\partial y}{\partial p_1} - y\left(x^2 + y^2 + z^2 \right)^{\frac{-1}{2}} \left(x \frac{\partial x}{\partial p_1} + y \frac{\partial y}{\partial p_1} \right)}{\left(x^2 + y^2 + z^2 \right)}$$

$$\frac{\partial S_{Cz}}{\partial p_1} = -\frac{z\left(x^2 + y^2 + z^2 \right)^{\frac{-1}{2}} \left(x \frac{\partial x}{\partial p_1} + y \frac{\partial y}{\partial p_1} \right)}{\left(x^2 + y^2 + z^2 \right)}$$

$$\frac{\partial S_{Bx}}{\partial p_1} = \frac{\partial S_{Cx}}{\partial p_1} \qquad \frac{\partial S_{By}}{\partial p_1} = -\frac{\partial S_{Cy}}{\partial p_1} \qquad \frac{\partial S_{Bz}}{\partial p_1} = -\frac{\partial S_{Cz}}{\partial p_1}$$

$$\frac{\partial S_{Ox}}{\partial p_1} = (\cos\kappa\cos\phi - \sin\kappa\sin\omega\sin\phi)\frac{\partial S_{Bx}}{\partial p_1} - \sin\kappa\cos\omega\frac{\partial S_{By}}{\partial p_1}$$
$$+ (\cos\kappa\sin\phi + \sin\kappa\sin\omega\cos\phi)\frac{\partial S_{Bz}}{\partial p_1}$$

$$\frac{\partial S_{Oy}}{\partial p_1} = (\sin\kappa\cos\phi + \cos\kappa\sin\omega\sin\phi)\frac{\partial S_{Bx}}{\partial p_1} + \cos\kappa\cos\omega\frac{\partial S_{By}}{\partial p_1}$$
$$+ (\sin\kappa\sin\phi - \cos\kappa\sin\omega\cos\phi)\frac{\partial S_{Bz}}{\partial p_1}$$

$$\frac{\partial S_{Oz}}{\partial p_1} = -\cos\omega\sin\phi\frac{\partial S_{Bx}}{\partial p_1} + \sin\omega\frac{\partial S_{By}}{\partial p_1} + \cos\omega\cos\phi\frac{\partial S_{Bz}}{\partial p_1}$$

$$\frac{\partial S_{Ex}}{\partial p_1} = r_{11}\frac{\partial S_{Ox}}{\partial p_1} + r_{12}\frac{\partial S_{Oy}}{\partial p_1} + r_{13}\frac{\partial S_{Oz}}{\partial p_1}$$
$$\frac{\partial S_{Ey}}{\partial p_1} = r_{21}\frac{\partial S_{Ox}}{\partial p_1} + r_{22}\frac{\partial S_{Oy}}{\partial p_1} + r_{23}\frac{\partial S_{Oz}}{\partial p_1}$$
$$\frac{\partial S_{Ez}}{\partial p_1} = r_{31}\frac{\partial S_{Ox}}{\partial p_1} + r_{32}\frac{\partial S_{Oy}}{\partial p_1} + r_{33}\frac{\partial S_{Oz}}{\partial p_1}$$

$$\frac{\partial X_0}{\partial p_1} = \frac{\partial s}{\partial p_1}S_{Ex} + s\frac{\partial S_{Ex}}{\partial p_1}$$
$$\frac{\partial Y_0}{\partial p_1} = \frac{\partial s}{\partial p_1}S_{Ey} + s\frac{\partial S_{Ey}}{\partial p_1}$$
$$\frac{\partial Z_0}{\partial p_1} = \frac{\partial s}{\partial p_1}S_{Ez} + s\frac{\partial S_{Ez}}{\partial p_1}$$

$$\frac{\partial s}{\partial p_1} = \frac{\left(-\frac{\partial \beta}{\partial p_1} - \frac{1}{2}(\beta^2 - 4\alpha\gamma)^{\frac{-1}{2}}\left(2\beta\frac{\partial\beta}{\partial p_1} - 4\alpha\frac{\partial\gamma}{\partial p_1} - 4\gamma\frac{\partial\alpha}{\partial p_1}\right)\right) * 2\alpha - 2\frac{\partial\alpha}{\partial p_1}\left(-\beta - \sqrt{-\beta^2 - 4\alpha\gamma}\right)}{4 * \alpha^2}$$

$$\frac{\partial \alpha}{\partial p_1} = \frac{2 * S_{Ex} * \frac{\partial S_{Ex}}{\partial p_1} + 2 * S_{Ey} * \frac{\partial S_{Ey}}{\partial p_1}}{a^2} + \frac{2 * S_{Ez} * \frac{\partial S_{Ez}}{\partial p_1}}{b^2}$$

$$\frac{\partial \beta}{\partial p_1} = \frac{X_{cam} * \frac{\partial S_{Ex}}{\partial p_1} + Y_{cam} * \frac{\partial S_{Ey}}{\partial p_1}}{a^2} + \frac{Z_{cam} * \frac{\partial S_{Ez}}{\partial p_1}}{b^2}$$

$$\frac{\partial \gamma}{\partial p_1} = 0$$

$$\frac{\partial\lambda}{\partial p_1}=\frac{1}{1+\left(\frac{Y_0}{X_0}\right)^2}*\left(\frac{X_0*\frac{\partial Y_0}{\partial p_1}-Y_0*\frac{\partial X_0}{\partial p_1}}{X_0^2}\right)$$

$$\frac{\partial\phi}{\partial p_1}=\frac{\left[\frac{\partial Z_o}{\partial p_1}\sqrt{X_o^2+Y_o^2}-\left(X_o\frac{\partial X_o}{\partial p_1}+Y_o\frac{\partial Y_o}{\partial p_1}\right)*\left(X_o^2+Y_o^2\right)^{\frac{-1}{2}}*Z_o\right]}{\left(1+\frac{Z_o^2}{\left(X_o^2+Y_o^2\right)\left(1-\frac{e^2N}{N+h}\right)}\right)*\left(1-\frac{e^2N}{N+h}\right)*\left(X_o^2+Y_o^2\right)}$$

C.7 Partial Derivative with respect to p_2

$$\frac{\partial x'}{\partial p_2}=0 \qquad \frac{\partial y'}{\partial p_2}=0 \qquad \frac{\partial z'}{\partial p_2}=0 \qquad \frac{\partial r}{\partial p_2}=0$$

$$\frac{\partial x}{\partial p_2}=-2x'y' \qquad \frac{\partial y}{\partial p_2}=y'\left(-2y'-\frac{r^2}{y'}\right) \qquad \frac{\partial z}{\partial p_2}=0$$

$$\frac{\partial S_{Cx}}{\partial p_2}=\frac{\left(x^2+y^2+z^2\right)^{\frac{1}{2}}\frac{\partial x}{\partial p_2}-x\left(x^2+y^2+z^2\right)^{\frac{-1}{2}}\left(x\frac{\partial x}{\partial p_2}+y\frac{\partial y}{\partial p_2}\right)}{\left(x^2+y^2+z^2\right)}$$

$$\frac{\partial S_{Cy}}{\partial p_2}=\frac{\left(x^2+y^2+z^2\right)^{\frac{1}{2}}\frac{\partial y}{\partial p_2}-y\left(x^2+y^2+z^2\right)^{\frac{-1}{2}}\left(x\frac{\partial x}{\partial p_2}+y\frac{\partial y}{\partial p_2}\right)}{\left(x^2+y^2+z^2\right)}$$

$$\frac{\partial S_{Cz}}{\partial p_2}=-\frac{z\left(x^2+y^2+z^2\right)^{\frac{-1}{2}}\left(x\frac{\partial x}{\partial p_2}+y\frac{\partial y}{\partial p_2}\right)}{\left(x^2+y^2+z^2\right)}$$

$$\frac{\partial S_{Bx}}{\partial p_2}=\frac{\partial S_{Cx}}{\partial p_2} \qquad \frac{\partial S_{By}}{\partial p_2}=-\frac{\partial S_{Cy}}{\partial p_2} \qquad \frac{\partial S_{Bz}}{\partial p_2}=-\frac{\partial S_{Cz}}{\partial p_2}$$

$$\frac{\partial S_{Ox}}{\partial p_2}=\left(\cos\kappa\cos\phi-\sin\kappa\sin\omega\sin\phi\right)\frac{\partial S_{Bx}}{\partial p_2}-\sin\kappa\cos\omega\frac{\partial S_{By}}{\partial p_2}$$
$$+\left(\cos\kappa\sin\phi+\sin\kappa\sin\omega\cos\phi\right)\frac{\partial S_{Bz}}{\partial p_2}$$

$$\frac{\partial S_{Oy}}{\partial p_2}=\left(\sin\kappa\cos\phi+\cos\kappa\sin\omega\sin\phi\right)\frac{\partial S_{Bx}}{\partial p_2}+\cos\kappa\cos\omega\frac{\partial S_{By}}{\partial p_2}$$
$$+\left(\sin\kappa\sin\phi-\cos\kappa\sin\omega\cos\phi\right)\frac{\partial S_{Bz}}{\partial p_2}$$

$$\frac{\partial S_{Oz}}{\partial p_2} = -\cos\omega\sin\phi\frac{\partial S_{Bx}}{\partial p_2} + \sin\omega\frac{\partial S_{By}}{\partial p_2} + \cos\omega\cos\phi\frac{\partial S_{Bz}}{\partial p_2}$$

$$\frac{\partial S_{Ex}}{\partial p_2} = r_{11}\frac{\partial S_{Ox}}{\partial p_2} + r_{12}\frac{\partial S_{Oy}}{\partial p_2} + r_{13}\frac{\partial S_{Oz}}{\partial p_2}$$
$$\frac{\partial S_{Ey}}{\partial p_2} = r_{21}\frac{\partial S_{Ox}}{\partial p_2} + r_{22}\frac{\partial S_{Oy}}{\partial p_2} + r_{23}\frac{\partial S_{Oz}}{\partial p_2}$$
$$\frac{\partial S_{Ez}}{\partial p_2} = r_{31}\frac{\partial S_{Ox}}{\partial p_2} + r_{32}\frac{\partial S_{Oy}}{\partial p_2} + r_{33}\frac{\partial S_{Oz}}{\partial p_2}$$

$$\frac{\partial X_0}{\partial p_2} = \frac{\partial s}{\partial p_2}S_{Ex} + s\frac{\partial S_{Ex}}{\partial p_2}$$
$$\frac{\partial Y_0}{\partial p_2} = \frac{\partial s}{\partial p_2}S_{Ey} + s\frac{\partial S_{Ey}}{\partial p_2}$$
$$\frac{\partial Y_0}{\partial p_2} = \frac{\partial s}{\partial p_2}S_{Ez} + s\frac{\partial S_{Ez}}{\partial p_2}$$

$$\frac{\partial s}{\partial p_2} = \frac{\left(-\frac{\partial \beta}{\partial p_2} - \frac{1}{2}\left(\beta^2 - 4\alpha\gamma\right)^{\frac{-1}{2}}\left(2\beta\frac{\partial \beta}{\partial p_2} - 4\alpha\frac{\partial \gamma}{\partial p_2} - 4\gamma\frac{\partial \alpha}{\partial p_2}\right)\right) * 2\alpha - 2\frac{\partial \alpha}{\partial p_2}\left(-\beta - \sqrt{-\beta^2 - 4\alpha\gamma}\right)}{4 * \alpha^2}$$

$$\frac{\partial \alpha}{\partial p_2} = \frac{2 * S_{Ex} * \frac{\partial S_{Ex}}{\partial p_2} + 2 * S_{Ey} * \frac{\partial S_{Ey}}{\partial p_2}}{a^2} + \frac{2 * S_{Ez} * \frac{\partial S_{Ez}}{\partial p_2}}{b^2}$$

$$\frac{\partial \beta}{\partial p_2} = \frac{X_{cam} * \frac{\partial S_{Ex}}{\partial p_2} + Y_{cam} * \frac{\partial S_{Ey}}{\partial p_2}}{a^2} + \frac{Z_{cam} * \frac{\partial S_{Ez}}{\partial p_2}}{b^2}$$

$$\frac{\partial \gamma}{\partial p_2} = 0$$

$$\frac{\partial \lambda}{\partial p_2} = \frac{1}{1 + \left(\frac{Y_0}{X_0}\right)^2} * \left(\frac{X_0 * \frac{\partial Y_0}{\partial p_2} - Y_0 * \frac{\partial X_0}{\partial p_2}}{X_0^2}\right)$$

$$\frac{\partial \phi}{\partial p_2} = \frac{\left[\frac{\partial Z_o}{\partial p_2}\sqrt{X_o^2 + Y_o^2} - \left(X_o\frac{\partial X_o}{\partial p_2} + Y_o\frac{\partial Y_o}{\partial p_2}\right) * \left(X_o^2 + Y_o^2\right)^{\frac{-1}{2}} * Z_o\right]}{\left(1 + \frac{Z_o^2}{\left(X_o^2 + Y_o^2\right)\left(1 - \frac{e^2 N}{N + h}\right)}\right) * \left(1 - \frac{e^2 N}{N + h}\right) * \left(X_o^2 + Y_o^2\right)}$$

C.8 Partial Derivative with respect to ω

$$\frac{\partial x'}{\partial \omega} = 0 \qquad \frac{\partial y'}{\partial \omega} = 0 \qquad \frac{\partial z'}{\partial \omega} = 0 \qquad \frac{\partial r}{\partial \omega} = 0$$

$$\frac{\partial x}{\partial \omega} = 0 \qquad \frac{\partial y}{\partial \omega} = 0 \qquad \frac{\partial z}{\partial \omega} = 0$$

$$\frac{\partial S_{Cx}}{\partial \omega} = 0 \qquad \frac{\partial S_{Cy}}{\partial \omega} = 0 \qquad \frac{\partial S_{Cz}}{\partial \omega} = 0$$

$$\frac{\partial S_{Bx}}{\partial \omega} = 0 \qquad \frac{\partial S_{By}}{\partial \omega} = 0 \qquad \frac{\partial S_{Bz}}{\partial \omega} = 0$$

$$\frac{\partial S_{Ox}}{\partial \omega} = -\sin\kappa\cos\omega\sin\phi * S_{Bx} + \sin\kappa\sin\omega * S_{By} + \sin\kappa\cos\omega\cos\phi * S_{Bz}$$
$$\frac{\partial S_{Oy}}{\partial \omega} = \cos\kappa\cos\omega\sin\phi * S_{Bx} - \cos\kappa\sin\omega * S_{By} - \cos\kappa\cos\omega\cos\phi * S_{Bz}$$
$$\frac{\partial S_{Oz}}{\partial \omega} = \sin\omega\sin\phi * S_{Bx} + \cos\omega * S_{By} - \sin\omega\cos\phi * S_{Bz}$$

$$\frac{\partial S_{Ex}}{\partial \omega} = r_{11}\frac{\partial S_{Ox}}{\partial \omega} + r_{12}\frac{\partial S_{Oy}}{\partial \omega} + r_{13}\frac{\partial S_{Oz}}{\partial \omega}$$
$$\frac{\partial S_{Ey}}{\partial \omega} = r_{21}\frac{\partial S_{Ox}}{\partial \omega} + r_{22}\frac{\partial S_{Oy}}{\partial \omega} + r_{23}\frac{\partial S_{Oz}}{\partial \omega}$$
$$\frac{\partial S_{Ez}}{\partial \omega} = r_{31}\frac{\partial S_{Ox}}{\partial \omega} + r_{32}\frac{\partial S_{Oy}}{\partial \omega} + r_{33}\frac{\partial S_{Oz}}{\partial \omega}$$

$$\frac{\partial X_0}{\partial \omega} = \frac{\partial s}{\partial \omega}S_{Ex} + s\frac{\partial S_{Ex}}{\partial \omega}$$
$$\frac{\partial Y_0}{\partial \omega} = \frac{\partial s}{\partial \omega}S_{Ey} + s\frac{\partial S_{Ey}}{\partial \omega}$$
$$\frac{\partial Y_0}{\partial \omega} = \frac{\partial s}{\partial \omega}S_{Ez} + s\frac{\partial S_{Ez}}{\partial \omega}$$

$$\frac{\partial s}{\partial \omega} = \frac{\left(-\frac{\partial \beta}{\partial \omega} - \frac{1}{2}\left(\beta^2 - 4\alpha\gamma\right)^{\frac{-1}{2}}\left(2\beta\frac{\partial \beta}{\partial \omega} - 4\alpha\frac{\partial \gamma}{\partial \omega} - 4\gamma\frac{\partial \alpha}{\partial \omega}\right)\right) * 2\alpha - 2\frac{\partial \alpha}{\partial \omega}\left(-\beta - \sqrt{-\beta^2 - 4\alpha\gamma}\right)}{4 * \alpha^2}$$

$$\frac{\partial \alpha}{\partial \omega} = \frac{2 * S_{Ex} * \frac{\partial S_{Ex}}{\partial \omega} + 2 * S_{Ey} * \frac{\partial S_{Ey}}{\partial \omega}}{a^2} + \frac{2 * S_{Ez} * \frac{\partial S_{Ez}}{\partial \omega}}{b^2}$$

$$\frac{\partial \beta}{\partial \omega} = \frac{X_{cam} * \frac{\partial S_{Ex}}{\partial \omega} + Y_{cam} * \frac{\partial S_{Ey}}{\partial \omega}}{a^2} + \frac{Z_{cam} * \frac{\partial S_{Ez}}{\partial \omega}}{b^2}$$

$$\frac{\partial \gamma}{\partial \omega} = 0$$

$$\frac{\partial \lambda}{\partial \omega} = \frac{1}{1+\left(\frac{Y_0}{X_0}\right)^2} * \left(\frac{X_0 * \frac{\partial Y_0}{\partial \omega} - Y_0 * \frac{\partial X_0}{\partial \omega}}{X_0^2} \right)$$

$$\frac{\partial \phi}{\partial \omega} = \frac{\left[\frac{\partial Z_o}{\partial \omega}\sqrt{X_o^2+Y_o^2} - \left(X_o \frac{\partial X_o}{\partial \omega} + Y_o \frac{\partial Y_o}{\partial \omega} \right) * \left(X_o^2+Y_o^2\right)^{\frac{-1}{2}} * Z_o \right]}{\left(1 + \frac{Z_o^2}{\left(X_o^2+Y_o^2\right)\left(1-\frac{e^2 N}{N+h}\right)} \right) * \left(1 - \frac{e^2 N}{N+h}\right) * \left(X_o^2+Y_o^2\right)}$$

C.9 Partial Derivative with respect to φ

$$\frac{\partial x'}{\partial \phi} = 0 \qquad \frac{\partial y'}{\partial \phi} = 0 \qquad \frac{\partial z'}{\partial \phi} = 0 \qquad \frac{\partial r}{\partial \phi} = 0$$

$$\frac{\partial x}{\partial \phi} = 0 \qquad \frac{\partial y}{\partial \phi} = 0 \qquad \frac{\partial z}{\partial \phi} = 0$$

$$\frac{\partial S_{Cx}}{\partial \phi} = 0 \qquad \frac{\partial S_{Cy}}{\partial \phi} = 0 \qquad \frac{\partial S_{Cz}}{\partial \phi} = 0$$

$$\frac{\partial S_{Bx}}{\partial \phi} = 0 \qquad \frac{\partial S_{By}}{\partial \phi} = 0 \qquad \frac{\partial S_{Bz}}{\partial \phi} = 0$$

$$\frac{\partial S_{Ox}}{\partial \phi} = (-\cos\kappa\sin\phi - \sin\kappa\sin\omega\cos\phi) * S_{Bx} + (\cos\kappa\cos\phi - \sin\kappa\sin\omega\sin\phi) * S_{Bz}$$

$$\frac{\partial S_{Oy}}{\partial \phi} = (-\sin\kappa\sin\phi + \cos\kappa\sin\omega\cos\phi) * S_{Bx} + (\sin\kappa\cos\phi + \cos\kappa\sin\omega\sin\phi) * S_{Bz}$$

$$\frac{\partial S_{Oz}}{\partial \phi} = (-\cos\omega\cos\phi) * S_{Bx} - \cos\omega\sin\phi * S_{Bz}$$

$$\frac{\partial S_{Ex}}{\partial \phi} = r_{11}\frac{\partial S_{Ox}}{\partial \phi} + r_{12}\frac{\partial S_{Oy}}{\partial \phi} + r_{13}\frac{\partial S_{Oz}}{\partial \phi}$$

$$\frac{\partial S_{Ey}}{\partial \phi} = r_{21}\frac{\partial S_{Ox}}{\partial \phi} + r_{22}\frac{\partial S_{Oy}}{\partial \phi} + r_{23}\frac{\partial S_{Oz}}{\partial \phi}$$

$$\frac{\partial S_{Ez}}{\partial \phi} = r_{31}\frac{\partial S_{Ox}}{\partial \phi} + r_{32}\frac{\partial S_{Oy}}{\partial \phi} + r_{33}\frac{\partial S_{Oz}}{\partial \phi}$$

$$\frac{\partial X_0}{\partial \phi} = \frac{\partial s}{\partial \phi} S_{Ex} + s \frac{\partial S_{Ex}}{\partial \phi}$$

$$\frac{\partial Y_0}{\partial \phi} = \frac{\partial s}{\partial \phi} S_{Ey} + s \frac{\partial S_{Ey}}{\partial \phi}$$

$$\frac{\partial Y_0}{\partial \phi} = \frac{\partial s}{\partial \phi} S_{Ez} + s \frac{\partial S_{Ez}}{\partial \phi}$$

$$\frac{\partial s}{\partial \phi} = \frac{\left(-\frac{\partial \beta}{\partial \phi} - \frac{1}{2}\left(\beta^2 - 4\alpha\gamma\right)^{\frac{-1}{2}} \left(2\beta \frac{\partial \beta}{\partial \phi} - 4\alpha \frac{\partial \gamma}{\partial \phi} - 4\gamma \frac{\partial \alpha}{\partial \phi} \right) \right) * 2\alpha - 2\frac{\partial \alpha}{\partial \phi}\left(-\beta - \sqrt{-\beta^2 - 4\alpha\gamma} \right)}{4 * \alpha^2}$$

$$\frac{\partial \alpha}{\partial \phi} = \frac{2 * S_{Ex} * \frac{\partial S_{Ex}}{\partial \phi} + 2 * S_{Ey} * \frac{\partial S_{Ey}}{\partial \phi}}{a^2} + \frac{2 * S_{Ez} * \frac{\partial S_{Ez}}{\partial \phi}}{b^2}$$

$$\frac{\partial \beta}{\partial \phi} = \frac{X_{cam} * \frac{\partial S_{Ex}}{\partial \phi} + Y_{cam} * \frac{\partial S_{Ey}}{\partial \phi}}{a^2} + \frac{Z_{cam} * \frac{\partial S_{Ez}}{\partial \phi}}{b^2}$$

$$\frac{\partial \gamma}{\partial \phi} = 0$$

$$\frac{\partial \lambda}{\partial \phi} = \frac{1}{1 + \left(\frac{Y_0}{X_0}\right)^2} * \left(\frac{X_0 * \frac{\partial Y_0}{\partial \phi} - Y_0 * \frac{\partial X_0}{\partial \phi}}{X_0^2} \right)$$

$$\frac{\partial \varphi}{\partial \phi} = \frac{\left[\frac{\partial Z_o}{\partial \phi} \sqrt{X_o^2 + Y_o^2} - \left(X_o \frac{\partial X_o}{\partial \phi} + Y_o \frac{\partial Y_o}{\partial \phi} \right) * \left(X_o^2 + Y_o^2 \right)^{\frac{-1}{2}} * Z_o \right]}{\left(1 + \frac{Z_o^2}{\left(X_o^2 + Y_o^2 \right)\left(1 - \frac{e^2 N}{N + h} \right)} \right) * \left(1 - \frac{e^2 N}{N + h} \right) * \left(X_o^2 + Y_o^2 \right)}$$

C.10 Partial Derivative with respect to κ

$$\frac{\partial x'}{\partial \kappa} = 0 \qquad \frac{\partial y'}{\partial \kappa} = 0 \qquad \frac{\partial z'}{\partial \kappa} = 0 \qquad \frac{\partial r}{\partial \kappa} = 0$$

$$\frac{\partial x}{\partial \kappa} = 0 \qquad \frac{\partial y}{\partial \kappa} = 0 \qquad \frac{\partial z}{\partial \kappa} = 0$$

$$\frac{\partial S_{Cx}}{\partial \kappa} = 0 \qquad \frac{\partial S_{Cy}}{\partial \kappa} = 0 \qquad \frac{\partial S_{Cz}}{\partial \kappa} = 0$$

$$\frac{\partial S_{Bx}}{\partial \kappa} = 0 \qquad \frac{\partial S_{By}}{\partial \kappa} = 0 \qquad \frac{\partial S_{Bz}}{\partial \kappa} = 0$$

$$\frac{\partial S_{Ox}}{\partial \kappa} = \left(-\sin\kappa\cos\phi - \cos\kappa\sin\omega\sin\phi\right) * S_{Bx} - \cos\kappa\cos\omega * S_{By}$$
$$+\left(-\sin\kappa\sin\phi + \cos\kappa\sin\omega\cos\phi\right) * S_{Bz}$$

$$\frac{\partial S_{Oy}}{\partial \kappa} = \left(\cos\kappa\cos\phi - \sin\kappa\sin\omega\sin\phi\right) * S_{Bx} - \sin\kappa\cos\omega * S_{By}$$
$$+\left(\cos\kappa\sin\phi + \sin\kappa\sin\omega\cos\phi\right) * S_{Bz}$$

$$\frac{\partial S_{Oz}}{\partial \kappa} = 0$$

$$\frac{\partial S_{Ex}}{\partial \kappa} = r_{11}\frac{\partial S_{Ox}}{\partial \kappa} + r_{12}\frac{\partial S_{Oy}}{\partial \kappa} + r_{13}\frac{\partial S_{Oz}}{\partial \kappa}$$
$$\frac{\partial S_{Ey}}{\partial \kappa} = r_{21}\frac{\partial S_{Ox}}{\partial \kappa} + r_{22}\frac{\partial S_{Oy}}{\partial \kappa} + r_{23}\frac{\partial S_{Oz}}{\partial \kappa}$$
$$\frac{\partial S_{Ez}}{\partial \kappa} = r_{31}\frac{\partial S_{Ox}}{\partial \kappa} + r_{32}\frac{\partial S_{Oy}}{\partial \kappa} + r_{33}\frac{\partial S_{Oz}}{\partial \kappa}$$

$$\frac{\partial X_0}{\partial \kappa} = \frac{\partial s}{\partial \kappa} S_{Ex} + s\frac{\partial S_{Ex}}{\partial \kappa}$$
$$\frac{\partial Y_0}{\partial \kappa} = \frac{\partial s}{\partial \kappa} S_{Ey} + s\frac{\partial S_{Ey}}{\partial \kappa}$$
$$\frac{\partial Y_0}{\partial \kappa} = \frac{\partial s}{\partial \kappa} S_{Ez} + s\frac{\partial S_{Ez}}{\partial \kappa}$$

$$\frac{\partial s}{\partial \kappa} = \frac{\left(-\frac{\partial \beta}{\partial \kappa} - \frac{1}{2}\left(\beta^2 - 4\alpha\gamma\right)^{\frac{-1}{2}}\left(2\beta\frac{\partial \beta}{\partial \kappa} - 4\alpha\frac{\partial \gamma}{\partial \kappa} - 4\gamma\frac{\partial \alpha}{\partial \kappa}\right)\right) * 2\alpha - 2\frac{\partial \alpha}{\partial \kappa}\left(-\beta - \sqrt{-\beta^2 - 4\alpha\gamma}\right)}{4 * \alpha^2}$$

$$\frac{\partial \alpha}{\partial \kappa} = \frac{2 * S_{Ex} * \frac{\partial S_{Ex}}{\partial \kappa} + 2 * S_{Ey} * \frac{\partial S_{Ey}}{\partial \kappa}}{a^2} + \frac{2 * S_{Ez} * \frac{\partial S_{Ez}}{\partial \kappa}}{b^2}$$

$$\frac{\partial \beta}{\partial \kappa} = \frac{X_{cam} * \frac{\partial S_{Ex}}{\partial \kappa} + Y_{cam} * \frac{\partial S_{Ey}}{\partial \kappa}}{a^2} + \frac{Z_{cam} * \frac{\partial S_{Ez}}{\partial \kappa}}{b^2}$$

$$\frac{\partial \gamma}{\partial \kappa} = 0$$

$$\frac{\partial \lambda}{\partial \kappa} = \frac{1}{1 + \left(\frac{Y_0}{X_0}\right)^2} * \left(\frac{X_0 * \frac{\partial Y_0}{\partial \kappa} - Y_0 * \frac{\partial X_0}{\partial \kappa}}{X_0^2}\right)$$

$$\frac{\partial\phi}{\partial\kappa}=\frac{\left[\frac{\partial Z_o}{\partial\kappa}\sqrt{X_o^2+Y_o^2}-\left(X_o\frac{\partial X_o}{\partial\kappa}+Y_o\frac{\partial Y_o}{\partial\kappa}\right)*\left(X_o^2+Y_o^2\right)^{\frac{-1}{2}}*Z_o\right]}{\left(1+\frac{Z_o^2}{\left(X_o^2+Y_o^2\right)\left(1-\frac{e^2N}{N+h}\right)}\right)*\left(1-\frac{e^2N}{N+h}\right)*\left(X_o^2+Y_o^2\right)}$$

C.11 Partial Derivative with respect to c

$$\frac{\partial x'}{\partial c}=-x''+\frac{width}{2}\qquad\qquad \frac{\partial y'}{\partial\kappa}=-y''+\frac{height}{2}\qquad\qquad \frac{\partial z'}{\partial c}=0$$

$$\frac{\partial r}{\partial c}=\frac{1}{2}\left(x'^2+y'^2\right)^{\frac{-1}{2}}\left(2x'\frac{\partial x'}{\partial c}+2y'\frac{\partial y'}{\partial c}\right)$$

$$\frac{\partial x}{\partial c}=\frac{\partial x'}{\partial c}\left[1-k_1r^2-k_2r^4-2p_1x'-2p_2y'-\frac{p_1r^2}{x'}\right]$$

$$+x'\left(2k_1r\frac{\partial r}{\partial c}-4k_2r^3\frac{\partial r}{\partial c}-2p_1\frac{\partial x'}{\partial c}-2p_2\frac{\partial y'}{\partial c}-\frac{2rp_1x'\frac{\partial r}{\partial c}-p_1r^2\frac{\partial x'}{\partial c}}{x'^2}\right)$$

$$\frac{\partial y}{\partial c}=\frac{\partial y'}{\partial c}\left[1-k_1r^2-k_2r^4-2p_2y'-2p_1x'-\frac{p_2r^2}{y'}\right]$$

$$+y'\left(-2k_1r\frac{\partial r}{\partial c}-4k_2r^3\frac{\partial r}{\partial c}-2p_2\frac{\partial y'}{\partial c}-2p_1\frac{\partial x'}{\partial c}-\frac{2rp_2y'\frac{\partial r}{\partial c}-p_2r^2\frac{\partial y'}{\partial c}}{y'^2}\right)$$

$$\frac{\partial z}{\partial c}=0$$

$$\frac{\partial S_{Cx}}{\partial c}=\frac{\left(x^2+y^2+z^2\right)^{\frac{1}{2}}\frac{\partial x}{\partial c}-x\left(x^2+y^2+z^2\right)^{\frac{-1}{2}}\left(x\frac{\partial x}{\partial c}+y\frac{\partial y}{\partial c}\right)}{\left(x^2+y^2+z^2\right)}$$

$$\frac{\partial S_{Cy}}{\partial c}=\frac{\left(x^2+y^2+z^2\right)^{\frac{1}{2}}\frac{\partial y}{\partial c}-y\left(x^2+y^2+z^2\right)^{\frac{-1}{2}}\left(x\frac{\partial x}{\partial c}+y\frac{\partial y}{\partial c}\right)}{\left(x^2+y^2+z^2\right)}$$

$$\frac{\partial S_{Cz}}{\partial c}=-\frac{z\left(x^2+y^2+z^2\right)^{\frac{-1}{2}}\left(x\frac{\partial x}{\partial c}+y\frac{\partial y}{\partial c}\right)}{\left(x^2+y^2+z^2\right)}$$

$$\frac{\partial S_{Bx}}{\partial c}=\frac{\partial S_{Cx}}{\partial c}\qquad\qquad \frac{\partial S_{By}}{\partial\kappa}=-\frac{\partial S_{Cy}}{\partial c}\qquad\qquad \frac{\partial S_{Bz}}{\partial\kappa}=-\frac{\partial S_{Cz}}{\partial c}$$

$$\frac{\partial S_{Ox}}{\partial c} = (\cos\kappa\cos\phi - \sin\kappa\sin\omega\sin\phi)\frac{\partial S_{Bx}}{\partial c} - \sin\kappa\cos\omega\frac{\partial S_{By}}{\partial c}$$
$$+(\cos\kappa\sin\phi + \sin\kappa\sin\omega\cos\phi)\frac{\partial S_{Bz}}{\partial c}$$

$$\frac{\partial S_{Oy}}{\partial c} = (\sin\kappa\cos\phi + \cos\kappa\sin\omega\sin\phi)\frac{\partial S_{Bx}}{\partial c} + \cos\kappa\cos\omega\frac{\partial S_{By}}{\partial c}$$
$$+(\sin\kappa\sin\phi - \cos\kappa\sin\omega\cos\phi)\frac{\partial S_{Bz}}{\partial c}$$

$$\frac{\partial S_{Oz}}{\partial c} = -\cos\omega\sin\phi\frac{\partial S_{Bx}}{\partial c} + \sin\omega\frac{\partial S_{By}}{\partial c} + \cos\omega\cos\phi\frac{\partial S_{Bz}}{\partial c}$$

$$\frac{\partial S_{Ex}}{\partial c} = r_{11}\frac{\partial S_{Ox}}{\partial c} + r_{12}\frac{\partial S_{Oy}}{\partial c} + r_{13}\frac{\partial S_{Oz}}{\partial c}$$
$$\frac{\partial S_{Ey}}{\partial c} = r_{21}\frac{\partial S_{Ox}}{\partial c} + r_{22}\frac{\partial S_{Oy}}{\partial c} + r_{23}\frac{\partial S_{Oz}}{\partial c}$$
$$\frac{\partial S_{Ez}}{\partial c} = r_{31}\frac{\partial S_{Ox}}{\partial c} + r_{32}\frac{\partial S_{Oy}}{\partial c} + r_{33}\frac{\partial S_{Oz}}{\partial c}$$

$$\frac{\partial X_0}{\partial c} = \frac{\partial s}{\partial c}S_{Ex} + s\frac{\partial S_{Ex}}{\partial c}$$
$$\frac{\partial Y_0}{\partial c} = \frac{\partial s}{\partial c}S_{Ey} + s\frac{\partial S_{Ey}}{\partial c}$$
$$\frac{\partial Y_0}{\partial c} = \frac{\partial s}{\partial c}S_{Ez} + s\frac{\partial S_{Ez}}{\partial c}$$

$$\frac{\partial s}{\partial c} = \frac{\left(-\frac{\partial\beta}{\partial p_2} - \frac{1}{2}(\beta^2 - 4\alpha\gamma)^{\frac{-1}{2}}\left(2\beta\frac{\partial\beta}{\partial c} - 4\alpha\frac{\partial\gamma}{\partial c} - 4\gamma\frac{\partial\alpha}{\partial c}\right)\right) * 2\alpha - 2\frac{\partial\alpha}{\partial c}\left(-\beta - \sqrt{-\beta^2 - 4\alpha\gamma}\right)}{4 * \alpha^2}$$

$$\frac{\partial\alpha}{\partial c} = \frac{2 * S_{Ex} * \frac{\partial S_{Ex}}{\partial c} + 2 * S_{Ey} * \frac{\partial S_{Ey}}{\partial c}}{a^2} + \frac{2 * S_{Ez} * \frac{\partial S_{Ez}}{\partial c}}{b^2}$$
$$\frac{\partial\beta}{\partial c} = \frac{X_{cam} * \frac{\partial S_{Ex}}{\partial c} + Y_{cam} * \frac{\partial S_{Ey}}{\partial c}}{a^2} + \frac{Z_{cam} * \frac{\partial S_{Ez}}{\partial c}}{b^2}$$
$$\frac{\partial\gamma}{\partial c} = 0$$

$$\frac{\partial\lambda}{\partial c} = \frac{1}{1 + \left(\frac{Y_0}{X_0}\right)^2} * \left(\frac{X_0 * \frac{\partial Y_0}{\partial c} - Y_0 * \frac{\partial X_0}{\partial c}}{X_0^2}\right)$$

$$\frac{\partial \phi}{\partial c} = \frac{\left[\frac{\partial Z_o}{\partial c} \sqrt{X_o^2 + Y_o^2} - \left(X_o \frac{\partial X_o}{\partial c} + Y_o \frac{\partial Y_o}{\partial c} \right) * \left(X_o^2 + Y_o^2 \right)^{\frac{-1}{2}} * Z_o \right]}{\left(1 + \frac{Z_o^2}{\left(X_o^2 + Y_o^2 \right)\left(1 - \frac{e^2 N}{N+h} \right)} \right) * \left(1 - \frac{e^2 N}{N+h} \right) * \left(X_o^2 + Y_o^2 \right)}$$

C.12 Partial Derivative with respect to X_{cam}

$$\frac{\partial x'}{\partial X_{cam}} = 0 \qquad \frac{\partial y'}{\partial X_{cam}} = 0 \qquad \frac{\partial z'}{\partial X_{cam}} = 0$$

$$\frac{\partial r}{\partial X_{cam}} = 0 \qquad \frac{\partial x}{\partial X_{cam}} = 0 \qquad \frac{\partial y}{\partial X_{cam}} = 0 \qquad \frac{\partial z}{\partial X_{cam}} = 0$$

$$\frac{\partial S_{Cx}}{\partial X_{cam}} = 0 \qquad \frac{\partial S_{Cy}}{\partial X_{cam}} = 0 \qquad \frac{\partial S_{Cz}}{\partial X_{cam}} = 0$$

$$\frac{\partial S_{Bx}}{\partial X_{cam}} = 0 \qquad \frac{\partial S_{By}}{\partial X_{cam}} = 0 \qquad \frac{\partial S_{Bz}}{\partial X_{cam}} = 0$$

$$\frac{\partial S_{Ox}}{\partial X_{cam}} = 0 \qquad \frac{\partial S_{Oy}}{\partial X_{cam}} = 0 \qquad \frac{\partial S_{Oz}}{\partial X_{cam}} = 0$$

$$\frac{\partial S_{Ex}}{\partial X_{cam}} = S_{Ox} \frac{\partial r_{11}}{\partial X_{cam}} + S_{Oy} \frac{\partial r_{12}}{\partial X_{cam}} + S_{Oz} \frac{\partial r_{13}}{\partial X_{cam}}$$

$$\frac{\partial S_{Ey}}{\partial X_{cam}} = S_{Ox} \frac{\partial r_{21}}{\partial X_{cam}} + S_{Oy} \frac{\partial r_{22}}{\partial X_{cam}} + S_{Oz} \frac{\partial r_{23}}{\partial X_{cam}}$$

$$\frac{\partial S_{Ez}}{\partial X_{cam}} = S_{Ox} \frac{\partial r_{31}}{\partial X_{cam}} + S_{Oy} \frac{\partial r_{32}}{\partial X_{cam}} + S_{Oz} \frac{\partial r_{33}}{\partial X_{cam}}$$

$$\frac{\partial X_0}{\partial X_{cam}} = 1 + \frac{\partial s}{\partial X_{cam}} S_{Ex} + s \frac{\partial S_{Ex}}{\partial X_{cam}}$$

$$\frac{\partial Y_0}{\partial X_{cam}} = \frac{\partial s}{\partial X_{cam}} S_{Ey} + s \frac{\partial S_{Ey}}{\partial X_{cam}}$$

$$\frac{\partial Z_0}{\partial X_{cam}} = \frac{\partial s}{\partial X_{cam}} S_{Ez} + s \frac{\partial S_{Ez}}{\partial X_{cam}}$$

$$\frac{\partial s}{\partial X_{cam}} = \frac{\left(-\frac{\partial \beta}{\partial X_{cam}} - \frac{1}{2}\left(\beta^2 - 4\alpha\gamma\right)^{\frac{-1}{2}} \left(2\beta \frac{\partial \beta}{\partial X_{cam}} - 4\alpha \frac{\partial \gamma}{\partial X_{cam}} - 4\gamma \frac{\partial \alpha}{\partial X_{cam}} \right) \right) * 2\alpha - 2 \frac{\partial \alpha}{\partial X_{cam}} \left(-\beta - \sqrt{-\beta^2 - 4\alpha\gamma} \right)}{4 * \alpha^2}$$

$$\frac{\partial \alpha}{\partial X_{cam}} = 0 \qquad \frac{\partial \beta}{\partial X_{cam}} = \frac{S_{Ex}}{a^2} \qquad \frac{\partial \gamma}{\partial X_{cam}} = \frac{2X_{cam}}{a^2}$$

$$\frac{\partial \lambda}{\partial X_{cam}} = \frac{1}{1+\left(\frac{Y_0}{X_0}\right)^2} * \left(\frac{X_0 * \frac{\partial Y_0}{\partial X_{cam}} - Y_0 * \frac{\partial X_0}{\partial X_{cam}}}{X_0^2} \right)$$

$$\frac{\partial \phi}{\partial X_{Cam}} = \frac{\left[\frac{\partial Z_o}{\partial X_{Cam}} \sqrt{X_o^2 + Y_o^2} - \left(X_o \frac{\partial X_o}{\partial X_{Cam}} + Y_o \frac{\partial Y_o}{\partial X_{Cam}} \right) * \left(X_o^2 + Y_o^2 \right)^{\frac{-1}{2}} * Z_o \right]}{\left(1 + \frac{Z_o^2}{\left(X_o^2 + Y_o^2 \right)\left(1 - \frac{e^2 N}{N+h} \right)} \right) * \left(1 - \frac{e^2 N}{N+h} \right) * \left(X_o^2 + Y_o^2 \right)}$$

C.13 Partial Derivative with respect to Y_{cam}

$$\frac{\partial x'}{\partial Y_{cam}} = 0 \qquad \frac{\partial y'}{\partial Y_{cam}} = 0 \qquad \frac{\partial z'}{\partial Y_{cam}} = 0$$

$$\frac{\partial r}{\partial Y_{cam}} = 0 \qquad \frac{\partial x}{\partial Y_{cam}} = 0 \qquad \frac{\partial y}{\partial Y_{cam}} = 0 \qquad \frac{\partial z}{\partial Y_{cam}} = 0$$

$$\frac{\partial S_{Cx}}{\partial Y_{cam}} = 0 \qquad \frac{\partial S_{Cy}}{\partial Y_{cam}} = 0 \qquad \frac{\partial S_{Cz}}{\partial Y_{cam}} = 0$$

$$\frac{\partial S_{Bx}}{\partial Y_{cam}} = 0 \qquad \frac{\partial S_{By}}{\partial Y_{cam}} = 0 \qquad \frac{\partial S_{Bz}}{\partial Y_{cam}} = 0$$

$$\frac{\partial S_{Ox}}{\partial Y_{cam}} = 0 \qquad \frac{\partial S_{Oy}}{\partial Y_{cam}} = 0 \qquad \frac{\partial S_{Oz}}{\partial Y_{cam}} = 0$$

$$\frac{\partial S_{Ex}}{\partial Y_{cam}} = S_{Ox} \frac{\partial r_{11}}{\partial Y_{cam}} + S_{Oy} \frac{\partial r_{12}}{\partial Y_{cam}} + S_{Oz} \frac{\partial r_{13}}{\partial Y_{cam}}$$

$$\frac{\partial S_{Ey}}{\partial Y_{cam}} = S_{Ox} \frac{\partial r_{21}}{\partial Y_{cam}} + S_{Oy} \frac{\partial r_{22}}{\partial Y_{cam}} + S_{Oz} \frac{\partial r_{23}}{\partial Y_{cam}}$$

$$\frac{\partial S_{Ez}}{\partial Y_{cam}} = S_{Ox} \frac{\partial r_{31}}{\partial Y_{cam}} + S_{Oy} \frac{\partial r_{32}}{\partial Y_{cam}} + S_{Oz} \frac{\partial r_{33}}{\partial Y_{cam}}$$

$$\frac{\partial X_0}{\partial Y_{cam}} = \frac{\partial s}{\partial Y_{cam}} S_{Ex} + s\frac{\partial S_{Ex}}{\partial Y_{cam}}$$

$$\frac{\partial Y_0}{\partial Y_{cam}} = 1 + \frac{\partial s}{\partial Y_{cam}} S_{Ey} + s\frac{\partial S_{Ey}}{\partial Y_{cam}}$$

$$\frac{\partial Z_0}{\partial Y_{cam}} = \frac{\partial s}{\partial Y_{cam}} S_{Ez} + s\frac{\partial S_{Ez}}{\partial Y_{cam}}$$

$$\frac{\partial s}{\partial Y_{cam}} = \frac{\left(-\frac{\partial \beta}{\partial Y_{cam}} - \frac{1}{2}\left(\beta^2 - 4\alpha\gamma\right)^{\frac{-1}{2}}\left(2\beta\frac{\partial \beta}{\partial Y_{cam}} - 4\alpha\frac{\partial \gamma}{\partial Y_{cam}} - 4\gamma\frac{\partial \alpha}{\partial Y_{cam}}\right)\right) * 2\alpha - 2\frac{\partial \alpha}{\partial Y_{cam}}\left(-\beta - \sqrt{-\beta^2 - 4\alpha\gamma}\right)}{4 * \alpha^2}$$

$$\frac{\partial \alpha}{\partial Y_{cam}} = 0 \qquad \frac{\partial \beta}{\partial Y_{cam}} = \frac{S_{Ey}}{a^2} \qquad \frac{\partial \gamma}{\partial Y_{cam}} = \frac{2Y_{cam}}{a^2}$$

$$\frac{\partial \lambda}{\partial Y_{cam}} = \frac{1}{1 + \left(\frac{Y_0}{X_0}\right)^2} * \left(\frac{X_0 * \frac{\partial Y_0}{\partial Y_{cam}} - Y_0 * \frac{\partial X_0}{\partial Y_{cam}}}{X_0^2}\right)$$

$$\frac{\partial \phi}{\partial Y_{Cam}} = \frac{\left[\frac{\partial Z_o}{\partial Y_{Cam}}\sqrt{X_o^2 + Y_o^2} - \left(X_o\frac{\partial X_o}{\partial Y_{Cam}} + Y_o\frac{\partial Y_o}{\partial Y_{Cam}}\right) * \left(X_o^2 + Y_o^2\right)^{\frac{-1}{2}} * Z_o\right]}{\left(1 + \frac{Z_o^2}{\left(X_o^2 + Y_o^2\right)\left(1 - \frac{e^2 N}{N+h}\right)}\right) * \left(1 - \frac{e^2 N}{N+h}\right) * \left(X_o^2 + Y_o^2\right)}$$

C.14 Partial Derivative with respect to Z_{cam}

$$\frac{\partial x'}{\partial Z_{cam}} = 0 \qquad \frac{\partial y'}{\partial Z_{cam}} = 0 \qquad \frac{\partial z'}{\partial Z_{cam}} = 0$$

$$\frac{\partial r}{\partial Z_{cam}} = 0 \qquad \frac{\partial x}{\partial Z_{cam}} = 0 \qquad \frac{\partial y}{\partial Z_{cam}} = 0 \qquad \frac{\partial z}{\partial Z_{cam}} = 0$$

$$\frac{\partial S_{Cx}}{\partial Z_{cam}} = 0 \qquad \frac{\partial S_{Cy}}{\partial Z_{cam}} = 0 \qquad \frac{\partial S_{Cz}}{\partial Z_{cam}} = 0$$

$$\frac{\partial S_{Bx}}{\partial Z_{cam}} = 0 \qquad \frac{\partial S_{By}}{\partial Z_{cam}} = 0 \qquad \frac{\partial S_{Bz}}{\partial Z_{cam}} = 0$$

$$\frac{\partial S_{Ox}}{\partial Z_{cam}} = 0 \qquad \frac{\partial S_{Oy}}{\partial Z_{cam}} = 0 \qquad \frac{\partial S_{Oz}}{\partial Z_{cam}} = 0$$

$$\frac{\partial S_{Ex}}{\partial Z_{cam}} = S_{Ox}\frac{\partial r_{11}}{\partial Z_{cam}} + S_{Oy}\frac{\partial r_{12}}{\partial Z_{cam}} + S_{Oz}\frac{\partial r_{13}}{\partial Z_{cam}}$$

$$\frac{\partial S_{Ey}}{\partial Z_{cam}} = S_{Ox}\frac{\partial r_{21}}{\partial Z_{cam}} + S_{Oy}\frac{\partial r_{22}}{\partial Z_{cam}} + S_{Oz}\frac{\partial r_{23}}{\partial Z_{cam}}$$

$$\frac{\partial S_{Ez}}{\partial Z_{cam}} = S_{Ox}\frac{\partial r_{31}}{\partial Z_{cam}} + S_{Oy}\frac{\partial r_{32}}{\partial Z_{cam}} + S_{Oz}\frac{\partial r_{33}}{\partial Z_{cam}}$$

$$\frac{\partial X_0}{\partial Z_{cam}} = \frac{\partial s}{\partial Z_{cam}} S_{Ex} + s\frac{\partial S_{Ex}}{\partial Z_{cam}}$$

$$\frac{\partial Y_0}{\partial Z_{cam}} = \frac{\partial s}{\partial Z_{cam}} S_{Ey} + s\frac{\partial S_{Ey}}{\partial Z_{cam}}$$

$$\frac{\partial Z_0}{\partial Z_{cam}} = 1 + \frac{\partial s}{\partial Z_{cam}} S_{Ez} + s\frac{\partial S_{Ez}}{\partial Z_{cam}}$$

$$\frac{\partial s}{\partial Z_{cam}} = \frac{\left(-\frac{\partial \beta}{\partial Z_{cam}} - \frac{1}{2}\left(\beta^2 - 4\alpha\gamma\right)^{\frac{-1}{2}}\left(2\beta\frac{\partial \beta}{\partial Z_{cam}} - 4\alpha\frac{\partial \gamma}{\partial Z_{cam}} - 4\gamma\frac{\partial \alpha}{\partial Z_{cam}}\right)\right) * 2\alpha - 2\frac{\partial \alpha}{\partial Z_{cam}}\left(-\beta - \sqrt{-\beta^2 - 4\alpha\gamma}\right)}{4 * \alpha^2}$$

$$\frac{\partial \alpha}{\partial Z_{cam}} = 0 \qquad \frac{\partial \beta}{\partial Z_{cam}} = \frac{S_{Ex}}{b^2} \qquad \frac{\partial \gamma}{\partial Z_{cam}} = \frac{2Z_{cam}}{b^2}$$

$$\frac{\partial \lambda}{\partial Z_{cam}} = \frac{1}{1 + \left(\frac{Y_0}{X_0}\right)^2} * \left(\frac{X_0 * \frac{\partial Y_0}{\partial Z_{cam}} - Y_0 * \frac{\partial X_0}{\partial Z_{cam}}}{X_0^2}\right)$$

$$\frac{\partial \phi}{\partial Z_{Cam}} = \frac{\left[\frac{\partial Z_o}{\partial Z_{Cam}}\sqrt{X_o^2 + Y_o^2} - \left(X_o\frac{\partial X_o}{\partial Z_{Cam}} + Y_o\frac{\partial Y_o}{\partial Z_{Cam}}\right) * \left(X_o^2 + Y_o^2\right)^{\frac{-1}{2}} * Z_o\right]}{\left(1 + \frac{Z_o^2}{\left(X_o^2 + Y_o^2\right)\left(1 - \frac{e^2 N}{N + h}\right)}\right) * \left(1 - \frac{e^2 N}{N + h}\right) * \left(X_o^2 + Y_o^2\right)}$$

C.15 Partial Derivative with respect to εh

$$\frac{\partial d}{\partial \varepsilon h} = \tan(z) \qquad \frac{\partial \lambda}{\partial d} = \sin\alpha\frac{V}{c}\frac{1}{\cos\phi} \qquad \frac{\partial \lambda}{\partial \varepsilon h} = \tan z \sin\alpha\frac{V}{c}\frac{1}{\cos\phi}$$

$$\frac{\partial \phi}{\partial d} = \cos\alpha\frac{V^3}{c} \qquad \frac{\partial \phi}{\partial \varepsilon h} = \tan z\cos\alpha\frac{V^3}{c}$$

C.16 Partial Derivative with respect to x" (x pixel coordinate)

$$\frac{\partial x'}{\partial x''} = -c \qquad \frac{\partial y'}{\partial x''} = 0 \qquad \frac{\partial z'}{\partial x''} = 0$$

$$\frac{\partial r}{\partial x''}=\frac{1}{2}\left(x'^2+y'^2\right)^{\frac{-1}{2}}\left(2x'\frac{\partial x'}{\partial x''}+2y'\frac{\partial y'}{\partial x''}\right)$$

$$\frac{\partial x}{\partial x''}=\frac{\partial x'}{\partial x''}\left[1-k_1r^2-k_2r^4-2p_1x'-2p_2y'-\frac{p_1r^2}{x'}\right]$$
$$+x'\left(2k_1r\frac{\partial r}{\partial x''}-4k_2r^3\frac{\partial r}{\partial x''}-2p_1\frac{\partial x'}{\partial x''}-2p_2\frac{\partial y'}{\partial x''}-\frac{2rp_1x'\frac{\partial r}{\partial x''}-p_1r^2\frac{\partial x'}{\partial x''}}{x'^2}\right)$$

$$\frac{\partial y}{\partial x''}=\frac{\partial y'}{\partial x''}\left[1-k_1r^2-k_2r^4-2p_2y'-2p_1x'-\frac{p_2r^2}{y'}\right]$$
$$+y'\left(-2k_1r\frac{\partial r}{\partial x''}-4k_2r^3\frac{\partial r}{\partial x''}-2p_2\frac{\partial y'}{\partial x''}-2p_1\frac{\partial x'}{\partial x''}-\frac{2rp_2y'\frac{\partial r}{\partial x''}-p_2r^2\frac{\partial y'}{\partial x''}}{y'^2}\right)$$

$$\frac{\partial z}{\partial x''}=0$$

$$\frac{\partial S_{Cx}}{\partial x''}=\frac{\left(x^2+y^2+z^2\right)^{\frac{1}{2}}\frac{\partial x}{\partial x''}-x\left(x^2+y^2+z^2\right)^{\frac{-1}{2}}\left(x\frac{\partial x}{\partial x''}+y\frac{\partial y}{\partial x''}\right)}{\left(x^2+y^2+z^2\right)}$$

$$\frac{\partial S_{Cy}}{\partial x''}=\frac{\left(x^2+y^2+z^2\right)^{\frac{1}{2}}\frac{\partial y}{\partial x''}-y\left(x^2+y^2+z^2\right)^{\frac{-1}{2}}\left(x\frac{\partial x}{\partial x''}+y\frac{\partial y}{\partial x''}\right)}{\left(x^2+y^2+z^2\right)}$$

$$\frac{\partial S_{Cz}}{\partial x''}=-\frac{z\left(x^2+y^2+z^2\right)^{\frac{-1}{2}}\left(x\frac{\partial x}{\partial x''}+y\frac{\partial y}{\partial x''}\right)}{\left(x^2+y^2+z^2\right)}$$

$$\frac{\partial S_{Bx}}{\partial x''}=\frac{\partial S_{Cx}}{\partial x''}\qquad\frac{\partial S_{By}}{\partial x''}=-\frac{\partial S_{Cy}}{\partial x''}\qquad\frac{\partial S_{Bz}}{\partial x''}=-\frac{\partial S_{Cz}}{\partial x''}$$

$$\frac{\partial S_{Ox}}{\partial x''}=\left(\cos\kappa\cos\phi-\sin\kappa\sin\omega\sin\phi\right)\frac{\partial S_{Bx}}{\partial x''}-\sin\kappa\cos\omega\frac{\partial S_{By}}{\partial x''}$$
$$+\left(\cos\kappa\sin\phi+\sin\kappa\sin\omega\cos\phi\right)\frac{\partial S_{Bz}}{\partial x''}$$

$$\frac{\partial S_{Oy}}{\partial x''}=\left(\sin\kappa\cos\phi+\cos\kappa\sin\omega\sin\phi\right)\frac{\partial S_{Bx}}{\partial x''}+\cos\kappa\cos\omega\frac{\partial S_{By}}{\partial x''}$$
$$+\left(\sin\kappa\sin\phi-\cos\kappa\sin\omega\cos\phi\right)\frac{\partial S_{Bz}}{\partial x''}$$

$$\frac{\partial S_{Oz}}{\partial x''}=-\cos\omega\sin\phi\frac{\partial S_{Bx}}{\partial x''}+\sin\omega\frac{\partial S_{By}}{\partial x''}+\cos\omega\cos\phi\frac{\partial S_{Bz}}{\partial x''}$$

$$\frac{\partial S_{Ex}}{\partial x''}=r_{11}\frac{\partial S_{Ox}}{\partial x''}+r_{12}\frac{\partial S_{Oy}}{\partial x''}+r_{13}\frac{\partial S_{Oz}}{\partial x''}$$

$$\frac{\partial S_{Ey}}{\partial x''}=r_{21}\frac{\partial S_{Ox}}{\partial x''}+r_{22}\frac{\partial S_{Oy}}{\partial x''}+r_{23}\frac{\partial S_{Oz}}{\partial x''}$$

$$\frac{\partial S_{Ez}}{\partial x''} = r_{31}\frac{\partial S_{Ox}}{\partial x''} + r_{32}\frac{\partial S_{Oy}}{\partial x''} + r_{33}\frac{\partial S_{Oz}}{\partial x''}$$

$$\frac{\partial X_0}{\partial x''} = \frac{\partial s}{\partial x''}S_{Ex} + s\frac{\partial S_{Ex}}{\partial x''}$$

$$\frac{\partial Y_0}{\partial x''} = \frac{\partial s}{\partial x''}S_{Ey} + s\frac{\partial S_{Ey}}{\partial x''}$$

$$\frac{\partial Y_0}{\partial x''} = \frac{\partial s}{\partial x''}S_{Ez} + s\frac{\partial S_{Ez}}{\partial x''}$$

$$\frac{\partial s}{\partial x''} = \frac{\left(-\frac{\partial \beta}{\partial x''} - \frac{1}{2}\left(\beta^2 - 4\alpha\gamma\right)^{\frac{-1}{2}}\left(2\beta\frac{\partial \beta}{\partial x''} - 4\alpha\frac{\partial \gamma}{\partial x''} - 4\gamma\frac{\partial \alpha}{\partial x''}\right)\right) * 2\alpha - 2\frac{\partial \alpha}{\partial x''}\left(-\beta - \sqrt{-\beta^2 - 4\alpha\gamma}\right)}{4 * \alpha^2}$$

$$\frac{\partial \alpha}{\partial x''} = \frac{2 * S_{Ex} * \frac{\partial S_{Ex}}{\partial x''} + 2 * S_{Ey} * \frac{\partial S_{Ey}}{\partial x''}}{a^2} + \frac{2 * S_{Ez} * \frac{\partial S_{Ez}}{\partial x''}}{b^2}$$

$$\frac{\partial \beta}{\partial x''} = \frac{X_{cam} * \frac{\partial S_{Ex}}{\partial x''} + Y_{cam} * \frac{\partial S_{Ey}}{\partial x''}}{a^2} + \frac{Z_{cam} * \frac{\partial S_{Ez}}{\partial x''}}{b^2}$$

$$\frac{\partial \gamma}{\partial x''} = 0$$

$$\frac{\partial \lambda}{\partial x''} = \frac{1}{1 + \left(\frac{Y_0}{X_0}\right)^2} * \left(\frac{X_0 * \frac{\partial Y_0}{\partial x''} - Y_0 * \frac{\partial X_0}{\partial x''}}{X_0^2}\right)$$

$$\frac{\partial \phi}{\partial x''} = \frac{\left[\frac{\partial Z_o}{\partial x''}\sqrt{X_o^2 + Y_o^2} - \left(X_o\frac{\partial X_o}{\partial x''} + Y_o\frac{\partial Y_o}{\partial x''}\right) * \left(X_o^2 + Y_o^2\right)^{\frac{-1}{2}} * Z_o\right]}{\left(1 + \frac{Z_o^2}{\left(X_o^2 + Y_o^2\right)\left(1 - \frac{e^2 N}{N + h}\right)}\right) * \left(1 - \frac{e^2 N}{N + h}\right) * \left(X_o^2 + Y_o^2\right)}$$

C.17 Partial Derivative with respect to y” (y pixel coordinate)

$$\frac{\partial x'}{\partial y''} = 0 \qquad \frac{\partial x'}{\partial y''} = -c \qquad \frac{\partial r}{\partial y''} = \frac{1}{2}\left(x'^2 + y'^2\right)^{\frac{-1}{2}}\left(2x'\frac{\partial x'}{\partial y''} + 2y'\frac{\partial y'}{\partial y''}\right)$$

$$\frac{\partial x}{\partial y''}=\frac{\partial x'}{\partial y''}\left[1-k_1r^2-k_2r^4-2p_1x'-2p_2y'-\frac{p_1r^2}{x'}\right]$$
$$+x'\left(2k_1r\frac{\partial r}{\partial y''}-4k_2r^3\frac{\partial r}{\partial y''}-2p_1\frac{\partial x'}{\partial y''}-2p_2\frac{\partial y'}{\partial y''}-\frac{2rp_1x'\frac{\partial r}{\partial y''}-p_1r^2\frac{\partial x'}{\partial y''}}{x'^2}\right)$$

$$\frac{\partial y}{\partial y''}=\frac{\partial y'}{\partial y''}\left[1-k_1r^2-k_2r^4-2p_2y'-2p_1x'-\frac{p_2r^2}{y'}\right]$$
$$+y'\left(-2k_1r\frac{\partial r}{\partial y''}-4k_2r^3\frac{\partial r}{\partial y''}-2p_2\frac{\partial y'}{\partial y''}-2p_1\frac{\partial x'}{\partial y''}-\frac{2rp_2y'\frac{\partial r}{\partial y''}-p_2r^2\frac{\partial y'}{\partial y''}}{y'^2}\right)$$

$$\frac{\partial z}{\partial y''}=0$$
$$\frac{\partial S_{Cx}}{\partial y''}=\frac{\left(x^2+y^2+z^2\right)^{\frac{1}{2}}\frac{\partial x}{\partial y''}-x\left(x^2+y^2+z^2\right)^{\frac{-1}{2}}\left(x\frac{\partial x}{\partial y''}+y\frac{\partial y}{\partial y''}\right)}{\left(x^2+y^2+z^2\right)}$$
$$\frac{\partial S_{Cy}}{\partial y''}=\frac{\left(x^2+y^2+z^2\right)^{\frac{1}{2}}\frac{\partial y}{\partial y''}-y\left(x^2+y^2+z^2\right)^{\frac{-1}{2}}\left(x\frac{\partial x}{\partial y''}+y\frac{\partial y}{\partial y''}\right)}{\left(x^2+y^2+z^2\right)}$$
$$\frac{\partial S_{Cz}}{\partial y''}=-\frac{z\left(x^2+y^2+z^2\right)^{\frac{-1}{2}}\left(x\frac{\partial x}{\partial y''}+y\frac{\partial y}{\partial y''}\right)}{\left(x^2+y^2+z^2\right)}$$

$$\frac{\partial S_{Bx}}{\partial y''}=\frac{\partial S_{Cx}}{\partial y''}\qquad\frac{\partial S_{By}}{\partial y''}=-\frac{\partial S_{Cy}}{\partial y''}\qquad\frac{\partial S_{Bz}}{\partial y''}=-\frac{\partial S_{Cz}}{\partial y''}$$

$$\frac{\partial S_{Ox}}{\partial y''}=\left(\cos\kappa\cos\phi-\sin\kappa\sin\omega\sin\phi\right)\frac{\partial S_{Bx}}{\partial y''}-\sin\kappa\cos\omega\frac{\partial S_{By}}{\partial y''}$$
$$+\left(\cos\kappa\sin\phi+\sin\kappa\sin\omega\cos\phi\right)\frac{\partial S_{Bz}}{\partial y''}$$
$$\frac{\partial S_{Oy}}{\partial y''}=\left(\sin\kappa\cos\phi+\cos\kappa\sin\omega\sin\phi\right)\frac{\partial S_{Bx}}{\partial y''}+\cos\kappa\cos\omega\frac{\partial S_{By}}{\partial y''}$$
$$+\left(\sin\kappa\sin\phi-\cos\kappa\sin\omega\cos\phi\right)\frac{\partial S_{Bz}}{\partial y''}$$
$$\frac{\partial S_{Oz}}{\partial y''}=-\cos\omega\sin\phi\frac{\partial S_{Bx}}{\partial y''}+\sin\omega\frac{\partial S_{By}}{\partial y''}+\cos\omega\cos\phi\frac{\partial S_{Bz}}{\partial y''}$$
$$\frac{\partial S_{Ex}}{\partial y''}=r_{11}\frac{\partial S_{Ox}}{\partial y''}+r_{12}\frac{\partial S_{Oy}}{\partial y''}+r_{13}\frac{\partial S_{Ox}}{\partial y''}$$
$$\frac{\partial S_{Ey}}{\partial y''}=r_{21}\frac{\partial S_{Ox}}{\partial y''}+r_{22}\frac{\partial S_{Oy}}{\partial y''}+r_{23}\frac{\partial S_{Ox}}{\partial y''}$$
$$\frac{\partial S_{Ez}}{\partial y''}=r_{31}\frac{\partial S_{Ox}}{\partial y''}+r_{32}\frac{\partial S_{Oy}}{\partial y''}+r_{33}\frac{\partial S_{Oz}}{\partial y''}$$

$$\frac{\partial X_0}{\partial y''} = \frac{\partial s}{\partial y''} S_{Ex} + s\frac{\partial S_{Ex}}{\partial y''}$$

$$\frac{\partial Y_0}{\partial y''} = \frac{\partial s}{\partial y''} S_{Ey} + s\frac{\partial S_{Ey}}{\partial y''}$$

$$\frac{\partial Y_0}{\partial y''} = \frac{\partial s}{\partial y''} S_{Ez} + s\frac{\partial S_{Ez}}{\partial y''}$$

$$\frac{\partial s}{\partial y''} = \frac{\left(-\frac{\partial \beta}{\partial y''} - \frac{1}{2}\left(\beta^2 - 4\alpha\gamma\right)^{\frac{-1}{2}}\left(2\beta\frac{\partial \beta}{\partial y''} - 4\alpha\frac{\partial \gamma}{\partial y''} - 4\gamma\frac{\partial \alpha}{\partial y''}\right)\right) * 2\alpha - 2\frac{\partial \alpha}{\partial y''}\left(-\beta - \sqrt{-\beta^2 - 4\alpha\gamma}\right)}{4 * \alpha^2}$$

$$\frac{\partial \alpha}{\partial y''} = \frac{2 * S_{Ex} * \frac{\partial S_{Ex}}{\partial y''} + 2 * S_{Ey} * \frac{\partial S_{Ey}}{\partial y''}}{a^2} + \frac{2 * S_{Ez} * \frac{\partial S_{Ez}}{\partial y''}}{b^2}$$

$$\frac{\partial \beta}{\partial y''} = \frac{X_{cam} * \frac{\partial S_{Ex}}{\partial y''} + Y_{cam} * \frac{\partial S_{Ey}}{\partial y''}}{a^2} + \frac{Z_{cam} * \frac{\partial S_{Ez}}{\partial y''}}{b^2}$$

$$\frac{\partial \gamma}{\partial y''} = 0$$

$$\frac{\partial \lambda}{\partial y''} = \frac{1}{1 + \left(\frac{Y_0}{X_0}\right)^2} * \left(\frac{X_0 * \frac{\partial Y_0}{\partial y''} - Y_0 * \frac{\partial X_0}{\partial y''}}{X_0^2}\right)$$

$$\frac{\partial \phi}{\partial y''} = \frac{\left[\frac{\partial Z_o}{\partial y''}\sqrt{X_o^2 + Y_o^2} - \left(X_o\frac{\partial X_o}{\partial y''} + Y_o\frac{\partial Y_o}{\partial y''}\right) * \left(X_o^2 + Y_o^2\right)^{\frac{-1}{2}} * Z_o\right]}{\left(1 + \frac{Z_o^2}{\left(X_o^2 + Y_o^2\right)\left(1 - \frac{e^2 N}{N + h}\right)}\right) * \left(1 - \frac{e^2 N}{N + h}\right) * \left(X_o^2 + Y_o^2\right)}$$